



MODELING OF ASYMMETRIC INTERMODULATION DISTORTION AND MEMORY  
EFFECTS OF POWER AMPLIFIERS

A THESIS SUBMITTED TO  
THE GRADUATE SCHOOL OF NATURAL AND APPLIED SCIENCES  
OF  
MIDDLE EAST TECHNICAL UNIVERSITY

BY

AHMET HAYRETTİN YÜZER

IN PARTIAL FULFILLMENT OF THE REQUIREMENTS  
FOR  
THE DEGREE OF DOCTOR OF PHILOSOPHY  
IN  
ELECTRICAL AND ELECTRONICS ENGINEERING

MAY 2011

Approval of the thesis:

**MODELING OF ASYMMETRIC INTERMODULATION DISTORTION AND MEMORY  
EFFECTS OF POWER AMPLIFIERS**

submitted by **AHMET HAYRETTİN YÜZER** in partial fulfillment of the requirements for  
the degree of  
**Doctor of Philosophy in Electrical and Electronics Engineering Department, Middle  
East Technical University** by,

Prof. Dr. Canan Özgen  
Dean, Graduate School of **Natural and Applied Sciences**

\_\_\_\_\_

Prof. Dr. İsmet Erkmen  
Head of Department, **Electrical and Electronics Engineering**

\_\_\_\_\_

Assoc. Prof. Dr. Şimşek DEMİR  
Supervisor, **Electrical and Electronics Engineering**

\_\_\_\_\_

**Examining Committee Members:**

Prof. Dr. Canan Toker  
Electrical and Electronics Engineering, METU

\_\_\_\_\_

Assoc. Prof. Dr. Şimşek Demir  
Electrical and Electronics Engineering, METU

\_\_\_\_\_

Prof. Dr. Hayrettin Köymen  
Electrical and Electronics Engineering, Bilkent University

\_\_\_\_\_

Prof. Dr. Nevzat Yıldırım  
Electrical and Electronics Engineering, METU

\_\_\_\_\_

Prof. Dr. Sencer Koç  
Electrical and Electronics Engineering, METU

\_\_\_\_\_

**Date:**

\_\_\_\_\_

**I hereby declare that all information in this document has been obtained and presented in accordance with academic rules and ethical conduct. I also declare that, as required by these rules and conduct, I have fully cited and referenced all material and results that are not original to this work.**

Name, Last Name: AHMET HAYRETTİN YÜZER

Signature :

# ABSTRACT

## MODELING OF ASYMMETRIC INTERMODULATION DISTORTION AND MEMORY EFFECTS OF POWER AMPLIFIERS

YÜZER, Ahmet Hayrettin

Ph.D, Department of Electrical and Electronics Engineering

Supervisor : Assoc. Prof. Dr. Şimşek DEMİR

May 2011, 157 pages

This dissertation is focused on developing a new passband behavioral model in order to account for asymmetric intermodulation distortion resulted from memory effect.

First, a measurement setup is prepared to measure the AM/AM, AM/PM distortion, magnitudes and the phases of intermodulation (IMD) and fundamental (FUND) components which are created by the amplifier where phase is calculated only by measuring magnitudes. Then, responses of a sample amplifier are measured for different excitation situations (center frequency and tone spacing are swept).

A new modeling technique, namely Odd Order Modeling (OOM), is proposed which has unequal time delay terms. The reason of unequal time delay addition is the change of effective channel length according to the average power passing through that channel. These unequal delays create asymmetry in the IMD components. General Power Series Expansion (GPSE) model is also extracted, OOM and GPSE model performances are compared by using NMSE metric. In order to improve model performance, even order terms with envelope of input are added. It is mathematically proven that even order terms with envelope of the input have contribution to IMD and FUND components'. This improved version of modeling is named

as Even Order modeling (EOM). EOM model performance is compared with the others' performance for two-tone excitation measurement results. It is shown that EOM gives the most accurate result. Model performance is checked for unequal four-tone signal as well.

EOM model is applied to baseband DPD circuit after making some modifications. Model linearization performance is compared with the performances of the other memory polynomial modeling techniques.

Keywords: Phase measurement, Behavioral modeling, Intermodulation distortion, unequal time delay, thermal modeling, even order contribution

# ÖZ

## GÜÇ YÜKSELTİCİLERİNDE ARAKİPLEME BOZULUMUNDAKİ BAKIŞIMSIZLIĞIN VE HAFIZA ETKİSİNİN MODELLENMESİ

YÜZER, Ahmet Hayrettin

Doktora, Elektrik ve Elektronik Mühendisliği Bölümü

Tez Yöneticisi : Doç. Dr. Şimşek DEMİR

Mayıs 2011, 157 sayfa

Bu tezde hafıza etkisinin sebep olduğu asimetrik arakiplenim bozulumunu modellemek için geçirme bandında çalışan bir davranışsal modelleme geliştirmeye odaklanılmış ve aşağıda özetlenen sonuçlar elde edilmiştir:

İlk olarak, güç yükselticinin oluşturduğu AM/AM ve AM/PM bozulumu ile temel bileşenin ve bozulumun büyüklük ve fazının ölçülebilmesi için ölçüm sistemi hazırlanmıştır. Karmaşık sayıların toplamı kuramına dayanan bir denklem ile sadece büyüklük değerleri ölçülerek açı hesaplaması yapılmaktadır. Sonrasında, değişik uyarım durumlarında örnek bir güç yükseltici cevabı ölçülmüştür (farklı merkez frekansına ve farklı tonlar arası frekansına sahip uyarım işaretleri).

Tek terimli modelleme (OOM) olarak isimlendirilen modelleme yöntemi önerilmiştir ki bu yöntem eşit olmayan zaman gecikmesi terimlerine sahiptir. Zaman geciktirme terimleri asimetri oluşturmak için eklenmiştir. Eş olmayan zaman gecikmesi eklemenin sebebi şudur; transistorun etkin kanal uzunluğu üzerinden geçen gücün ortalama değerini göre değişmektedir. Genel üssel seri açılım model (GPSE) parametrelili de elde edildikten sonra GPSE ve OOM model başarımları NMSE ölçeği yardımıyla karşılaştırılmıştır. Model başarımlarını arttırmak

için Çift dereceli terimlerin IMD' ye ve FUND' e herhangi bir etkisi yoktur. Giriş işaretinin zarfı ile beraber modelleme denkleminde eklenen çift dereceli terimlerin IMD' ye ve FUND' e etkisi matematiksel olarak ispatlanmıştır. Geliştirilen bu modele çift dereceli modelleme (EOM) ismi verilmiştir. İki ton uyarımı sonuçlarına göre EOM model başarımı diğer modelleme başarımları ile karşılaştırılmıştır. EOM modelleme tekniğinin en doğru sonucu verdiği gösterilmiştir. Sonra EOM başarımı bir önceki paragrafta belirtilen değişik uyarım durumları için alınan ölçüm sonuçları ile karşılaştırılmış ve modelin geçerlilik bölgesi  $f_0 \pm \%20$  olarak gözlemlenmiştir. EOM model başarımı eş olmayan büyüklük değerine sahip dört onlu uyarım işareti için de kontrol edilmiştir.

Bazı değişikliklerin/uyumlaştırmaların ardından EOM model taban bant DPD devresine uygulanmıştır. Modelin başarımı diğer iki hafıza etkisi modelleme yöntemlerinin başarımları ile karşılaştırılmıştır.

Anahtar Kelimeler: Faz ölçümü, davranışsal modelleme, arakipleme bozulumu, eşit olmayan zaman gecikmesi, ısıl etkinin modellenmesi, çift terim katkısı

*To my wife Huriye, my son Ahmet Efe  
and to  
my parents*

## ACKNOWLEDGMENTS

I am heartily thankful to my supervisor, Prof. Dr. Şimşek Demir, whose encouragement, guidance and support from the initial to the final level enabled me to present this thesis. He showed me different ways to approach a research problem and the need to be persistent to accomplish any goal. He taught me that, How I can broaden my horizon while trying to find a way for any problem.

I would like to thank Prof. Dr. Hayrettin Köymen and Prof. Dr. Sencer Koç for their valuable suggestions during the whole period and for their time during the Progress Committee meetings.

I am also grateful to Prof. Dr. Fadhel Ghannouchi, for hosting me at Iradio Lab/University of Calgary for six months, and I deeply appreciate his guidance, invaluable comments and suggestions during my study on baseband application of proposed modeling technique(EOM).

I am also would like to thank to my dear friends Dr. Evren Ekmekçi, Dr. Tansu Filik, Oğuzhan Erdem, Umut Tilki, Sebahattin Topal, Yılmaz Kalkan, Barış Özyer, Akif Durdu, and Atilla Dönük for their support and friendship through these years.

I would like to thank my former roommates:Dr. Mehmet Ünlü, Dr. Kağan Toplalı, İlker Co-mart, Çağrı Çetintepe, Ömer Bayraktar, Özgehan Şahin, Ramazan Çetin, Amin Ronaghzadeh, Pejman Mohammadi, Caner Güçlü and Ozan D. Gürbüz and latter roommates:Öznur Türkmen and Yusuf Sevinç for his friendship and company who made my times in the department enjoyable and worthy.

I acknowledge ASELSAN A.Ş. for supporting me through the project titled as "Güç Yükselticinin Davranışsal Modelinin (GÜYDAM) Belirlenmesi" which is the passband application part of my thesis.

I also would like to thank to Mohamed Helaoui, Aidin Bassam, Erhan Sağlamyürek, Fatih Yılmaz, Serdar Durdağı, Shubhrajit Bhattacharjee, Ramzi Darraji, Saeed Rezaei Nazifi, Karun Rawat, Meenakshi Rawat, Mayada Younes, Dhikra Saffar and Andrew Kwan who are my fel-

lows in the University of Calgary, for their help and friendship. I am also grateful to Ivana L. D'Adamo, Sarsu family, Uyanik family and Nurgel family for helping hand for formal issues related with Canada Government, to accommodate in Calgary and recreation myself after a busy week.

I am also very grateful to my mother Fatma Yüzer, my brothers and my sisters for their sincere love and endless support during my life.

Finally, I want to thank to the one special in my life, my lovely wife Huriye Yüzer, for their support and love that keep me eager and hopeful to accomplish this thesis. I could not have completed my thesis without her unlimited support and patience.

# TABLE OF CONTENTS

ABSTRACT . . . . .	iv
ÖZ . . . . .	vi
DEDICATON . . . . .	viii
ACKNOWLEDGMENTS . . . . .	ix
TABLE OF CONTENTS . . . . .	xi
LIST OF TABLES . . . . .	xiv
LIST OF FIGURES . . . . .	xv
CHAPTERS	
1 Introduction . . . . .	1
1.1 Motivations and Objectives of This Study . . . . .	1
1.2 Organization of This Dissertation . . . . .	2
1.3 Original Contributions . . . . .	2
2 Memory Effect of Power Amplifier and Linear-Nonlinear Modeling . . . . .	4
2.1 Introduction . . . . .	4
2.2 Memory Effect . . . . .	5
2.2.1 Electrical Memory Effect . . . . .	6
2.2.2 Thermal Memory Effect . . . . .	7
2.3 Amplifier Nonlinearities . . . . .	8
2.4 Amplifier Behavioral Modeling Types . . . . .	15
2.4.1 Baseband Behavioral Modeling . . . . .	16
2.4.2 Passband Behavioral Modeling . . . . .	17
2.4.3 Relation Between Baseband Coefficient and Passband Coefficient . . . . .	17
2.5 Common Nonlinear Behavioral Models . . . . .	18

	2.5.1	Memoryless Nonlinear Modeling . . . . .	19
	2.5.2	Nonlinear Modeling with Memory . . . . .	22
	2.5.2.1	Volterra Series . . . . .	22
	2.5.2.2	Wiener, Hammerstein and Wiener-Hammerstein Models . . . . .	24
	2.5.2.3	Parallel Wiener Model . . . . .	27
	2.5.2.4	Multi-Slice Behavioral Modeling . . . . .	29
	2.5.2.5	Memory Polynomial Models . . . . .	30
	2.6	Summary . . . . .	33
3		Measurement Setup and Measurement Results . . . . .	34
	3.1	Introduction . . . . .	34
	3.2	Measurement Setup . . . . .	35
	3.3	AM/AM Measurement . . . . .	38
	3.4	Phase Measurement . . . . .	38
	3.5	AM/PM Measurement . . . . .	40
	3.6	Phase Calibration for Signal Generators . . . . .	49
	3.7	Measurement Results . . . . .	50
	3.8	Conclusion . . . . .	69
4		Theory of Power Series with Unequal Time Delay Behavioral Model, Param- eter Extraction and Comparison . . . . .	71
	4.1	Introduction . . . . .	71
	4.2	Model Architecture . . . . .	72
	4.2.1	Asymmetry Creation . . . . .	77
	4.3	Extraction Procedure for Modeling . . . . .	79
	4.4	NMSE Metric for Model Comparison . . . . .	80
	4.5	Verification and Model Comparison . . . . .	81
	4.6	EOM Model Validity Range . . . . .	93
	4.6.1	EOM Model Validity Range Investigation for Two-Tone excitation . . . . .	93
	4.6.2	EOM model Validity Range Investigation for Unequal Four- Tone excitation . . . . .	107
	4.7	Summary . . . . .	118

5	Baseband Applications of EOM Modeling . . . . .	120
5.1	Introduction . . . . .	120
5.2	Modification on EOM modeling . . . . .	121
5.2.1	Evaluation Metrics . . . . .	121
5.2.2	Extraction Algorithm for MPSD . . . . .	122
5.3	Thermal Memory Effect Modeling and Linearization Application . .	124
5.4	Electrical Memory Effect Modeling Application . . . . .	127
5.5	Summary . . . . .	130
6	Conclusion and Future work . . . . .	131
6.1	Conclusion . . . . .	131
6.2	Future Research . . . . .	136
	REFERENCES . . . . .	137
A	Intermediate Steps of Phase Difference Calculation Equation Derivation . . .	141
B	Expansion for the polynomial order terms . . . . .	142
C	Unequal Four-Tone Comparison Graphs . . . . .	149
	CURRICULUM VITAE . . . . .	156

## LIST OF TABLES

### TABLES

Table 3.1 Sample LUT . . . . .	51
Table 4.1 The coefficients of GPSE modeling extracted by using measurement results of 10MHz/1kHz . . . . .	81
Table 4.2 The coefficients of OOM modeling extracted by using measurement results of 10MHz/1kHz . . . . .	82
Table 4.3 The coefficients of EOM modeling extracted by using measurement results of 10MHz/1kHz . . . . .	82
Table 4.4 NMSE values . . . . .	89
Table 4.5 Measured frequency spectra of unequal four-tone signal created by I/Q mod- ulator . . . . .	109
Table 4.6 Measured frequency spectra of the amplifier response to the unequal four- tone excitation . . . . .	110
Table 4.7 Frequency spectra of model output calculated in Matlab by using FFT com- mand for unequal four-tone excitation . . . . .	111
Table 4.8 Normalized square error of measured value and estimated model output . .	112
Table 5.1 Forward Models' performance comparison for GPSE, MPM with unit delay, MPM with sparse delay and MPSD . . . . .	127
Table 5.2 Inverse Models' performance comparison of GPSE, MPM with unit delay, MPM with sparse delay and MPSD . . . . .	127
Table 5.3 Delay Values . . . . .	128
Table 5.4 Comparison of the MPM and MPSD Models based on the MEMR, NMSE and ACEPR values . . . . .	128

## LIST OF FIGURES

### FIGURES

Figure 2.1 Structure of Behavioral model . . . . .	5
Figure 2.2 Memory sources in integrated circuit of power amplifier [6] . . . . .	6
Figure 2.3 IMD3 amplitude versus frequency spacing [7] . . . . .	7
Figure 2.4 Measured lower and upper IMD3 sidebands as a function of output power for a)20MHz, b)1MHz and c)5kHz tone spacing [8] . . . . .	9
Figure 2.5 Heat flow from the device. (a) Physical and (b) electrical lumped element [9]	10
Figure 2.6 Simulation results for a) Gain & magnitude of Pout vs Pin and b)phase of Pout vs Pin for <b>linear behavior</b> of sample amplifier designed in ADS2009 . . . . .	11
Figure 2.7 Simulation results for a) Gain & AM/AM and b)AM/PM <b>nonlinear be-</b> <b>havior</b> of sample amplifier designed in ADS2009 . . . . .	12
Figure 2.8 Measurement results for a) Gain and b)output power vs input power <b>non-</b> <b>linear behavior</b> of sample amplifier#2 measured at iradio lab. University of Calgary	13
Figure 2.9 Frequency spectra of (a) a one-tone continuous wave input and (b) the corresponding output . . . . .	15
Figure 2.10 Frequency spectra of (a) a two-tone continuous wave input and (b) the corresponding output . . . . .	15
Figure 2.11 Frequency spectra of (a) a one-tone WCDMA input and (b) the correspond- ing output . . . . .	16
Figure 2.12 Block diagram of a) Wiener, b)Hammerstein and c)Wiener-Hammerstein Models . . . . .	25
Figure 2.13 Dual Branch Wiener-Hammerstein model Structure . . . . .	27
Figure 2.14 Block diagram of Parallel Wiener Model . . . . .	28
Figure 2.15 A two-slice nonlinear system behavioral model . . . . .	30

Figure 2.16 Modified Multi-Slice Behavioral Modeling . . . . .	30
Figure 2.17 Structure of Memory Polynomial Model with <u>unit delay</u> . . . . .	31
Figure 2.18 Structure of Memory Polynomial Model with <u>sparse delay</u> . . . . .	31
Figure 3.1 Schematic representation of Measurement setup . . . . .	36
Figure 3.2 Photograph of Measurement setup . . . . .	37
Figure 3.3 Photograph of Amplifier . . . . .	37
Figure 3.4 Flow chart for one-tone phase difference measurement for a predefined power level . . . . .	41
Figure 3.5 Phase measurement technique validation setup . . . . .	42
Figure 3.6 Phase difference between former and latter state . . . . .	42
Figure 3.7 Power level vs. phase difference between "SGA" and "SGC" . . . . .	43
Figure 3.8 Power level vs. phase difference between "SGB" and "SGC" . . . . .	43
Figure 3.9 in-phase four-tone signal creation . . . . .	44
Figure 3.10 Addition for the signals having equal magnitude and 120° phase difference	46
Figure 3.11 Flow chart for AM/PM measurement for full range power level . . . . .	47
Figure 3.12 Repeated phase measurement result of through line . . . . .	48
Figure 3.13 Repeated phase measurement result of sample amplifier . . . . .	48
Figure 3.14 Magnitude and phase measurement result of one-tone excitation having 10MHz working frequency . . . . .	52
Figure 3.15 Magnitude and phase measurement results of a)IMDL, b)IMDU, c)FUNDL and d)FUNDU for two-tone excitation having 10MHz/1kHz . . . . .	56
Figure 3.16 Magnitude and phase measurement results of a)IMDL, b)IMDU, c)FUNDL and d)FUNDU for two-tone excitation having 8MHz/1kHz . . . . .	58
Figure 3.17 Magnitude and phase measurement results of a)IMDL, b)IMDU, c)FUNDL and d)FUNDU for two-tone excitation having 9MHz/1kHz . . . . .	60
Figure 3.18 Magnitude and phase measurement results of a)IMDL, b)IMDU, c)FUNDL and d)FUNDU for two-tone excitation having 11MHz/1kHz . . . . .	62
Figure 3.19 Magnitude and phase measurement results of a)IMDL, b)IMDU, c)FUNDL and d)FUNDU for two-tone excitation having 12MHz/1kHz . . . . .	64

Figure 3.20 Magnitude and phase measurement results of a)IMDL, b)IMDU, c)FUNDL and d)FUNDU for two-tone excitation having 10MHz/300Hz . . . . .	66
Figure 3.21 Magnitude and phase measurement results of a)IMDL, b)IMDU, c)FUNDL and d)FUNDU for two-tone excitation having 10MHz/3.3kHz . . . . .	68
Figure 4.1 Block diagram representation of OOM . . . . .	73
Figure 4.2 Power series with unequal time delay behavioral model with even order terms	76
Figure 4.3 Asymmetry creation mechanism . . . . .	79
Figure 4.4 Comparison between magnitudes and phases of measurement and OOM model outputs for 10MHz/1kHz input excitation for a) ImdL b) ImdU c)FundL and d) FundU components . . . . .	85
Figure 4.5 Comparison between magnitudes and phases of measurement and EOM model outputs for 10MHz/1kHz input excitation for a) ImdL b) ImdU c)FundL and d) FundU components . . . . .	87
Figure 4.6 Comparison between magnitudes and phases of measurement and EOM model outputs for 10MHz one-tone excitation . . . . .	88
Figure 4.7 Comparison of three modeling for a)magnitude and b)phase of IMDL component for 10MHz/1kHz excitation signal . . . . .	90
Figure 4.8 Comparison of three modeling for a)magnitude and b)phase of IMDU component for 10MHz/1kHz excitation signal . . . . .	91
Figure 4.9 Comparison of three modeling for a)magnitude and b)phase of FUNDL component for 10MHz/1kHz excitation signal . . . . .	92
Figure 4.10 Comparison of three modeling for a)magnitude and b)phase of FUNDU component for 10MHz/1kHz excitation signal . . . . .	94
Figure 4.12 EOM modeling asymmetry representation performance for a)magnitude and b)phase of IMD signals . . . . .	95
Figure 4.13 Comparison between magnitudes and phases of measurement and EOM model outputs for 8MHz/1kHz input excitation for a) ImdL b) ImdU c)FundL and d) FundU components . . . . .	97

Figure 4.14 Comparison between magnitudes and phases of measurement and EOM model outputs for 9MHz/1kHz input excitation for a) ImdL b) ImdU c)FundL and d) FundU components . . . . .	99
Figure 4.15 Comparison between magnitudes and phases of measurement and EOM model outputs for 11MHz/1kHz input excitation for a) ImdL b) ImdU c)FundL and d) FundU components . . . . .	101
Figure 4.16 Comparison between magnitudes and phases of measurement and EOM model outputs for 12MHz/1kHz input excitation for a) ImdL b) ImdU c)FundL and d) FundU components . . . . .	103
Figure 4.17 Comparison between magnitudes and phases of measurement and EOM model outputs for 10MHz/300Hz input excitation for a) ImdL b) ImdU c)FundL and d) FundU components . . . . .	105
Figure 4.18 Comparison between magnitudes and phases of measurement and EOM model outputs for 10MHz/3.3kHz input excitation for a) ImdL b) ImdU c)FundL and d) FundU components . . . . .	113
Figure 4.19 Measured frequency spectra of five sample excitation signal for unequal four-tone for a)full range and b)zoomed to fundamental tone . . . . .	114
Figure 4.20 Comparison between measurement results and model outputs for four-tone input excitation for five different power levels ( $-8.18dBm$ to $2.25dBm$ ). . . . .	117
Figure 5.1 Shaped memory delay values for 101-WCDMA excitation scenario . . . . .	123
Figure 5.2 Difference between magnitude of IMDL and magnitude of IMDU to distinguish the region where thermal memory effect dominates . . . . .	125
Figure 5.3 DPD and an amplifier output power versus input power [54] . . . . .	126
Figure 5.4 Linearization line-up [54] . . . . .	126
Figure 5.5 Frequency spectra of model estimation and measurement result for 101_WCDMA excitation scenario . . . . .	129
Figure 5.6 Zoomed version frequency spectra of model estimation and measurement results for 101_WCDMA excitation scenario . . . . .	129
Figure C.1 Comparison between measurement and model outputs for four-tone (10MHz/1kHz) input excitation for five different power levels ( $-12.8dBm$ to $4.26dBm$ ). . . . .	155

# CHAPTER 1

## Introduction

### 1.1 Motivations and Objectives of This Study

There is a growing demand for amplifier characterization in these days because more information about amplifier behavior such as gain compression, saturation power, adjacent channel power ratio (ACPR), asymmetry in the intermodulation distortion (IMD) etc., are required in designing complicated systems involving amplifiers. Amplifiers introduce nonlinearities especially when operating near or beyond 1 dB compression point ( $P_{1dB}$ ); however numerous amplifiers used in telecommunication applications are operated in a weakly nonlinear regime due to linearity requirements [1]. Many researchers are working on linearization techniques which can be used to decrease effect of nonlinearities of amplifiers. First step of linearization may be to have a behavioral amplifier model. The better amplifier model we have, the more success we will have in linearization. There is inherent asymmetry in the fundamental components (FUND) and inter-modulation distortion (IMD) components at the output of an amplifier when excited with more than one tone [2]. One of the main aims of this dissertation is to develop a model which can represent asymmetry in both magnitude and phase of FUND and IMD components.

Amplifier models are used to estimate/calculate the spectral components (FUND, IMD etc.) at the output of an amplifier. A computer is used to calculate these components when behavioral model is used in simulation. FPGA or microprocessor is used to calculate these components when behavioral model is used in a circuit (Feedforward Linearizer, DPD, ...). In the design process, simple calculations are preferred. Therefore, behavioral model order should be as small as possible to decrease the calculation time. Another aim of this dissertation is

decreasing the nonlinearity order of modeling/that is decreasing the model complexity.

## **1.2 Organization of This Dissertation**

In the first part of the second chapter of this dissertation, explanation about memory effect types, passband and baseband modeling techniques are given. Then in the second part, literature review of common modeling techniques is outlined. In the third chapter, measurement setup preparation steps are explained. AM/AM and AM/PM measurement procedure and phase calibration technique are explained in detail in this chapter as well. In the fourth chapter, firstly, theory of modeling techniques, extraction procedure are explained with asymmetry creation mechanism. Secondly, comparison results of extracted models are given for verification purpose. Finally, EOM validity range investigation results are given. In the fifth chapter, baseband DPD application results of proposed model are given. Finally, in the sixth chapter, conclusion of the research is summarized and some future work are listed.

## **1.3 Original Contributions**

The issues of modeling asymmetric intermodulation distortion is presented in this dissertation. In order to find model parameters, amplifier response must be measured. In addition to AM/AM measurement, AM/PM measurement is needed for successful model extraction. AM/PM measurement is difficult for passband signal. Therefore, a measurement setup is prepared which has ability to measure AM/AM, AM/PM distortion, magnitudes and phases of intermodulation (IMD) and fundamental (FUND) components and magnitudes of unequal four-tone signal. This is the first original contribution of this dissertation.

Proposed modeling technique is based on power series expansion. Time delay terms are added to each order of polynomial terms to create asymmetry between IMDL and IMDU. Unlike the memory polynomial models, time delay values are not equal for each order term. So, unequal time delay terms are used in modeling equation, thus new modeling technique is proposed which gives more accurate result than GPSE. This is another original contribution of this dissertation.

Unless any modification is applied, even order terms do not have any contribution to IMD and

FUND components. There is no paper in literature which shows the even order modification to get contribution to the IMD and FUND for passband modeling. It is mathematically proven that even order term can contribute to the IMD and FUND components as long as envelope of input signal is added to that term. This is another original contribution of this dissertation.

When amplifier is excited with GSM signal thermal memory is dominated. So, a modeling technique is needed having thermal memory modeling ability to construct DPD system for base station. Proposed modeling technique is applied to baseband DPD circuit after making some modification. This is the first time, thermal memory effect is modeled with a polynomial modeling technique. Forward modeling, Inverse modeling and linearization performance is better than other techniques.

## CHAPTER 2

# Memory Effect of Power Amplifier and Linear-Nonlinear Modeling

### 2.1 Introduction

There are perfectly good transistor characterization techniques. However, utilizing these models towards an amplifier design is also a complicated process. Low noise amplifier and power amplifier have different utilization methods. Similarly wideband amplifiers and high gain amplifiers or high linearity and high efficiency amplifiers have contradicting requirements. When considering system design the detailed amplifier circuit is not required, but its performance as a function of frequency, type of excitation, input power level etc. becomes critical. So, there is a growing demand for amplifier characterization. Information about amplifier behavior such as gain compression, saturation power, adjacent channel power ratio (ACPR), asymmetry in the intermodulation distortion (IMD) and so on are required in system designs. Usually most challenging amplifier designs are power amplifiers.

Power amplifier models can be divided into two parts; physical modeling and behavioral modeling. Designer should have knowledge about the elements used in the power amplifier while trying to get a physical modeling. Output power can be calculated by using mathematical definition of components and transistor's nonlinear relation. This type of power amplifier modeling is used in circuit level simulation which takes long time. Behavioral models are used in system level simulation. There is no need to have knowledge about the elements which are included to the power amplifier circuit while trying to get behavioral model of it. While trying to characterize amplifier, it should be taken into account that PA's are designed to be used generally in telecommunication systems. But, "DSP/telecommunication engineers

do not work with the deterministic standard RF metrics” [3] such as quiescent point, bias circuit, number of section used in the input matching circuit, ... . They generally work with statistical metrics and data. So, there is a gap between DSP/telecommunication engineers and RF engineers. This gap is resulted from the nature of the design specifications in between two disciplines. Properly managed and well defined behavioral model can bridge that gap [3].

Behavioral model accuracy depends on parameter extraction techniques and model structure. Moreover, behavioral model parameters depend on excitation type and condition. Therefore, there are a number of behavioral models in literature. These models are often built from observed/measured data and relate the results of a process to its stimuli with a purely mathematical relationship. Behavioral Modeling is therefore often thought to be merely a form of multidimensional curve fitting [4]. Behavioral model black box structure is as given in Figure 2.1.

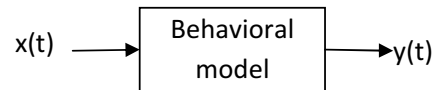


Figure 2.1: Structure of Behavioral model

## 2.2 Memory Effect

If the instantaneous time output of the system is effected by the input of the previous time, it is said that this system has memory. This is the shortest/basic definition of memory. There is another definition given in literature as ”distortion itself is not memory effect, but only non-constant distortion behavior at different modulation frequencies can be regarded as one [5]”. Memory Effects are seen at the output of an amplifier as asymmetry in between lower band IMD (IMDL) and upper band IMD (IMDU) components. FUND and IMD components’ creation are explained in section 2.3 on page 8. Most of off-the-shelf amplifiers have memory effect and memory is the main source of degradation in the performance of PA. Memory characterization and canceling the effects of memory are not resolved yet and these are active research areas. Memory can be due to mainly two reasons; Electrical Memory Effect and Thermal Memory Effect. Sources of memory effect for power amplifier are illustrated in Figure 2.2 [6]. Bias circuit, matching circuit, excitation signal having wide bandwidth, matching

circuit and transistor are the main sources of Electrical (Short Time) Memory Effect. Electrical Memory Effect can be reduced (minimize) while designing bias circuit and matching circuit. Heat sink, excitation signal having narrow bandwidth and transistor can be some of the reasons for Thermal (Long Time) Memory Effect. Minimizing the Thermal Memory Effect which is caused by transistor temperature dependent electrical parameter is very difficult. In order to visualize the Thermal Memory Effect at the output of amplifier Boumaiza [7] *et al.* excited the 90-W peak lateral double-diffused metal-oxide-semiconductor (LDMOS) PA with two tone having different frequency spacing then measured the magnitude of IMD3 for different frequency spacing for a constant input power level. Magnitude of IMD3 is given in Figure 2.3 [7]. Tornblad *et al.* also [8] investigated IMD3 power level versus output power for three specific tone spacing (20MHz, 1MHz and 5kHz) for Infineon product PTFA191001E (1.9GHz, 100W amplifier). IMD power level versus output power level graph is showed in Figure 2.4.

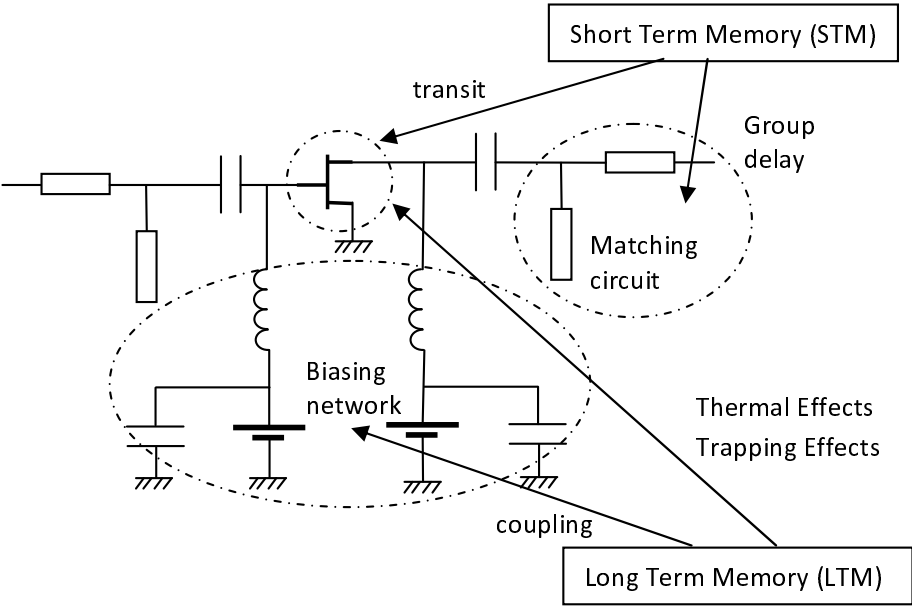


Figure 2.2: Memory sources in integrated circuit of power amplifier [6]

**2.2.1 Electrical Memory Effect**

As it is stated in the previous section, a power amplifier may have both electrical and thermal memory effects. The major source of electrical memory effect is variation in the terminal

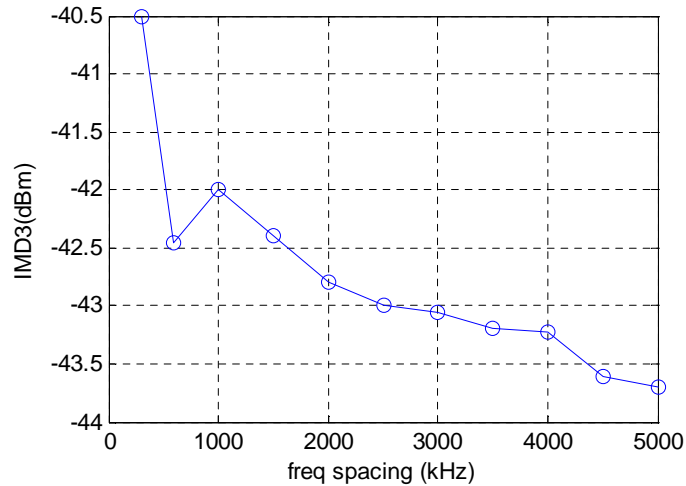


Figure 2.3: IMD3 amplitude versus frequency spacing [7]

impedances with respect to bandwidth of input signal [7].

When the output spectra of amplifier is investigated, in some cases, Thermal Memory Effect is dominated by Electrical Memory Effect. If power amplifier is excited with a modulated wide band signal such as WCDMA or just a two-tone having wider tone separation, IMD at the output of amplifier is mostly affected by electrical memory effect. As it is shown in Figure 2.4a, there is asymmetry in between IMDL and IMDU for wide band excitation signal. This asymmetry is caused by frequency dependent baseband impedance. Since memory effect is created by frequency dependent baseband impedance for wide band signal, it affects the IMDL and IMDU components in different amounts which create asymmetry in between IMDL and IMDU. There are a number of electrical memory modeling techniques in literature. Some of those modeling techniques, considering Electrical Memory Effect, are explained shortly in section 2.5.

### 2.2.2 Thermal Memory Effect

Gain variation caused by temperature dependent transistor parameter is the major source of thermal memory effect. Electrical Memory Effect is dominated by Thermal Memory effect when amplifier is excited with a modulated signal having narrow bandwidth such as GSM or a two-tone signal having narrow frequency separation. Considering Figure 2.3, it can be said that thermal memory effect on IMD level decrease when the frequency separation

increase. For example, there is approximately 10dB asymmetry in between IMDL and IMDU components when the amplifier is excited with a signal having 5kHz tone spacing as shown in Figure 2.4c [8]. Moreover, there is no specific frequency separation limit for thermal memory effect creation, it depends on amplifier and environment structure.

Physical and lumped element representation of heat flow diagram from the device are given in Figure 2.5 [9]. Tornblad reported that time constant for die and for package are  $\sim 90\mu s$  and  $\sim 370\mu s$  respectively. This means that temperature response of amplifier lag in the signal passing through amplifier approximately 3kHz and 10kHz due to die and package structure. Delayed temperature value effect the temperature dependent transistor parameter [10].

### 2.3 Amplifier Nonlinearities

Behavioral modeling was defined as relation between input and output previously. Each modeling technique has own modeling function and mathematical bases. Therefore, before starting explain modeling techniques, it had better give some basic nonlinear definitions.

Behavioral modeling function, input-output relation, can be classify as static function part or dynamic function part. In static function, output is defined according to the *instantaneous input*. Static function may be either linear or nonlinear as given in (2.1) and (2.2), respectively.

$$y|_{linear}(t) = G \cdot x(t) \quad (2.1)$$

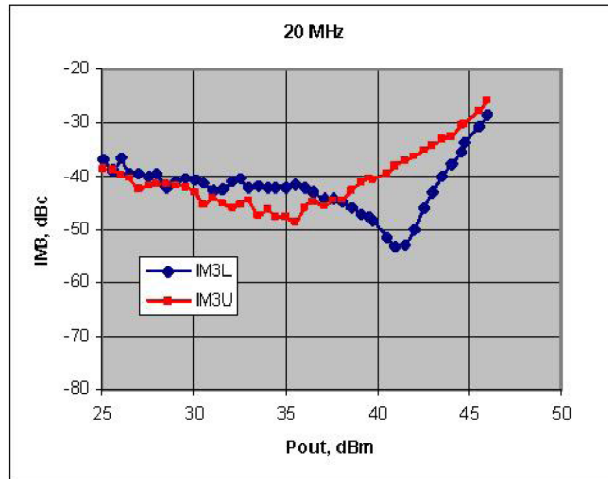
$$y|_{nonlinear}(t) = f(G) \cdot x(t) \quad (2.2)$$

where  $x(t)$  is time domain input signal,  $y(t)$  is time domain output signal,  $G$  is constant and  $f(G)$  is the function contains powers of  $G$  as well as first order.

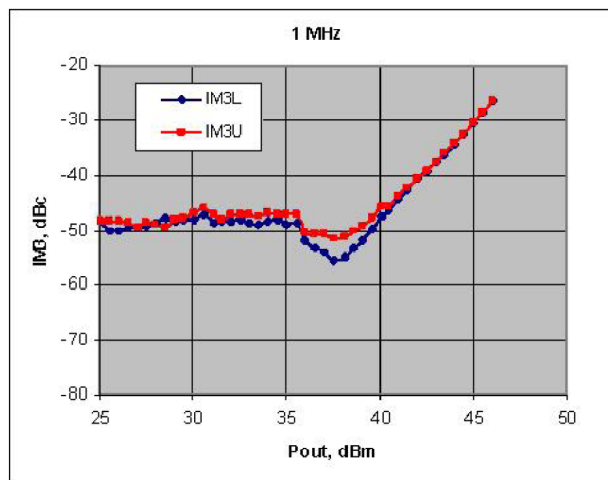
Static function does not has any relation between previous time input and current time output. In contrast, dynamic function has a relation between current time output and previous time input as well as current time input. In other words, having previous time dependency means dynamic function has memory effect. Dynamic function may also be either linear or nonlinear as given in (2.3) and (2.4) .

$$y|_{linear}(t) = G \cdot x(t - \phi_G) \quad (2.3)$$

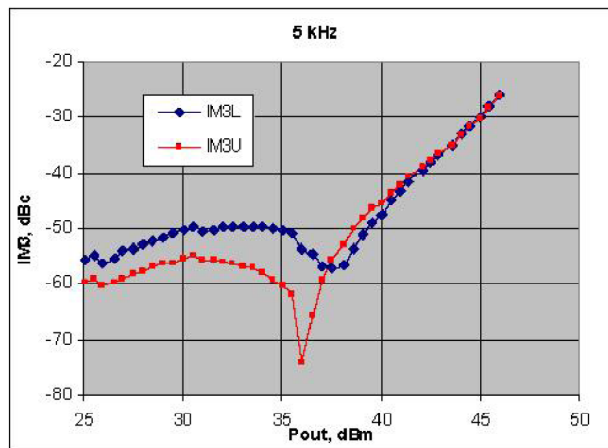
$$y|_{nonlinear}(t) = f(G) \cdot x(t - f(\phi_G)) \quad (2.4)$$



(a) tonespacing 20Mz



(b) tonespacing 1MHz



(c) tonespacing 5kHz

Figure 2.4: Measured lower and upper IMD3 sidebands as a function of output power for a)20MHz, b)1MHz and c)5kHz tone spacing [8]

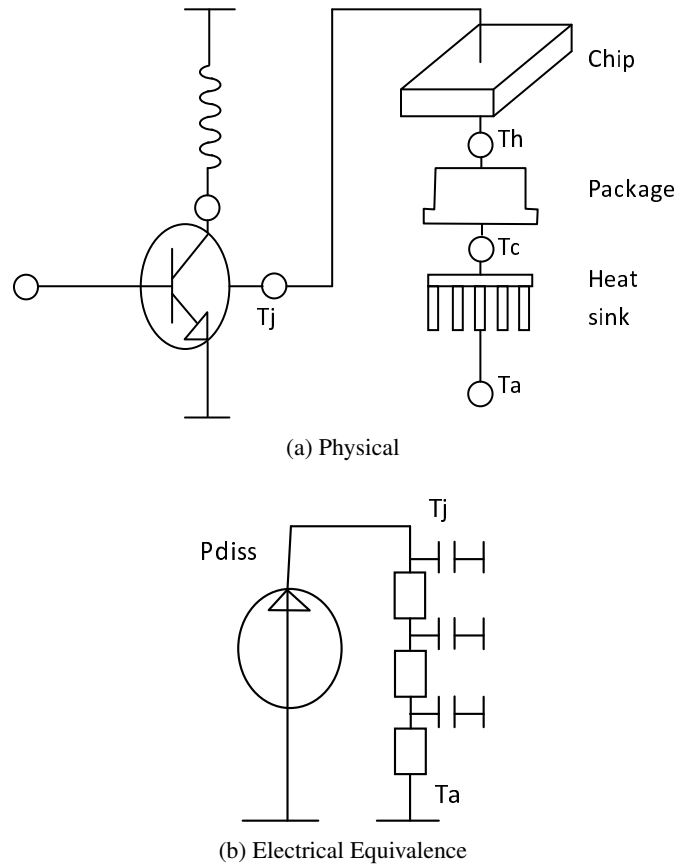
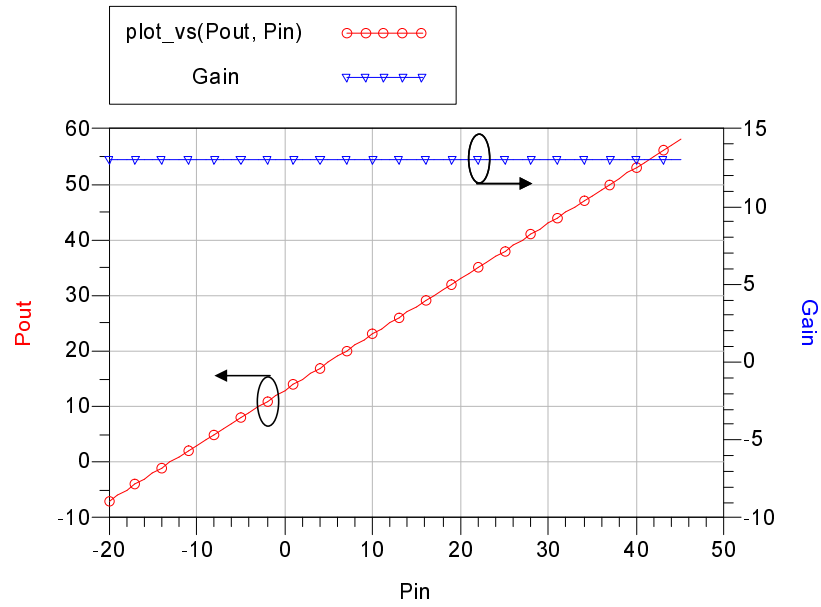


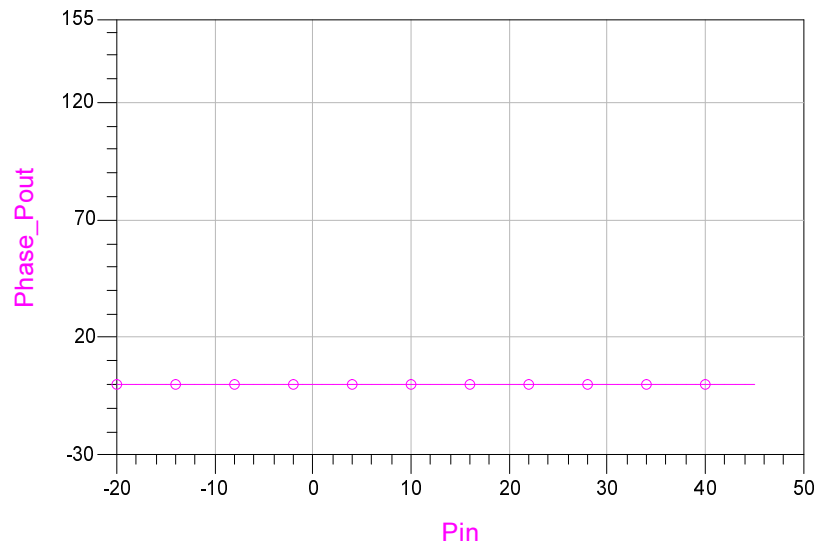
Figure 2.5: Heat flow from the device. (a) Physical and (b) electrical lumped element [9]

where  $\phi_G$  represents the phase of  $G$ .

In order to visualize the linear and nonlinear amplification effect on amplifier output, a project is prepared in ADS2009. Amplifier is excited with one-tone Continuous Wave (CW) signal and then gain vs input power, output power vs input power and phase of output power vs input are plotted for linear and nonlinear amplification case as given in Figure 2.6 and Figure 2.7, respectively. In these graphs, blue colored trace represents the gain of amplifier, red colored trace represents the magnitude of output signal and purple colored trace represents the phase of output signal. Gain and phase are constant for all excitation levels for linear amplification case as seen from Figure 2.6a and Figure 2.6b. Gain is decreasing when input power level exceed  $P_{1dB}$  point for the nonlinear amplification case. Although phase is approximately constant for the power level lower than  $P_{1dB}$ , phase starts change when the input power exceed  $P_{1dB}$ . If the system has memory, output power level of PA becomes as given in Figure 2.8b and corresponding gain become as given in Figure 2.8a.

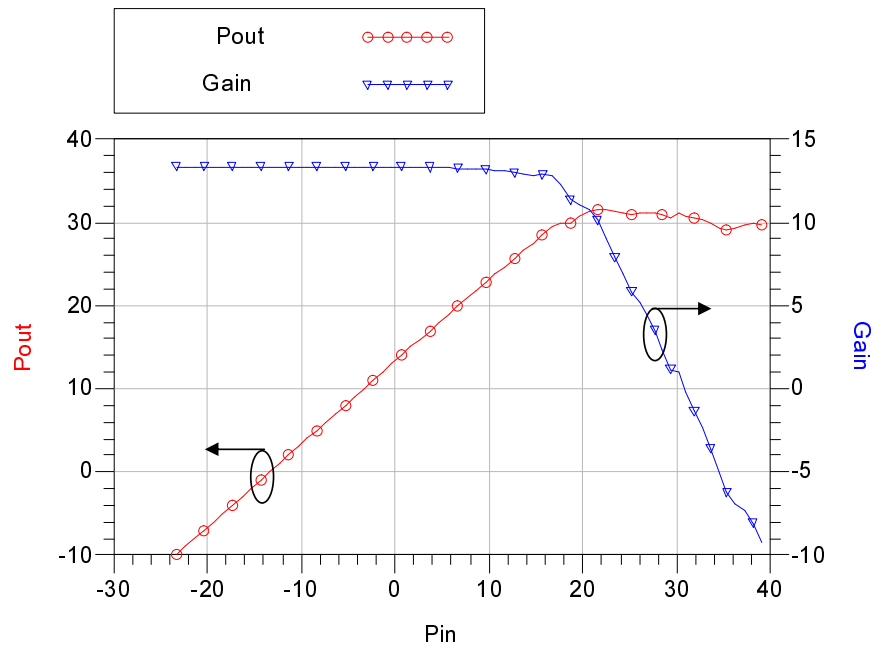


(a) Gain and magnitude of Pout vs Pin for linear amplification

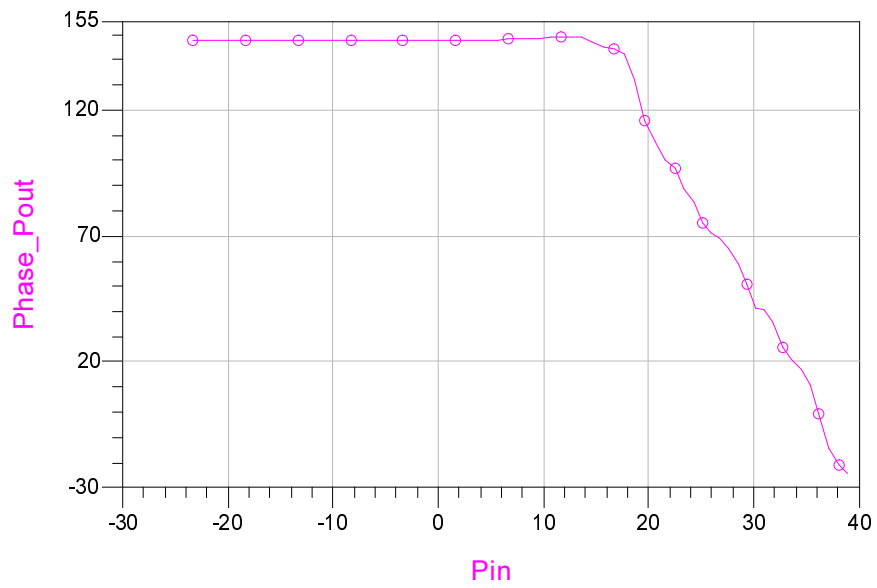


(b) phase of Pout vs Pin for linear amplification

Figure 2.6: Simulation results for a) Gain & magnitude of Pout vs Pin and b) phase of Pout vs Pin for **linear behavior** of sample amplifier designed in ADS2009

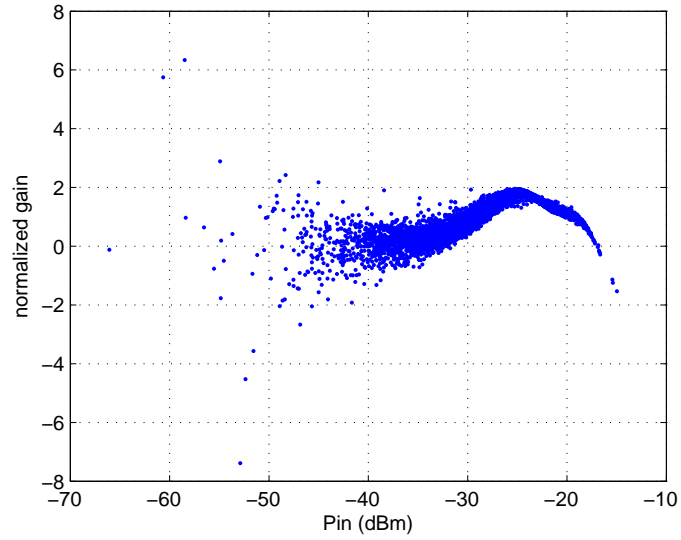


(a) Gain and AM/AM

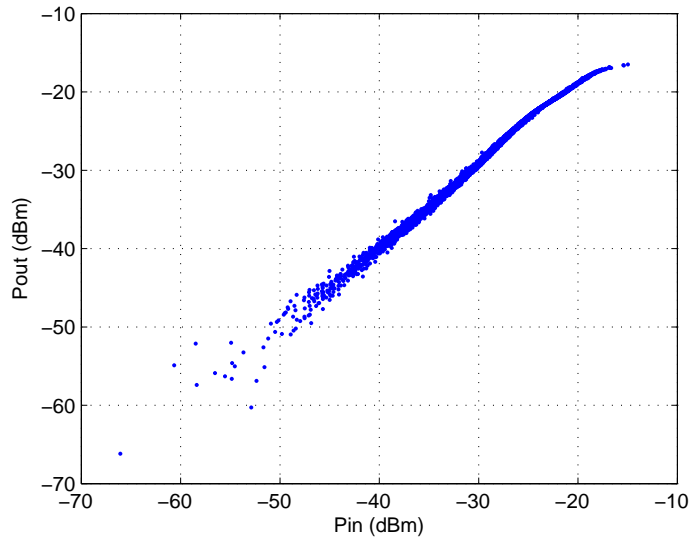


(b) AM/PM

Figure 2.7: Simulation results for a) Gain & AM/AM and b)AM/PM **nonlinear behavior** of sample amplifier designed in ADS2009



(a) Normalized Gain



(b) output power vs input power

Figure 2.8: Measurement results for a) Gain and b)output power vs input power **nonlinear behavior** of sample amplifier#2 measured at iradio lab. University of Calgary

Hereafter, modeling with static function will be named as *memoryless modeling* and modeling with dynamic function will be named as *modeling with memory* in this dissertation. Also, finding the coefficients of model equations will be named as *model extraction/model coefficient extraction*. Because almost all power amplifier models are composed of nonlinear equations, model coefficients can not be extracted arithmetically easily. Therefore, model extraction procedure/technique is important/needed step.

One-tone and two-tone excitation signal can be represented mathematically as given in (2.5) and (2.6), respectively. Output representation of linear modeling becomes as given in (2.7) and (2.8) after substituting (2.5) and (2.6) into (2.1).

$$x_{1Tone}(t) = V \cdot \cos \omega_c t \quad (2.5)$$

$$x_{2Tone}(t) = V_1 \cdot \cos \omega_1 t + V_2 \cdot \cos \omega_2 t \quad (2.6)$$

$$y_{1Tone}(t) = G \cdot V \cdot \cos \omega_c t \quad (2.7)$$

$$y_{2Tone}(t) = G \cdot V_1 \cdot \cos \omega_1 t + G \cdot V_2 \cdot \cos \omega_2 t \quad (2.8)$$

If the nonlinear function  $f(G)$  given in (2.2) is taken as power series, as given in (2.9), output representation of nonlinear modeling become as given in (2.10) and (2.11) after substituting (2.5) and (2.6) in to (2.2).

$$y = \sum_{k=1}^K a_k \cdot x^k \quad (2.9)$$

$$y_{1Tone}(t) = a_1 \cdot V \cdot \cos \omega_c t + a_2 \cdot V^2 \cdot \cos^2 \omega_c t + \dots + a_K \cdot V^K \cdot \cos^K \omega_c t \quad (2.10)$$

$$y_{2Tone}(t) = a_1 \cdot V_1 \cdot \cos \omega_1 t + a_1 \cdot V_2 \cdot \cos \omega_2 t + a_2 \cdot (V_1 \cdot \cos \omega_1 t + V_2 \cdot \cos \omega_2 t)^2 + \dots + a_K \cdot (V_1 \cdot \cos \omega_1 t + V_2 \cdot \cos \omega_2 t)^K \quad (2.11)$$

Frequency spectra of continuous wave input and corresponding output both for one-tone and for two-tone are given in Figure 2.9a, Figure 2.9b, Figure 2.10a and Figure 2.10b, respectively. The components placed at  $f = f_1$  is named as lower band fundamental (FUNDL) signal and the other one placed at  $f = f_2$  is named as upper band fundamental (FUNDU) signal in Figure 2.10. Similarly, the component placed at  $f = 2f_1 - f_2$  is named as lower band intermodulation distortion (IMDL) and the other one placed at  $f = 2f_2 - f_1$  is named as upper band intermodulation distortion (IMDU) in Figure 2.10b.

Frequency spectra of WCDMA input and corresponding output for one carrier is given in Figure 2.11a and Figure 2.11b respectively.

Magnitude or/and phase of components showed on frequency spectra are measured in order to find model coefficients,  $a_k$ . Generally, model coefficients are found by equating model function with measurement result. When the model function is not linear as given in (2.11), model coefficient can not be found arithmetically. Optimization, iteration, active learning and pseudo inverse are some of the techniques to find the model coefficients. Almost all technique use curve fitting.

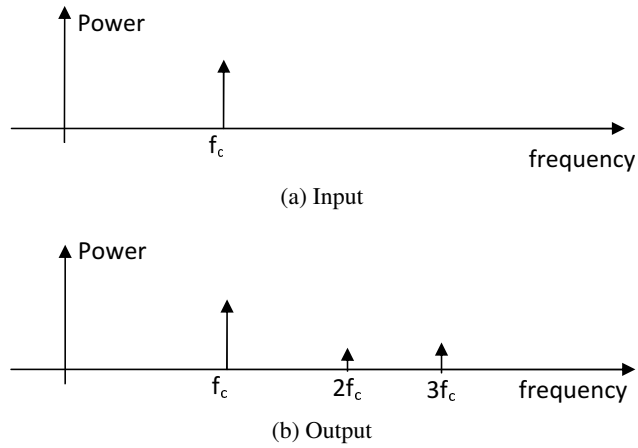


Figure 2.9: Frequency spectra of (a) a one-tone continuous wave input and (b) the corresponding output

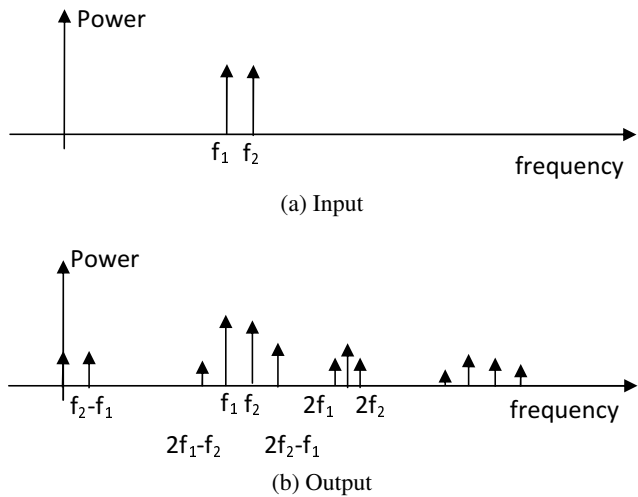


Figure 2.10: Frequency spectra of (a) a two-tone continuous wave input and (b) the corresponding output

## 2.4 Amplifier Behavioral Modeling Types

Behavioral modeling is defined as finding the mathematical relation between input and output as stated previously. Because of this definition, behavioral modeling can be thought as a multi dimensional curve fitting process. Modeling procedure can be summarized as follows:

- Excite the PA with desired signal type ( one - tone, two - tone, multi-tone or modulated signal).
- Measure the input and output signal/spectra.

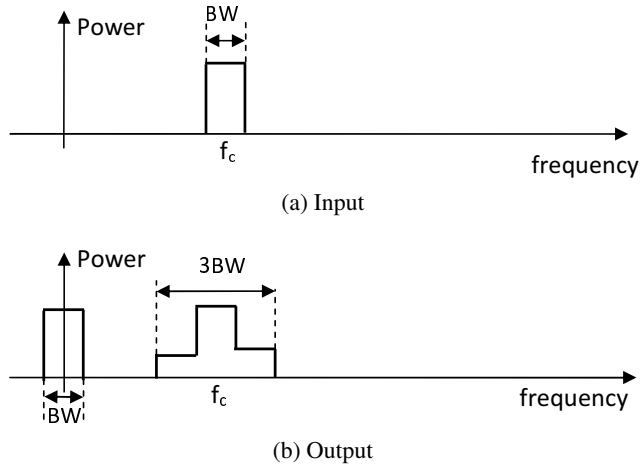


Figure 2.11: Frequency spectra of (a) a one-tone WCDMA input and (b) the corresponding output

- Extract model parameters by equating measurement values with model equations.

Behavioral models can be placed in one of two types of modeling techniques according to excitation and output signal; Baseband Model and Passband Model. Baseband model suppresses the carrier frequency component and only interested with envelope signal. In contrast to this, passband model depends on each cycle of carrier frequency as well as envelope signal.

#### 2.4.1 Baseband Behavioral Modeling

Envelope of the signal or distortion of envelope signal can be modeled with this type of modeling technique. Therefore, this type of modeling technique is appropriate for the system with baseband signal. On the other hand, harmonic distortion of the carrier can not be modeled with this modeling technique because there is no term representing the RF frequency in the modeling equation. Baseband signal is composed of two scalar numbers  $I(t)$  and  $Q(t)$ , defined as in-phase and quadrature components. Time domain complex baseband signal mathematical representation is as given in (2.12).

$$V_i(t) = I_i(t) + jQ_i(t) = |V_i(t)|\angle V_i(t) \quad (2.12)$$

When it is needed to simulate the whole transceiver system including baseband model, baseband to passband conversion is required since transceiver system is working with high frequency signal. Passband to baseband conversion is explained shortly in 2.4.3 [3].

Output signal for baseband modeling can be represented with Memory Polynomial modeling (MPM) as given in (2.13).

$$V_o[n] = \sum_{m=0}^{M-1} \sum_{k=1}^K a_{k,m} \cdot V_i[n-m] \cdot |V_i[n-m]|^{k-1} \quad (2.13)$$

where  $V_i$  and  $V_o$  are the input and the estimated output baseband complex discrete signal, and  $a_{k,m}$ ,  $M$  and  $K$  are the model coefficients, memory depth and the nonlinearity order respectively.

### 2.4.2 Passband Behavioral Modeling

Both RF frequency and envelope signal can be represented in passband modeling. Hence, both harmonic distortion of carrier and distortion of envelope signal can be modeled with passband modeling technique. But, since passband model has a number of cycles related with only RF signal for one cycle of information (Envelope) signal, time domain simulation of passband modeling consumes much more time than the time needed for baseband modeling simulation. Therefore, carrier frequency based analysis, harmonic balance analysis preferred to simulate passband modeling. Time domain two-tone input excitation signal can be represented in passband as given in (2.14).

$$\begin{aligned} V_i(t) &= V_c \cos \omega_c t \times V_m \cos \omega_m t \\ &= \frac{V_c V_m}{2} \times \cos(\omega_c - \omega_m)t + \frac{V_c V_m}{2} \times \cos(\omega_c + \omega_m)t \end{aligned} \quad (2.14)$$

where  $V_c$  represents maximum value of magnitude of carrier signal,  $V_m$  represents maximum value of magnitude of message (Envelope) signal,  $\omega_c$  represents carrier frequency in radian per second and  $\omega_m$  represents envelope signal's frequency in radian per second. Time domain output signal for passband modeling can be represented as given in (2.15) for power series modeling technique.

$$V_o(t) = a_1 V_i(t) + a_3 V_i^3(t) + a_5 V_i^5(t) \quad (2.15)$$

### 2.4.3 Relation Between Baseband Coefficient and Passband Coefficient

The coefficients which are extracted by using passband signal cannot be used in baseband model directly. After making some transformation, these coefficients can be used in baseband.

A signal having high frequency term can be represented in terms of baseband signal as given in (2.16).

$$\begin{aligned}
rf(t) &= I(t) \cos \omega_c t + Q(t) \sin \omega_c t \\
&= \text{Re} \{ [I(t) + jQ(t)] \times [\cos \omega_c t - j \sin \omega_c t] \} \\
&= \text{Re} \{ [I(t) + jQ(t)] e^{-j\omega_c t} \} \\
&= \frac{1}{2} \{ [I(t) + jQ(t)] e^{-j\omega_c t} + [I(t) + jQ(t)] e^{j\omega_c t} \}
\end{aligned} \tag{2.16}$$

Considering the (2.16), passband signal can be rewritten as follows:

$$rf(t) = C(t)e^{-j\omega_c t} + C^*(t)e^{j\omega_c t} \tag{2.17}$$

where  $C(t) = I(t) + jQ(t)$ .  $C^*(t)$  represents complex conjugate of  $C(t)$ . Then, after substituting (2.17) in to the (2.15), passband modeling and baseband modeling became as given in (2.18) and (2.19) respectively [11].

$$V_o(t)|_{w_c} = [k_1 + \frac{3}{4}k_3|C(t)|^2 + \frac{5}{8}k_5|C(t)|^4] \cdot [C(t)e^{-j\omega_c t} + C^*(t)e^{j\omega_c t}] \tag{2.18}$$

$$V_o(t)|_{BB} = [k_1 + \frac{3}{4}k_3|C(t)|^2 + \frac{5}{8}k_5|C(t)|^4] \cdot C(t) \tag{2.19}$$

## 2.5 Common Nonlinear Behavioral Models

Behavioral model is represented as a black box as given in Figure 2.1. So, user only need to know model equation/function, whatever that system contains is not of interest. If it is aimed that 2<sup>nd</sup> and 3<sup>rd</sup> harmonic shouldn't be at the output of amplifier, it can be filtered out easily. Therefore, while trying to get model, it is assumed that output is filtered around carrier frequency. The signal which is at the active and adjacent channel are out of interest. Conversely, hence IMD is an in-band distortion, it is much more difficult to filter out. Therefore, it is focused on modeling of IMD signal in this dissertation just like most of the researchers do who are working on amplifier modeling. While trying to propose a new behavioral model, three subjects should be explained/determined carefully; model structure, measurement setup and model parameter extraction algorithm. Although user do not have to have information about what the system contains, researchers have to have knowledge about PA structure/circuit to capture most properties of that system. The more knowledge we have about amplifier non-linear behavior and sources of nonlinearity, the better model we can develop. In addition to

this, although user don't have to have detailed information about structure, s/he had better to have knowledge about DUT (PA) behavior. For instance, if the amplifier has memory effect, a model with memory terms should be used. Otherwise, if memoryless model is used, performance of the system having that model wouldn't be as good as wanted.

After choosing appropriate model having ability to get good estimation performance for the system to be modeled, model parameters should be extracted. Measurement type and measurement setup are another important issues for successful model parameter extraction step. Measurement setup is prepared by considering what kind of measurement is required for model extraction. While one-tone measurement is enough for some modeling types, some other modeling types require different measurement types such as two-tone, multi-tone, base-band signal measurement. Model performance depends on extraction success and model extraction success is depend on fitting performance [12]. Common and mostly used nonlinear behavioral models and extraction algorithms which are previously reported in literature are explained in next section.

### 2.5.1 Memoryless Nonlinear Modeling

#### General Power Series Expression (GPSE)

Power series function is the workhorse of the most of the behavioral modeling techniques. GPSE is developed by simplifying the Volterra-Series modeling [13]. After simplification, memory effect representation ability has been lost. Therefore, GPSE is defined as *memoryless version* of Volterra-Series modeling. Moreover, this simplification resulted in limited usage of this technique for PA behavioral modeling [14]. In contrast, GPSE modeling can be usable as long as the PA doesn't has memory effect or has a negligible amount. Indeed power series is frequently used in modeling combined with other techniques. GPSE modeling is used both for bandpass modeling and passband modeling.

Mathematical definition of GPSE is as follows:

$$V_o(t) = \sum_{k=1}^K a_{2k-1} \cdot (V_i(t))^{2k-1} \quad (2.20)$$

where  $V_i$  and  $V_o$  represent time domain input and output signals respectively.  $a_{2k-1}$  are the

model coefficients. if  $a_{2k-1}$  coefficients are assumed as real-valued, only AM/AM or AM/PM nonlinear behavior of PA can be modeled; it is impossible to model both AM/AM and AM/PM characteristics. Huang *at al.* [15] used power series to estimate only AM/AM behavior with real-valued model coefficient. Arno *at al.* [16] used two different power series function having real-valued model coefficients to model both AM/AM and AM/PM nonlinear behavior. One of the power series function is used for AM/AM and the other one is used for AM/PM.

In order to model AM/PM nonlinear behavior as well as AM/AM nonlinear behavior with using only one power series expression,  $a_{2k-1}$  coefficients should be chosen as complex numbers [17], [18], [13]. if (2.6) is substituted into the GPSE modeling equation, (2.20), we will get the result as given in (2.21) considering  $K=3$ .

$$V_o(t) = a_1 (V_1 \cos(\omega_1 t) + V_2 \cos(\omega_2 t)) + a_3 (V_1 \cos(\omega_1 t) + V_2 \cos(\omega_2 t))^3 + a_5 (V_1 \cos(\omega_1 t) + V_2 \cos(\omega_2 t))^5 \quad (2.21)$$

If we expand (2.21), we will get (2.22). Hence (2.22) contains higher order trigonometric function, it is difficult to calculate distortion and fundamental components. Simplified version of (2.22) is given in (2.23a).

$$\begin{aligned} V_o(t) = & a_5 V_1^5 \cos^5 \omega_1 t + 5a_5 V_1^4 V_2 \cos^4 \omega_1 t \cos \omega_2 t + 10a_5 V_1^3 V_2^2 \cos^3 \omega_1 t \cos^2 \omega_2 t \\ & + a_3 V_1^3 \cos^3 \omega_1 t + 10a_3 V_1^2 V_2^3 \cos^2 \omega_1 t \cos^3 \omega_2 t + 3a_3 V_1^2 V_2 \cos^2 \omega_1 t \cos \omega_2 t \\ & + 5a_5 V_1 V_2^4 \cos \omega_1 t \cos^4 \omega_2 t + 3a_3 V_1 V_2^2 \cos \omega_1 t \cos^2 \omega_2 t + a_1 V_1 \cos \omega_1 t \\ & + a_5 V_2^5 \cos^5 \omega_2 t + a_3 V_2^3 \cos^3 \omega_2 t + a_1 V_2 \cos \omega_2 t \end{aligned} \quad (2.22)$$

In order to facilitate phasor domain representation, (2.23a) is rewritten in the form as given in (2.23b). The terms having "  $\cos(\omega_1 t)$  " multiplier (terms having red colored font) named as  $V_{FUNDL}$  and the terms having "  $\cos(2\omega_1 t - \omega_2 t)$  " multiplier (terms having blue colored font) named as  $V_{IMDL}$  (See the section 2.3 at the page 14 for the definition of FUNDL, FUNDU, IMDL and IMDU).

$$\begin{aligned}
V_o(t) = & V_1 a_1 \cos \omega_1 t + V_2 a_1 \cos \omega_2 t + \frac{3}{4} V_1^3 a_3 \cos \omega_1 t + \frac{3}{4} V_2^3 a_3 \cos \omega_2 t \\
& + \frac{1}{4} V_1^3 a_3 \cos 3\omega_1 t + \frac{5}{8} V_1^5 a_5 \cos \omega_1 t + \frac{1}{4} V_2^3 a_3 \cos 3\omega_2 t + \frac{5}{8} V_2^5 a_5 \cos \omega_2 t \\
& + \frac{5}{16} V_1^5 a_5 \cos 3\omega_1 t + \frac{1}{16} V_1^5 a_5 \cos 5\omega_1 t + \frac{5}{16} V_2^5 a_5 \cos 3\omega_2 t \\
& + \frac{1}{16} V_2^5 a_5 \cos 5\omega_2 t + \frac{3}{2} V_1 V_2^2 a_3 \cos \omega_1 t \\
& + \frac{3}{2} V_1^2 V_2 a_3 \cos \omega_2 t + \frac{15}{8} V_1 V_2^4 a_5 \cos \omega_1 t + \frac{15}{8} V_1^4 V_2 a_5 \cos \omega_2 t \\
& + \frac{3}{4} V_1 V_2^2 a_3 \cos (\omega_1 t - 2\omega_2 t) + \frac{3}{4} V_1 V_2^2 a_3 \cos (\omega_1 t + 2\omega_2 t) \\
& + \frac{3}{4} V_1^2 V_2 a_3 \cos (2\omega_1 t + \omega_2 t) + \frac{3}{4} V_1^2 V_2 a_3 \cos (2\omega_1 t - \omega_2 t) \\
& + \frac{5}{4} V_1 V_2^4 a_5 \cos (\omega_1 t - 2\omega_2 t) + \frac{5}{4} V_1 V_2^4 a_5 \cos (\omega_1 t + 2\omega_2 t) \\
& + \frac{5}{4} V_1^4 V_2 a_5 \cos (2\omega_1 t + \omega_2 t) + \frac{5}{4} V_1^4 V_2 a_5 \cos (2\omega_1 t - \omega_2 t) \\
& + \frac{5}{16} V_1 V_2^4 a_5 \cos (\omega_1 t - 4\omega_2 t) + \frac{5}{16} V_1 V_2^4 a_5 \cos (\omega_1 t + 4\omega_2 t) \\
& + \frac{5}{16} V_1^4 V_2 a_5 \cos (4\omega_1 t + \omega_2 t) + \frac{5}{16} V_1^4 V_2 a_5 \cos (4\omega_1 t - \omega_2 t) \\
& + \frac{15}{4} V_1^3 V_2^2 a_5 \cos \omega_1 t + \frac{15}{4} V_1^2 V_2^3 a_5 \cos \omega_2 t + \frac{5}{4} V_1^3 V_2^2 a_5 \cos 3\omega_1 t \\
& + \frac{5}{4} V_1^2 V_2^3 a_5 \cos 3\omega_2 t + \frac{15}{8} V_1^2 V_2^3 a_5 \cos (2\omega_1 t + \omega_2 t) \\
& + \frac{15}{8} V_1^3 V_2^2 a_5 \cos (\omega_1 t - 2\omega_2 t) + \frac{15}{8} V_1^3 V_2^2 a_5 \cos (\omega_1 t + 2\omega_2 t) \\
& + \frac{15}{8} V_1^2 V_2^3 a_5 \cos (2\omega_1 t - \omega_2 t) + \frac{5}{8} V_1^2 V_2^3 a_5 \cos (2\omega_1 t - 3\omega_2 t) \\
& + \frac{5}{8} V_1^2 V_2^3 a_5 \cos (2\omega_1 t + 3\omega_2 t) + \frac{5}{8} V_1^3 V_2^2 a_5 \cos (3\omega_1 t - 2\omega_2 t) \\
& + \frac{5}{8} V_1^3 V_2^2 a_5 \cos (3\omega_1 t + 2\omega_2 t)
\end{aligned} \tag{2.23a}$$

$$\begin{aligned}
V_o(t) = & V_{FUNDL} \cdot \cos(\omega_1 t) + V_{FUNDU} \cdot \cos(\omega_2 t) + V_{IMDL} \cdot \cos(2\omega_1 t - \omega_2 t) \\
& + V_{IMDU} \cdot \cos(2\omega_2 t - \omega_1 t) + V_{2HL} \cdot \cos(2\omega_1 t) + V_{2HU} \cdot \cos(2\omega_2 t) + \dots
\end{aligned} \tag{2.23b}$$

Passband model works on the signal having high frequency components, so magnitude and phase of frequency components are measured to extract model coefficients. Working with phasor domain is easier than working with time domain for passband modeling because time domain measurement is much more difficult for the signal having both high and low frequency component. At this point, new phasor domain definition is needed since phasor domain is defined on one-frequency but there are more than one frequency components in (2.23a). In order to overcome this problem each components are represented in phasor domain w.r.t. its

own frequency. In other words,  $V_{FUNDL}$  is represented in phasor domain w.r.t.  $\omega_1$  radian frequency and  $V_{IMDL}$  is represented in phasor domain w.r.t.  $2\omega_1 - \omega_2$  radian frequency. Phase of FUNDL component is defined w.r.t.  $\omega_1$  frequency and phase of FUNDU component is defined w.r.t.  $\omega_2$  frequency. Hence, phase representation of "1 nsec time delay" is different for both FUNDL and FUNDU. Considering this definition, phasor domain representation of IMDL, IMDU, FUNDL and FUNDU components are as given in (2.24).

$$V_{IMDL} = \frac{3}{4}a_3V_1^2V_2 + a_5\left(\frac{5}{4}V_1^4V_2 + \frac{15}{8}V_1^2V_2^3\right) \quad (2.24a)$$

$$V_{IMDU} = \frac{3}{4}a_3V_1V_2^2 + a_5\left(\frac{5}{4}V_1V_2^4 + \frac{15}{8}V_1^3V_2^2\right) \quad (2.24b)$$

$$V_{FUNDL} = a_1V_1 + a_3\left(\frac{3}{4}V_1^3 + \frac{3}{2}V_1V_2^2\right) + a_5\left(\frac{5}{8}V_1^5 + \frac{15}{8}V_1V_2^4 + \frac{15}{4}V_1^3V_2^2\right) \quad (2.24c)$$

$$V_{FUNDU} = a_1V_2 + a_3\left(\frac{3}{4}V_2^3 + \frac{3}{2}V_1^2V_2\right) + a_5\left(\frac{5}{8}V_2^5 + \frac{15}{8}V_1^4V_2 + \frac{15}{4}V_1^2V_2^3\right) \quad (2.24d)$$

If equal amplitude excitation is assumed,  $V_1 = V_2$ , IMD components will be of equal amplitude,  $V_{IMDL} = V_{IMDU}$ . This means that there is no asymmetry in the IMD expression, (2.24a) and (2.24b). However, as demonstrated in Figure 2.10b and Figure 2.11b at page 15, there is an inherent asymmetrical distribution of IMD components. This is the disadvantage of this modeling technique.

In order to extract the coefficients, magnitude of IMD and FUND components are measured and then measurement values and (2.24) is equated.

## 2.5.2 Nonlinear Modeling with Memory

### 2.5.2.1 Volterra Series

Volterra Series Method for behavioral modeling is one of the oldest techniques for nonlinear circuit analysis. Vito Volterra reported this technique in 1959 in "Theory of Functionals and of Integro-Differential Equations" [19]. Then Wiener stated that this technique could be applied to the time invariant nonlinear circuit. Volterra Series modeling mathematical representation

in the passband is as follows :

$$\begin{aligned}
y(t) &= \sum_{n=1}^{\infty} y_n(t) \\
y_n(t) &= \int_{-\infty}^{\infty} h_1(t - \tau_1) V_i(\tau_1) d\tau_1 \\
&+ \int_{-\infty}^{\infty} \int_{-\infty}^{\infty} h_2(t - \tau_1, t - \tau_2) x_i(\tau_1) x_i(\tau_2) d\tau_1 d\tau_2 \\
&+ \int_{-\infty}^{\infty} \int_{-\infty}^{\infty} \int_{-\infty}^{\infty} h_3(t - \tau_1, t - \tau_2, t - \tau_3) x_i(\tau_1) x_i(\tau_2) x_i(\tau_3) d\tau_1 d\tau_2 d\tau_3 + \dots \\
&= \int_{-\infty}^{\infty} \dots \int_{-\infty}^{\infty} \int_{-\infty}^{\infty} h_n(\tau_1, \dots, \tau_n) \prod_{p=1}^n x(t - \tau_p) d\tau_p
\end{aligned} \tag{2.25}$$

where x and y represents time domain input and output signal,  $h_1(t - \tau_1)$ ,  $h_2(t - \tau_1, t - \tau_2)$  are called the  $n^{th}$  order Volterra Kernel or  $n^{th}$  order impulse response.

Maas *et al.* [20] used Volterra series to examine analytically intermodulation distortion of heterojunction bipolar transistors. Nonlinear currents are used to explain the reason of intermodulation distortion. Nonlinear currents are represented by Volterra series. In order to investigate cascading effect on intermodulation distortion, Volterra series is used again [21]. Volterra series can be used for cascaded systems to estimate IMD as long as amplifier is working in weakly nonlinear regime. Carvalho *et al.* [22] used Volterra series modeling technique to estimate third order IMD and explain asymmetry. Carvalho represented power amplifier model in mildly nonlinear behavior with a circuit having voltage dependent nonlinear resistor and capacitance as well as linear components. Volterra kernels can only be found by making specific measurements for each of them separately. When model order increase, measurement of Volterra kernel is getting more difficult. Therefore, Carvalho limited his work with third order IMD. Roy *et al.* [23] tried to develop a iterative technique to overcome this measurement requirement. He developed a method but, unfortunately the method was prone to measurement noise.

Boyd *et al.* [24] proposed a number of procedures to measure kernels directly from frequency measurement. But he has to limit his work in weakly nonlinear regime with third order. Evans *et al.* [25] proposed an improved method. They designed input signals to measure Volterra kernels in a short time period but they encountered practical problems to test it on nonlinear systems.

Wang *et al.* [26] defined nonlinear s-parameter based Volterra series. Nonlinear gain is es-

timated successfully for wide frequency band for weakly nonlinear regime, but there is not enough information about IMD asymmetry estimation performance. Verbeyst *et al.* [27] used Volterra series to estimate load impedance curve related to output power or gain of amplifier.

Maqusi [28] tried to characterize nonlinear distortion in cable television system. He simplified the Volterra Series in order to diminish the number of kernels to be find by measurement. Maqusi's simplified version is as given in (2.26). He reported that, when the Volterra series is simplified, model estimation accuracy is diminished too.

To sum up, "The Volterra series analysis is well suited to the simulation of nonlinear microwave devices and circuits, in particular in the weakly and mildly nonlinear regime." [29]. Volterra series has two main disadvantages; it works well in weakly or mildly nonlinear regime and Volterra kernels could be find by making special measurements.

$$y(t) = \sum_{n=1}^{\infty} y_n(t) \quad (2.26a)$$

$$y_n(t) = \int_0^{\infty} h_n(\tau) x^n(t - \tau) d\tau \quad (2.26b)$$

### 2.5.2.2 Wiener, Hammerstein and Wiener-Hammerstein Models

Wiener and Hammerstein modeling techniques can be used to represent nonlinear IMD since they can create asymmetry. Both models have one memoryless nonlinear function and one dynamic linear function. Nevertheless, another modeling technique is also reported namely Wiener-Hammerstein (3-box Modeling) which is composed of by merging the Wiener and the Hammerstein method. Block diagrams of Wiener, Hammerstein and Wiener-Hammerstein are as given in Figure 2.12. In these block diagrams  $f(\bullet)$  represents memoryless power series (static nonlinear function),  $H(S)$  and  $K(S)$  represent linear filters. Hence memory effect is defined frequency dependent, it can be modeled with linear filter.

Static nonlinear box describes the AM/AM and AM/PM nonlinear behavior at the center frequency of excitation signal. The linear filters,  $H(S)$  and  $K(S)$ , describe the frequency dependent deviations at the AM/AM and AM/PM behavior w.r.t. AM/AM and AM/PM behavior described at center frequency. Mathematical representation of static nonlinear function is as follows:

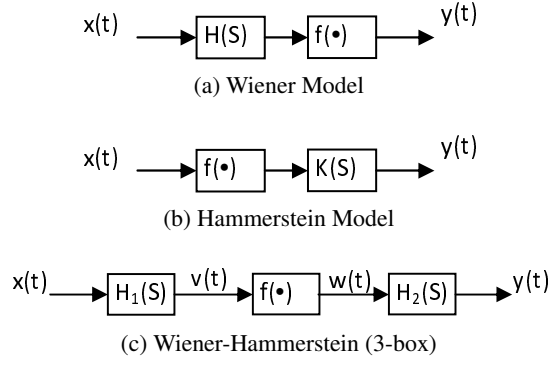


Figure 2.12: Block diagram of a) Wiener, b) Hammerstein and c) Wiener-Hammerstein Models

$$w(t) = \sum_{k=1}^n a_k v^k(t) \quad (2.27)$$

In order to represent AM/PM nonlinear behavior as well as AM/AM behavior  $a_k$  coefficients given in (2.27) are chosen as complex numbers as stated in section 2.5.1 on page 19. Input excitation signal at center frequency can be represented as given in (2.28a) in time domain and as given in (2.28b) in phasor domain.

$$x_c(t) = A \cos(2\pi f_c t + \theta) \quad (2.28a)$$

$$\hat{x}_c = A e^{j\theta} \quad (2.28b)$$

where  $A$  represents the maximum amplitude value of signal,  $f_c$  represents center frequency,  $\hat{x}_c$  represent phasor representation of  $x_c$ , and  $\theta$  represents the phase w.r.t  $t=0$ . Corresponding output mathematical representation is as follows:

$$\begin{aligned} \hat{y}_c &= \sum_{k=0}^{(n-1)/2} a_{2k+1} |H_1(f_c) \hat{x}_c|^{2k} H_1(f_c) H_2(f_c) \hat{x}_c \\ &= \sum_{k=0}^{(n-1)/2} a_{2k+1} A^{2k+1} e^{j\theta} \end{aligned} \quad (2.29)$$

where  $a_{2k+1}$  represents model coefficients. Although, filters are normalized to center frequency,  $H_1(f_c) = 1$  and  $H_2(f_c) = 1$ , value of filters are not equal to one for other frequencies.

For example, when excitation signal at  $f_1$  frequency, output signal is as given in (2.30).

$$\hat{y}_c = \sum_{k=0}^{(n-1)/2} a_{2k+1} |H_1(f_1) A e^{j\theta}|^{2k} |H_2(f_1)| e^{j(\theta_{H_1(f_1)} + \theta_{H_2(f_1)})} \quad (2.30)$$

where  $A e^{j\theta} = \hat{x}_1$ ,  $\theta_{H_1(f_1)}$  and  $\theta_{H_2(f_1)}$  represents the phase response of linear filter  $H_1$  and  $H_2$  respectively.

Since the static nonlinear function represents AM/AM and AM/PM behavior memoryless modeling explained in section 2.5.1, model coefficient extraction procedure is very similar. Memoryless function coefficients are extracted for center frequency excitation. Linear filters are extracted by using numerical fitting. Linear filters are described as given in (2.31).

$$H_1(f) = \frac{H_{ss}(f)}{|H_{sat}(f)|} \quad (2.31a)$$

$$H_2(f) = |H_{sat}(f)| e^{(\phi - \angle H_{ss}(f))} \quad (2.31b)$$

where  $\phi$  is equal to  $(\theta_{H_1(f)} + \theta_{H_2(f)})$ ,  $H_{ss}(f)$  and  $H_{sat}(f)$  represent small-signal response and saturation response of PA and these responses are measured over the interested frequency band in linear region and at the  $P_{1dB}$  point, respectively with using network analyzer.

Hammerstein method is used in [30] and in [31] with baseband signal. [31] used an iterative method to find model coefficients. Greblecki [32] and Billings *et al.* [33] used Wiener modeling to characterize amplifier with baseband signal.

3-box modeling technique is used with both baseband signal and passband signal. Bai [34] used 3-box modeling to get model of nonlinear behavior of amplifier with baseband signal. Model coefficients are found in two steps. The first one is the least square algorithm and the other one is the singular value decomposition. A matrix is composed at the first step and then it is solved at the second step to find coefficients values. Crama *et al.* [35] used the 3-box modeling with passband signal.

Sano *et al.* [36] and Taringou *et al.* [37] used 3-box modeling in baseband predistorter. Sano found coefficient with iterative technique.

Ghannouchi *et al.* [38] used a model which is a bit different than 3-box modeling. He connected both models in parallel instead of merging them. So, this new model has 4 boxes as

given in Figure 2.13. In this figure, Hammerstein modeling placed at upper branch and wiener modeling placed at lower branch. The number of coefficients are increased with this new modeling and model performance improved by 3dB.

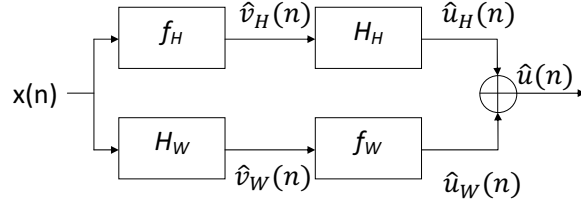


Figure 2.13: Dual Branch Wiener-Hammerstein model Structure

To sum up, disadvantages are resulted mainly from dynamic linear filters' limitations. Dynamic filters used for asymmetry creation are designed according to one-tone measurement results. So, filter behavior doesn't have flexibility to adopt frequency changes. Moreover, since filters are designed according to passband one-tone measurement result, long term memory effect can not be modeled with this technique. There is a small frequency separation relative to the working frequency between IMDL and IMDU. So, in order to create so much asymmetry between magnitude of IMDL and IMDU, filter order should be high.

### 2.5.2.3 Parallel Wiener Model

Ku *et al.* [39] proposed a new modeling namely "Parallel Wiener Modeling" in order to capture long time memory effect as well as short time memory effect. The model is an improved version of the Wiener modeling. Block diagram of Parallel Wiener Model is as given in Figure 2.14. In this diagram,  $F_i(\bullet)$  is a complex-valued polynomial function and  $H_i(\omega)$  is a linear filter same as in Wiener modeling.

The first branch line is chosen as a memoryless model, so  $H_1(\omega)$  is chosen as in time domain  $h_1(t) = \delta(t)$ . Coefficient of  $F_1(\bullet)$  is extracted from AM/AM and AM/PM responses to the one tone excitation. The other linear filters  $H_i(\omega_m)$ , ( $i = 2, \dots, p$ ) are extracted using the cross-correlation function of the input called  $r(t)$  and the error function  $\varepsilon_{i-1}$ .  $r(t)$  is defined as the envelope of the two-tone input signal as given in (2.32) and  $\varepsilon_{i-1}$  is defined as the difference

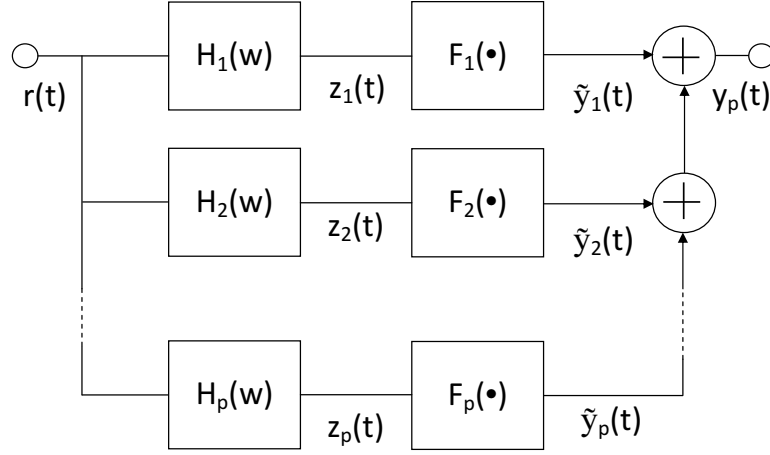


Figure 2.14: Block diagram of Parallel Wiener Model

between the output of the  $i^{th}$  nonlinear branch ( $\tilde{y}_i(t)$ ) and frequency-dependent complex power series  $F(r, \omega_m)$  as given in (2.34). Coefficients of  $F_i(\bullet)$  are chosen such that mean square error,  $\varepsilon_i^2$ , is minimized. New branches are added until the value of  $\varepsilon_i^2$  become less than a predefined threshold.

it is reported by the author that this modeling technique is also used in DPD. Better than 10dB improvement is seen in the ACPR for low power amplifier, but due to more memory effect the DPD performance for high power amplifier is worse.

$$r(t) = A \cos \omega_m(t) \quad (2.32)$$

$$\begin{aligned} y_p(t) &= \sum_{i=1}^p \tilde{y}_i(t) \\ &= \sum_{i=1}^p F_i(z_i(t)) \\ &= \sum_{i=1}^p \sum_{k=1}^n a_{2k-1,i} (A|H_i(\omega_m)| \cos(\omega_m t + \Omega_i(\omega_m)))^{2k-1} \end{aligned} \quad (2.33)$$

$$\begin{aligned} \varepsilon_i &= F(r(t), \omega_m) - \tilde{y}_i(t) \\ &= F(r(t), \omega_m) - \sum_{s=1}^i \tilde{y}_s(t), \quad i = 1, \dots, p. \end{aligned} \quad (2.34)$$

#### 2.5.2.4 Multi-Slice Behavioral Modeling

Walker *et al.* [10] give a new modeling technique named as Multi-Slice Behavioral Modeling based on Wiener-Hammerstein Modeling. Structure of the proposed model for two-slice is as given in Figure 2.15. In this model, each slice is added to represent a specific amplifier behavior. "The first slice captures single-nonlinearity effects present in the system under investigation which can include both even and odd-ordered effects. Additional slices capture nonlinearities in series such as even-order baseband upconversion, thermal effects, or other memory effects" [10] on page 72. This means that each slice has a memoryless nonlinear function and linear filters for specific frequency band similar to Wiener-Hammerstein Model. So, this structure can be named as a modified Wiener-Hammerstein model.  $f(\bullet)$  is odd-ordered polynomial function which represents memoryless nonlinearity and  $g(\bullet)$  is even-order polynomial function which represents memoryless nonlinearity.  $H(s)$  and  $K(s)$  is pre and post-linear networks respectively.  $H(s)$  and  $K(s)$  should capture memory effects since  $f(\bullet)$  and  $g(\bullet)$  not have memory effects.

This modeling technique requires the following measurement:

- One-tone AM/AM and AM/PM behavior, frequency is swept over band of interest.
- Magnitude and phase of IMD for constant frequency separation, while two-tone power level is sweeping.
- Magnitude and phase of IMD for constant frequency separation, while two-tone power level is sweeping.

Parameter extraction is performed after making an assumption that, contributors are independent for different slices. Therefore, at first, first slice parameters are extracted by using one-tone measurement result. Then, second slice parameters are extracted by using two-tone measurement result. Disadvantages of this modeling is the too much measurement results requirement.

Jang *et al.* [12] tried to simplify the "Multi-Slice Behavioral Model". Structure of simplified version of Multi-Slice modeling is as given in Figure 2.16. Dynamic linear filters are omitted from the first slice, and model performance is deteriorated. It is required to increase model order to the 17<sup>th</sup> even for one-tone AM/AM and AMP/PM modeling, while dynamic range for

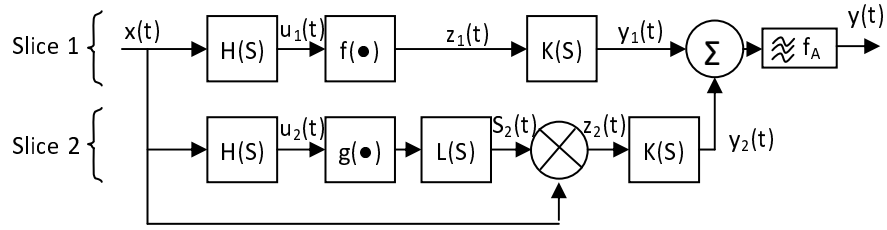


Figure 2.15: A two-slice nonlinear system behavioral model

AM/AM is approximately  $14dB$  and total phase change is approximately  $1.5^\circ$ . First slice is used to estimate odd-order fundamental response, so the nonlinear block in the first slice,  $NL_1$ , was extracted from single tone AM-AM and AM-PM characteristics at the center frequency. The second slice is used to represent baseband memory effect which result in asymmetric spectral regrowth. Coefficients of even-order polynomial,  $NL_2$ , are found by using same procedure applied to  $NL_1$ , but this time two-tone excitation measurement results are used.

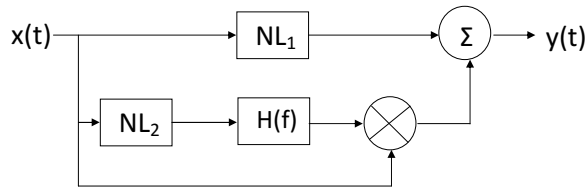


Figure 2.16: Modified Multi-Slice Behavioral Modeling

### 2.5.2.5 Memory Polynomial Models

Memory Polynomial Model (MPM) consists of delay taps and a nonlinear static function which is similar to GPSE. There are two different MPM models in literature w.r.t. delay types; MPM with unit delay and MPM with sparse delay. Block model representation for these two modeling types are as given in Figure 2.17 and Figure 2.18. These models are developed by truncating the Volterra Modeling. Both models are defined on passband.

Unit delay considers only diagonal element of Volterra Series, and thus the number of coefficients used in modeling is reduced [40], [41]. Ding *et al.* [40] reported that the advantage of memory polynomial is keeping the number of coefficient on the order of  $M \times K$ . However it was  $M^K$  for Volterra Series.

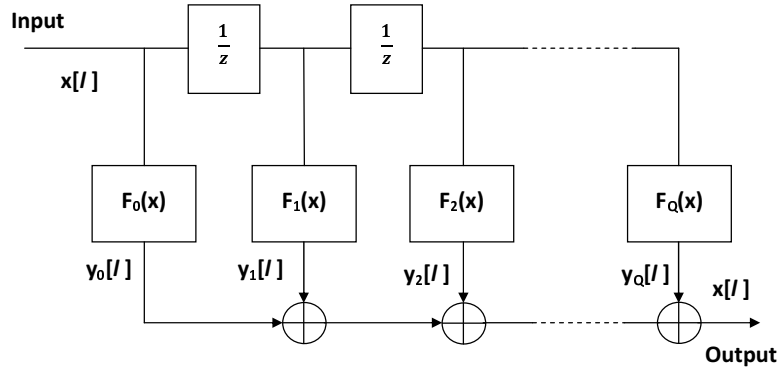


Figure 2.17: Structure of Memory Polynomial Model with unit delay

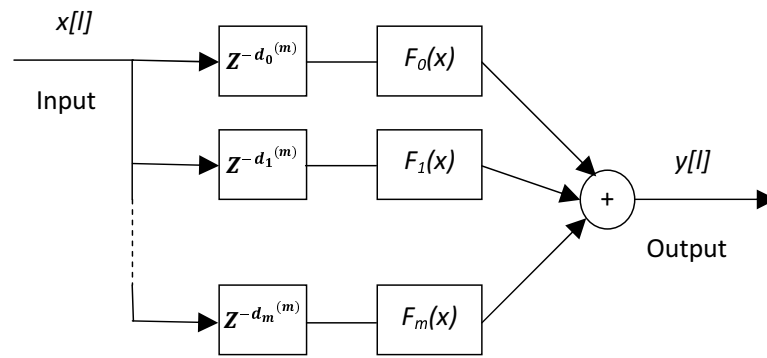


Figure 2.18: Structure of Memory Polynomial Model with sparse delay

Mathematical representation of MPM with unit delay is as follows:

$$y[n] = \sum_{q=0}^{M-1} \sum_{k=1}^K a_{k,q} |x[n-q]|^{k-1} \cdot x[n-q] \quad (2.35)$$

where  $x[n]$  and  $y[n]$  represents discrete input and output complex baseband signal respectively,  $a_{k,q}$  represents the complex-valued polynomial coefficients,  $K$  represent the polynomial function order, and  $M$  represents the memory depth (the number of delay taps). Maximum delay value which will be applied to the input signal is equal to the number which is one less than the number of delay taps. If the number of delay taps is chosen as 5, total number of unknown coefficients will be  $5 \times K$ . So, it is almost impossible to get model of long time memory effect.

Hence memory delay value is known for the model, extraction of model consists of finding the values of  $a_{k,q}$  coefficients.  $a_{k,q}$  values can be found by following the procedure given below

for MPM model with unit delay. As a first step, (2.35) is rewritten in matrix form as given in (2.36).

$$\vec{y} = \vec{a} \times \vec{x} \quad (2.36)$$

where  $\vec{y}$ ,  $\vec{a}$  and  $\vec{x}$  are defined as follows:

- $\vec{y} = [y(1) \ \cdots \ y(N)]^T$ , N is the number of samples
- $\vec{a} = [a_{1,0} \ a_{2,0} \ \cdots \ a_{K,0} \ \cdots \ a_{K,M-1}]$

$$\bullet \ \vec{x} = \begin{pmatrix} B_{1,0}(1) & \cdots & B_{1,0}(N) \\ B_{2,0}(1) & \cdots & B_{2,0}(N) \\ \vdots & \ddots & \vdots \\ B_{K,0}(1) & \cdots & B_{K,0}(N) \\ \vdots & \ddots & \vdots \\ B_{K,M-1}(1) & \cdots & B_{K,M-1}(N) \end{pmatrix}$$

where  $B_{K,M-1}(N) = |x(N - (M - 1))|^{K-1} \cdot x(N - (M - 1))$

After calculating  $\vec{y}$  and  $\vec{x}$  matrices, model coefficients can be calculated by using (2.37).

$$\vec{a} = \vec{y} \times \text{pinv}(\vec{x}) \quad (2.37)$$

where  $\text{pinv}(\vec{x})$  is pseudo inverse of  $\vec{x}$ .

Zhou *et al.* [42] used memory polynomial with sparse delay technique in DPD circuit. Coefficients are extracted by using adaptive RLS algorithm.

Mathematical representation of MPM with sparse delay is as follows:

$$y[n] = \sum_{q=0}^{M-1} \sum_{k=1}^K a_{k,q} |x[n - d_q^{(M)}]|^{k-1} \cdot x[n - d_q^{(M)}] \quad (2.38)$$

where  $d_q^{(M)}$  is the sparse delay values for the M branches. Coefficient extraction algorithm is similar to MPM model with unit delay. Moreover, this time sparse delay value should be found as well. To do this, the definition of  $B_{k,q}$  used in  $\vec{x}$  is updated as given in (2.39).  $d_q^{(M)}$  is

chosen as a random number and then model estimation error is calculated by using the metric MEMR suggested by Ku *et al.* [43]. If MEMR value is better than a predefined threshold, the delay value is stored.

$$B_{k,q}(N) = \left| x(N - d_q^{(M)}) \right|^{K-1} \cdot x(N - d_q^{(M)}) \quad (2.39)$$

Nan *et al.* [44] used memory polynomial modeling with sparse delay technique in DPD circuit. He reported that sparse delay gives better result than unit delay.

Since this modeling has gained ability to have higher delay value, this model can be represent long term memory. However, thermal memory is mostly effected by the first order or may be the third order depending on amplifier die and physical size. So, time delay value of the first order and the third order shouldn't be equal for good model performance. But, it is impossible to apply unequal time delay with this modeling.

## 2.6 Summary

Amplifier nonlinear behavior representation is an intriguing area for the system designer. Since the behavior is not linear, special techniques are required to investigate and predict the effects of an amplifier within a complex system. One of the properties of an amplifier to be considered is its memory effect. Memory effect types and sources of them are explained. There are a number of techniques in literature and the frequently used ones are outlined in this chapter. Besides the advantages, disadvantages are summarized. Some of disadvantages are related with the working frequency band (baseband or passband) and some of them are related with the modeling structure (special measurement requirement for the each parameter extraction, unable to model one of the memory effect types or application problem for real system).

## CHAPTER 3

### Measurement Setup and Measurement Results

#### 3.1 Introduction

Amplifier characterization is an important issue especially in the design of amplifiers and systems involving amplifiers such as linearizers and wireless communication systems. Behavioral modeling is one of the characterization techniques where a mathematical relation between input and output is constructed. There are a number of behavioral modeling techniques published in the literature. First step of modeling is the measurement of the magnitudes and phases of the signals at the input and the output of the amplifier. When an amplifier is excited with a one-tone signal or a multi-tone signal, AM/AM and AM/PM distortion at the output. When an amplifier is excited with a multi-tone signal, inter-modulation distortion (IMD) components are observed at the output of the amplifier as well. Magnitudes and phases of these signals are needed to extract an accurate model. Several measurement setups [45] - [49] are proposed to measure these quantities.

In this chapter, a new measurement technique is introduced which is used to measure both the magnitudes and the phases of signals generated by the amplifier. The measurement setup given in Figure 3.1 is prepared to measure AM/AM, AM/PM distortion, magnitudes and phases of intermodulation (IMD) and fundamental (FUND) components which are created by the amplifier. Indeed this measurement setup can be used for general phase measurement purposes. However, before starting measurement, input dynamic range, working frequency and frequency separation for phase measurement for multi-tone and maximum excitation power level should be investigated carefully. There is some limitation for the measurement setup such as AWSG sensitivity limits the maximum frequency separation for in-phase four-tone

generation. Phase measurement setup has been constructed to calculate/measure phase difference by measuring only magnitudes. An equation is derived based on complex number addition to calculate phase difference.

### 3.2 Measurement Setup

Measurement setup as given in Figure 3.1 is prepared to measure both magnitude and phase of one-tone and two-tone signals, because those measurement results are needed to get behavioral model of the power amplifier. In order to measure AM/AM response for one-tone, one signal generator(E8257C, "SGA") and one spectrum analyzer(E4408A, "SA") is added to the measurement setup and to measure AM/AM response for two-tone, one more signal generator (E8257D, "SGB") is added. There are two signal generators at the measurement setup since each signal generator has one-tone generation ability and one power combiner is added to the measurement setup to create two-tone signal in order to combine the signal generated by "SGA" and "SGB". Power level of the signal created at the output of amplifier is decreased by adding attenuator for SA safety. Value of attenuation is given as an example, actual attenuation amount is determined by measurements.

In order to measure phase, one more signal generator (E8267D, "SGC") for phase reference, digital attenuator (Hittite HMC472LP4) for wider dynamic range and one more power combiner are added to the measurement setup. The 10MHz reference signal generated by "SGC" is transferred to others for phase lock. A computer on which "Agilent VEE" program is working is added to the measurement setup and is connected to each instrument via GPIB cables to take data quickly for repetitive measurements.

A sample amplifier has been taken from "ASELSAN A.Ş." under the project titled as "Güç Yükselticinin Davranışsal Modelinin (GÜYDAM) Belirlenmesi". This sample amplifier whose maximum gain is 45.7dB around working frequency, saturation peak power is more than 390W (56dBm) and output  $P_{1dB}$  is 53.35dBm, is examined in this dissertation. The amplifier is composed of more than one stage (driver and main amplifier) and has push-pull output. ASELSAN company preserves the right to keep the other parameters and circuit schematic confidential.

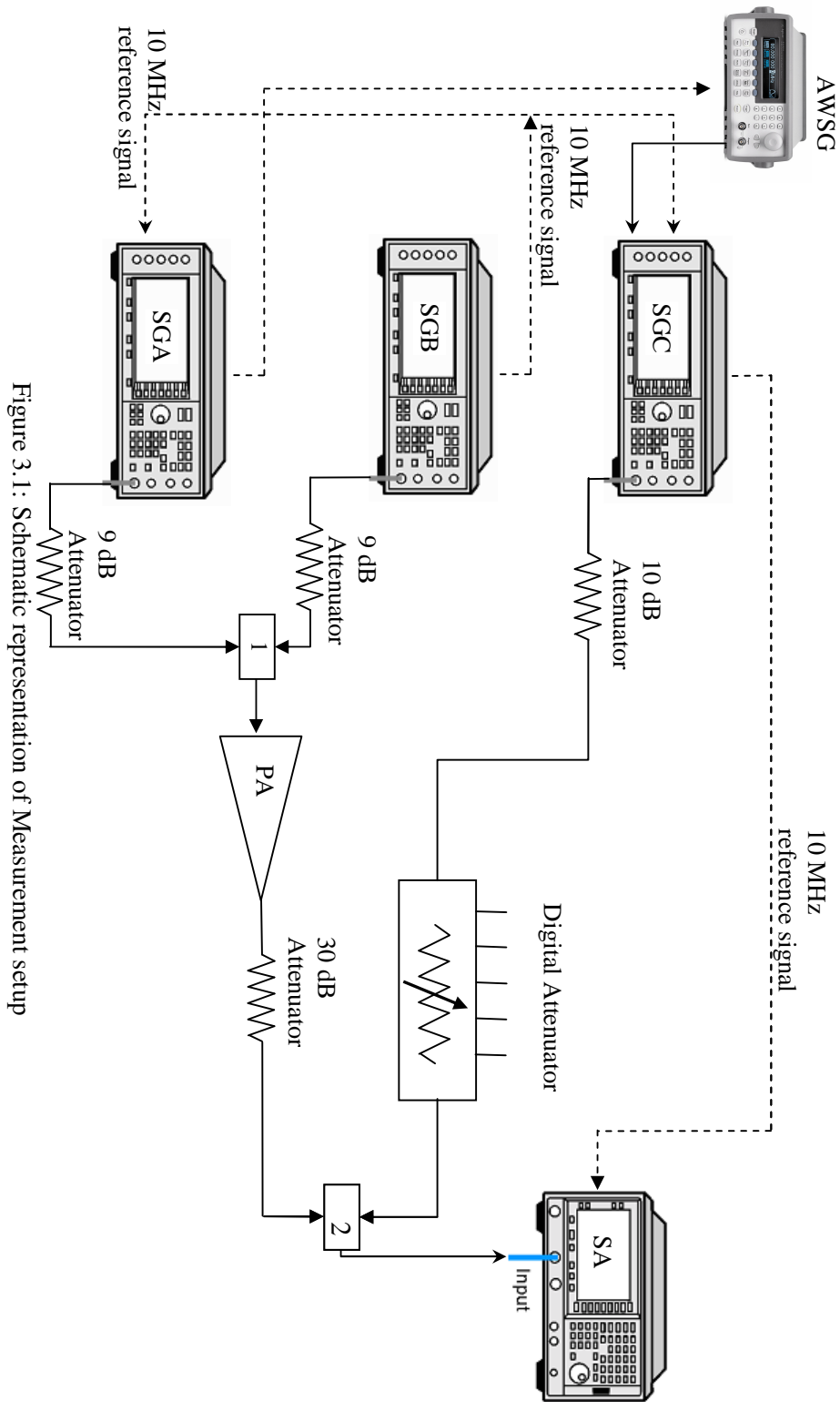


Figure 3. 1: Schematic representation of Measurement setup



Figure 3.2: Photograph of Measurement setup

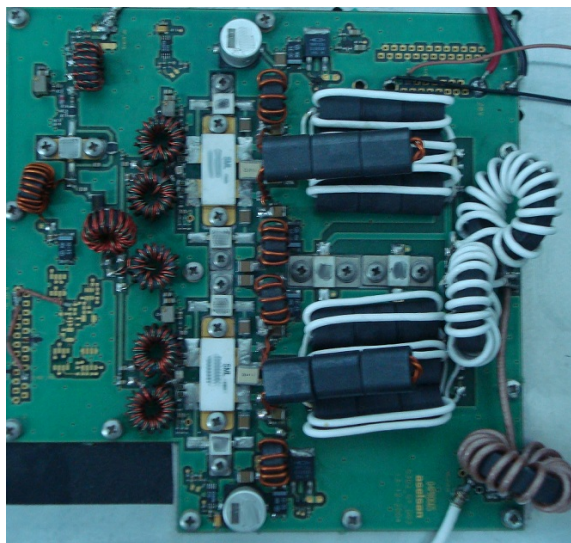


Figure 3.3: Photograph of Amplifier

### 3.3 AM/AM Measurement

One-tone AM/AM measurement procedure is straight forward.

There are some important points to perform reliable two-tone AM/AM measurement. Frequency of "SGA" is set equal to the FUNDL frequency and frequency of "SGB" is set equal to the FUNDU's frequency. After setting the frequency of signal generators, power level of signal generators are adjusted. Since excitation frequencies are known, center frequency of SA is adjusted to the average value of the signal generators' frequencies. Span of SA is adjusted equal to 5 times of frequency separation among fundamental tones. After two sweeps, SA sweep function is stopped, and then four magnitude (IMDL, IMDU, FUNDL and FUNDU) values are measured at the same screen. As a result, measurement error due to SA sweeping and time difference is minimized by measuring all magnitudes at the same sweep screen. Then, just after readout, signal generator output is disabled in order to prevent overwarming the amplifier. At this time, measured values are stored to an excel table and signal generators are adjusted for the next power level measurement.

### 3.4 Phase Measurement

Phase measurement is performed based on complex number addition. The signal at the output of the amplifier is assumed as the first complex number and the signal created by "SGC" is assumed as the second complex number. Then, after measuring the magnitudes of these signal by "SA", output of both signal generators are enabled at the same time and then magnitude of the signal at the output of second combiner is measured. This data gives information about the combined power level. Phase difference between the signal at the output of the amplifier and the "SGC" can be calculated mathematically by using (3.2).

Magnitude of the signal at the output of the amplifier and the magnitude of the signal created by "SGC" are named as  $m_{SG1}$ ,  $m_{SG2}$  and the phases are named as  $\phi_1$ ,  $\phi_2$ , respectively. Then, magnitude of the combined signal is named as  $m_{tot}$  and phase is named as  $\phi_{tot}$ . (3.1) is valid for this measurement setup since the signal at the output of second combiner, namely "2", can be represented with a complex number. Phase difference can be calculated(measured) by measuring only magnitudes of signal with "SA" by using (3.2). Intermediate steps of

derivation from (3.1) to (3.2) are given in Appendix A.

$$m_{SG1}\angle\phi_1 + m_{SG2}\angle\phi_2 = m_{tot}\angle\phi_{tot} \quad (3.1)$$

$$|\phi_1 - \phi_2| = \cos^{-1}\left(\frac{m_{tot}^2 - m_{SG1}^2 - m_{SG2}^2}{2 \cdot m_{SG1} \cdot m_{SG2}}\right) \quad (3.2)$$

Flow chart for one-tone phase difference measurement procedure for a predefined power level is as given in Figure 3.4. It is not expected that, there will be a phase difference among "SGA", "SGB" and "SGC" in a short time since the phases of instruments are fixed w.r.t. each other with the 10MHz reference cable.

A special setup as given in Figure 3.5 is designed to check this phase difference calculation theory. Firstly, phase difference between signal generators (E8257C and E8267D) are set as 180° by following the flow chart given in Figure 3.4. Secondly, phase of second signal generator (E8267D) is increased 1°, then phase difference calculated by using (3.2). Second step is repeated for 360 times and phases are stored as  $\theta_i, i = 1, 2, \dots, 360$ . Third, latter step phase difference is subtracted from the former step phase difference and plotted as given in Figure 3.6 (i.e.  $\theta_i - \theta_{i-1}$ ).

It can be said by considering the results given in Figure 3.6 that, phase difference can be calculated by using this technique successfully. Since "cosine" function is used to calculate phase difference, sign of calculated phase difference should be reversed when the actual phase difference value greater than 180°. In other words, while actual phase is 181°, cosine function gives 179°. Therefore at the beginning, sign of phase difference should be investigate carefully. There is a small error at the phase difference calculation when phase difference is close to 0°. SA noise and calculator digit number (sensitivity) are disturbing the measurement result when phase difference between signal generators is close to 0°. During the phase measurement for 360 steps power level of signal generators are not changed.

The phase calculation theory which is mathematically represented in (3.2) is also checked with the measurement setup in Figure 3.1 while the power level of signal generator are sweeping. Firstly, PA is replaced with the through line and phase difference between "SGA" and "SGC" is adjusted close to 120°. At that time, output power of signal generators are  $-13dBm$ . Power

level of signal generators are increased from  $-13dBm$  to  $13dBm$  with  $1dB$  steps without making any change in the phase of signal generators. After every increment in the magnitude, phase difference is measured. Increment in the magnitude of signal generators and phase measurement process are repeated many times, then results of three cycles are plotted in Figure 3.7.

Power level versus phase difference measurement is performed for "SGB" and "SGC" too. Results of this measurement are given in Figure 3.8.

Although phases of signal generators were not changed during the measurement period, phase differences between signal generators for different power levels changed unexpectedly. This error is different for "SGA" and "SGB" and, the value of change is bigger than the value of acceptable error for real measurement setup. Considering three repeated cycles, it can be said that change in the phase can be recovered by using a Look-Up-Table (LUT). Preparation for LUT for phase recovery is explained in section 3.6 in detail.

### 3.5 AM/PM Measurement

"SGA", "SGC" and "SA" instruments are enough to measure one-tone AM/PM measurement. Phase difference can be calculated by using (3.2). Frequency and power level of "SGA" is adjusted, then amplifier is excited.  $m_{SG1}$  represents the magnitude of the signal created at the output of the amplifier and  $\phi_1$  represents the phase of that signal.  $m_{SG2}$  represents the magnitude of the signal at the output of the digital attenuator.  $m_{tot}$  represents the magnitude of the signal at the input of "SA" when "SGA" and "SGC" output are enabled at the same time. After measuring the  $m_{SG1}$ ,  $m_{SG2}$  and  $m_{tot}$ , we can find " $|\phi_1 - \phi_2|$ " can be calculated by using (3.2). After increasing the power level of excitation signal, new phase difference value can be measured. These phase difference values are relative values w.r.t. the phase difference value measured in the beginning.

Two-tone AM/PM measurement needs one more step since there are more than one tone and it is needed to measure absolute phase difference between IMDL, IMDU, FUNDL and FUNDU. Although phase of signal generators are locked to each other with the  $10MHz$  reference cable, phase reference is lost when the frequency of signal generator is changed. This means that, after finishing the phase measurement for IMDL for the whole power level range, absolute

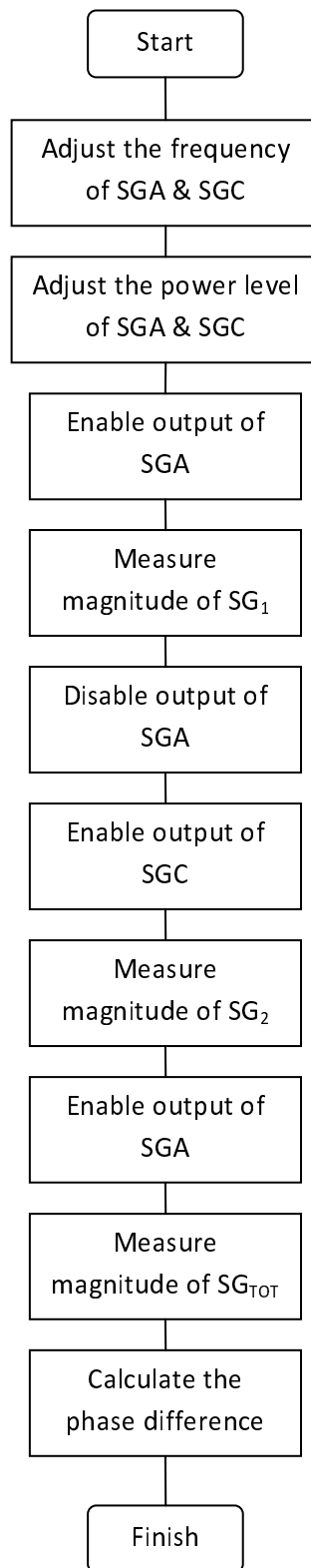


Figure 3.4: Flow chart for one-tone phase difference measurement for a predefined power level

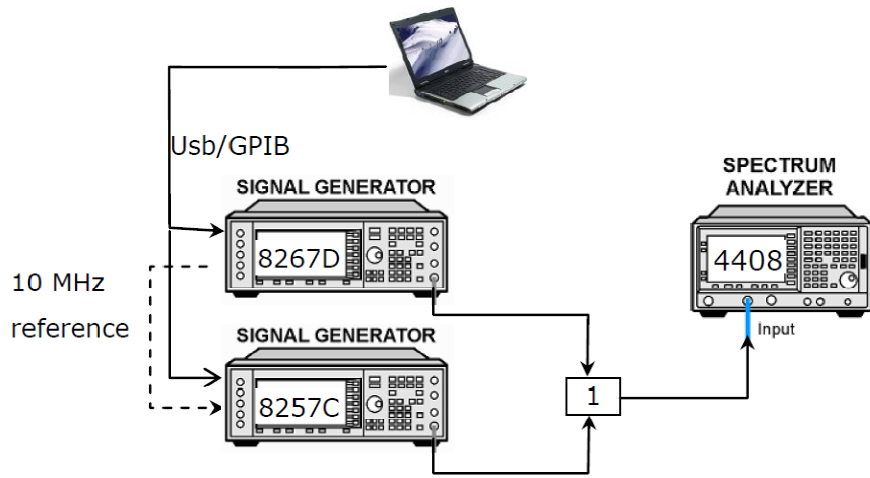


Figure 3.5: Phase measurement technique validation setup

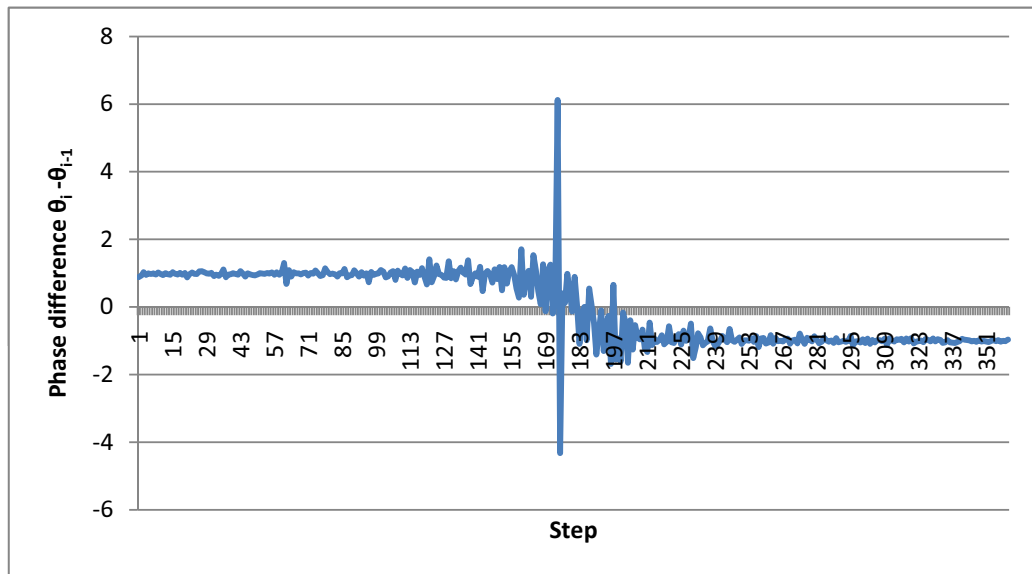


Figure 3.6: Phase difference between former and latter state

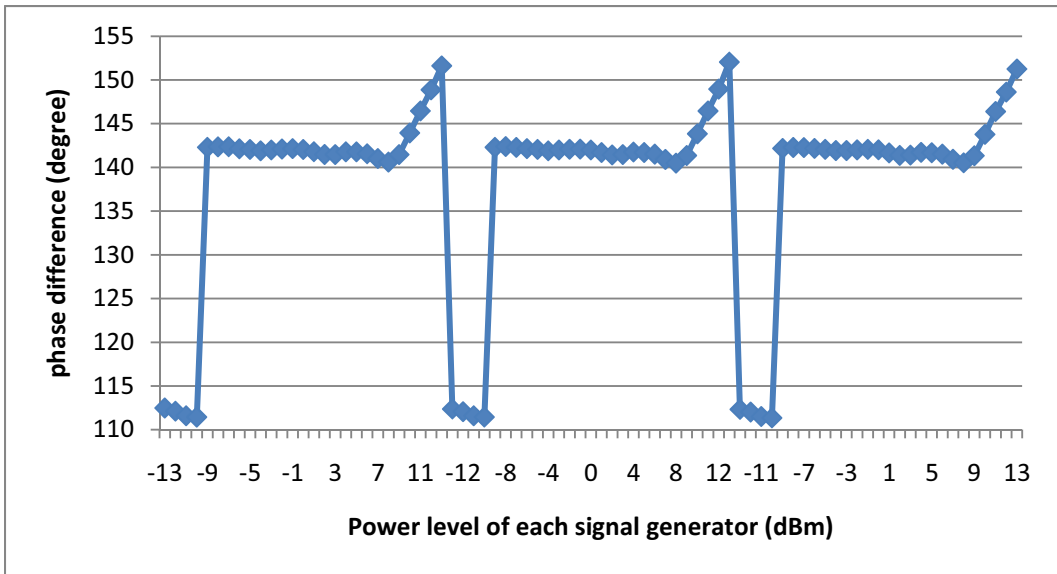


Figure 3.7: Power level vs. phase difference between "SGA" and "SGC"

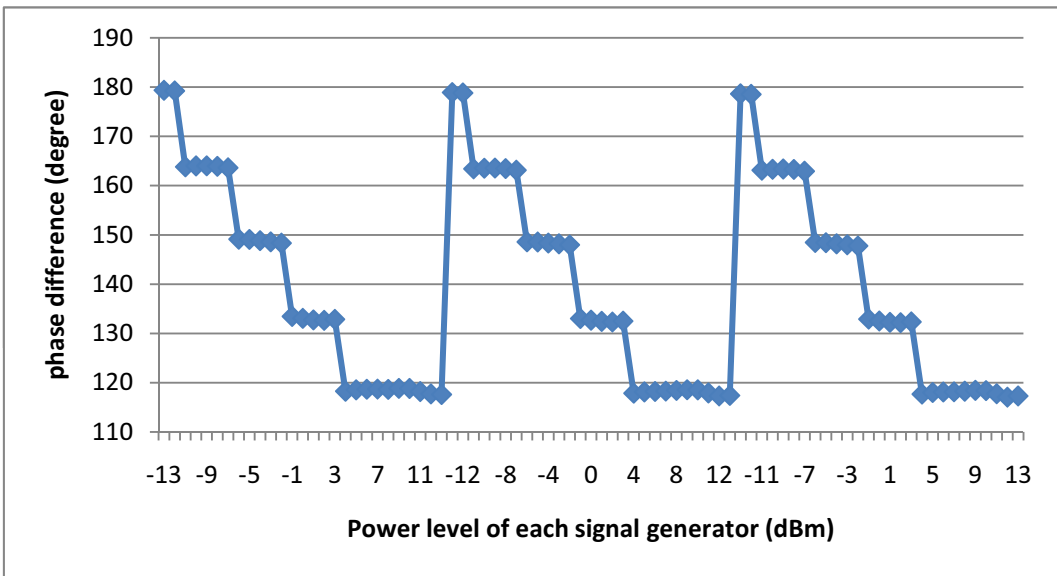


Figure 3.8: Power level vs. phase difference between "SGB" and "SGC"

phase difference for IMDU couldn't be measured since the frequency has been changed. Arbitrary wave shape generator (AWSG 33250) was added to the measurement setup to create four-tone signal having zero phase difference with each other. Firstly, four-tone signal (1Hz, 2Hz, 3Hz and 4Hz) having zero degree phase difference between each other is generated mathematically and is downloaded to the AWSG. The desired four-tone signal having frequency separation (1kHz, 1MHz, ...) can be created by adjusting the repetition frequency of AWSG, specifically, repetition frequency should be equal to the input excitation tone spacing namely  $\Delta f$ . Mathematical representation of AWSG output is as given in (3.3). The baseband four-tone signal created at the output of AWSG is applied to the "I" input of "SGC" I/Q modulator part, eight-tone Double Side Band Suppress Carrier (DSBSC) signal is created at the output of "SGC". Let's assume that phase of the signal created by AWSG is  $\phi_m$  and phase of the signal created by I/Q modulator section local oscillator is  $\phi_c$ . Phase of the tones having greater frequency than  $f_c$  became  $\phi_c + \phi_m$  as represented in Figure 3.9. In other words, there is  $0^\circ$  phase difference among upper four-tone of eight tone created at the output of "SGC" as given in (3.4).

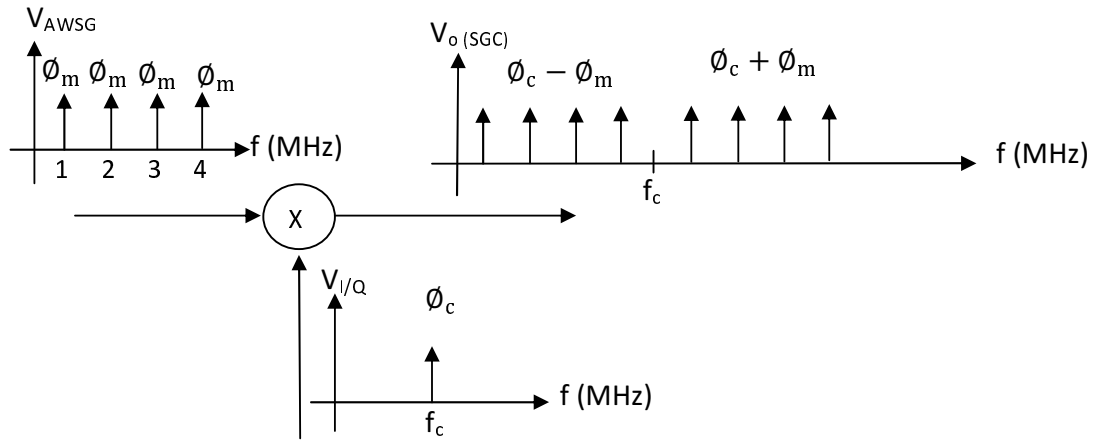


Figure 3.9: in-phase four-tone signal creation

$$\begin{aligned}
 V_{AWSG}(t) = & \cos(2\pi \cdot \Delta f \cdot t + \phi_m) + \cos(2\pi \cdot 2 \cdot \Delta f \cdot t + \phi_m) \\
 & + \cos(2\pi \cdot 3 \cdot \Delta f \cdot t + \phi_m) + \cos(2\pi \cdot 4 \cdot \Delta f \cdot t + \phi_m)
 \end{aligned} \tag{3.3}$$

where  $\Delta f = f_2 - f_1, f_2 > f_1$ .

$$V_{o(SGC)}(t) = \sum_{k=1}^4 \left[ \cos((\omega_c - 2 \cdot \pi \cdot k \cdot \Delta_f) \cdot t + \phi_m - \phi_c) \right] + \sum_{k=1}^4 \left[ \cos((\omega_c + 2 \cdot \pi \cdot k \cdot \Delta_f) \cdot t + \phi_m + \phi_c) \right] \quad (3.4)$$

where  $k = 1, 2, 3, 4$ .

First step of two-tone AM/PM measurement is the extraction of the lookup table (LUT) which is explained in section 3.6 in detail. Flow chart of AM/PM is as given in Figure 3.11. Frequency of "SGA" and "SGB" are adjusted equal to the frequency of FUNDL and FUNDU respectively. Baseband data which is needed for in-phase four-tone signal creation is downloaded to the AWSG and it is started to run. After being sure that eight-tone signal is seen at the screen of "SA", output of "SGC" is disabled. Power levels of "SGA" and "SGB" are set to the maximum level of desired dynamic range. Two-tone signal which is created at the output of the first combiner, "1", is applied to the amplifier. Four-tone signal is created at the output of the amplifier. There is no asymmetry in the magnitude of the eight-tone at the output of "SGC", but there is an asymmetry in the magnitude of the signal created at the output of the amplifier. Thus, phase measurement is performed tone-by-tone. First, phase of IMDL is measured. Center frequency of "SA" is adjusted to the IMDL frequency and span is chosen as equal to the two times frequency separation. Before starting measurement, one more initialization step is needed. In order to measure phase difference more precisely, magnitude of signals ( $m_{SG1}$  and  $m_{SG2}$ ) should be close to each other and phase difference between ( $m_{SG1}$  and  $m_{SG2}$ ) should be close to  $120^\circ$ . If there is  $120^\circ$  phase difference and magnitudes are equal ( $m_{SG1} = m_{SG2}$ ), magnitude of combined signal ( $m_{tot}$ ) will be equal to the  $m_{SG1}$  as shown in Figure 3.10 and as explained mathematically in (3.5). When the initialization process is finished, AM/PM measurement can be performed by following the flow chart given in Figure 3.11.

$$m_{tot} \angle \phi_{tot} = m_{SG1} \angle \phi_1 \text{ and } m_{SG2} \angle \phi_2$$

$$m_{tot} = m_{SG1} \cdot \cos(60) + m_{SG2} \cdot \cos(60) + j(m_{SG1} \cdot \cos(30) - m_{SG2} \cdot \cos(30))$$

$$m_{tot} |_{m_{SG1}=m_{SG2}} = m_{SG1} \quad (3.5)$$

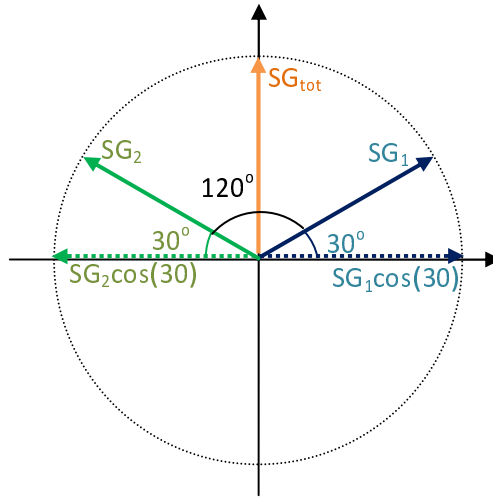


Figure 3.10: Addition for the signals having equal magnitude and  $120^\circ$  phase difference

A LUT is prepared for  $20dB$  dynamic range, then phase of through line and phase of FUNDL tone of another sample amplifier having  $33dB$  gain,  $27dBm$  output  $P_{1dB}$  are measured using this LUT for  $16dB$  and  $20dB$  dynamic range respectively. Measured results are plotted as given in Figure 3.12 and Figure 3.13. When input power change, there shouldn't be any change in the phase of through line theoretically. There was approximately  $15^\circ$  change in the phase of through line as given in Figure 3.7 when the power level of "SGA" and "SGC" are increased from  $-2dBm$  to  $-1dBm$  before phase calibration. Although the same signal generators are used, there is less than  $1^\circ$  change in the phase of through line for  $16dB$  dynamic range and there is a small difference for four repetitive measurement results for the whole dynamic range. There is maximum  $0.53^\circ$  phase difference between repetitive measurements. It is expected that, this value is being small for successive measurements because, while there are approximately  $128seconds$  of time difference between two measurements at repetitive measurement results for the same power level, there are  $8seconds$  of time difference for phase measurement of successive power levels. Phase measurements of PA are repeated with different LUT calibration data which is gathered at different time. Then phase of FUNDL tone of the sample amplifier is measured when PA is excited with two tone and plotted as given in Figure 3.13. There are approximately  $2^\circ$  change in the phase of FUNDL tone in  $20dB$  dynamic range for four repetitive measurements. Although there is a small discrepancy at the repetitive measurement results for the same power level, shape of phase is very close and this much of error is in the range of acceptable measurement error.

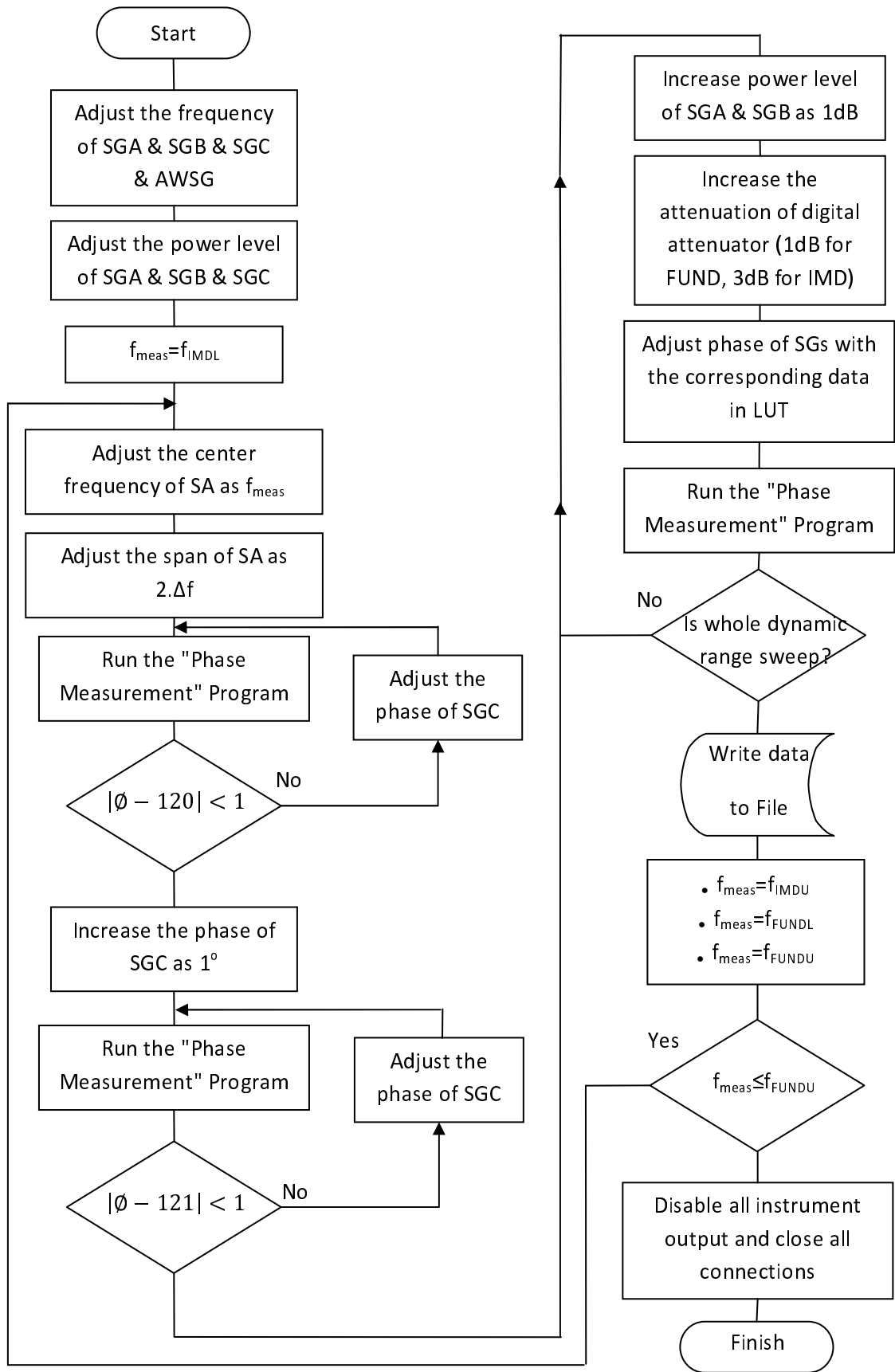


Figure 3.11: Flow chart for AM/PM measurement for full range power level

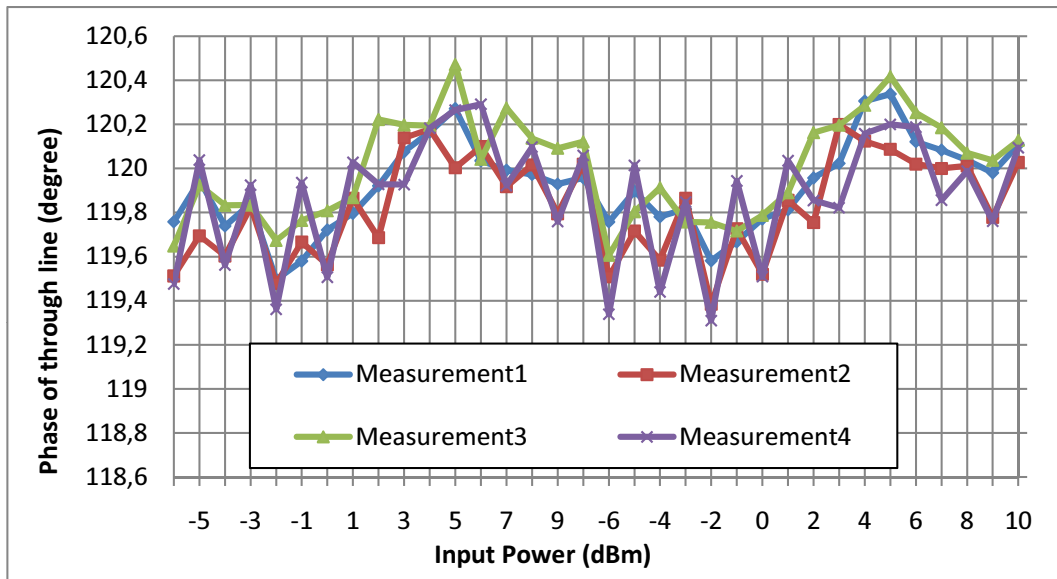


Figure 3.12: Repeated phase measurement result of through line

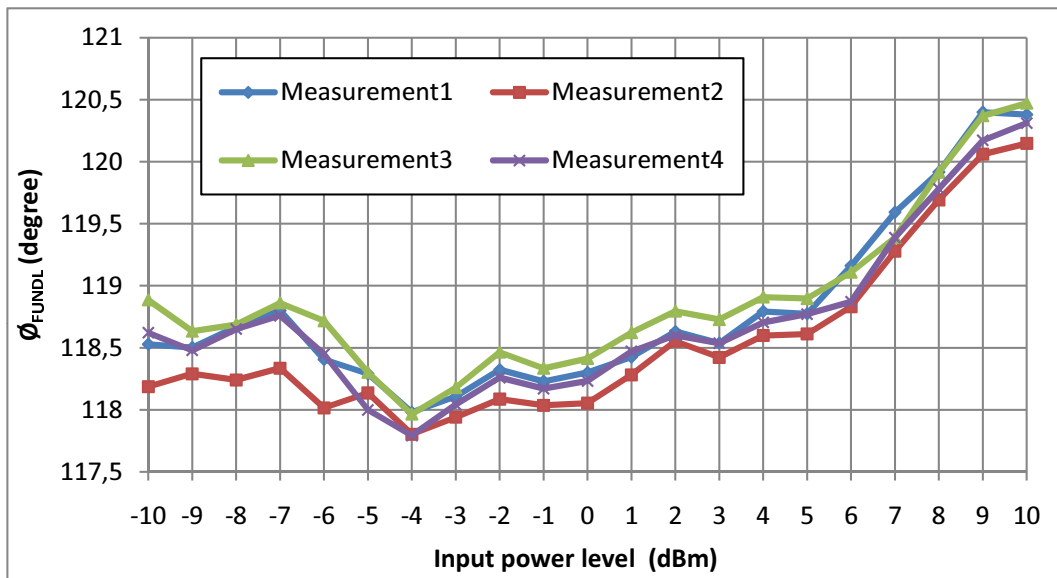


Figure 3.13: Repeated phase measurement result of sample amplifier

### 3.6 Phase Calibration for Signal Generators

Phase calibration and LUT construction are composed of two parts; training and verification. In the training part, LUT is prepared by making phase measurement for different power levels without making any change in the phase of signal generators. In the verification part, when power level of signal generator is changed, phase of signal generator is also set with corresponding the LUT data in order to get constant phase for through line. Training part is repeated until the ripple in the phase measurement results for verification part is less than  $1^\circ$  for the whole dynamic range.

Amplifier is removed from the measurement setup before starting the training part. There should be through connection instead of PA between power combiners at the measurement setup. Let's assume phase correction is needed for  $20dB$  dynamic range from  $10dBm$  to  $-10dBm$  power levels of the signal generators. Frequency of signal generators are set such that "SGA" frequency is equal to FUNDL tone and "SGB" frequency is equal to FUNDU tone. Then power level of both signal generators are set as  $10dBm$ . Phase of "SGA" is adjusted until phase difference between "SGA" and "SGC" is equal to  $120^\circ$ . At this time there might be two situations; either  $\angle SGC - \angle SGA = 180^\circ$  or  $\angle SGC - \angle SGA = -180^\circ$ . Hence, it should be accounted that absolute phase of "SGC" is greater than the absolute phase of "SGA" (i.e. This time if the phase of "SGC" is increased  $1^\circ$ , phase difference will be  $180^\circ$ . Conversely, if the phase difference is  $-180^\circ$ , after  $1^\circ$  increment in the phase of SGC, phase difference will be  $-179^\circ$  but the calculated phase difference value will be  $179^\circ$  due to nature cosine function. Then power level of only "SGA" is decreased by  $1dB$  from  $10dBm$  to  $9dBm$  and phase difference is measured. Assume phase difference is decreased to  $110^\circ$ . Inverse of difference between current phase difference measurement result and  $120^\circ$  is stored to the LUT as  $9dBm$  power level phase correction value for "SGA". In other words, when the power level of "SGA" is decreased from  $10dBm$  to  $9dBm$ , phase of "SGA" is  $10^\circ$  increased so that total phase difference for the new situation became  $110^\circ$ . In order to get  $120^\circ$ , when power level is decreased to  $9dBm$ , phase of "SGA" should be decreased by  $10^\circ$ . Next step is to find  $9dBm$  power level phase correction for "SGC". After power level of "SGC" is decreased to the  $9dBm$ , phase difference is measured, let us assume measurement result is  $95^\circ$ .  $9dBm$  power level phase correction value for "SGC" is calculated as  $15^\circ$ . This stair-step algorithm is performed until the corresponding phase correction of whole power levels for the signal

generators are learned.

Verification part is so similar to the training part. Power level of "SGA" and "SGC" are set as  $10dBm$  and frequency of "SGA" and "SGC" are set as FUNDL and FUNDU, respectively. Phase of "SGA" is adjusted until phase difference is equal to  $120^\circ$ . While power level of "SGA" is decreasing from  $10dBm$  to  $9dBm$  phase of signal generator is also decreased  $10^\circ$ . At this time measured phase difference between phase of "SGA" and "SGC" should be in the range of  $120^\circ \pm 0.5^\circ$ . Same operation is applied for "SGC" for  $9dBm$  power level. Phase correction is checked for the whole power level in the predefined dynamic range. If the ripple is smaller than  $1^\circ$  in the phase difference for the whole dynamic range, this LUT is accepted as verified for AM/PM measurement.

Training and verification procedure is applied for "SGB" too.

Digital attenuator is added to in the measurement setup as seen in Figure 3.1 in order to widen measurement setup's dynamic range. Digital attenuator is preferred instead of "SGC" since time versus phase behavior of digital attenuator is more stable. LUT is given in Table 3.1 as an example.

### 3.7 Measurement Results

Number of amplifier responses are measured and behavioral model has been extracted under this thesis. Two of those amplifiers have been taken from "ASELSAN A.Ş." under the GÜYDAM project. One of them is designed for HF band and the other one is designed for VHF band. In this thesis HF amplifier is chosen as the sample amplifier and results of HF amplifier are given in this section.

The amplifier is composed of more than one stage(driver and main amplifier) and has push-pull output. Saturation peak power for this sample amplifier is approximately  $390W$  ( $56dBm$ ), output  $P_{1dB}$  is  $53.35dBm$  and gain is  $45.7dB$ .

Magnitudes and phases of IMDL, IMDU, FUNDL and FUNDU components are measured for one-tone and two-tone continuous wave excitations.  $10MHz$  is chosen as the working frequency and  $1kHz$  is chosen as the frequency separation ( $10MHz/1kHz$ ) between FUNDL

Table 3.1: Sample LUT

SGA(dBm)	Corr <sub>SGA</sub> (°)	Dig. Att.(dB)	Corr <sub>Att</sub> (°)	SGC(dBm)	Corr <sub>SGC</sub> (°)
10	0.0	0	0	10	0
9	-2.20	1	0.7	9	-2.3
8	-4.60	2	2.1	8	-4.6
7	-7.20	3	4.3	7	-7.0
6	-9.50	4	5.9	6	-9.3
5	-11.80	5	8.9	5	-11.7
4	-14.00	6	11.3	4	-14.0
3	-16.20	7	14.6	3	-16.4
2	-18.40	8	15.4	2	-19.2
1	-20.60	9	16.3	1	-21.6
0	-22.80	10	17.8	0	-23.9
-1	-24.90	11	20.2	-1	-26.2
-2	-27.10	12	21.9	-2	-28.6
-3	-29.20	13	25.0	-3	-30.8
-4	-31.30	14	27.4	-4	-33.1
-5	-33.30	15	30.8	-5	-35.4
-6	-35.30	16	31.4	-6	-37.5
-7	-37.20	17	32.5	-7	-39.6
-8	-39.00	18	34.1	-8	-20.3
-9	-40.90	19	36.6	-9	-22.6
-10	-42.70	20	38.3	-10	-24.9

and FUNDU. These measurement results are used for modeling. Magnitudes of fundamental and IMD tones are also measured for unequal four-tone continuous wave.

Amplifier response for one-tone excitation is as given in Figure 3.14. Amplifier is derived beyond  $P_{1dB}$  power level. Amplifier gain is not constant and is increasing when input power increased until  $P_{in} = 8.7dBm$ . while the amplifier excitation power level increased from  $-10.3dBm$  to  $-4.3dBm$  then to  $8.7dBm$ , gain is increasing from  $43.2dB$  to  $43.7dB$  then to  $45.7dB$ , respectively. Maximum value of gain for this amplifier is  $45.7dB$ . When excitation power is increased to  $P_{1dB}$  power level gain is decreased to  $44.7dB$ . If the gain wouldn't change in a certain range(e.g. from  $-10.7dBm$  to  $0dBm$ ) like Class-A amplifier, coefficient extraction could be easy. This sample amplifier one-tone characteristic makes harder to get a

simple behavioral model. There is no range where phase is constant as well. Total change in the phase is  $3^\circ$ .

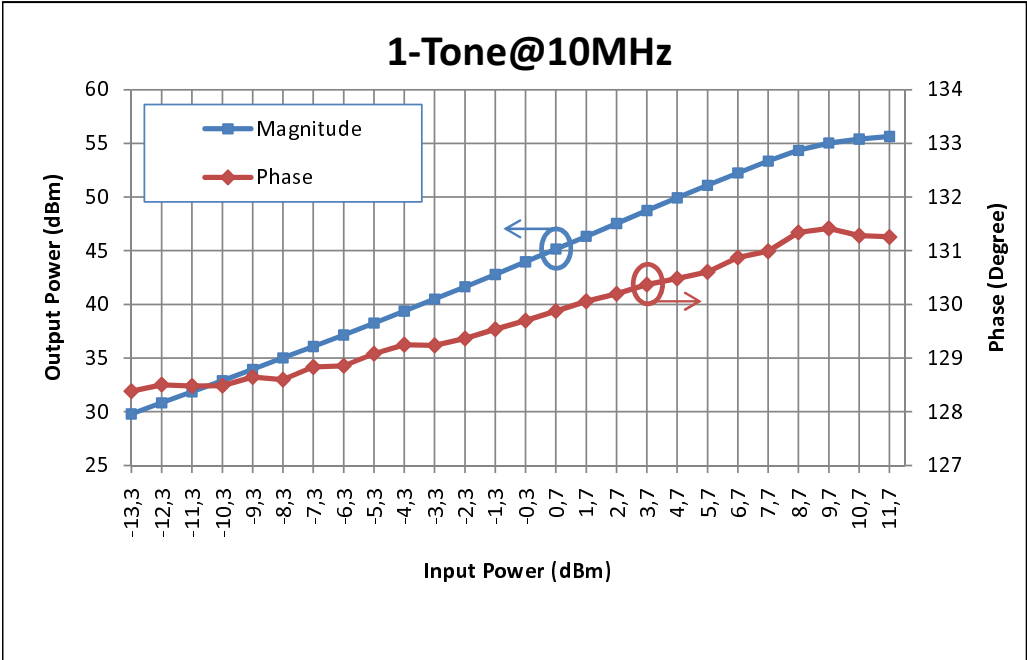


Figure 3.14: Magnitude and phase measurement result of one-tone excitation having 10MHz working frequency

It is stated previously that working frequency is 10MHz, i.e. frequency of FUNDL tone is chosen as equal to 10MHz and FUNDU tone is chosen as equal to  $10MHz + frequencyseparation$ . Thus, frequency of "SGA" is set to 10MHz and frequency of "SGB" is set to  $10.001MHz$  for two-tone excitation. Magnitudes and phases of IMDL, IMDU, FUNDL and FUNDU are measured for more than 15dB input dynamic range and are plotted as given in Figure 3.15. There is small asymmetry between magnitude of fundamental components which can be negligible. However, there is non-constant asymmetry in magnitudes of intermodulation components. Asymmetry increases to 10dB when input excitation level is 2.7dBm. While there is  $4.45^\circ$  change in the phase of FUNDL as shown in Figure 3.15c, it is less than  $3^\circ$  for FUNDU as shown in Figure 3.15d. Total phase change was  $3^\circ$  for one-tone excitation. It can be said that high nonlinearity order is required by considering the increasing rate and total change in the phase of intermodulation distortion (IMD) components as given in Figure 3.15a and Figure 3.15b. There is  $104.8^\circ$  and  $151^\circ$  total change for the phase of IMDL and the phase of IMDU, respectively. While asymmetry in between phase of IMDL and IMDU is  $-25^\circ$  for 3.7dBm input power level, it is increased to  $47.8^\circ$  for  $-1.3dBm$  input power level. This is the

most difficult point for behavioral modeling; approximately 10dB asymmetry (non-constant w.r.t. excitation power level) in the magnitude of IMD components and 151° change in the phase of IMDU in addition to this, there is more than 47° asymmetry (non-constant w.r.t. excitation power level) in the phase of IMD components.

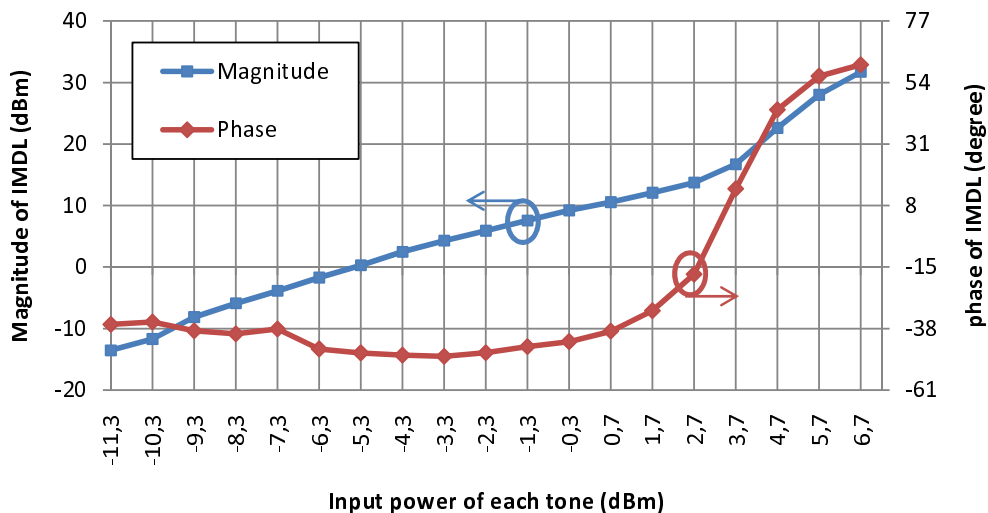
IMDL, IMDU, FUNDL and FUNDU will be named hereafter as "four components". Although, measurement results of two-tone (10MHz/1kHz) are enough for model parameter extraction, amplifier response for different two-tone excitation scheme(i.e. different center frequency and different frequency separation) and four-tone are measured for comparison and model validity range investigation. For this purpose, magnitudes and phases of four components are measured and plotted for 8MHz/1kHz, 9MHz/1kHz, 11MHz/1kHz and 12MHz/1kHz as given in Figure 3.16 – Figure 3.19 and plotted for 10MHz/300Hz, 10MHz/3.3kHz as given in Figure 3.20 and Figure 3.21, respectively. These measurement results are compared with the 10MHz/1kHz excitation measurement result because models is extracted according to 10MHz/1kHz measurement results.

There is no big difference between the magnitudes of the four components when the amplifier is excited with 8MHz/1kHz frequency separation w.r.t. the measurement result of 10MHz/1kHz frequency separation. Phase behavior of IMDL for 8MHz/1kHz is very similar to measurement result of 10MHz/1kHz. Phase behavior of IMDU for 8MHz/1kHz is very similar to measurement result of 10MHz/1kHz for the excitation power level which is lower than 1.7dBm. Increasing ratio w.r.t the input power in the phase of IMDU for 8MHz/1kHz is smaller than the ratio for 10MHz/1kHz measurement result. Increasing ratio of the phase of FUNDL and FUNDU for 8MHz/1kHz is greater than measurement results of 10MHz/1kHz. In contrast, phase behavior of fundamental tones are very similar. If the other measurement results (8MHz/1kHz – 12MHz/1kHz) frequency separation are investigate, similar explanation is valid for those measurement results. There is negligible difference in the magnitudes and is different increasing ratio. But there is small exception for the phase behavior of fundamental tones for the measurement results whose working frequencies are bigger than 10MHz. While the phases of fundamental tones are always increasing for 8MHz & 9MHz, it is constant for 10MHz and is decreasing for 11MHz & 12MHz excitation for the input power level which is greater than 3.7dBm. There is no special meaning(special case) for 3.7dBm power level for measurement setup. This special case may be related with the transistor properties and quiescent point.

If the measurement results for  $10\text{MHz}/300\text{Hz}$  frequency separation as given in Figure 3.20 are investigated, It can be said that amplifier behavior changes more than the change for  $8\text{MHz}$  excitation. Asymmetry in the magnitudes of IMD components has been lost. Both magnitude and phase of IMDL for  $300\text{Hz}$  separation is similar to measurement result of  $1\text{kHz}$ . But there is noticeably change for both magnitude of and phase of IMDU as it can be seen from Figure 3.20b. While input power level is low there is no difference, magnitude IMDU for  $300\text{Hz}$  frequency separation is increasing fast than the magnitude of IMDU for  $1\text{kHz}$  frequency separation. In contrast, total change in the magnitude is less than the total change in the magnitude for  $1\text{kHz}$  frequency separation measurement result. Moreover, there is a big change in the phase behavior. Total change in the phase of IMDU for  $300\text{Hz}$  frequency separation is less than the change in the phase of IMDU for  $1\text{kHz}$  frequency separation. Although there is small difference between the frequency of IMDL and the frequency of IMDU, there is an unexpected big difference in the phase of IMDL. The reason of this result is one of the possible future studies. There is a very small change in the phase of FUNDL and magnitude of FUNDU, conversely there is a big difference in the phase of FUNDU and magnitude of FUNDL.

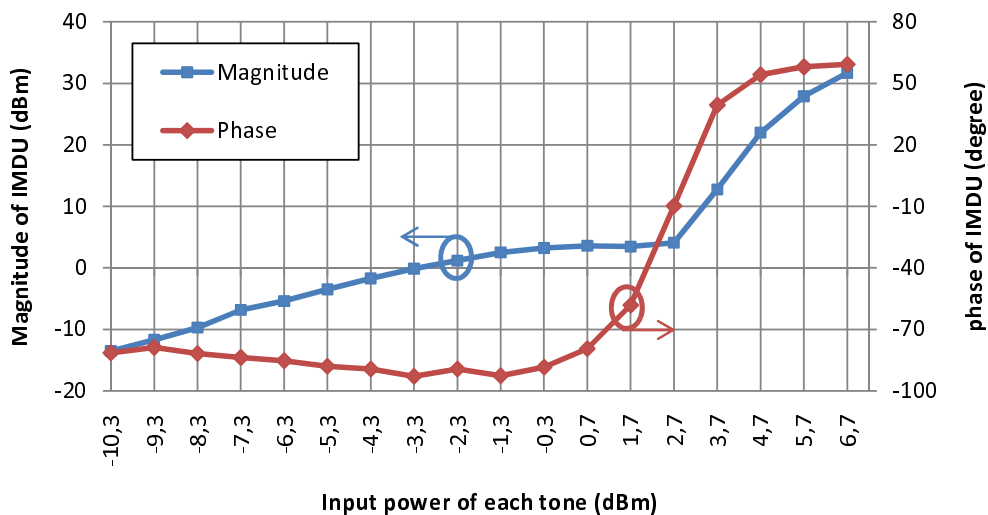
Magnitude of both FUNDL and FUNDU for  $3.3\text{kHz}$  frequency separation is very close to magnitude of FUNDL and FUNDU for  $1\text{kHz}$  frequency separation. The phase's behavior of FUNDL for  $3.3\text{kHz}$  frequency separation is similar to phase's behavior of FUNDL for  $1\text{kHz}$  frequency separation. There is small difference between phase of FUNDL for  $3.3\text{kHz}$  frequency separation and the phase of FUNDU for  $1\text{kHz}$  frequency separation and this difference is always lower than  $0.5^\circ$  which is negligible. It is difficult to say that intermodulation distortion measurement results belongs to the same amplifier by considering Figure 3.15a, Figure 3.15b, Figure 3.21a and Figure 3.21b. There are small similarities between  $3.3\text{kHz}$  frequency separation phase measurement results for IMDL and  $1\text{kHz}$  frequency separation phase measurement results for IMDL. If the x-axis could be shifted  $2\text{dB}$  to the left for the  $3.3\text{kHz}$  frequency separation measurement, measurement results would be similar. There is sweet-spot point in the magnitude of IMDU for  $3.3\text{kHz}$  frequency separation, but there isn't in the  $1\text{kHz}$  frequency separation measurement results.

### IMDL@10MHz with 1kHz Spacing

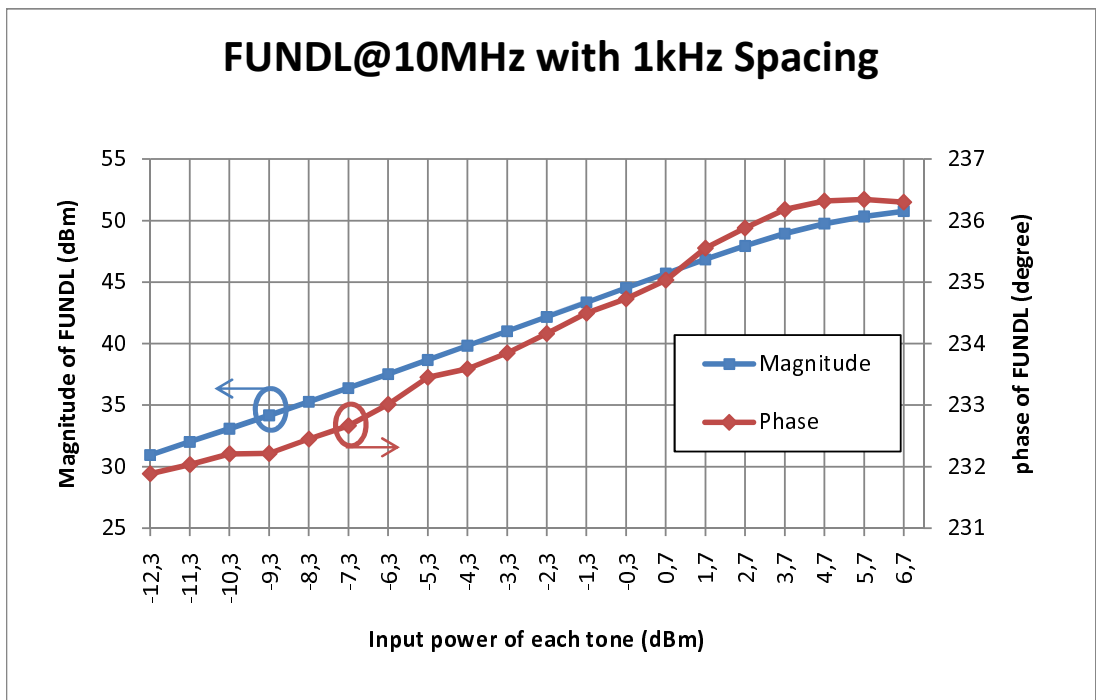


(a) Magnitude and phase measurement results of IMDL

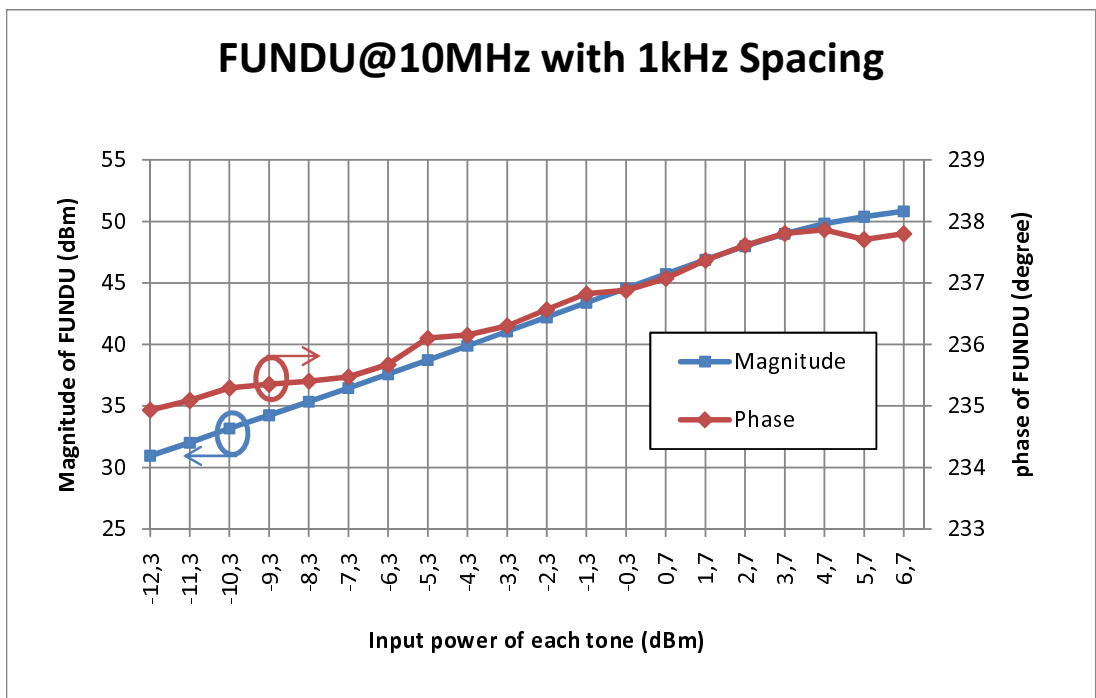
### IMDU@10MHz with 1kHz Spacing



(b) Magnitude and phase measurement results of IMDU



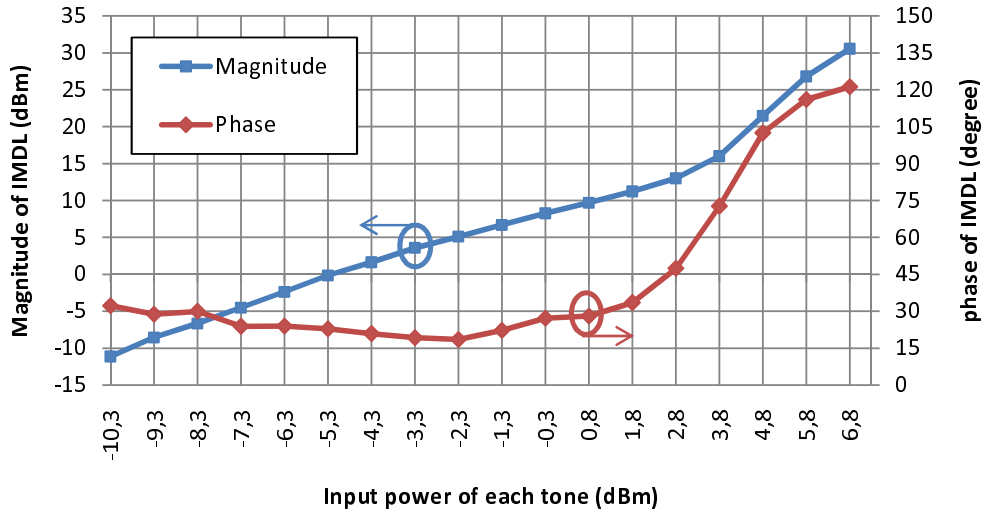
(c) Magnitude and phase measurement results of FUNDL



(d) Magnitude and phase measurement results of FUNDU

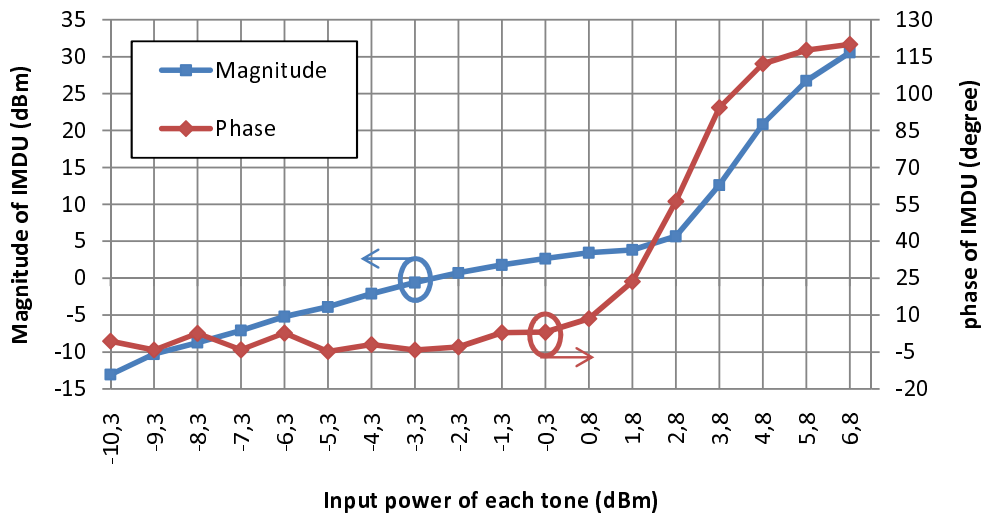
Figure 3.15: Magnitude and phase measurement results of a)IMDL, b)IMDU, c)FUNDL and d)FUNDU for two-tone excitation having 10MHz/1kHz

### IMDL@8MHz with 1kHz Spacing

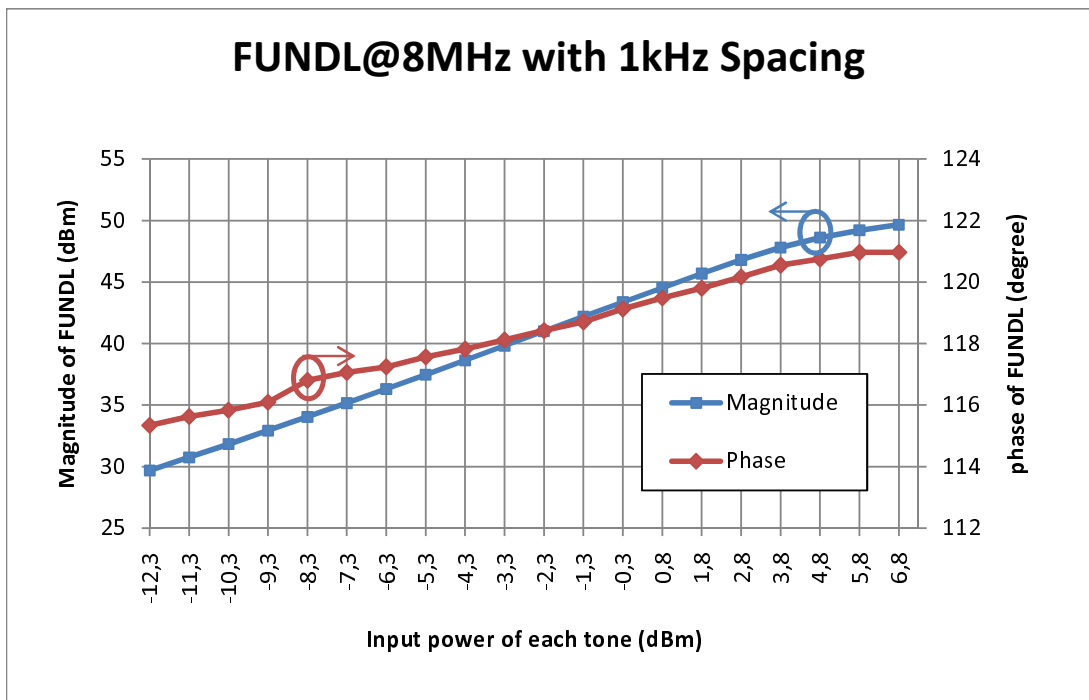


(a) Magnitude and phase measurement results of IMDL

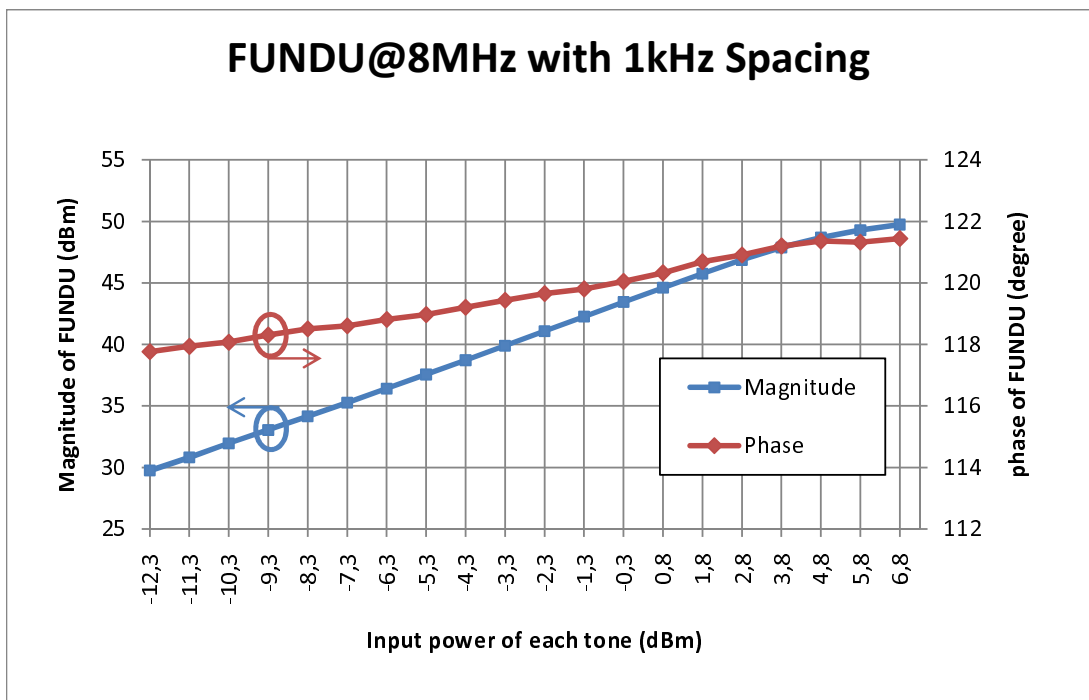
### IMDU@8MHz with 1kHz Spacing



(b) Magnitude and phase measurement results of IMDU



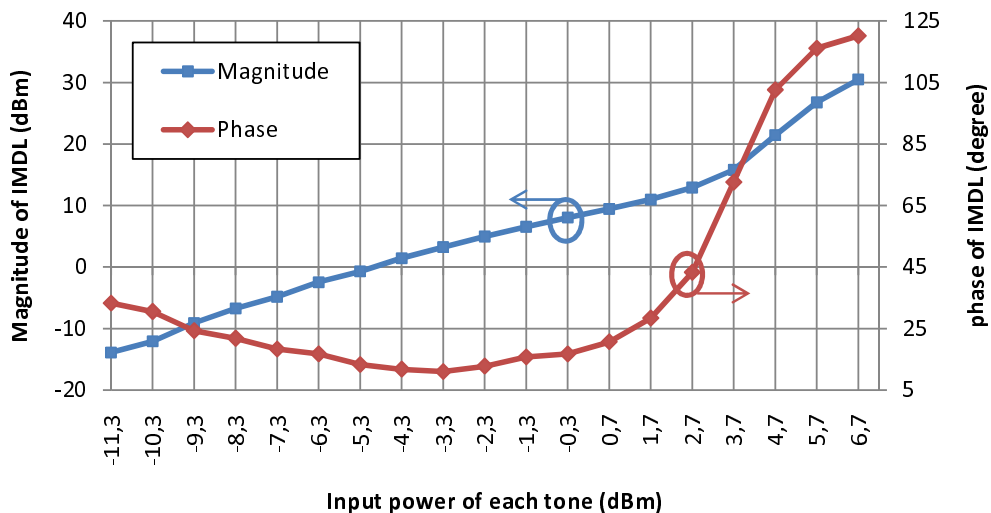
(c) Magnitude and phase measurement results of FUNDL



(d) Magnitude and phase measurement results of FUNDU

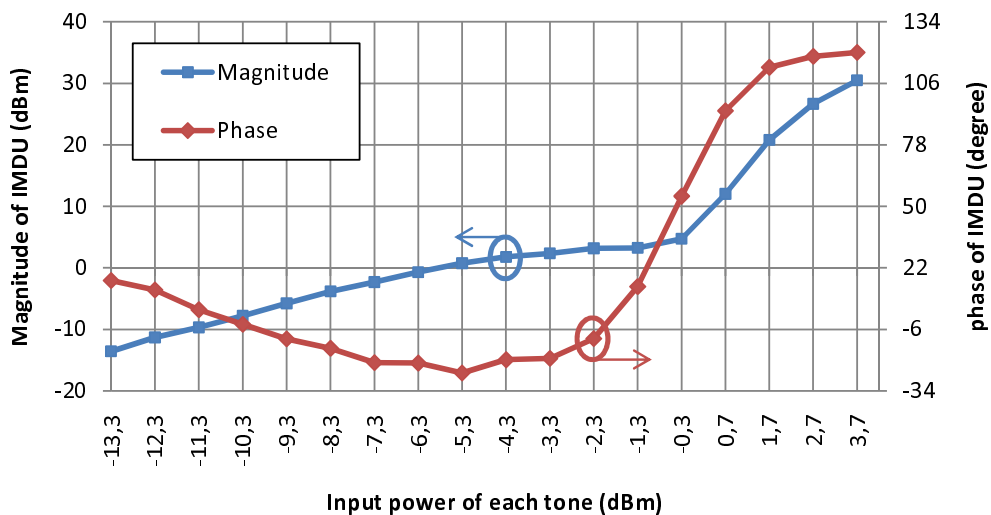
Figure 3.16: Magnitude and phase measurement results of a)IMDL, b)IMDU, c)FUNDL and d)FUNDU for two-tone excitation having  $8MHz/1kHz$ .

### IMDL@9MHz with 1kHz Spacing

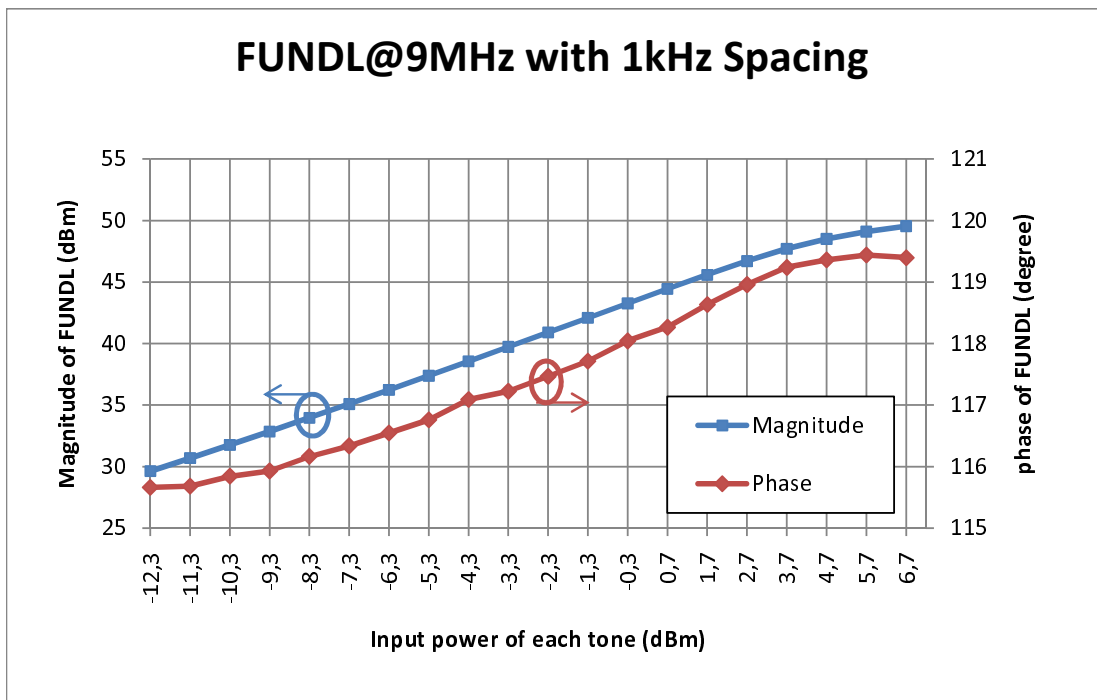


(a) Magnitude and phase measurement results of IMDL

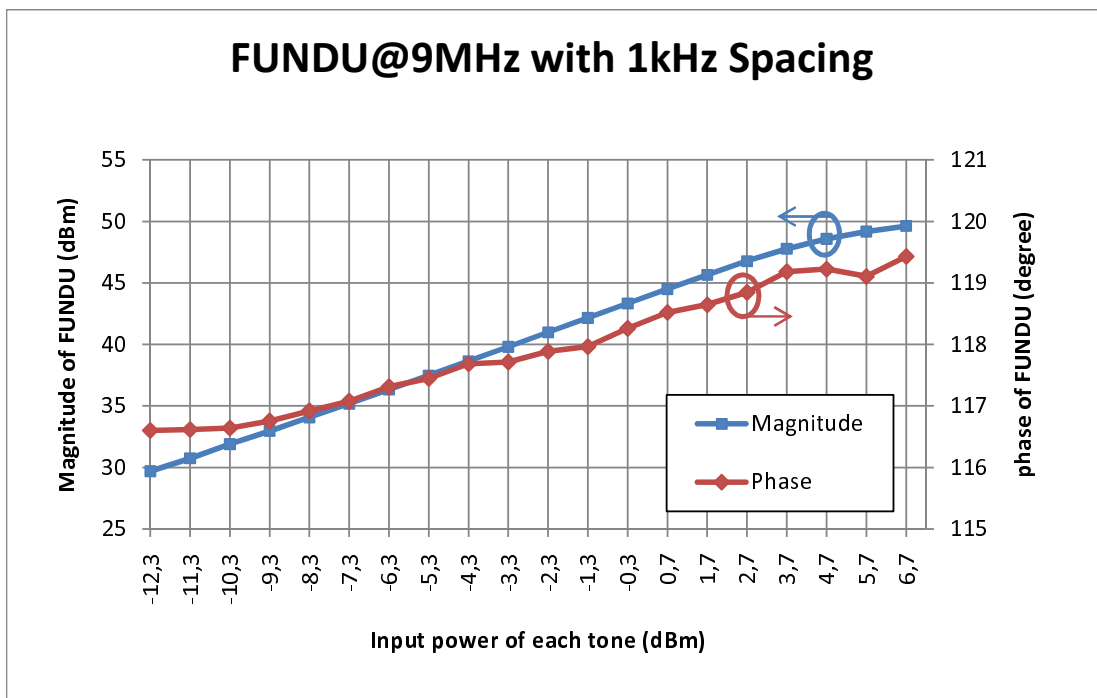
### IMDU@9MHz with 1kHz Spacing



(b) Magnitude and phase measurement results of IMDU



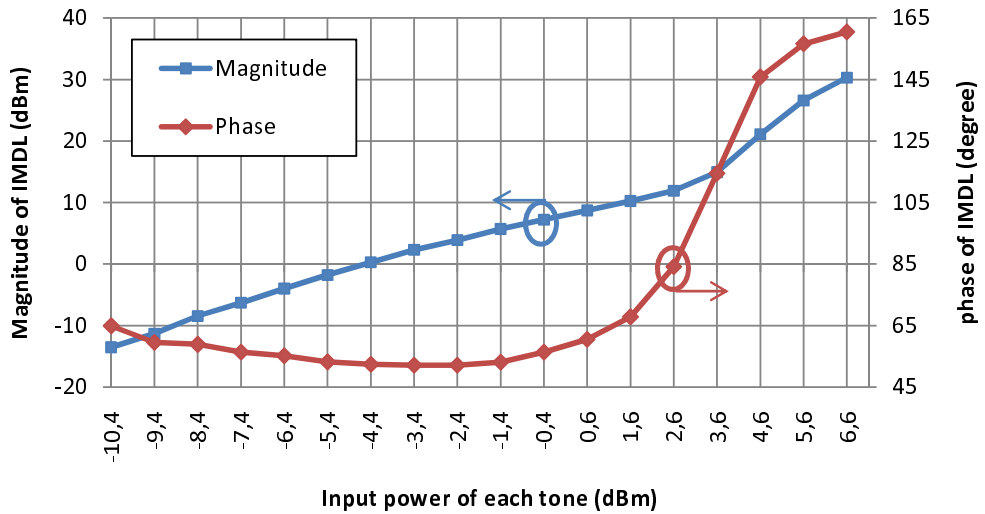
(c) Magnitude and phase measurement results of FUNDL



(d) Magnitude and phase measurement results of FUNDU

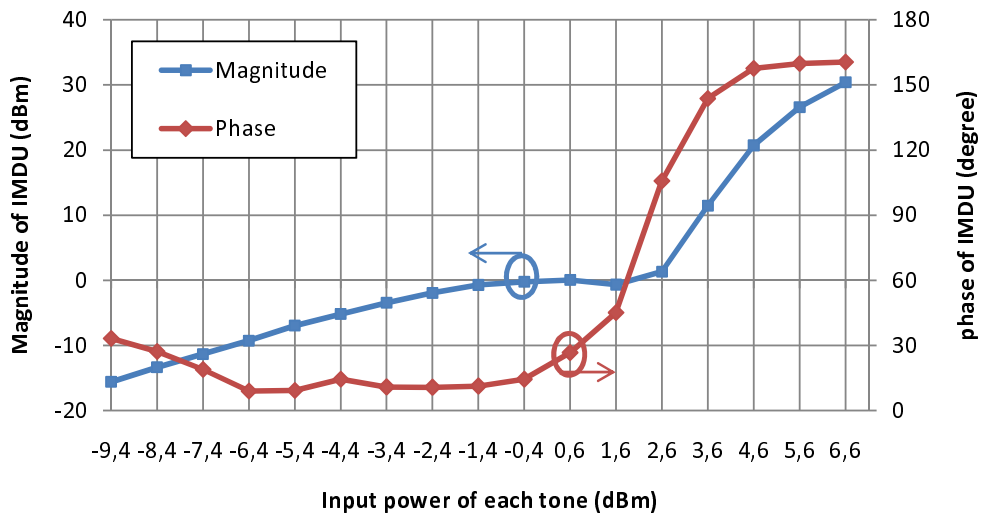
Figure 3.17: Magnitude and phase measurement results of a)IMDL, b)IMDU, c)FUNDL and d)FUNDU for two-tone excitation having  $9MHz/1kHz$

### IMDL@11MHz with 1kHz Spacing

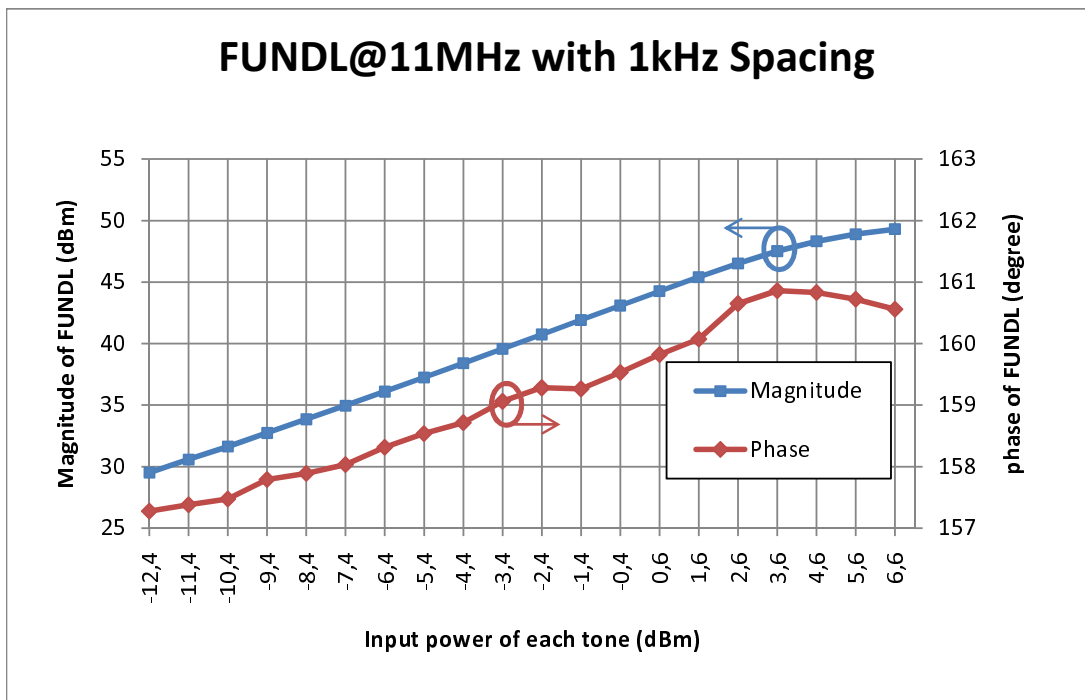


(a) Magnitude and phase measurement results of IMDL

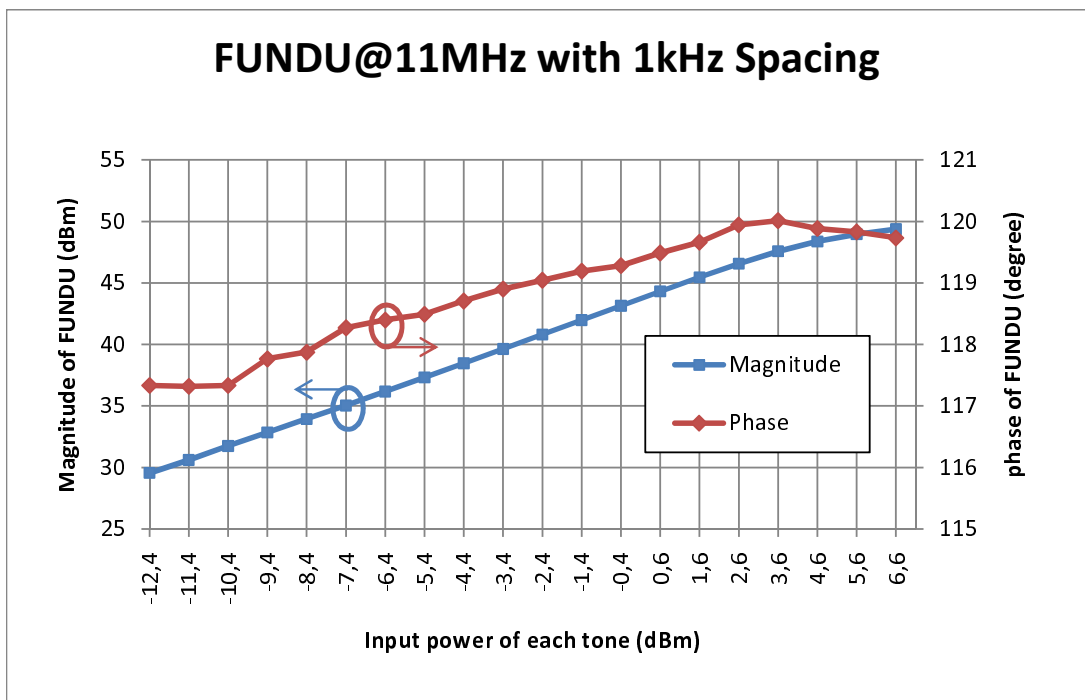
### IMDU@11MHz with 1kHz Spacing



(b) Magnitude and phase measurement results of IMDU



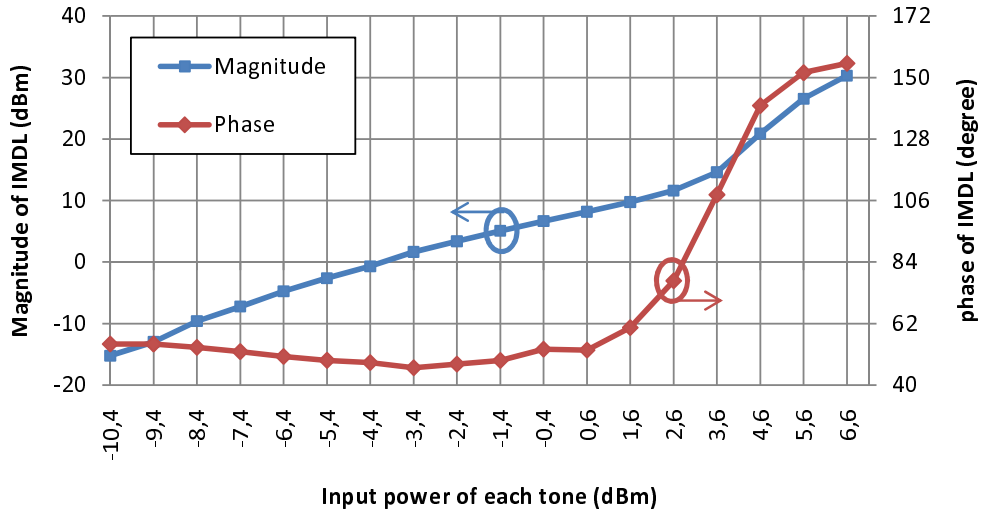
(c) Magnitude and phase measurement results of FUNDL



(d) Magnitude and phase measurement results of FUNDU

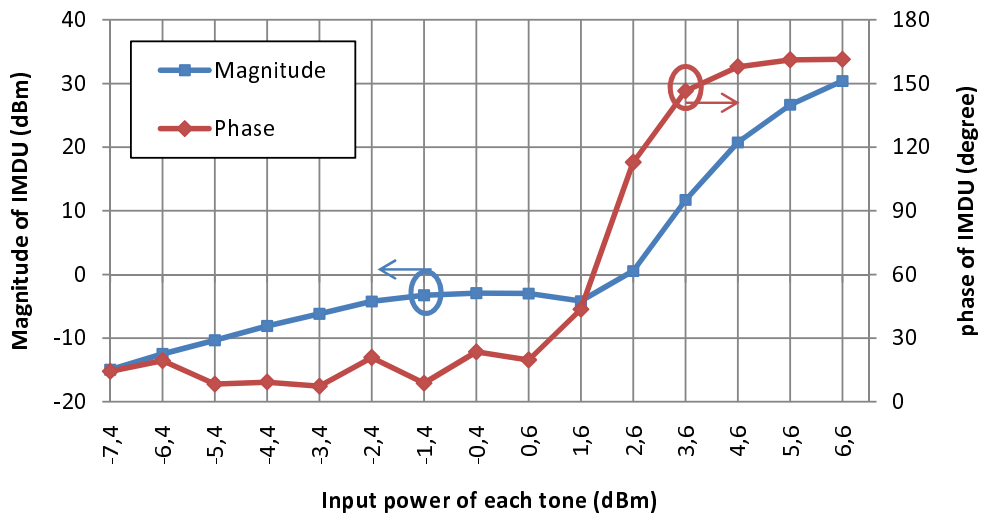
Figure 3.18: Magnitude and phase measurement results of a)IMDL, b)IMDU, c)FUNDL and d)FUNDU for two-tone excitation having  $11MHz/1kHz$

### IMDL@12MHz with 1kHz Spacing

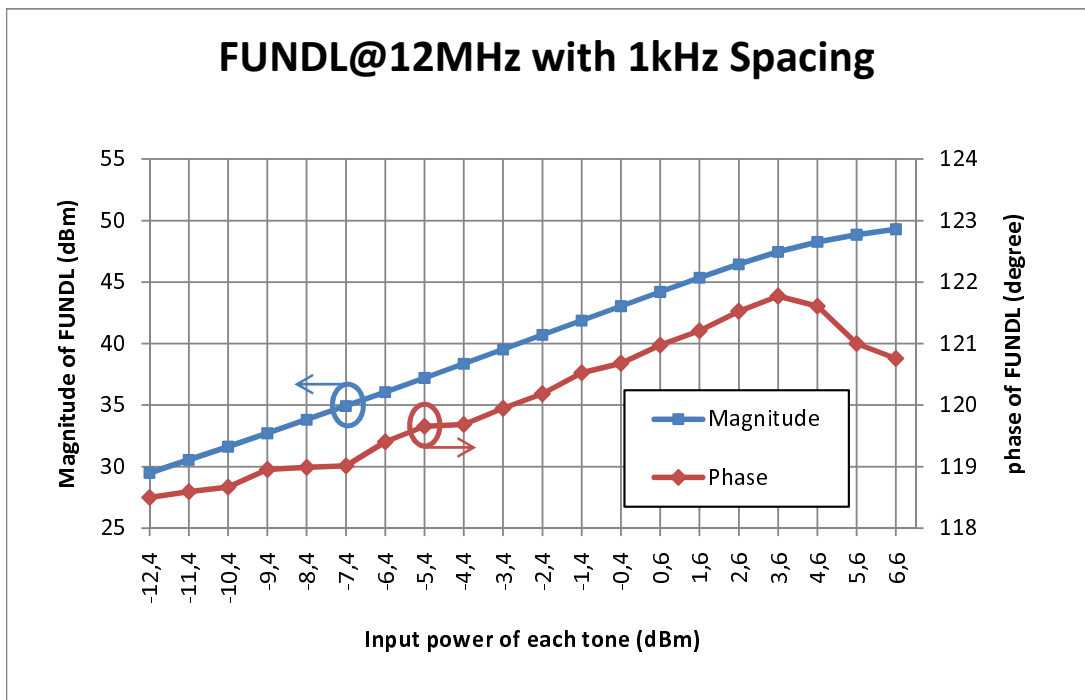


(a) Magnitude and phase measurement results of IMDL

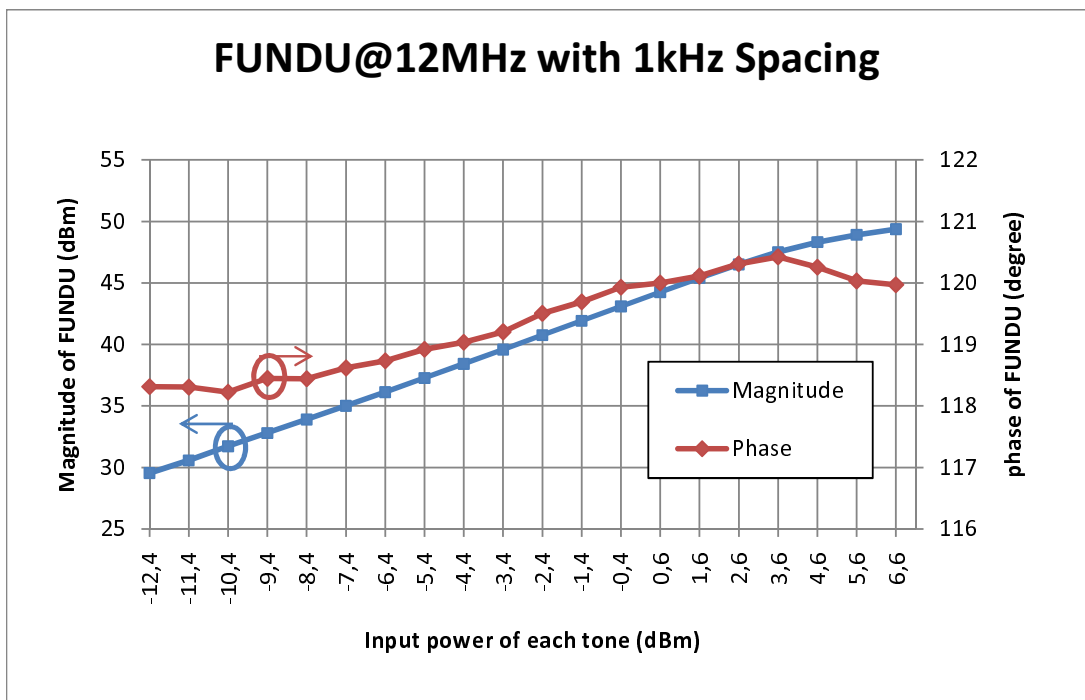
### IMDU@12MHz with 1kHz Spacing



(b) Magnitude and phase measurement results of IMDU

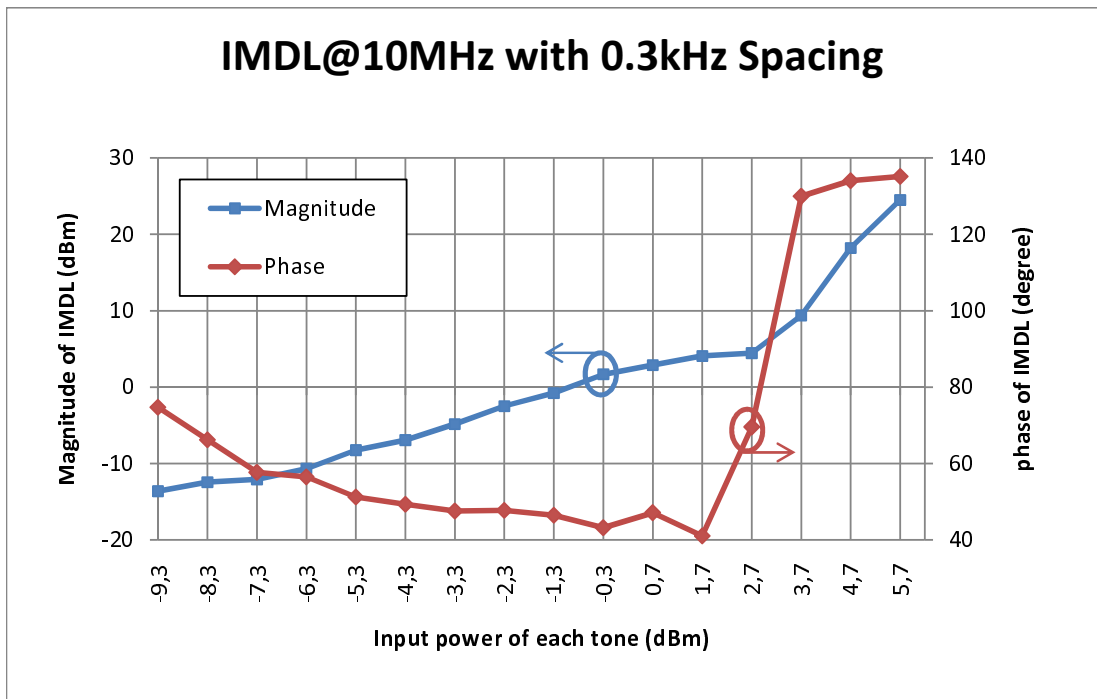


(c) Magnitude and phase measurement results of FUNDL

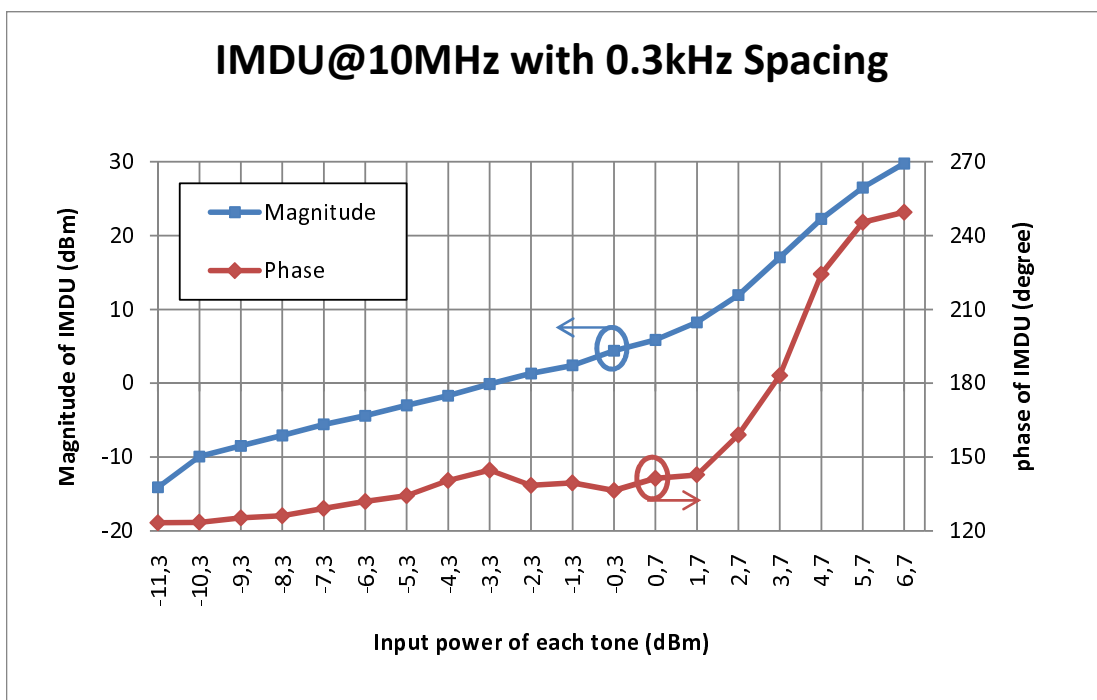


(d) Magnitude and phase measurement results of FUNDU

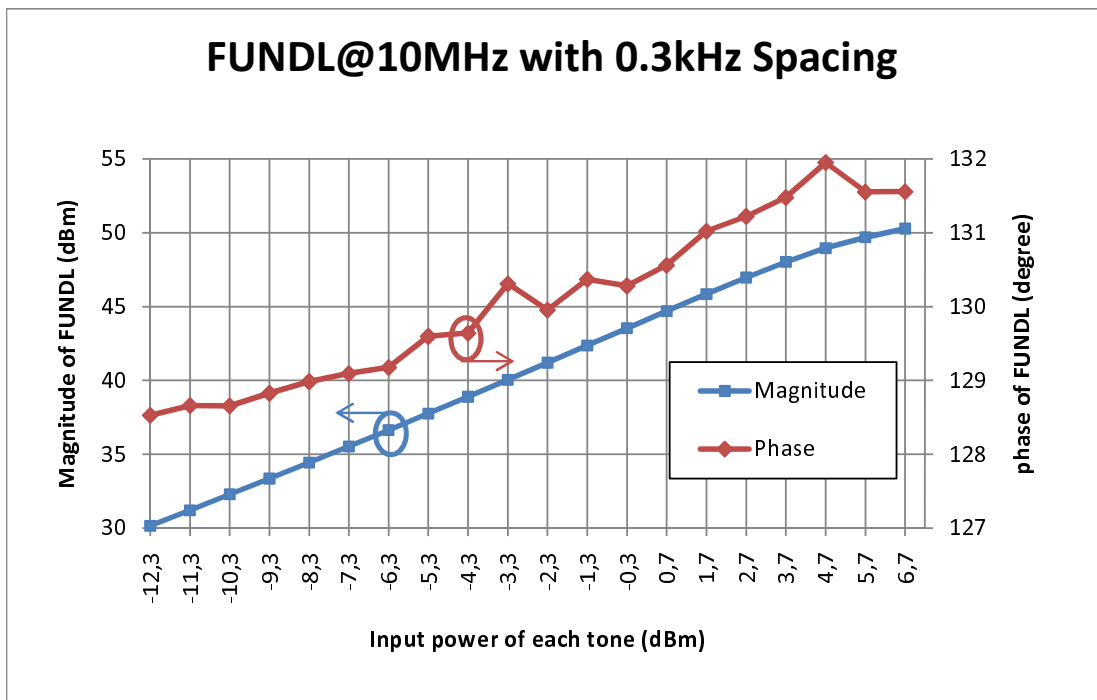
Figure 3.19: Magnitude and phase measurement results of a)IMDL, b)IMDU, c)FUNDL and d)FUNDU for two-tone excitation having 12MHz/1kHz



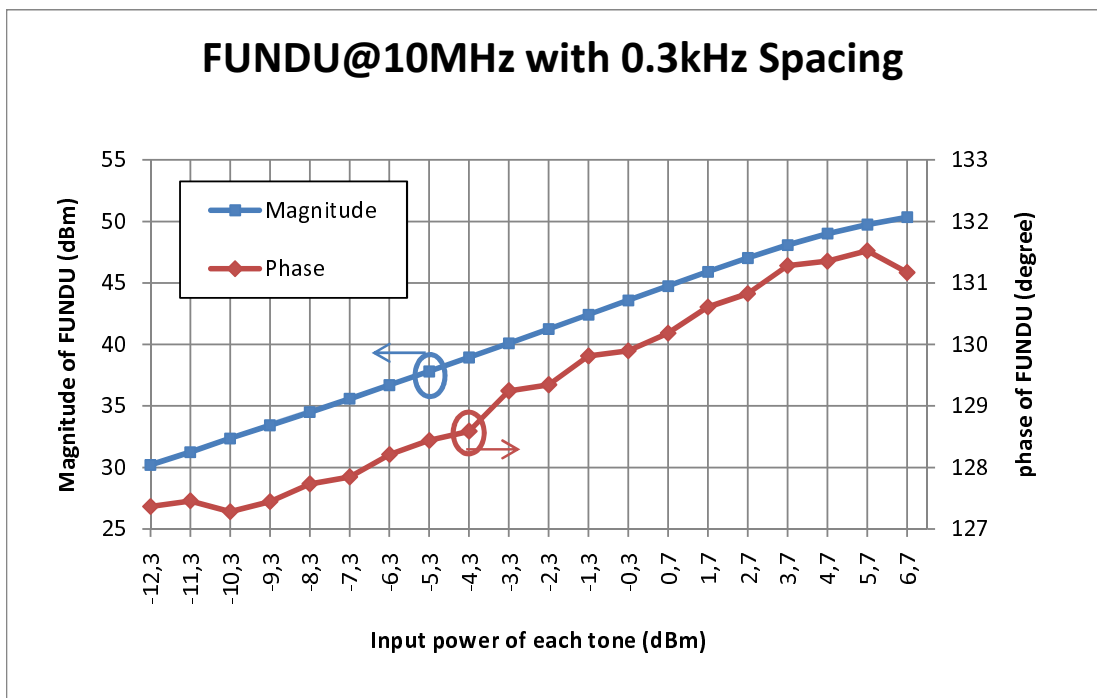
(a) Magnitude and phase measurement results of IMDL



(b) Magnitude and phase measurement results of IMDU

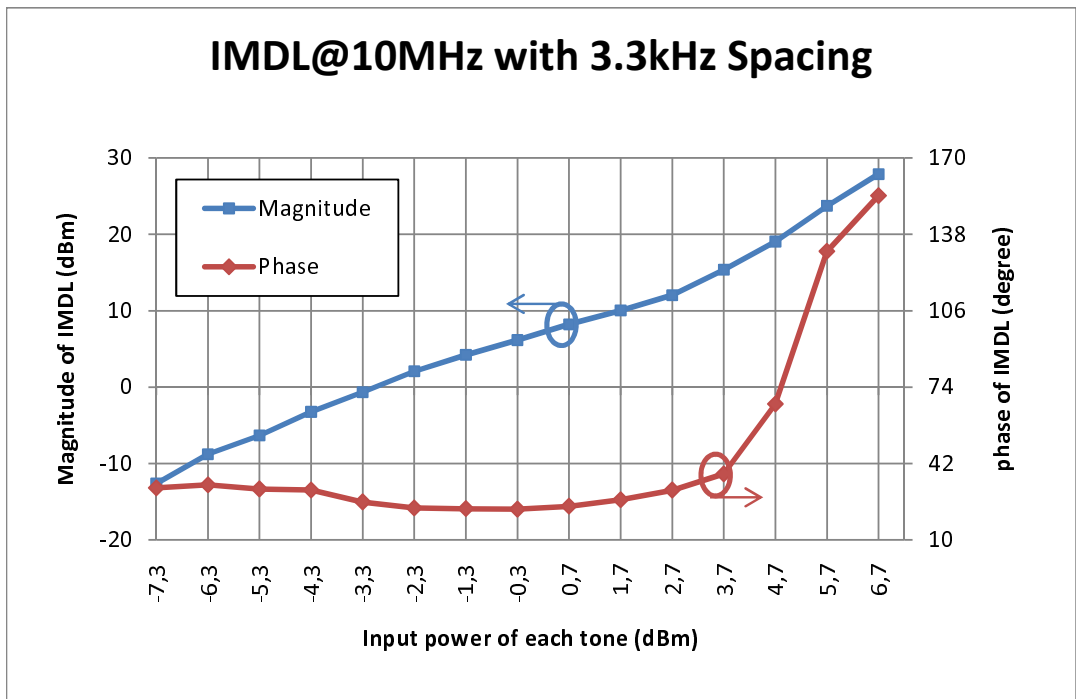


(c) Magnitude and phase measurement results of FUNDL

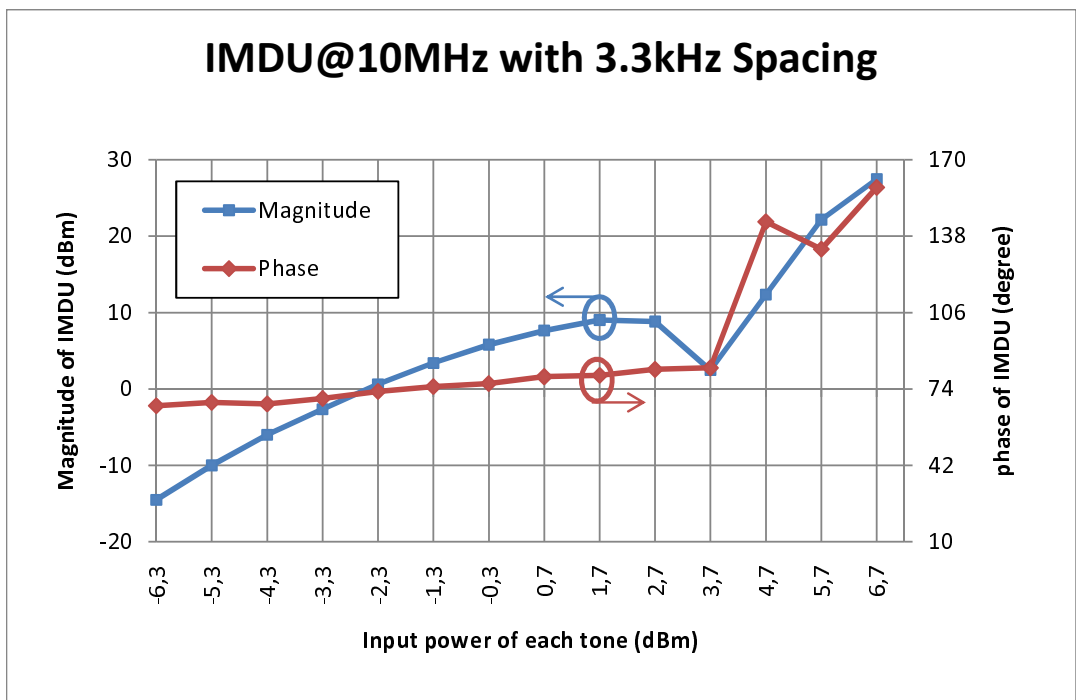


(d) Magnitude and phase measurement results of FUNDU

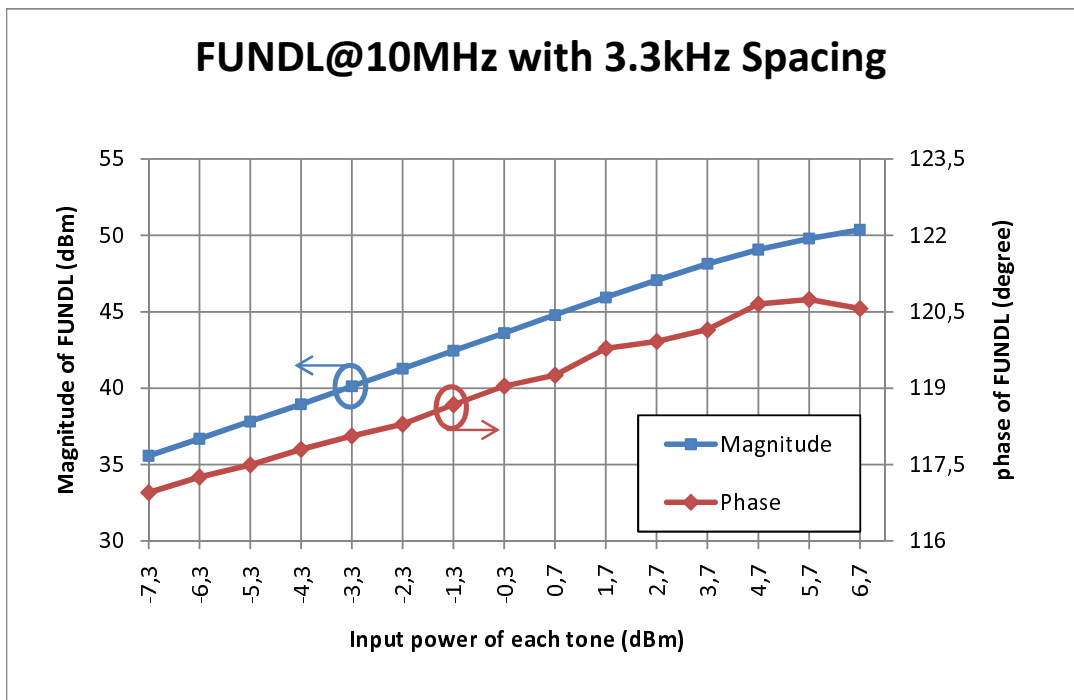
Figure 3.20: Magnitude and phase measurement results of a)IMDL, b)IMDU, c)FUNDL and d)FUNDU for two-tone excitation having 10MHz/300Hz



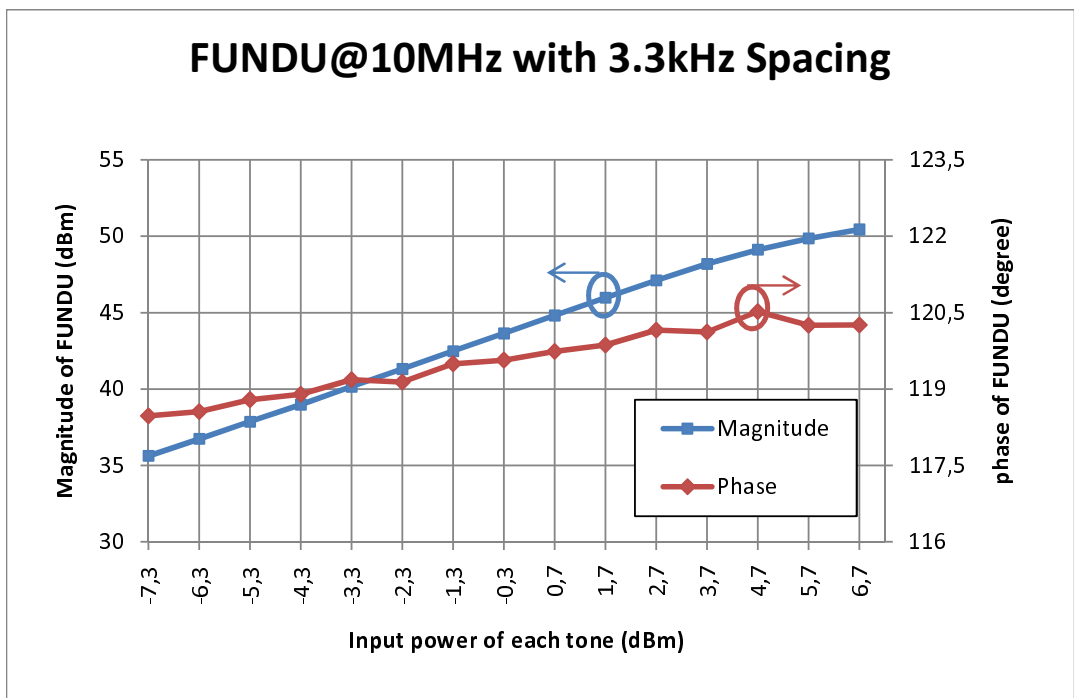
(a) Magnitude and phase measurement results of IMDL



(b) Magnitude and phase measurement results of IMDU



(c) Magnitude and phase measurement results of FUNDL



(d) Magnitude and phase measurement results of FUNDU

Figure 3.21: Magnitude and phase measurement results of a)IMDL, b)IMDU, c)FUNDL and d)FUNDU for two-tone excitation having 10MHz/3.3kHz

### 3.8 Conclusion

One of the important steps of modeling is to measure amplifier response which is essential for modeling. One-tone and two-tone AM/AM and AM/PM measurements are needed for modeling, thus a measurement setup is required to measure these properties of an amplifier. AM/PM measurement for two-tone excitation is difficult for RF signal, although AM/AM measurement is relatively easier. To do so, a new measurement setup is prepared. Two signal generators are used to create two-tone signal and one more signal generator is used as the reference signal for phase measurement and all instruments are connected each other with possible shortest cable to transfer the  $10\text{MHz}$  reference signal. A new equation is derived to calculate/measure phase difference by measuring magnitudes as given in (3.2). This equation is verified with a through line. While one of signal generator's phase is increased by  $1^\circ$  steps until  $360^\circ$ , phase difference was measured. Approximately  $1^\circ$  phase change is observed for all steps except around  $0^\circ$  phase difference. This error is related with calculation sensitivity of computer and "cosine" function used in phase calculation equation. Thus, this point has been considered during for all measurements. New measurement theory is checked for different power levels of signal generators as well. It is observed that there is a phase change when power level of signal generator is changed. Since the change in the phase is not random, phase calibration procedure is developed and a LUT is prepared in order to keep phase constant. Phase measurement is repeated many times for full dynamic range and results are plotted in Figure 3.12. There is maximum  $0.53^\circ$  phase difference between repetitive measurements. This value is smaller for successive measurements because, while there are approximately  $128\text{seconds}$  time difference between two repetitive measurements of the same power level, the time needed for phase measurement of successive power levels is  $8\text{seconds}$ .

One Arbitrary Wave Shape Generator(AWSG) is added to the measurement setup in order to measure the absolute phase difference among four components. Thus, four-tone signal having zero phase difference at each other could be generated. AWSG is used also for unequal four-tone creation as an excitation signal for model verification purpose.

One phase measurement cycle has been represented step-by-step in the flow chart as given in Figure 3.4 and full range phase measurement has been represented in the flow chart as given in Figure 3.11. A special computer program is prepared using "Agilent VEE" program to control instruments and to take data quickly by using these flowcharts. As a result of this, one

phase measurement cycle has been done in *8seconds*. Then, magnitudes and phases of four components are measured and plotted as given in Figure 3.16-Figure 3.19, for  $8MHz/1kHz$ - $12MHz/1kHz$  and plotted as given in Figure 3.20 and Figure 3.21 for  $10MHz/300Hz$ ,  $10MHz/3.3kHz$  frequency separation having  $10MHz$  working frequency, respectively. While there is small change in the behavior of the amplifier w.r.t. center frequency of two-tone, there is considerable change in the behavior of the amplifier w.r.t. frequency separation of two-tone.

## CHAPTER 4

### Theory of Power Series with Unequal Time Delay Behavioral Model, Parameter Extraction and Comparison

#### 4.1 Introduction

One of the main aims of this dissertation is to develop a model which predicts asymmetry between IMDL and IMDU. This asymmetry is resulted from memory effect. So, while trying to develop a new model, it is always checked that whether the new model has ability to create asymmetry mathematically between IMDL and IMDU or not. Since one other aim is simplicity in both model architecture and model parameter extraction procedure, the new model is based on power series expansion.

Model equation is defined for a passband signal and it is not developed for a special class of Amplifier. General amplifier behavior was taken in the consideration while trying to develop this model and the model has been verified with the sample amplifier which was a Class-B amplifier. This model can be used to get model of most type of amplifiers. In order to create asymmetry at the intermodulation distortion and fundamental components, *unequal time delay* terms are added to each order terms of polynomial series terms. Unequal time delay addition to each term is one of the original contributions of this thesis. Order of model function should be at least 5 in order to create asymmetry. Model order can be increased, if more accuracy is needed. Since model is defined as a time domain power series polynomial function, there is no limitation to add higher order. In contrast, for model simplicity, it is preferred to use the least order.

Since, even terms don't have any contribution to intermodulation distortion (IMD) and to fundamental (FUND) components, in the beginning only odd order terms are used in the

model. To prevent confusion with latter developed model, this new modeling technique is named as "Only Odd order Modeling" (OOM).

However, although there are a number of work claiming that even order can improve modeling success, there isn't any paper in literature which shows even terms' contribution to IMD and FUND components in passband by further work, OOM modeling is improved by adding even terms to the modeling equation and named as EOM. Another original contribution of this thesis is the development of a modeling technique having even order terms contributing to the IMD and FUND components. Envelope of the input excitation signal with even terms are added to the model to represent the baseband effect as well. This addition is vital, especially for baseband representation. Baseband signal is created as a result of spectral regrowth. after spectral regrowth. So that the model is capable of modeling the thermal memory effect as well.

## 4.2 Model Architecture

Model function is defined in time domain in order to be compatible with all kinds of excitation signals and for ease of the higher-order-term additions. In contrast, it is easier to study in frequency domain phasor representation for two-tone excitation. OOM mathematical representation is as follows;

$$V_o(t) = \sum_{k=1}^K a_{2k-1} V_i^{2k-1}(t - \tau_{2k-1}) \quad (4.1)$$

where " $V_i$ " and " $V_o$ " represent time domain input and output signal, respectively. " $a_{2k-1}$ " represents model coefficients to be found. " $K$ " represents the maximum nonlinearity order and " $\tau_{2k-1}$ " represents time delay for that term. Block diagram of OOM is given in Figure 4.1. Since it is focused on IMD and FUND tones in this dissertation and even order terms do not have any contribution to IMD and FUND components, (4.1) contains only odd order terms. Also, this fact is proved mathematically in (2.23) and (2.24) on page 20 for GPSE modeling and (4.2) for OOM. Therefore, OOM does not contain any even order terms at IMD and FUND equations. Continuous wave two-tone signal definition as an input is given in (4.3). After setting  $K=5$ (i.e. model order is 9) and substituting continuous wave two-tone signal given in (4.3) into (4.1), phasor representation of IMD and FUND components become as

given in (4.4) (Phasor representation transformation for multiple frequency is explained on page 21).

$$\begin{aligned}
 a_2 V_i(t - \tau_2) &= a_2 (V_1 \cos(\omega_1(t - \tau_2)) + V_1 \cos(\omega_2(t - \tau_2)))^2 \\
 &= V_1^2 a_2 + \frac{1}{2} V_1^2 a_2 \cos(2\omega_1 t - 2\omega_1 \tau_2) + \frac{1}{2} V_1^2 a_2 \cos(2\omega_2 t - 2\omega_2 \tau_2) \\
 &+ V_1^2 a_2 \cos(\omega_1 t + \omega_2 t - \omega_1 \tau_2 - \omega_2 \tau_2) \\
 &+ V_1^2 a_2 \cos(\omega_1 t - \omega_2 t - \omega_1 \tau_2 + \omega_2 \tau_2)
 \end{aligned} \tag{4.2}$$

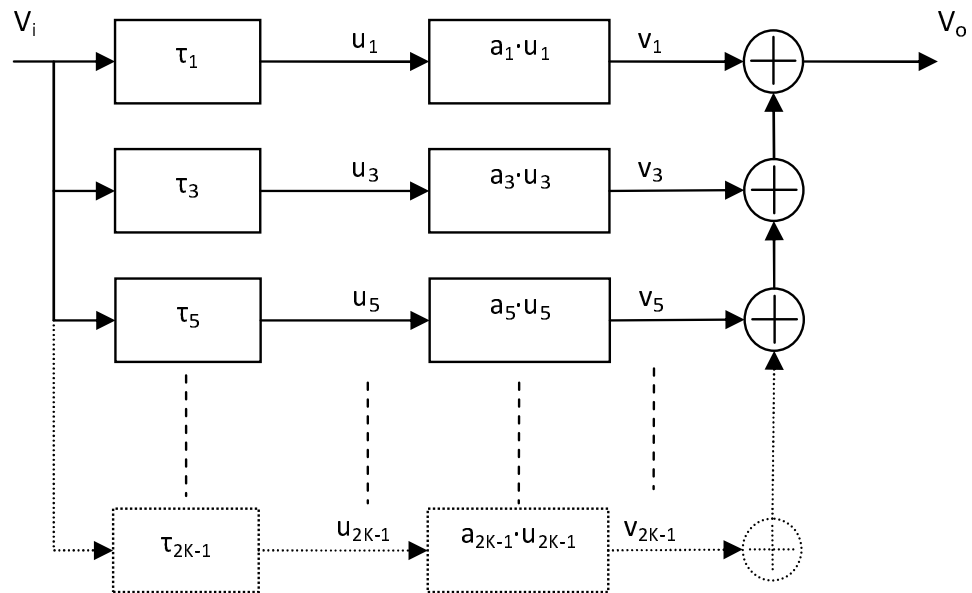


Figure 4.1: Block diagram representation of OOM

$$x(t) = V_1 \cdot \cos(\omega_1 t) + V_2 \cdot \cos(\omega_2 t) \tag{4.3}$$

$$V_o(t)|_{K=5} = a_1 V_i(t - \tau_1) + a_3 V_i^3(t - \tau_3) + a_5 V_i^5(t - \tau_5) + a_7 V_i^7(t - \tau_7) + a_9 V_i^9(t - \tau_9) \quad (4.4a)$$

$$V_o(t) = V_{FUNDL} \cdot \cos(\omega_1 t) + V_{FUNDU} \cdot \cos(\omega_2 t) + V_{IMDL} \cdot \cos(2\omega_1 t - \omega_2 t) + V_{IMDU} \cdot \cos(2\omega_2 t - \omega_1 t) + V_{2HL} \cos(2\omega_1 t) + V_{2HU} \cos(2\omega_2 t) + \dots \quad (4.4b)$$

$$V_{IMDL} = \frac{3}{4} a_3 V_1^3 \angle(-(2\omega_1 - \omega_2)\tau_3) + \frac{25}{8} a_5 V_1^5 \angle(-(2\omega_1 - \omega_2)\tau_5) + \frac{735}{64} a_7 V_1^7 \angle(-(2\omega_1 - \omega_2)\tau_7) + \frac{1323}{32} a_9 V_1^9 \angle(-(2\omega_1 - \omega_2)\tau_9) \quad (4.4c)$$

$$V_{IMDU} = \frac{3}{4} a_3 V_1^3 \angle(-(2\omega_2 - \omega_1)\tau_3) + \frac{25}{8} a_5 V_1^5 \angle(-(2\omega_2 - \omega_1)\tau_5) + \frac{735}{64} a_7 V_1^7 \angle(-(2\omega_2 - \omega_1)\tau_7) + \frac{1323}{32} a_9 V_1^9 \angle(-(2\omega_2 - \omega_1)\tau_9) \quad (4.4d)$$

$$V_{FUNDL} = a_1 V_1 \angle(-\omega_1 \tau_1) + \frac{9}{4} a_3 V_1^3 \angle(-\omega_1 \tau_3) + \frac{50}{8} a_5 V_1^5 \angle(-\omega_1 \tau_5) + \frac{1225}{64} a_7 V_1^7 \angle(-\omega_1 \tau_7) + \frac{3969}{64} a_9 V_1^9 \angle(-\omega_1 \tau_9) \quad (4.4e)$$

$$V_{FUNDU} = a_1 V_1 \angle(-\omega_2 \tau_1) + \frac{9}{4} a_3 V_1^3 \angle(-\omega_2 \tau_3) + \frac{50}{8} a_5 V_1^5 \angle(-\omega_2 \tau_5) + \frac{1225}{64} a_7 V_1^7 \angle(-\omega_2 \tau_7) + \frac{3969}{64} a_9 V_1^9 \angle(-\omega_2 \tau_9) \quad (4.4f)$$

The amplifier, measurement setup properties and measurement results are given in Chapter 3. Amplifier model is extracted by using these measurement results and comparison result with measurement results given in Figure 4.4. Although OOM modeling success is good in order to improve model success, even order terms are considered for the model.

If even terms are directly added to OOM, new model equation will be as given in (4.5). As it is stated previously and mathematically shown in (4.2), even terms, as given in (4.5), do not have any contribution to the IMD and FUND components. Therefore, some mathematical manipulation is required to get contribution from even terms to IMD and FUND components.

To do this,  $a_1$  and  $a_3$  coefficients are redefined as given in (4.6). Then if (4.6) is substituted in (4.1) by omitting prime sign and taking K as 3, modeling equation will become as in (4.7). The term having 6<sup>th</sup> order is omitted while (4.8a) is being written. The terms having red color font represent the contribution of the new added terms. These terms are considered as even order terms, due to  $V_{env} \cdot V_i$  multiplication. (4.6c) represents the two-tone envelope signal. IMD and FUND components are given in (4.8) after expanding the (4.7). Expanded version of each order term in (4.8a) is given in Appendix B. Even term contributions to the IMD and

FUND components can be seen at Appendix B as well.

Although work presented up to now is a passband modeling, this modeling can also be used in baseband modeling. There is no requirement to make modification on passband model equation to use in baseband; defining  $V_i$  and  $V_o$  in baseband is enough, some modification may be applied to improve model performance, but it is not necessary indeed. Another measurement setup and model extraction procedure should be used.

$$V_o(t) = \sum_{k=1}^5 a_k V_i^k(t - \tau_k) \quad (4.5a)$$

$$V_o(t) = a_1 V_i(t - \tau_1) + a_2 V_i^2(t - \tau_2) + a_3 V_i^3(t - \tau_3) + a_4 V_i^4(t - \tau_4) + a_5 V_i^5(t - \tau_5) \quad (4.5b)$$

$$a_1 = a_1' + a_2 \cdot V_{env}(t - \tau_1) \quad (4.6a)$$

$$a_3 = a_3' + a_4 \cdot V_{env}(t - \tau_3) \quad (4.6b)$$

$$V_{env}(t) = \frac{4V_1}{\pi} + \frac{8V_1}{\pi} \cos(\Delta\omega t) - \frac{8V_1}{15\pi} \cos(2\Delta\omega t) + \frac{8V_1}{35\pi} \cos(3\Delta\omega t) + \frac{8V_1}{63\pi} \cos(4\Delta\omega t) \quad (4.6c)$$

where  $\Delta\omega = |\omega_1 - \omega_2|$

$$V_o(t) = \sum_{k=1}^K (a_{2k-1} + a_{2k} \cdot V_{env}(t - \tau_{2k-1})) V_i^{2k-1}(t - \tau_{2k-1}) \quad (4.7)$$

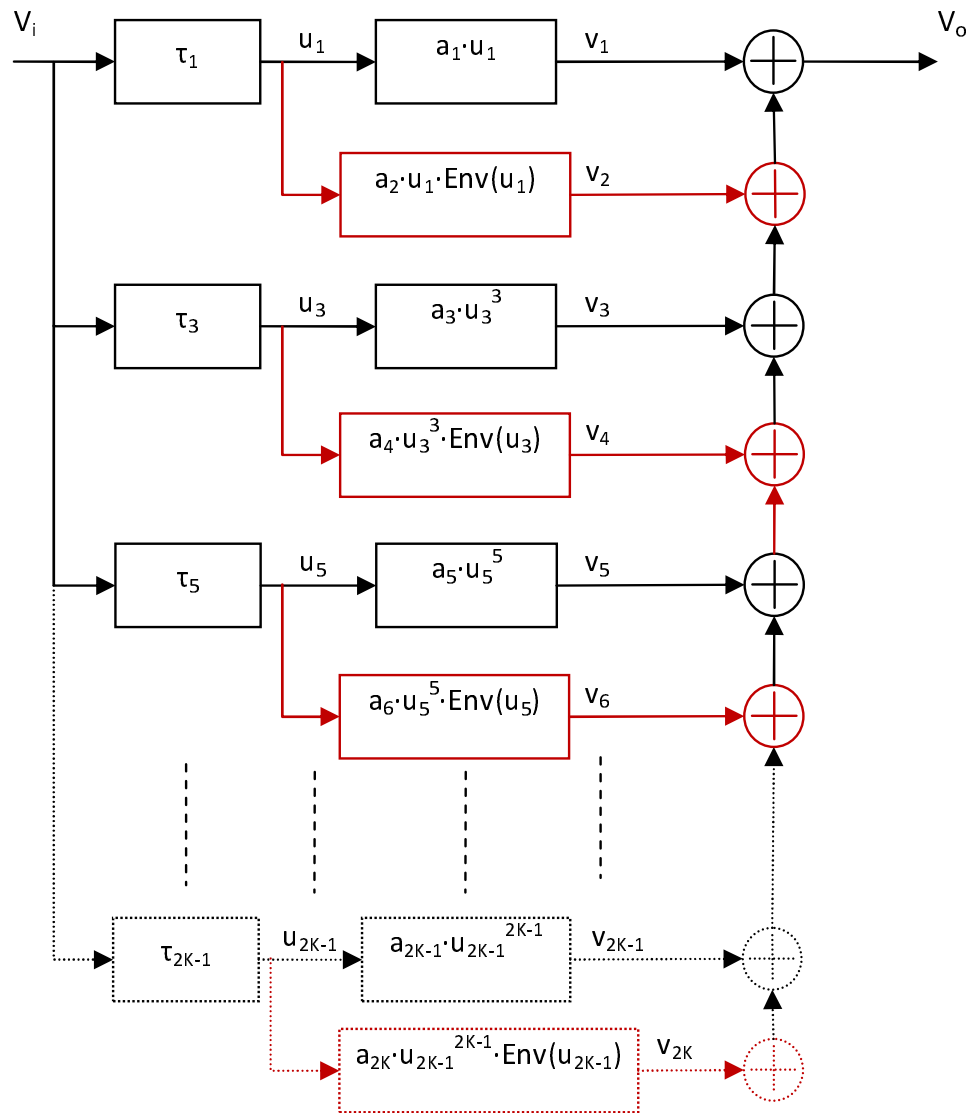


Figure 4.2: Power series with unequal time delay behavioral model with even order terms

$$V_o(t)|_{K=3} = (a_1 + a_2 V_{env}(t - \tau_1)) V_i(t - \tau_1) \quad (4.8a)$$

$$+ (a_3 + a_4 V_{env}(t - \tau_3)) V_i^3(t - \tau_3) + a_5 V_i^5(t - \tau_5)$$

$$V_{IMDL} = \frac{16}{15\pi} a_2 V_1^2 \angle(-(2\omega_1 - \omega_2)\tau_1) + \frac{3}{4} a_3 V_1^3 \angle(-(2\omega_1 - \omega_2)\tau_3) \quad (4.8b)$$

$$+ \frac{192}{35\pi} a_4 V_1^4 \angle(-(2\omega_1 - \omega_2)\tau_3) + \frac{25}{8} a_5 V_1^5 \angle(-(2\omega_1 - \omega_2)\tau_5)$$

$$V_{IMDU} = \frac{16}{15\pi} a_2 V_1^2 \angle(-(2\omega_2 - \omega_1)\tau_1) + \frac{3}{4} a_3 V_1^3 \angle(-(2\omega_2 - \omega_1)\tau_3) \quad (4.8c)$$

$$+ \frac{192}{35\pi} a_4 V_1^4 \angle(-(2\omega_2 - \omega_1)\tau_3) + \frac{25}{8} a_5 V_1^5 \angle(-(2\omega_2 - \omega_1)\tau_5)$$

$$V_{FL} = a_1 V_1 \angle(-\omega_1\tau_1) + \frac{16}{3\pi} a_2 V_1^2 \angle(-\omega_1\tau_1) \quad (4.8d)$$

$$+ \frac{9}{4} a_3 V_1^3 \angle(-\omega_1\tau_3) + \frac{64}{5\pi} a_4 V_1^4 \angle(-\omega_1\tau_3) + \frac{50}{8} a_5 V_1^5 \angle(-\omega_1\tau_5)$$

$$V_{FL} = a_1 V_1 \angle(-\omega_2\tau_1) + \frac{16}{3\pi} a_2 V_1^2 \angle(-\omega_2\tau_1) \quad (4.8e)$$

$$+ \frac{9}{4} a_3 V_1^3 \angle(-\omega_2\tau_3) + \frac{64}{5\pi} a_4 V_1^4 \angle(-\omega_2\tau_3) + \frac{50}{8} a_5 V_1^5 \angle(-\omega_2\tau_5)$$

#### 4.2.1 Asymmetry Creation

If the order of OOM model is limited to  $K=3$  and 6<sup>th</sup> order is omitted, model equation will be as given in (4.9) and IMD and FUND components will be as given in (4.10) for unequal two-tone excitation (input signal representation is given in (2.6)).

$$V_o(t) = a_1 V_i(t - \tau_1) + a_3 V_i^3(t - \tau_3) + a_5 V_i^5(t - \tau_5) \quad (4.9)$$

$$V_{IMDL} = \frac{3}{4}a_3V_1^2V_2\angle(-(2\omega_1 - \omega_2)\tau_3) + \frac{5}{4}a_5\left[V_1^4V_2 + \frac{3}{2}V_1^2V_2^3\right]\angle(-(2\omega_1 - \omega_2)\tau_5) \quad (4.10a)$$

$$V_{IMDU} = \frac{3}{4}a_3V_1V_2^2\angle(-(2\omega_2 - \omega_1)\tau_3) + \frac{5}{4}a_5\left[V_1V_2^4 + \frac{3}{2}V_1^3V_2^2\right]\angle(-(2\omega_2 - \omega_1)\tau_5) \quad (4.10b)$$

$$V_{FUNDL} = a_1V_1\angle(-\omega_1\tau_1) + a_3\left[\frac{3}{4}V_1^3 + \frac{3}{2}V_1V_2^2\right]\angle(-\omega_1\tau_3) + a_5\left[\frac{5}{8}V_1^5 + \frac{15}{8}V_1V_2^4 + \frac{15}{4}V_1^3V_2^2\right]\angle(-\omega_1\tau_5) \quad (4.10c)$$

$$V_{FUNDU} = a_1V_2\angle(-\omega_2\tau_1) + a_3\left[\frac{3}{4}V_2^3 + \frac{3}{2}V_1^2V_2\right]\angle(-\omega_2\tau_3) + a_5\left[\frac{5}{8}V_2^5 + \frac{15}{8}V_1^4V_2 + \frac{15}{4}V_1^2V_2^3\right]\angle(-\omega_2\tau_5) \quad (4.10d)$$

If equal amplitude excitation is assumed ( $V_1 = V_2$ ), (4.10a) and (4.10b) become as (4.11a) and (4.11b), respectively. It is obvious that IMDL and IMDU are composed of two vectors. If the term containing  $a_3$  named as  $\vec{A}$  and the term containing  $a_5$  named as  $\vec{B}$ , (4.11) becomes as (4.12). Magnitudes of  $\overline{A_L}$  and  $\overline{A_U}$  are equal but phases are different. In other words, IMDL and IMDU consist of two vectors. Assume there is a vector, namely  $\vec{c}$ , consisting the addition of other two vectors such as  $\vec{a}$  and  $\vec{b}$ . It is obvious from geometry that, if the phase of  $\vec{a}$  or  $\vec{b}$  is changed, magnitude and phase of new vector will not be equal to  $\vec{c}$ .

To sum up, IMDL and IMDU components consist of two vectors such that the vectors of IMDL has equal magnitude but different phase compared with the of IMDU. Thus, there should be asymmetry in both the magnitude and the phase of IMDL and IMDU as represented in Figure 4.3.

This situation is valid for FUNDL and FUNDU components as well.

$$V_{IMDL} = \frac{3}{4}a_3V_1^3\angle(-(2\omega_1 - \omega_2)\tau_3) + \frac{25}{8}a_5V_1^5\angle(-(2\omega_1 - \omega_2)\tau_5) \quad (4.11a)$$

$$V_{IMDU} = \frac{3}{4}a_3V_1^3\angle(-(2\omega_2 - \omega_1)\tau_3) + \frac{25}{8}a_5V_1^5\angle(-(2\omega_2 - \omega_1)\tau_5) \quad (4.11b)$$

$$\begin{aligned}
V_{IMDL} &= \overline{A_L} + \overline{B_L} \\
&= |\overline{A_L}| \angle (-(2\omega_1 - \omega_2) \tau_3) + |\overline{B_L}| \angle (-(2\omega_1 - \omega_2) \tau_5)
\end{aligned} \tag{4.12a}$$

$$\begin{aligned}
V_{IMDU} &= \overline{A_U} + \overline{B_U} \\
&= |\overline{A_U}| \angle \alpha (-(2\omega_2 - \omega_1) \tau_3) + |\overline{B_U}| \angle \alpha (-(2\omega_2 - \omega_1) \tau_5)
\end{aligned} \tag{4.12b}$$

where  $\alpha = \frac{2\omega_2 - \omega_1}{\omega_1 - \omega_2}$  and  $|\overline{A_L}| = |\overline{A_U}| = \frac{3}{4} a_3 V_1^3$ ,  $|\overline{B_L}| = |\overline{B_U}| = \frac{25}{8} a_5 V_1^5$ .

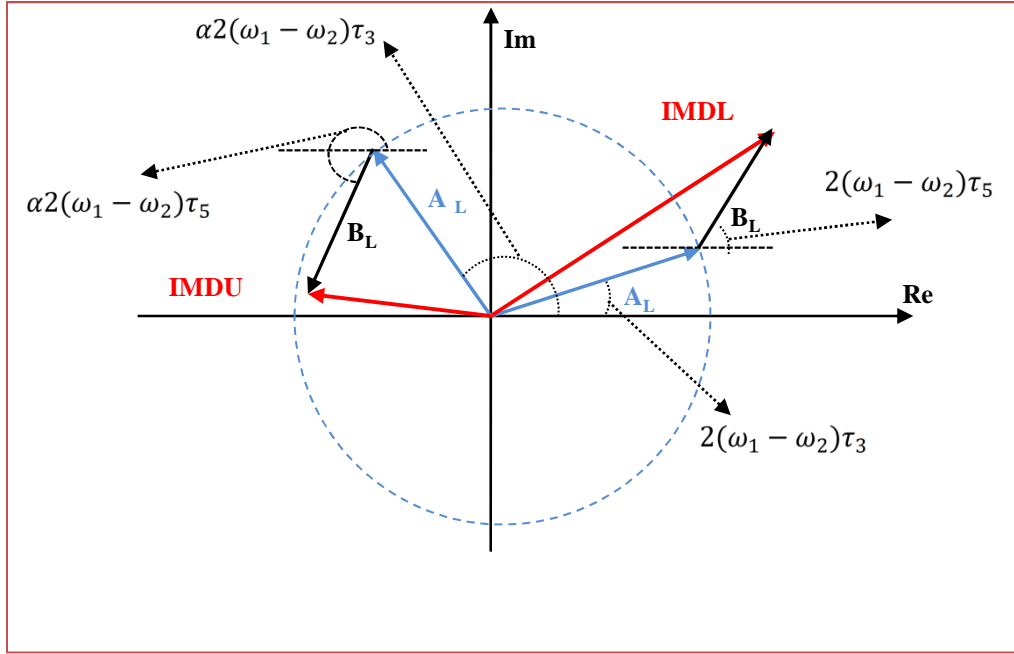


Figure 4.3: Asymmetry creation mechanism

### 4.3 Extraction Procedure for Modeling

As it is explained in section 2.1 on page 5 behavioral model is defined as a multidimensional curve fitting. Model parameter value can be found after a successful curve fitting procedure. All coefficients given in (4.7) are found at the same time according to extraction procedure for this new modeling technique instead of one-by-one. In contrast, there is an easier method which can be applied to limit coefficient value and can reduce the time required for model extraction. For example;  $a_1$  value is supposed to be close to the amplifier's small signal gain.

Two-tone continuous wave is used as an excitation(input) signal. A time aligned two-tone

signal is created by signal generators which are shown in Figure 3.1. Magnitudes and phases of IMD and FUND signals are measured from the output signal. After finishing all the measurement, corresponding model parameters can be found.

The coefficients  $a_k$  and  $\tau_k$  which are used for OOM&EOM modeling are found by equating the measurement results and (4.4)&(4.8) for both magnitude and phase for four different components (IMDL, IMDU, FUNDL and FUNDU). Since the equations are not linear, the coefficients cannot be found arithmetically. Therefore, the coefficients are found by using optimization tool of MATLAB program. A special program is written for this purpose. One of the MATLAB commands, "fmincon" constrained minimization function, is used in order to use limitation for coefficients. Least mean square cost function is used for optimization because there are four different components (IMDL, IMDU, FUNDL and FUNDU) which should be fit at the same time (i.e. using the same coefficient).

Amplifier response for a two-tone excitation signal is measured for approximately 16 dB dynamic range as given in Chapter 3. In order to diminish noise effect measurement is repeated number of times then they are averaged. The coefficients are listed in table at the succeeded section.

#### **4.4 NMSE Metric for Model Comparison**

Model parameters are found after multi dimensional curve fitting processes. An optimization technique is used to fit four components' estimation to the measurement result. A metric is needed to express the fitting success. There are a number of metrics published in the literature. The metrics which are mostly used are summarized in [50]; "Normalized Mean Square Error(NMSE), Memory Effect Modeling Ratio (MEMR), Adjacent Channel Error Power Ratio (ACPR) and Normalized Absolute Mean Spectrum Error (NAMSE)" [50].

In this thesis, NMSE which is reviewed below is used to evaluate the success of the model in passband.

Normalized mean square error (NMSE) is the metric which indicates the overall accuracy of a PA modeling for a single tone. In other words, NMSE value represents the model accuracy for a predefined dynamic range. Mathematical representation of NMSE is given as follows:

$$NMS E = 10 \log \left( \text{mean} \frac{|V_{meas} - V_{est}|^2}{|V_{meas}|^2} \right) \quad (4.13)$$

where  $V_{meas}$  and  $V_{est}$  represent the measured and estimated output signals.

## 4.5 Verification and Model Comparison

Model parameters are found by using optimization tool of Matlab program. Cost function for optimization is defined as to minimize least mean square error. Although optimization program suggests a solution this may not be the best one. In other words, optimization may be trapped to a local minima. Therefore extracted model is verified by comparing other modeling technique's results and other excitation situations. GPSE modeling technique is used for comparison.

GPSE modeling coefficients are tabulated in Table 4.1 which are extracted by using the measurement results of  $10MHz/1kHz$  excitation signal. OOM modeling coefficients are tabulated in Table 4.2 which are extracted by using the measurement results of  $10MHz/1kHz$  excitation signal. Comparison between OOM model estimations and magnitudes/phases of measurement results of four components (IMDL, IMDU, FUNDL and FUNDU) are given in Figure 4.4.

EOM modeling coefficients are tabulated in Table 4.3 which are extracted by using the measurement results of  $10MHz/1kHz$  excitation signal. Comparison between EOM model estimations and magnitudes/phases of measurement results, four components (IMDL, IMDU, FUNDL and FUNDU) are given in Figure 4.5. Comparison between EOM model estimations and magnitudes/phases of measurement for one tone excitation are given in Figure 4.6 as well.

Table 4.1: The coefficients of GPSE modeling extracted by using measurement results of  $10MHz/1kHz$

$a_1$	$a_2$	$a_3$	$a_4$	$a_5$	$a_7$	$a_9$
161.77+17i	0	73+15i	0	-83-10i	15+5i	2+2i

There is a sweet-spot point in the magnitude of IMDU, but there is not for IMDL for the measurement results of  $10MHz/1kHz$  excitation. Moreover, although there is a 10dB asymmetry

Table 4.2: The coefficients of OOM modeling extracted by using measurement results of 10MHz/1kHz

$a_1$	$a_2$	$a_3$	$a_4$	$a_5$	$a_7$	$a_9$
161	0	77.91	0	137	56.1	8.97
$\tau_1(\mu sec)$		$\tau_3(\mu sec)$		$\tau_5(\mu sec)$	$\tau_7(\mu sec)$	$\tau_9(\mu sec)$
0.00		25.8		4.059	2.717	10.183

Table 4.3: The coefficients of EOM modeling extracted by using measurement results of 10MHz/1kHz

$a_1$	$a_2$	$a_3$	$a_4$	$a_5$	$a_7$	$a_9$
156.2	25.2	54.38	-27.67	36.02	0	0
$\tau_1(\mu sec)$		$\tau_3(\mu sec)$		$\tau_5(\mu sec)$	$\tau_7(\mu sec)$	$\tau_9(\mu sec)$
0.00		34.43		0.272	0	0

between magnitude of IMDL and IMDU, OOM model behavior is similar to the amplifier behavior as shown in Figure 4.4a and Figure 4.4b. While maximum error for magnitude of IMDL is 5dB for the considered dynamic range, this maximum error increased to 10dB for magnitude of IMDU in the high power excitation situation. This error may be decreased by increasing the model order but this is not a desired solution due to simple model requirement. There is a small error in the magnitude and phase of fundamental components as shown in Figure 4.4c and Figure 4.4c. Although there is big error in magnitude of IMDU, error in the phase is small. Despite all this error, OOM represent asymmetry better than GPSE model representation. While the NMSE for IMDL of GPSE model estimation approximately 1.3dB better than the NMSE for IMDL of OOM model, OOM model estimation for IMDU is approximately 6dB better as shown in Table 4.4.

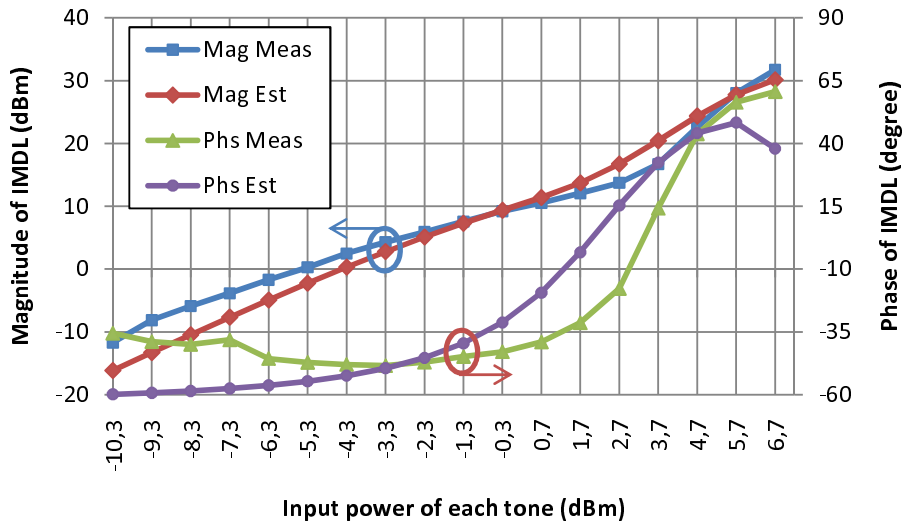
OOM model improved model estimation, although the improvement is limited. Then EOM model is developed to improve model estimation noticeably. There is always less than 1.3dB error for the whole dynamic range, except 4.7dBm input power level both for magnitude of IMDL and IMDU as given in Figure 4.5. This error is acceptable for the case of 10dB asymmetry. Phase of IMDL and IMDU estimation of EOM is also very good. There is approximately 15° error for phase of IMDU for high input power level, but this is not a big error if it is considered that total change in the phase is more than 150°. Estimation of intermodulation distortion is improved more than 10dB by EOM modeling w.r.t. the GPSE estimation

as shown in Table 4.4.

In order to visualize the improvement in the estimation of four components, measurement results and the outputs of three modeling techniques are plotted on the same graph separately for four components as given in Figure 4.7-Figure 4.10. Although the EOM model is using lower order than the other modeling technique, EOM always gives the best result. Since it is focused on to model asymmetry in the intermodulation component in this thesis, the others sometime gives better result at the estimation of **fundamental components** then EOM estimation. But, improvement of EOM's intermodulation distortion asymmetry modeling performance is much more better than in the fundamental asymmetry estimation. In order to emphasize the asymmetry modeling success of EOM, measurement results and EOM model estimation both for IMDL and for IMDU are plotted in the same graph as given in Figure 4.12. EOM model gives a small error for high excitation power level. Although there is a small error, EOM output behavior is similar to the amplifier behavior and behavior of the magnitude of the IMD estimated by EOM for high power level is follows the measurement result, and is not diverging to illogical power level.

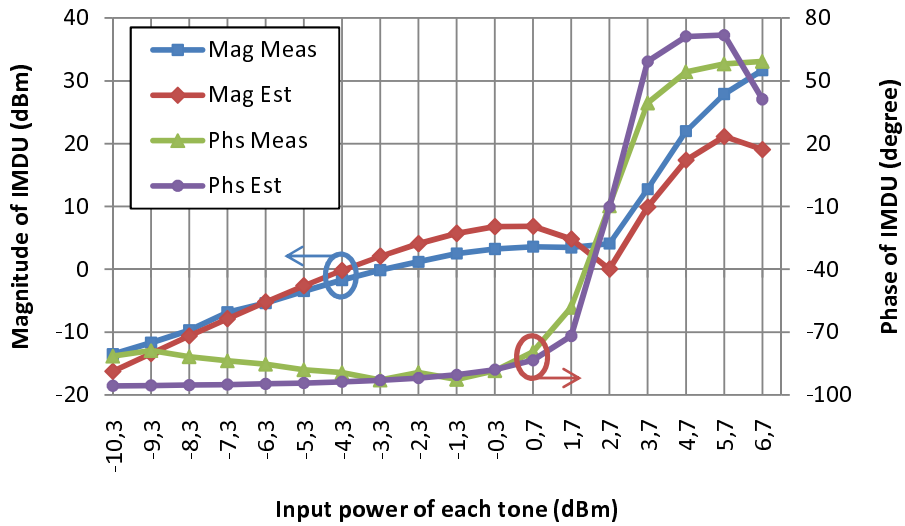
Effect of even order term addition to modeling equation can be seen from Figure 4.7 and Figure 4.8.

### IMDL@10MHz with 1kHz Spacing

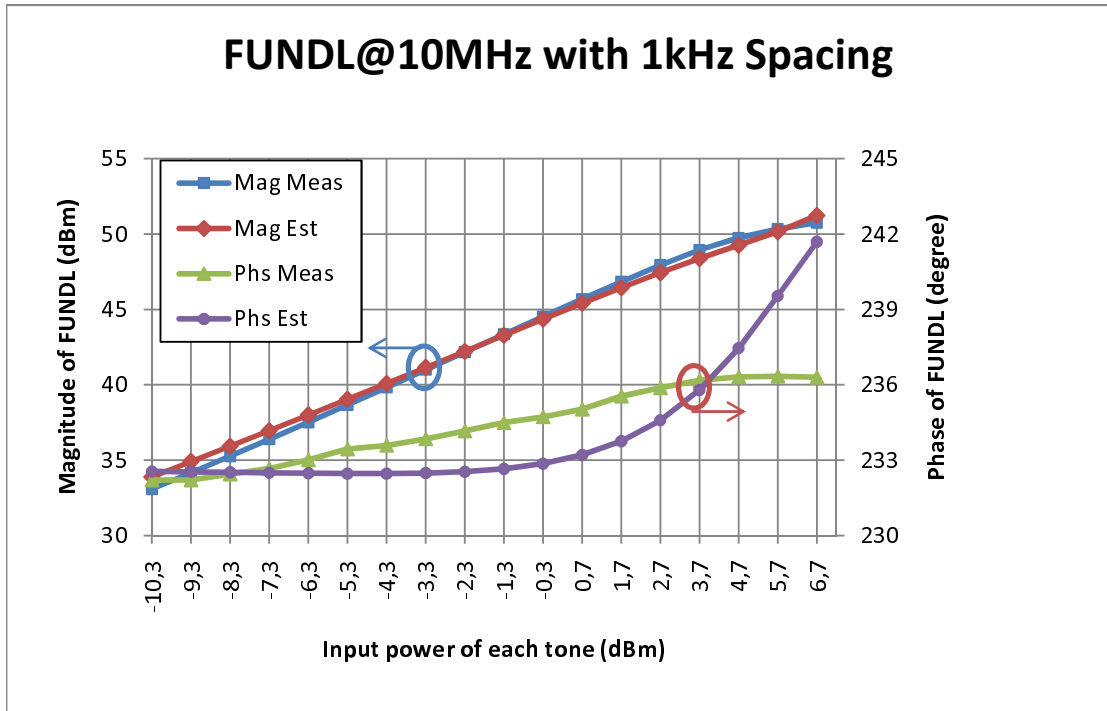


(a) Comparison of magnitude of and phase of IMDL which is estimated by OOM model

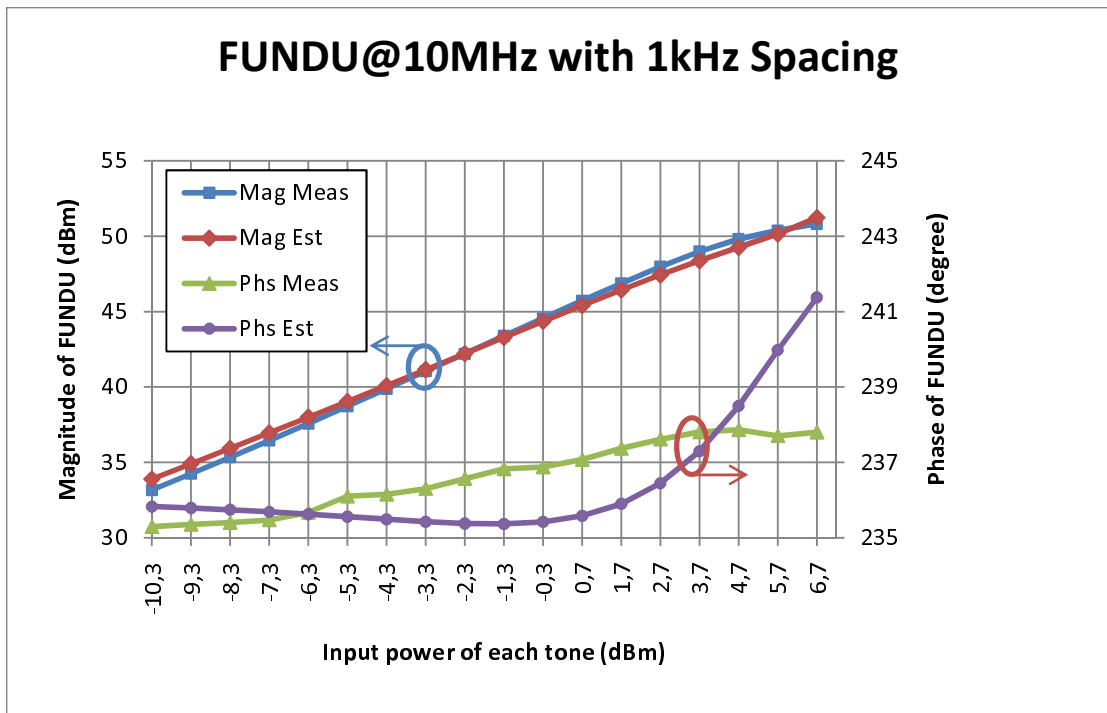
### IMDU@10MHz with 1kHz Spacing



(b) Comparison of magnitude of and phase of IMDU which is estimated by OOM model



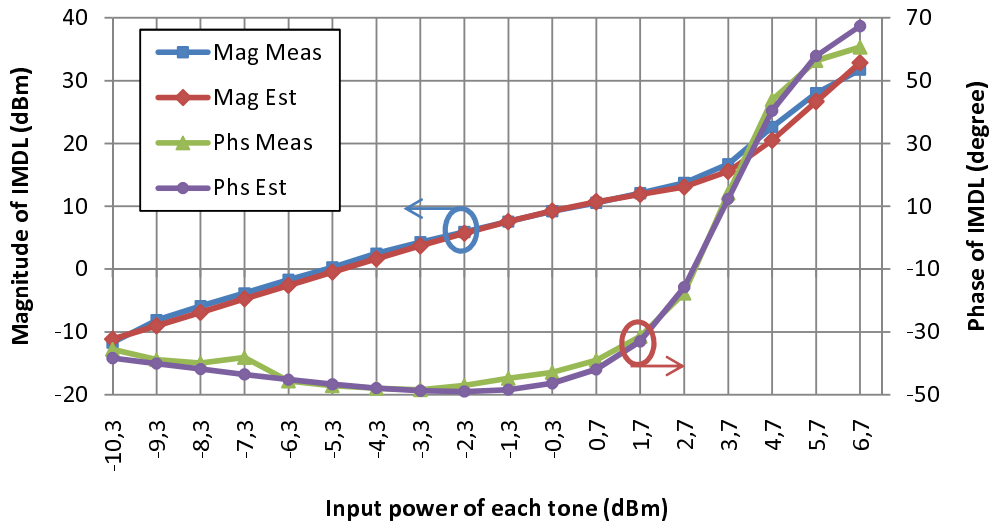
(c) Comparison of magnitude and phase of FUNDL which is estimated by OOM model



(d) Comparison of magnitude and phase of FUNDU which is estimated by OOM model

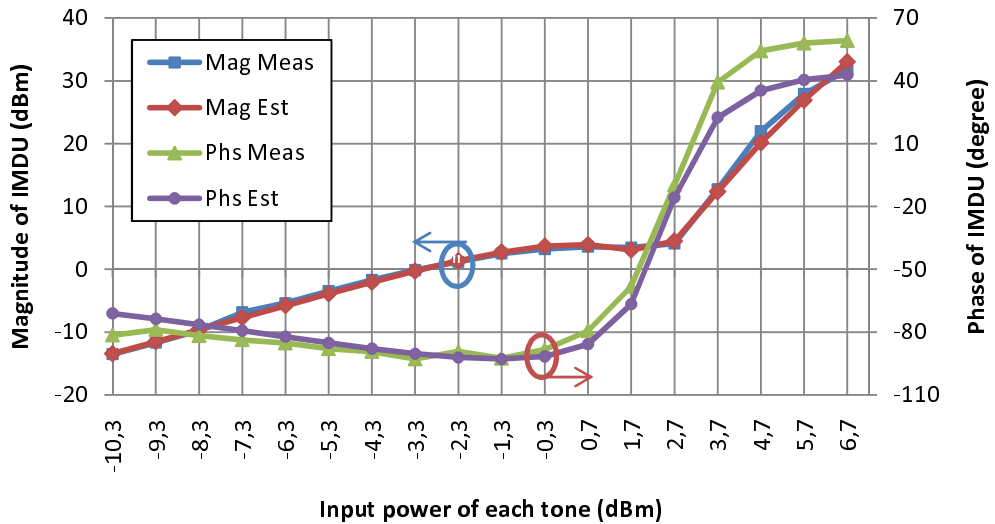
Figure 4.4: Comparison between magnitudes and phases of measurement and OOM model outputs for 10MHz/1kHz input excitation for a) ImdL b) ImdU c) FundL and d) FundU components

### IMDL@10MHz with 1kHz Spacing

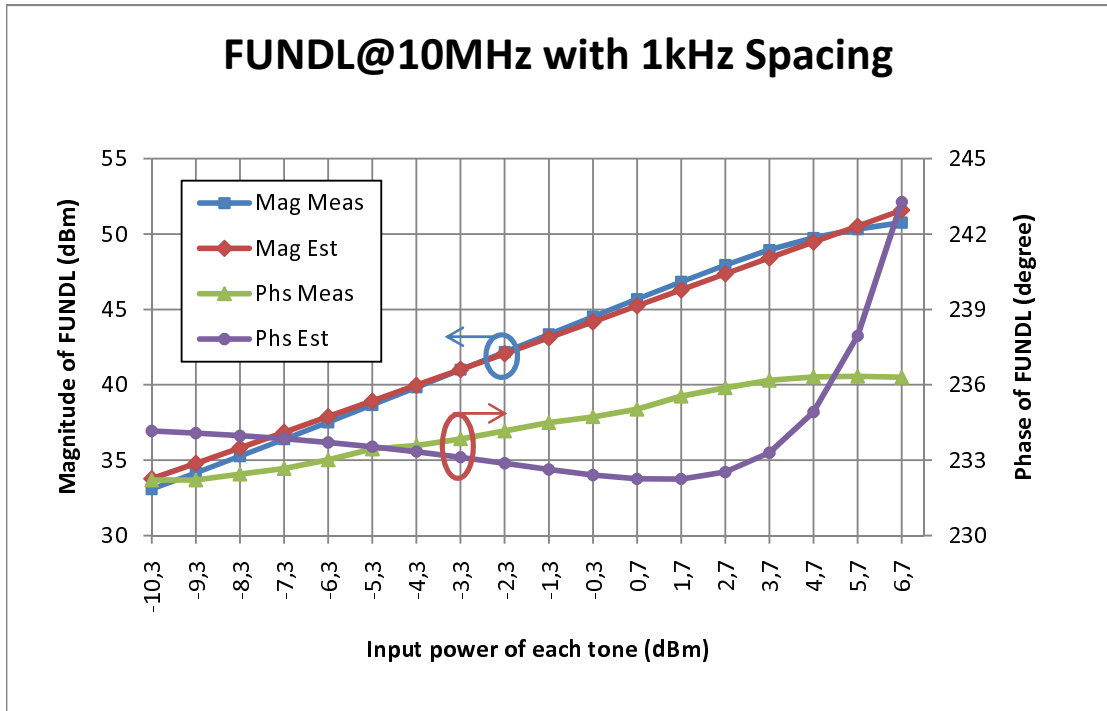


(a) Comparison of magnitude and phase of IMDL which is estimated by EOM model

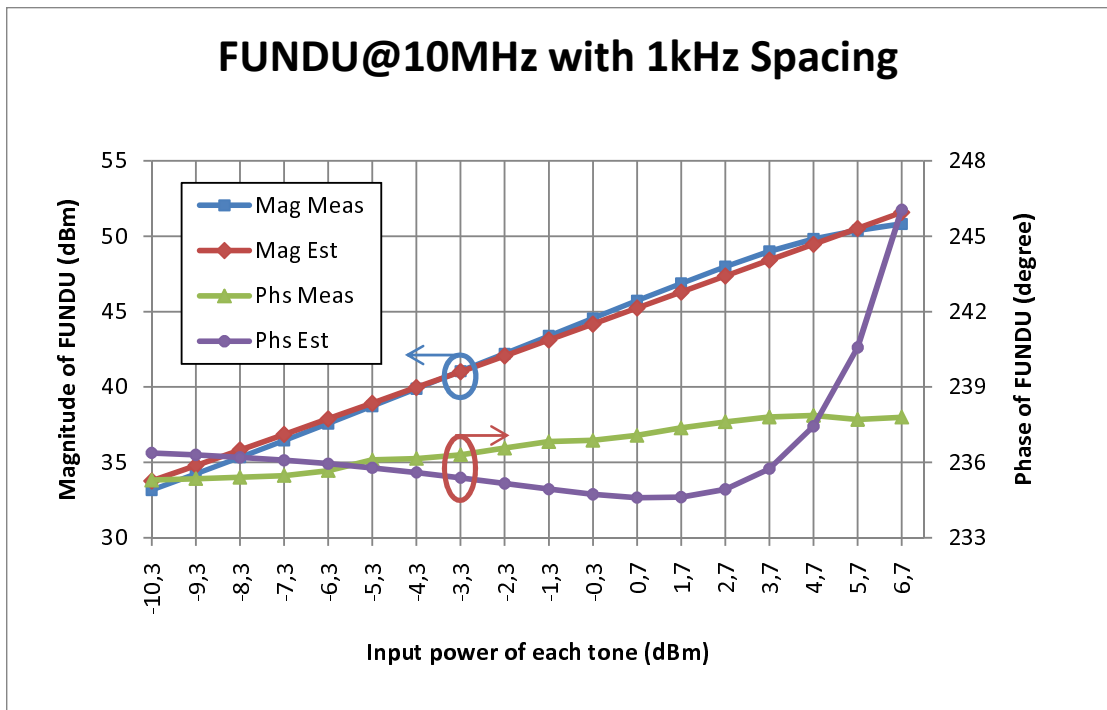
### IMDU@10MHz with 1kHz Spacing



(b) Comparison of magnitude and phase of IMDU which is estimated by EOM model



(c) Comparison of magnitude and phase of FUNDL which is estimated by EOM model



(d) Comparison of magnitude and phase of FUNDU which is estimated by EOM model

Figure 4.5: Comparison between magnitudes and phases of measurement and EOM model outputs for 10MHz/1kHz input excitation for a) ImdL b) ImdU c) FundL and d) FundU components

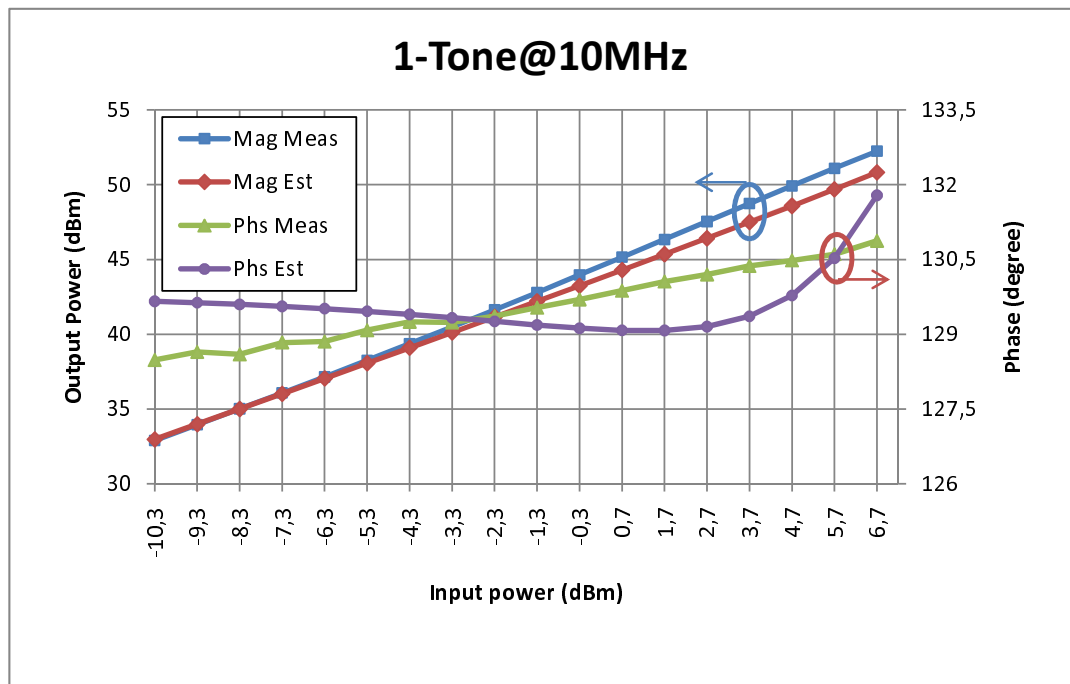
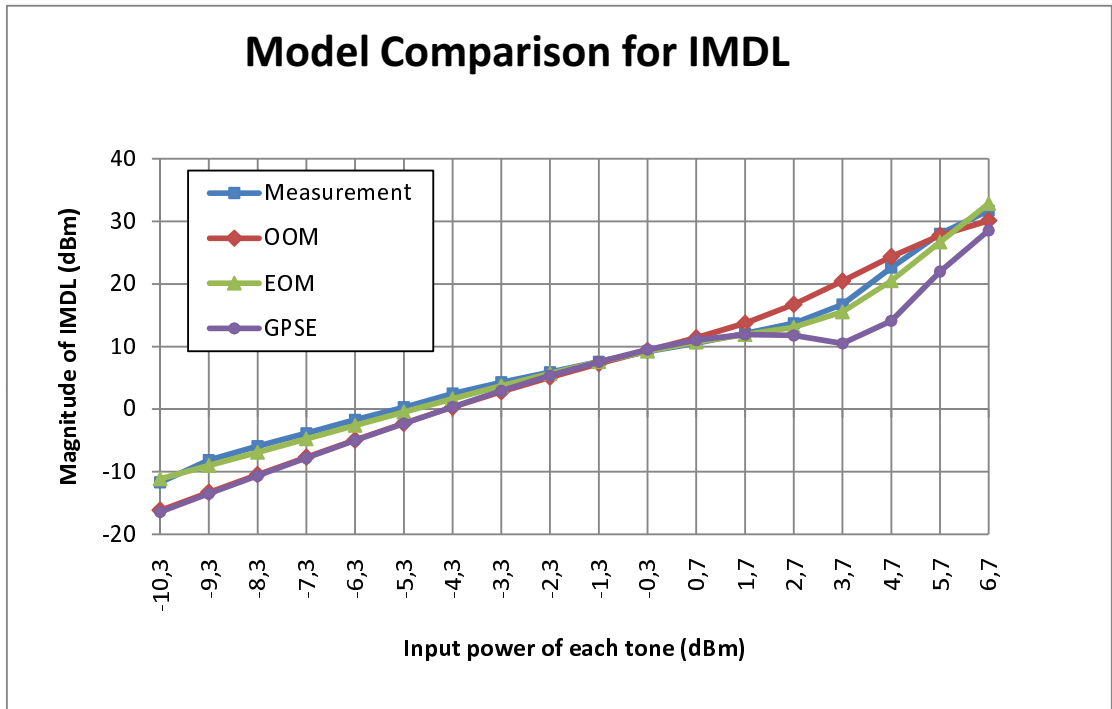


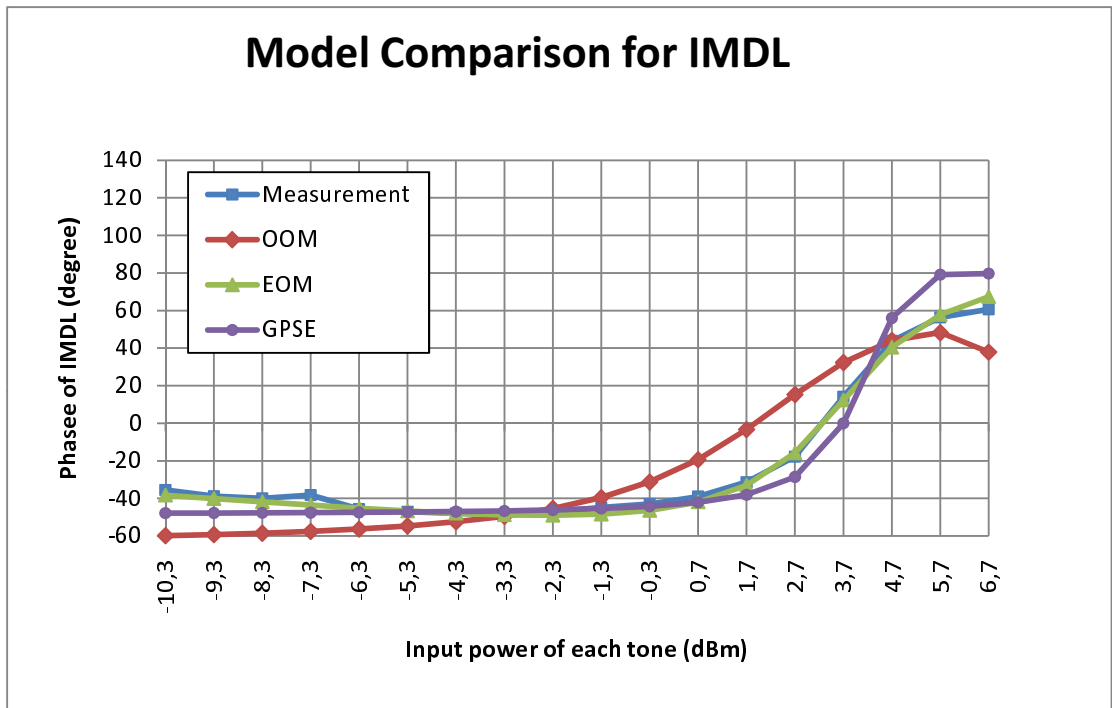
Figure 4.6: Comparison between magnitudes and phases of measurement and EOM model outputs for 10MHz one-tone excitation

Table 4.4: NMSE values

$f_c/\Delta f$	Component	GPSE	OOM	EOM
10MHz/1kHz	IMDL	-8.74	-7.45	-18.94
	IMDU	-1.90	-7.80	-13.68
	FUNDL	-24.73	-23.31	-23.07
	FUNDU	-25.37	-24.55	-22.88
8MHz/1kHz	IMDL	-9.03	-6.10	-15.53
	IMDU	-2.04	-3.22	-10.31
	FUNDL	-14.09	-14.52	-14.80
	FUNDU	-14.66	-15.50	-15.90
9MHz/1kHz	IMDL	-9.53	-6.52	-17.34
	IMDU	-1.00	-4.92	-13.27
	FUNDL	-13.88	-14.27	-14.55
	FUNDU	-14.41	-15.17	-15.57
11MHz/1kHz	IMDL	-10.34	-6.42	-13.41
	IMDU	3.93	-1.85	-2.80
	FUNDL	-13.30	-13.63	-13.87
	FUNDU	-13.69	-14.30	-14.65
12MHz/1kHz	IMDL	-10.36	-5.94	-9.86
	IMDU	7.40	3.16	2.21
	FUNDL	-13.18	-13.47	-13.72
	FUNDU	-13.56	-14.11	-14.47
10MHz/300Hz	IMDL	1.22	4.35	2.70
	IMDU	-5.75	-5.37	-8.75
	FUNDL	-17.00	-17.43	-18.17
	FUNDU	-17.36	-17.94	-18.67
10MHz/3.3kHz	IMDL	-5.90	-1.15	-3.25
	IMDU	0.17	12.83	8.61
	FUNDL	-18.82	-20.63	-20.53
	FUNDU	-19.13	-19.84	-19.51

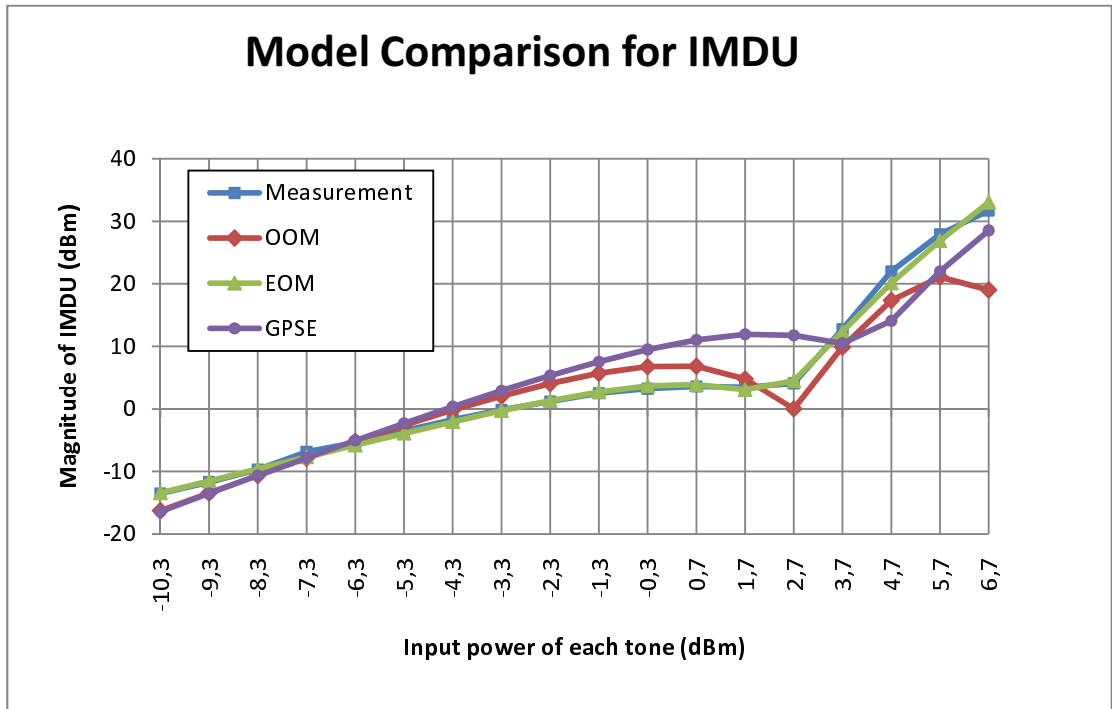


(a) Magnitude of IMDL

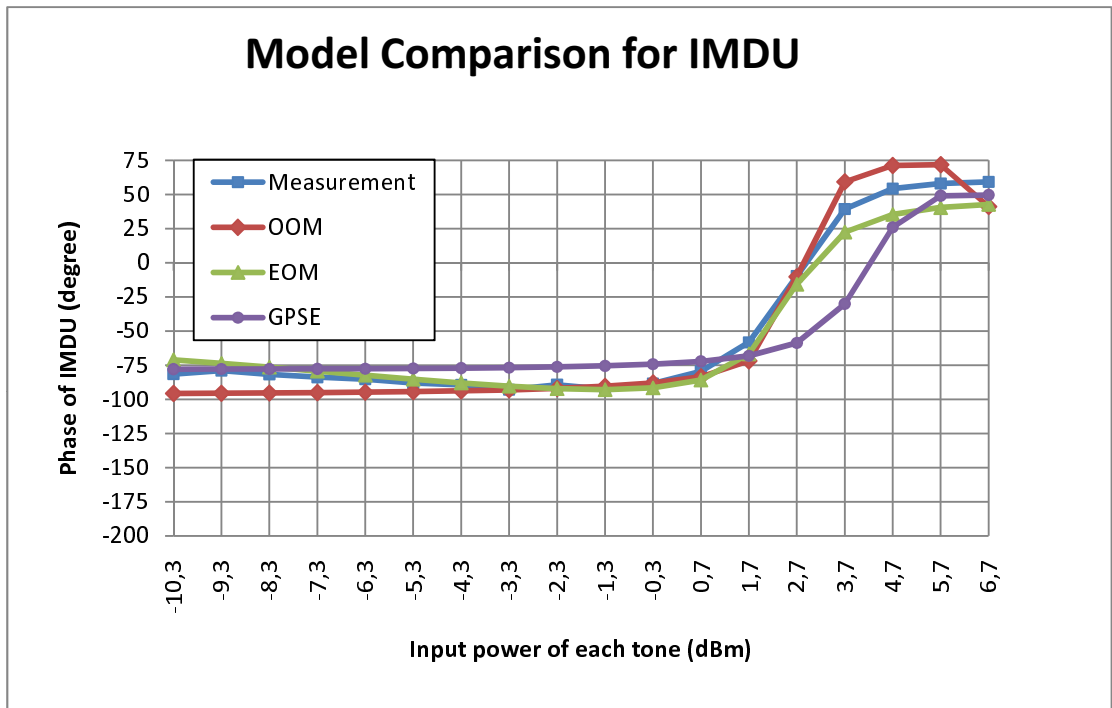


(b) Phase of IMDL

Figure 4.7: Comparison of three modeling for a) magnitude and b) phase of IMDL component for 10MHz/1kHz excitation signal

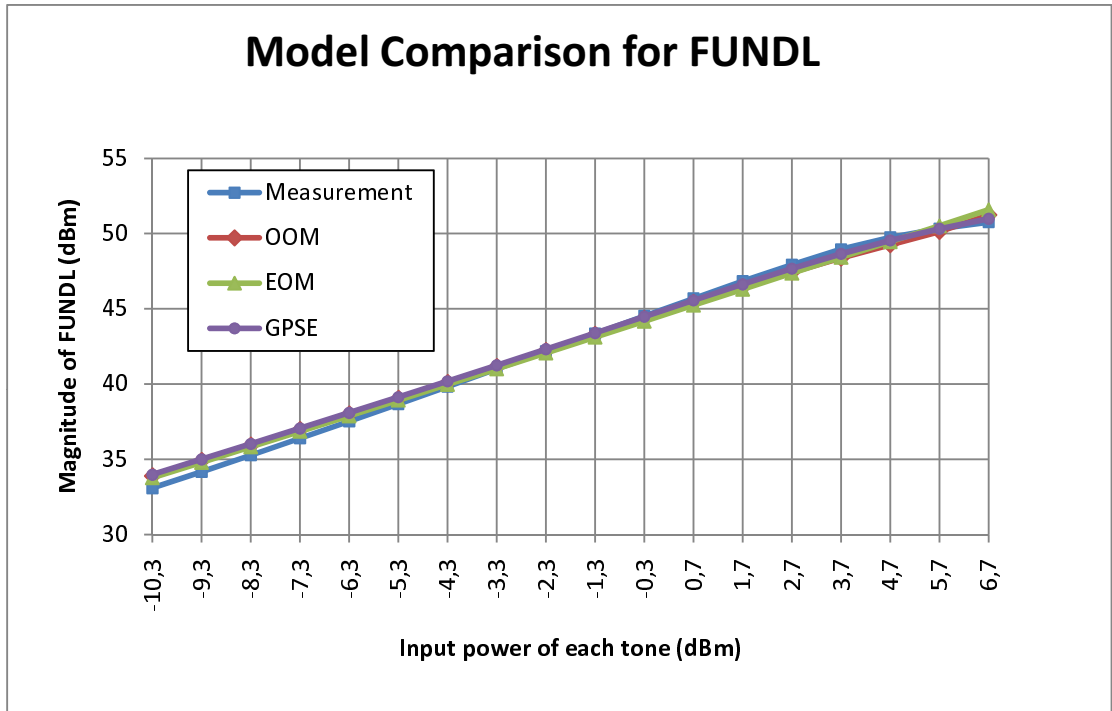


(a) Magnitude of IMDU

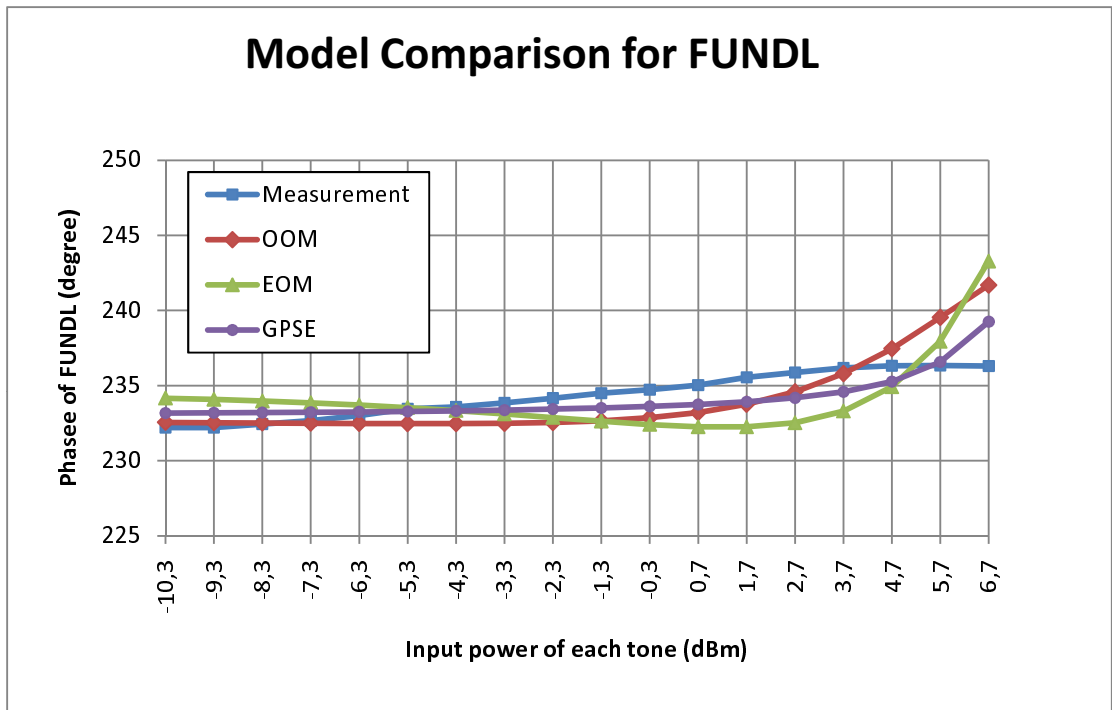


(b) Phase of IMDU

Figure 4.8: Comparison of three modeling for a) magnitude and b) phase of IMDU component for 10MHz/1kHz excitation signal



(a) Magnitude of FUNDL



(b) Phase of FUNDL

Figure 4.9: Comparison of three modeling for a)magnitude and b)phase of FUNDL component for 10MHz/1kHz excitation signal

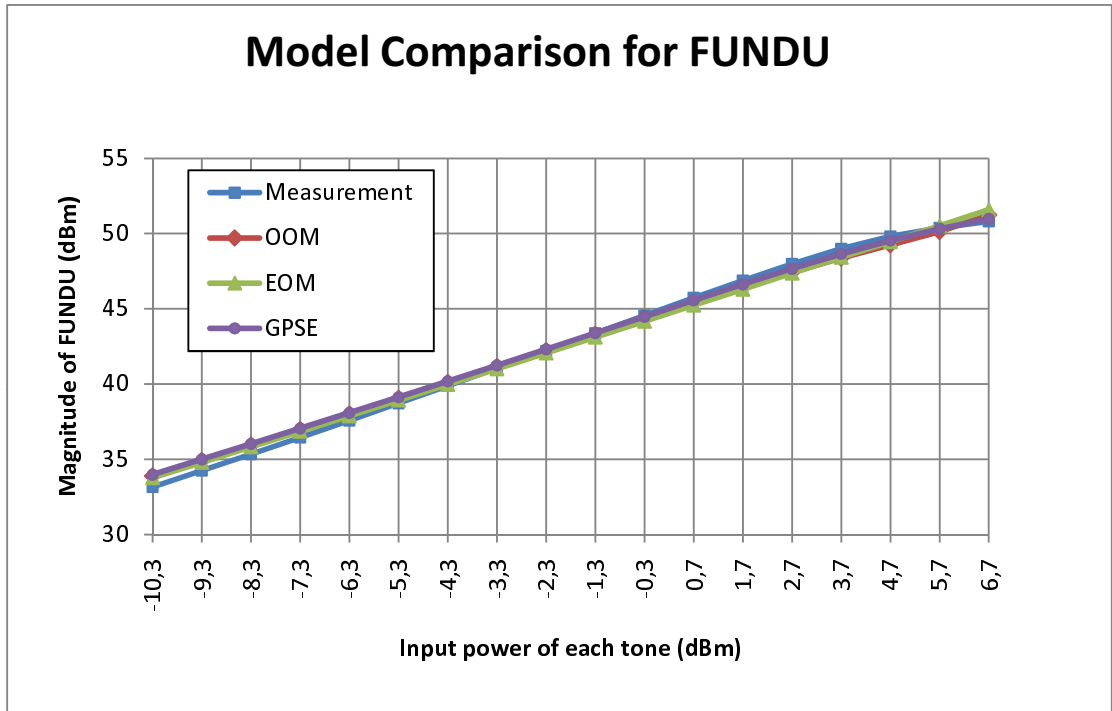
## 4.6 EOM Model Validity Range

### 4.6.1 EOM Model Validity Range Investigation for Two-Tone excitation

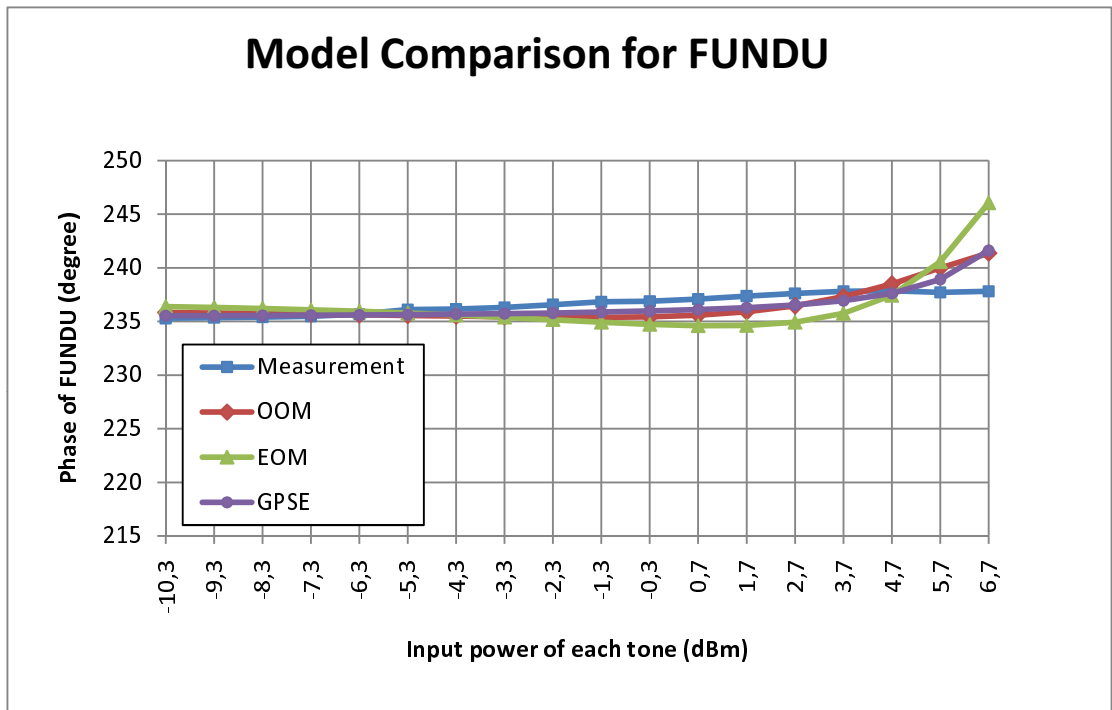
EOM model coefficients are found according to the measurement results of two-tone excitation. EOM model gives acceptable results for  $10\text{MHz}/1\text{kHz}$  two-tone excitation. Firstly, EOM model outputs for  $8\text{MHz}/1\text{kHz}$ ,  $9\text{MHz}/1\text{kHz}$ ,  $11\text{MHz}/1\text{kHz}$  and  $12\text{MHz}/1\text{kHz}$  are compared with the measurement results to check model sensitivity to the change of center frequency of excitation signal by using model parameters found according to the  $10\text{MHz}/1\text{kHz}$  measurement. Secondly, EOM model outputs for  $10\text{MHz}/300\text{Hz}$  and  $10\text{MHz}/3.3\text{kHz}$  are compared with the measurement results to check model sensitivity for change in the excitation tone's spacing. Finally, EOM model's validity is checked by using unequal amplitude four-tone excitation signal. Comparison in between magnitudes and phases of measurement result and EOM model outputs for two-tone excitation results (IMDL, IMDU, FUNDL and FUNDU) are given in Figure 4.13, Figure 4.14, Figure 4.15, Figure 4.16, Figure 4.17, and Figure 4.18 for the excitation  $8\text{MHz}/1\text{kHz}$ ,  $9\text{MHz}/1\text{kHz}$ ,  $11\text{MHz}/1\text{kHz}$ ,  $12\text{MHz}/1\text{kHz}$ ,  $10\text{MHz}/300\text{Hz}$  and  $10\text{MHz}/3.3\text{kHz}$ , respectively.

By considering the Figure 4.13-Figure 4.16, it can be said that changing the working frequency from  $8\text{MHz}$  to  $12\text{MHz}$  (i.e.  $f_o \pm \%20$ ) doesn't result in noticeable error at the output of model except magnitude of IMDU for  $12\text{MHz}/1\text{kHz}$ . Although there are small errors, all of them are in the acceptable error region.

There are acceptable results for phase of all components for two different frequency spacings as shown in  $10\text{MHz}/300\text{Hz}$  and  $10\text{MHz}/3.3\text{kHz}$  except the phase of IMDU for  $10\text{MHz}/3.3\text{kHz}$  excitation. Actually, phase of IMDU for  $10\text{MHz}/3.3\text{kHz}$  excitation shows unexpected behavior as an intermodulation distortion signal and behavior of it is not similar to other IMD signal's behavior. While total change in the phase of IMDL or IMDU is more than  $120^\circ$ , total phase change is approximately  $80^\circ$ . Moreover, phase of model shows unexpected behavior. While phase of model is following the measurement results for IMDL, it couldn't follow the phase of IMDU. Model estimation is in the acceptable region for magnitude of FUND components and magnitude of IMDU component, while frequency separation is changing. Errors at the magnitude of IMDL are bigger than expected value.

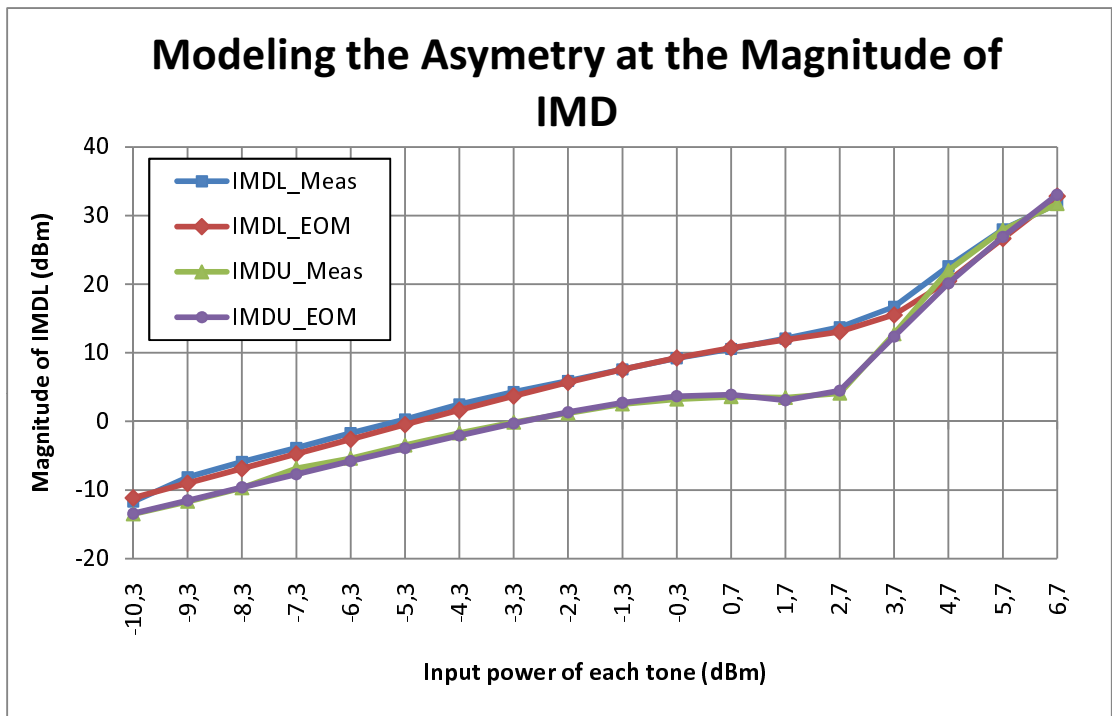


(a) Magnitude of FUNDU

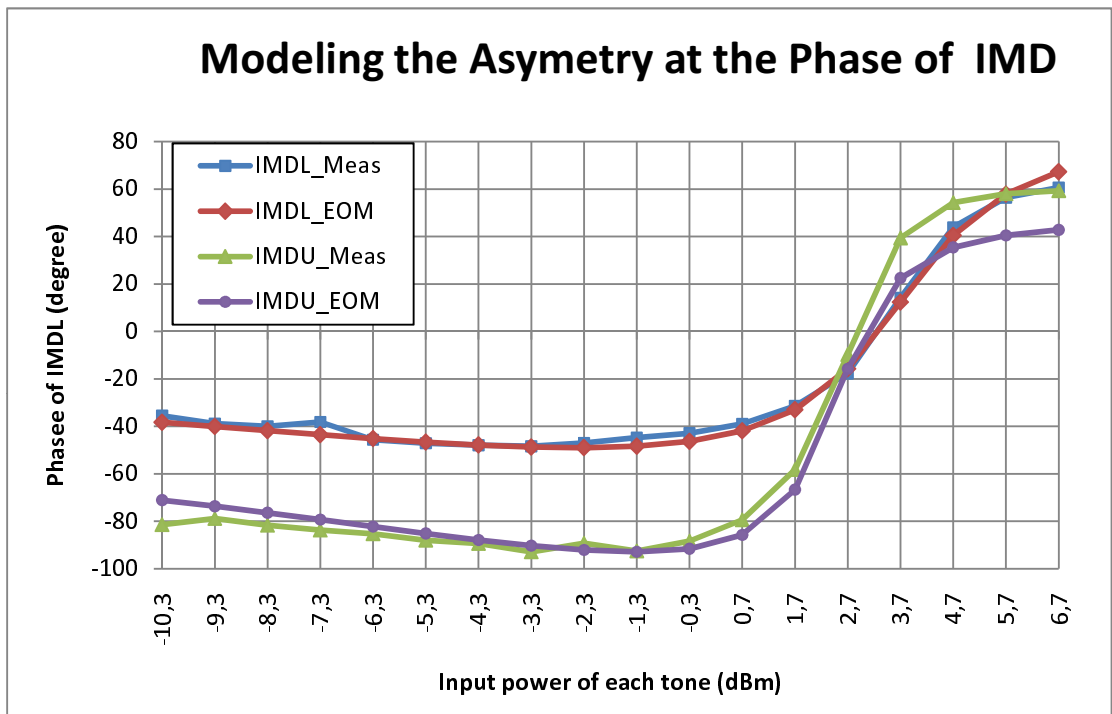


(b) Phase of FUNDU

Figure 4.10: Comparison of three modeling for a)magnitude and b)phase of FUNDU component for 10MHz/1kHz excitation signal



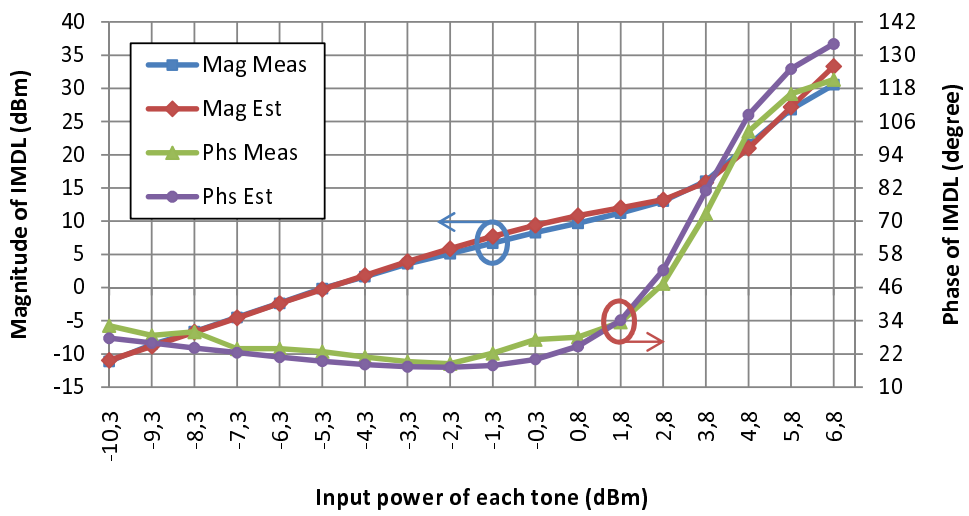
(a) Magnitude of IMD



(b) Phase of IMD

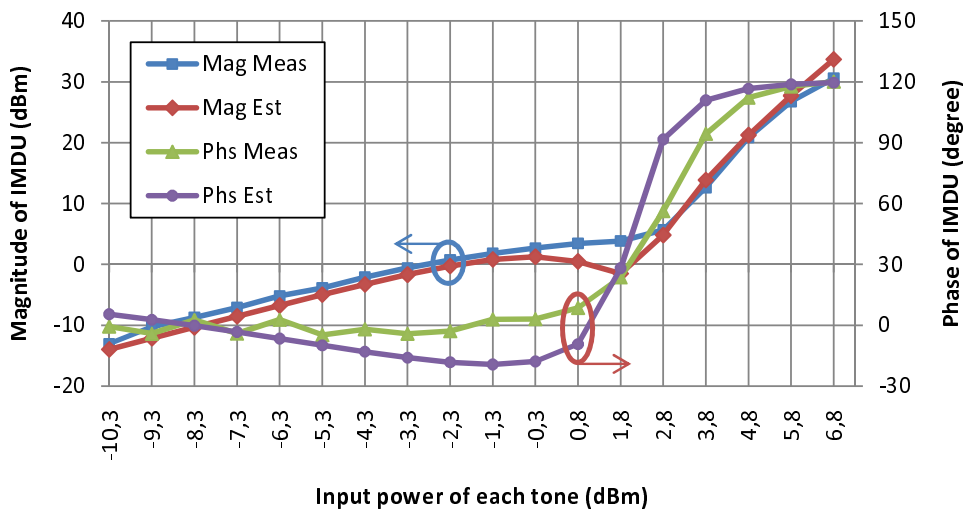
Figure 4.12: EOM modeling asymmetry representation performance for a)magnitude and b)phase of IMD signals

### IMDL@8MHz with 1kHz Spacing

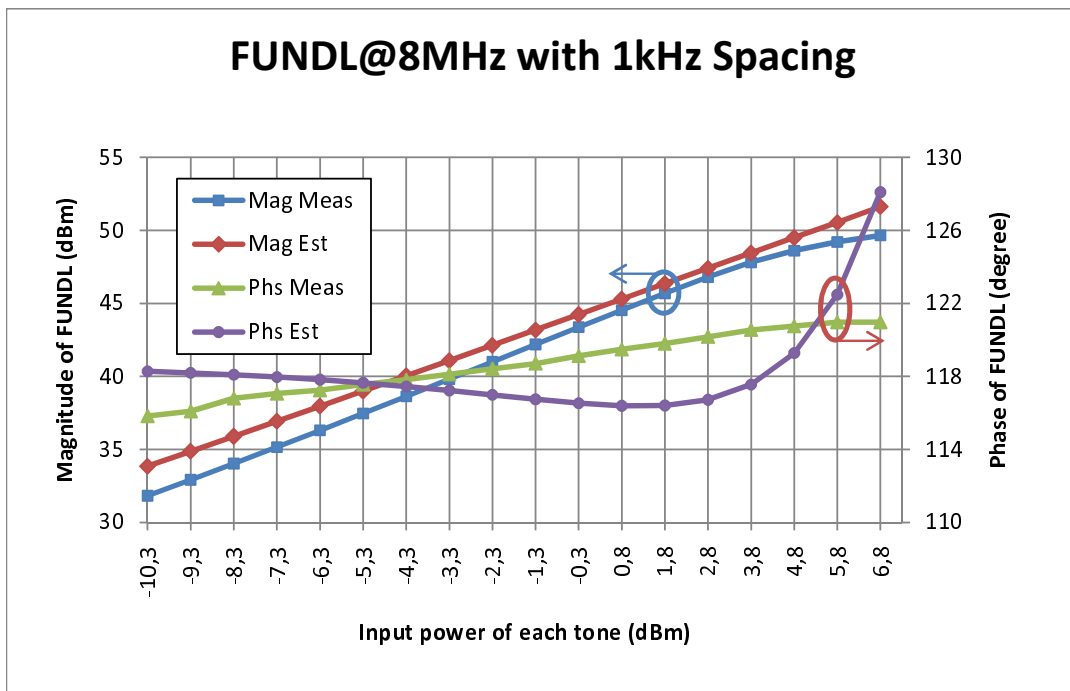


(a) Comparison of magnitude and phase of IMDL which is estimated by EOM model

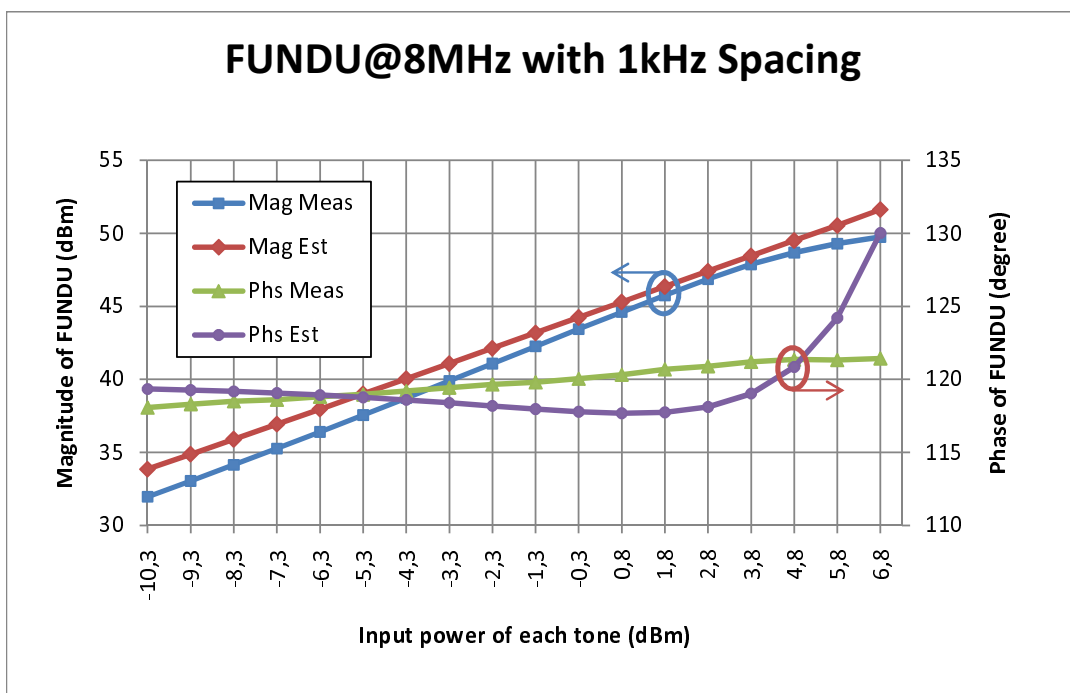
### IMDU@8MHz with 1kHz Spacing



(b) Comparison of magnitude and phase of IMDU which is estimated by EOM model

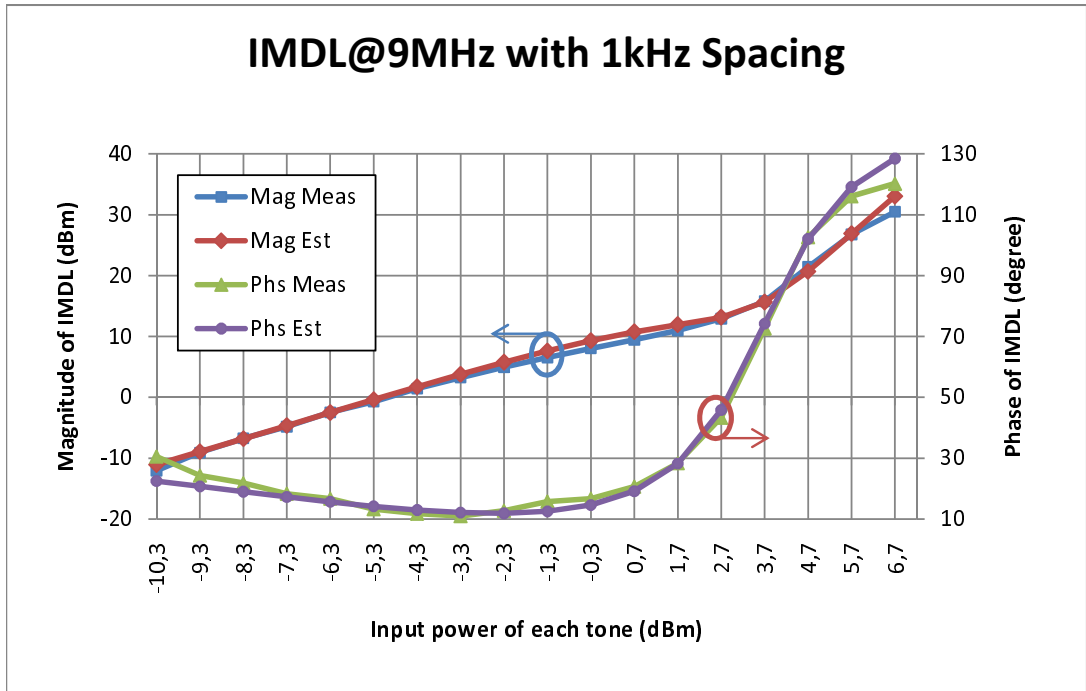


(c) Comparison of magnitude and phase of FUNDL which is estimated by EOM model

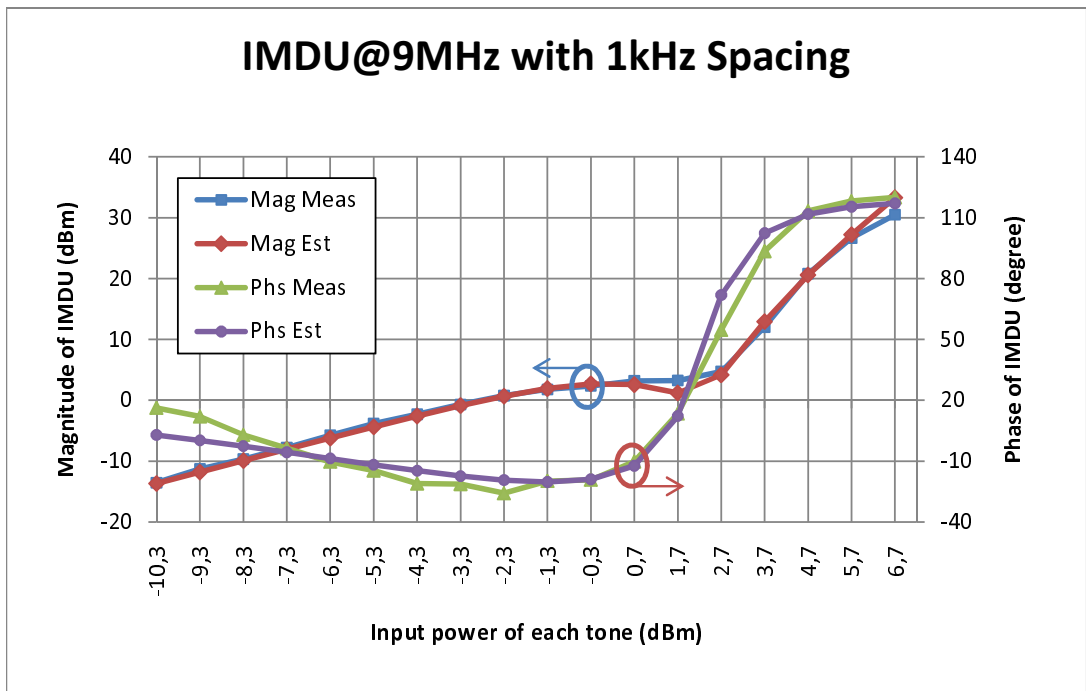


(d) Comparison of magnitude and phase of FUNDU which is estimated by EOM model

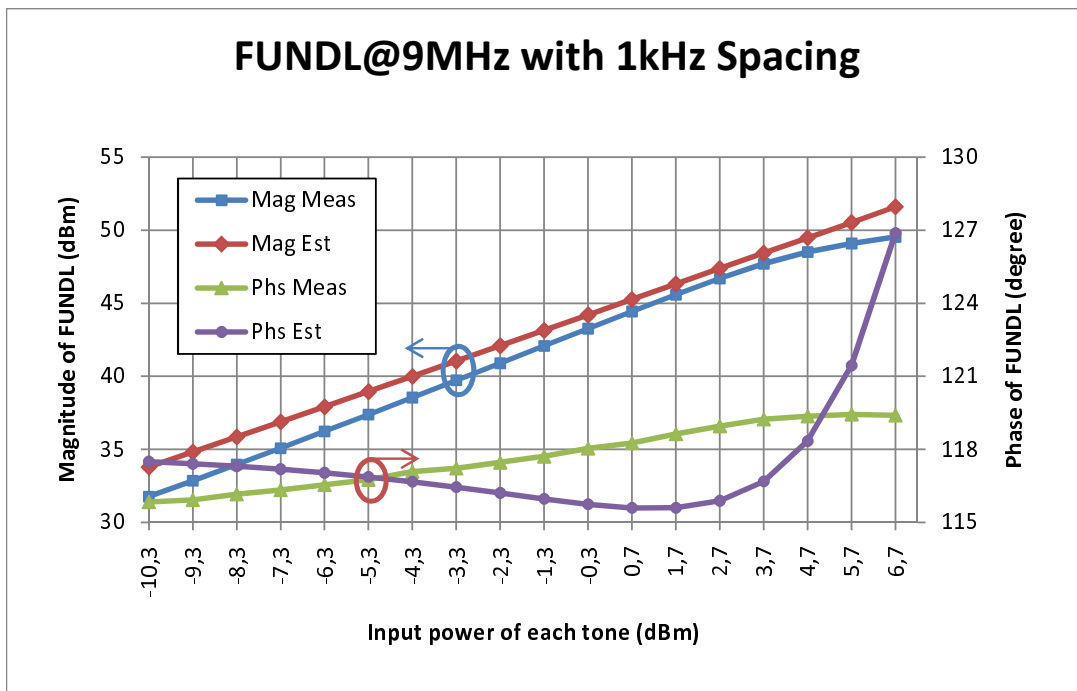
Figure 4.13: Comparison between magnitudes and phases of measurement and EOM model outputs for 8MHz/1kHz input excitation for a) ImdL b) ImdU c)FundL and d) FundU components



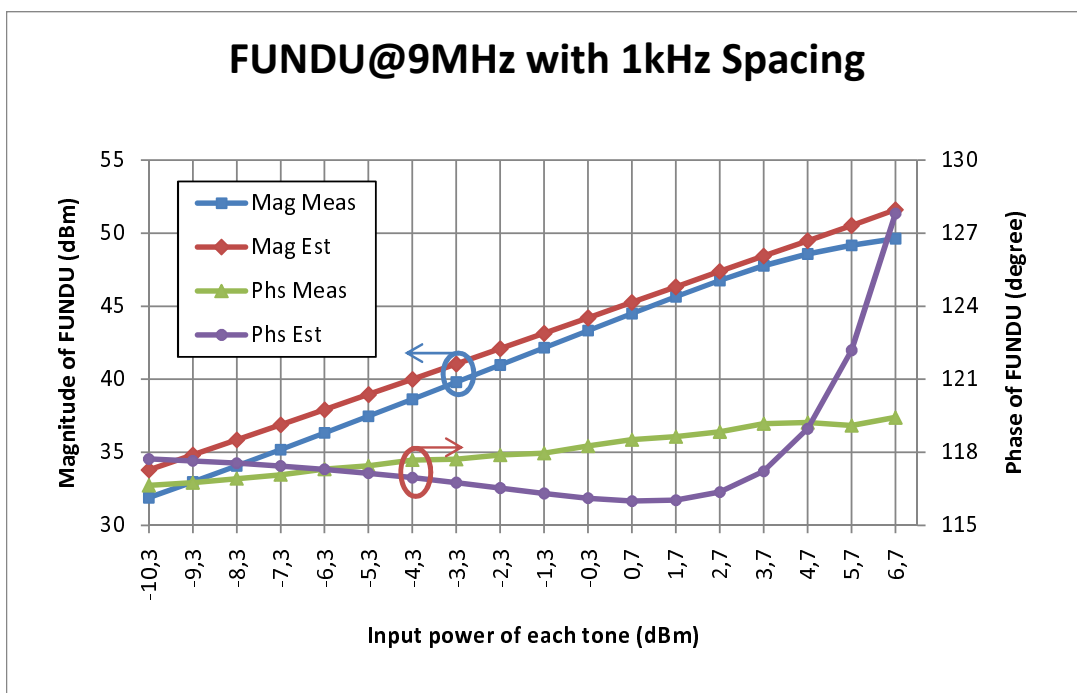
(a) Comparison of magnitude and phase of IMDL which is estimated by EOM model



(b) Comparison of magnitude and phase of IMDU which is estimated by EOM model

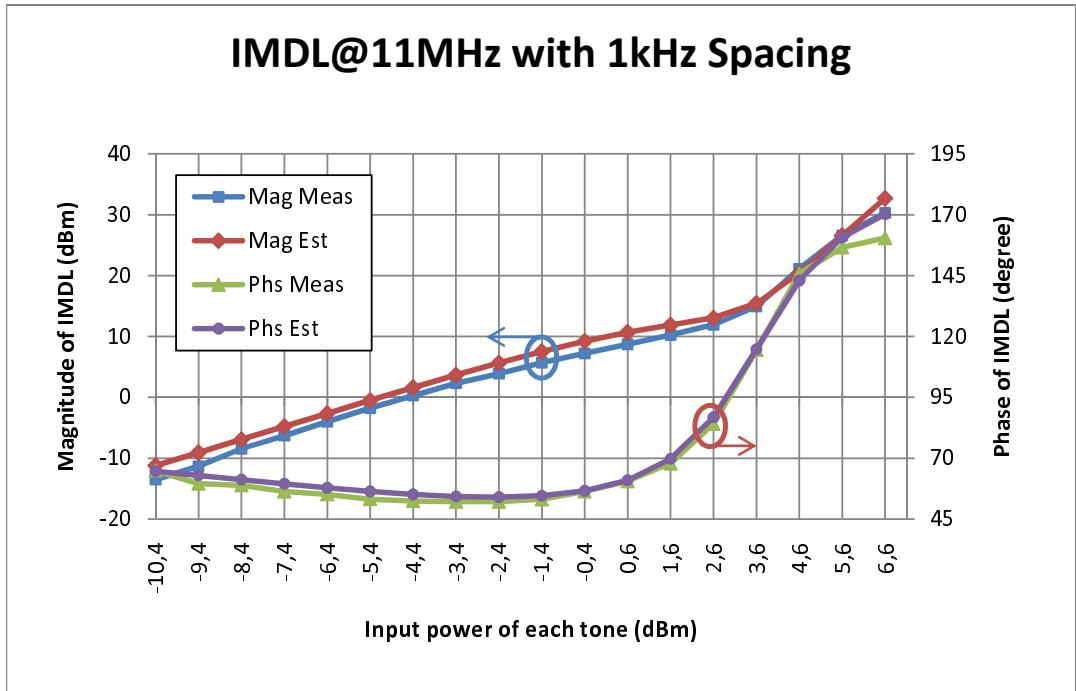


(c) Comparison of magnitude and phase of FUNDL which is estimated by EOM model

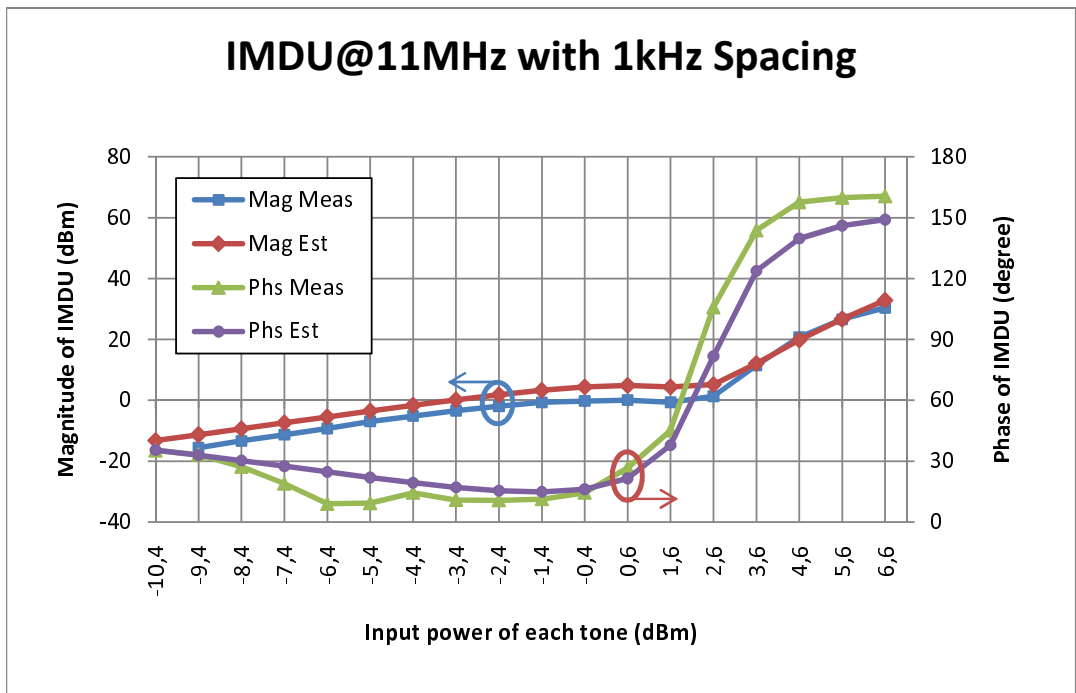


(d) Comparison of magnitude and phase of FUNDU which is estimated by EOM model

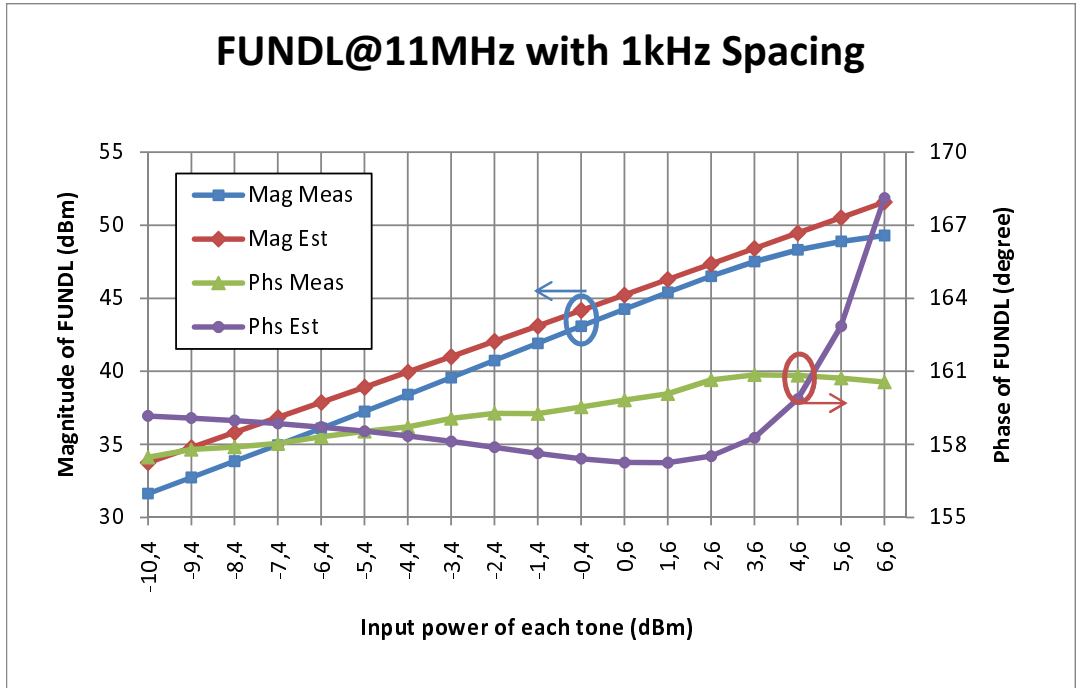
Figure 4.14: Comparison between magnitudes and phases of measurement and EOM model outputs for 9MHz/1kHz input excitation for a) ImdL b) ImdU c)FundL and d) FundU components



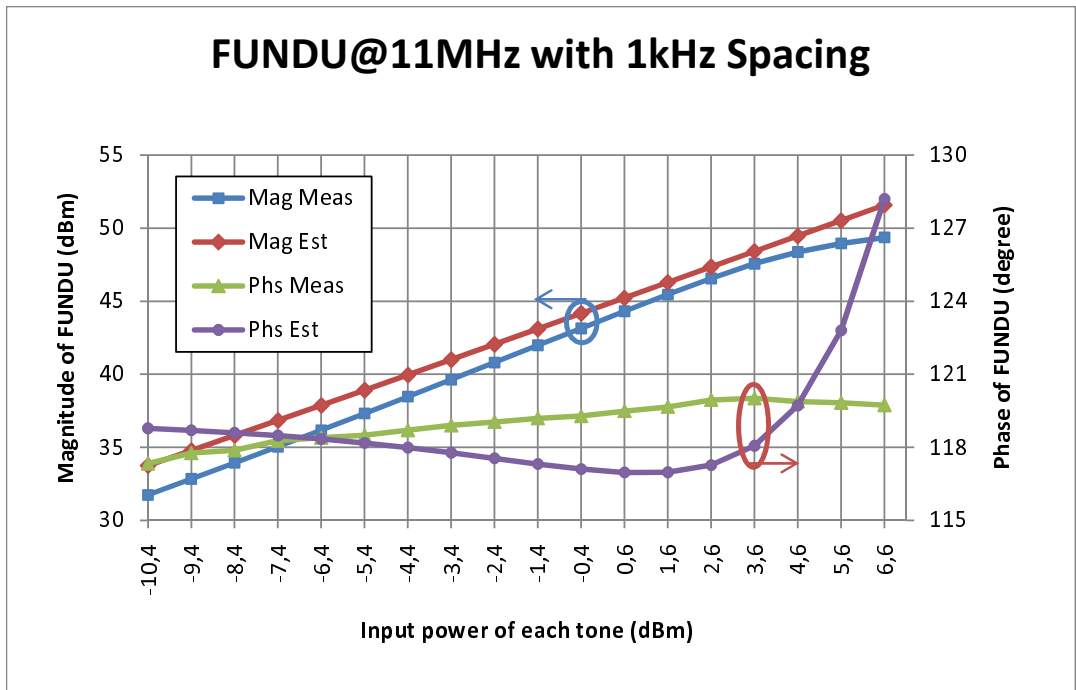
(a) Comparison of magnitude and phase of IMDL which is estimated by EOM model



(b) Comparison of magnitude and phase of IMDU which is estimated by EOM model

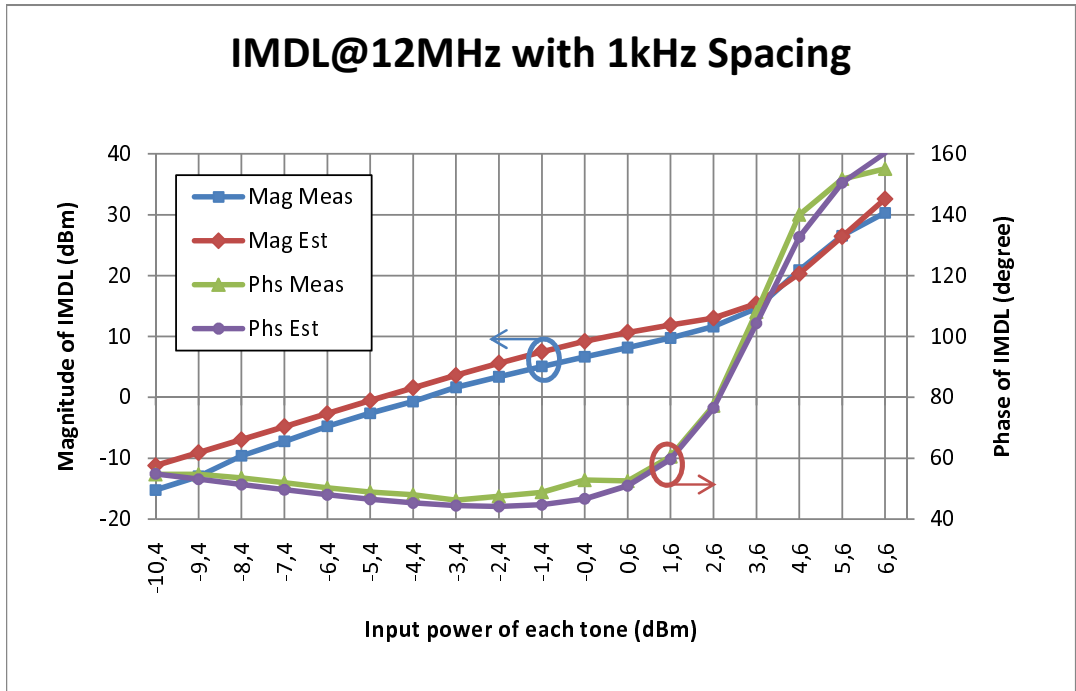


(c) Comparison of magnitude and phase of FUNDL which is estimated by EOM model

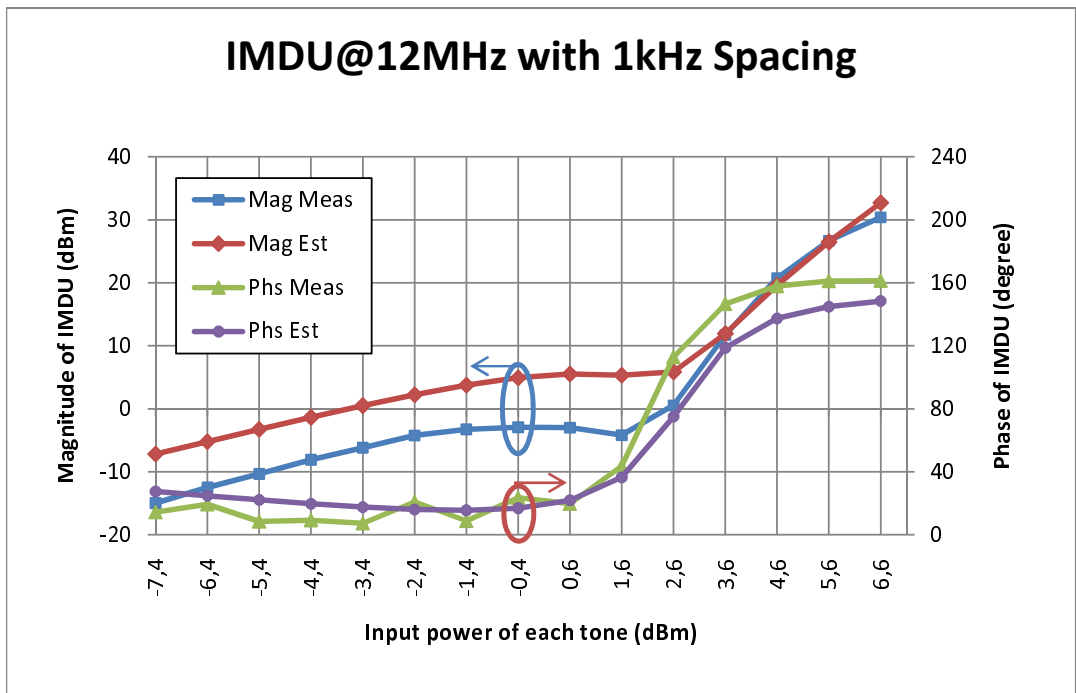


(d) Comparison of magnitude and phase of FUNDU which is estimated by EOM model

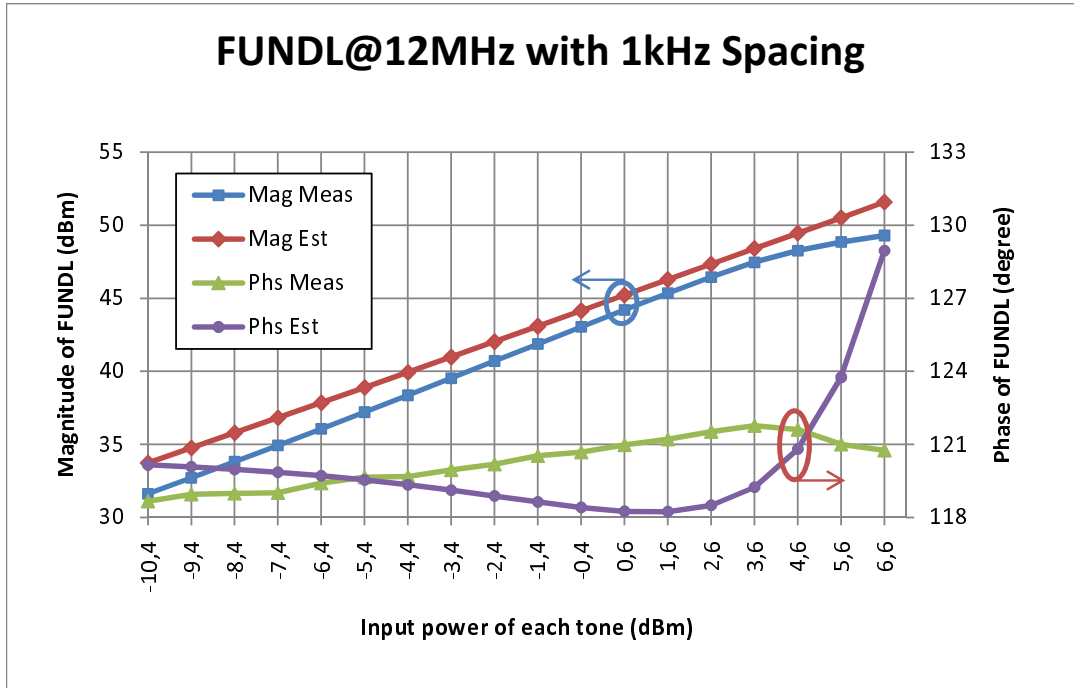
Figure 4.15: Comparison between magnitudes and phases of measurement and EOM model outputs for 11MHz/1kHz input excitation for a) ImdL b) ImdU c) FundL and d) FundU components



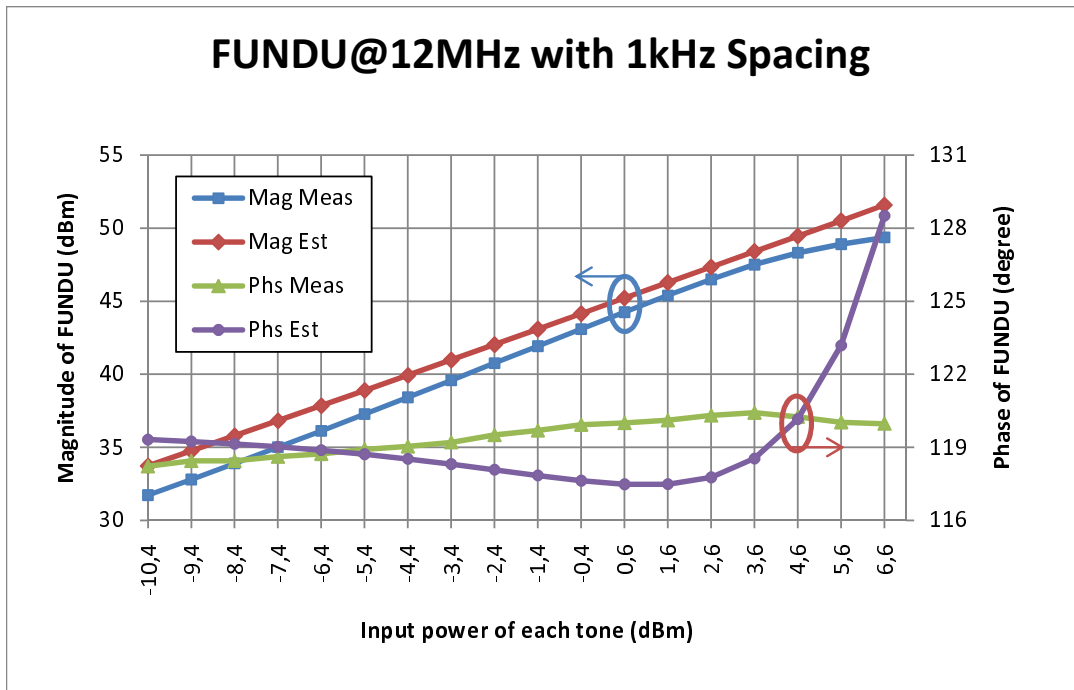
(a) Comparison of magnitude and phase of IMDL which is estimated by EOM model



(b) Comparison of magnitude and phase of IMDU which is estimated by EOM model

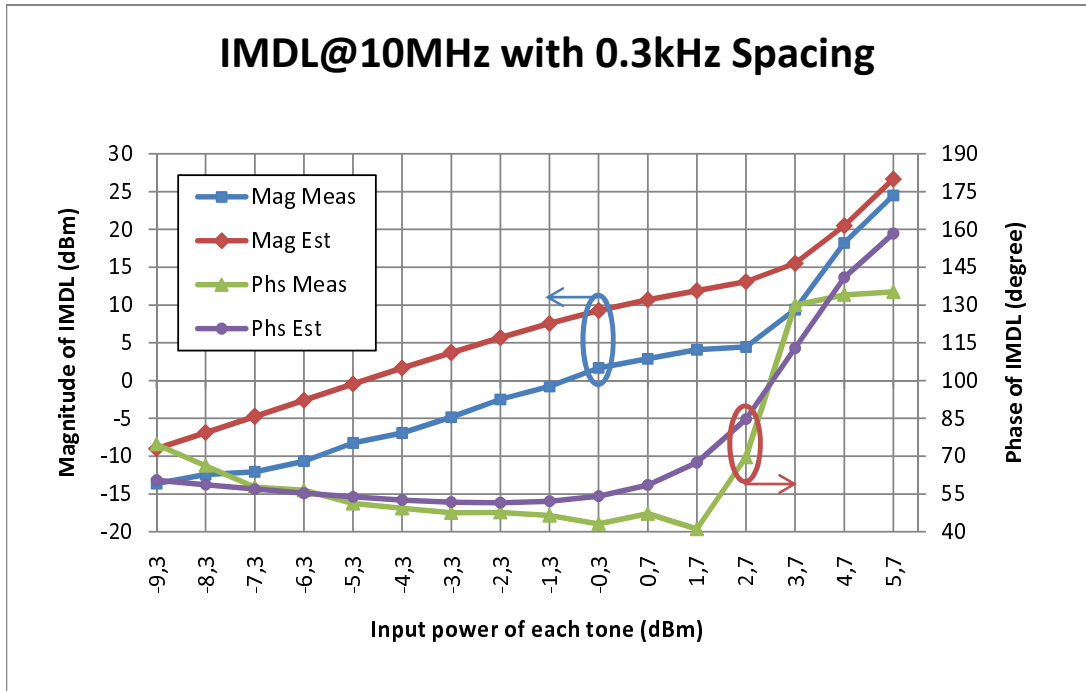


(c) Comparison of magnitude and phase of FUNDL which is estimated by EOM model

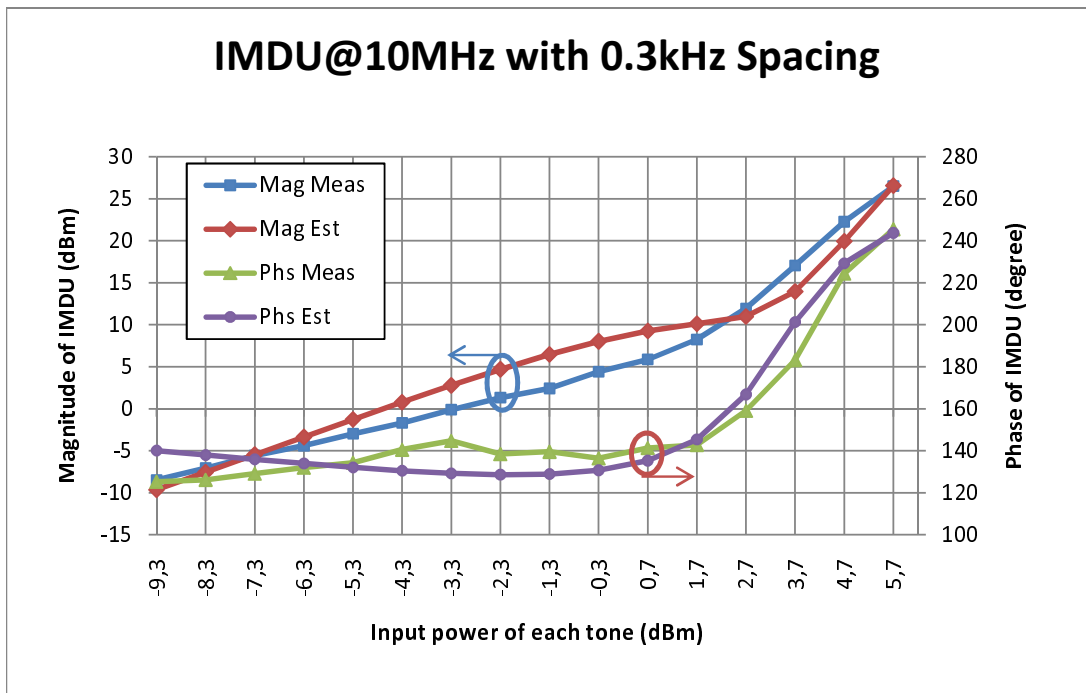


(d) Comparison of magnitude and phase of FUNDU which is estimated by EOM model

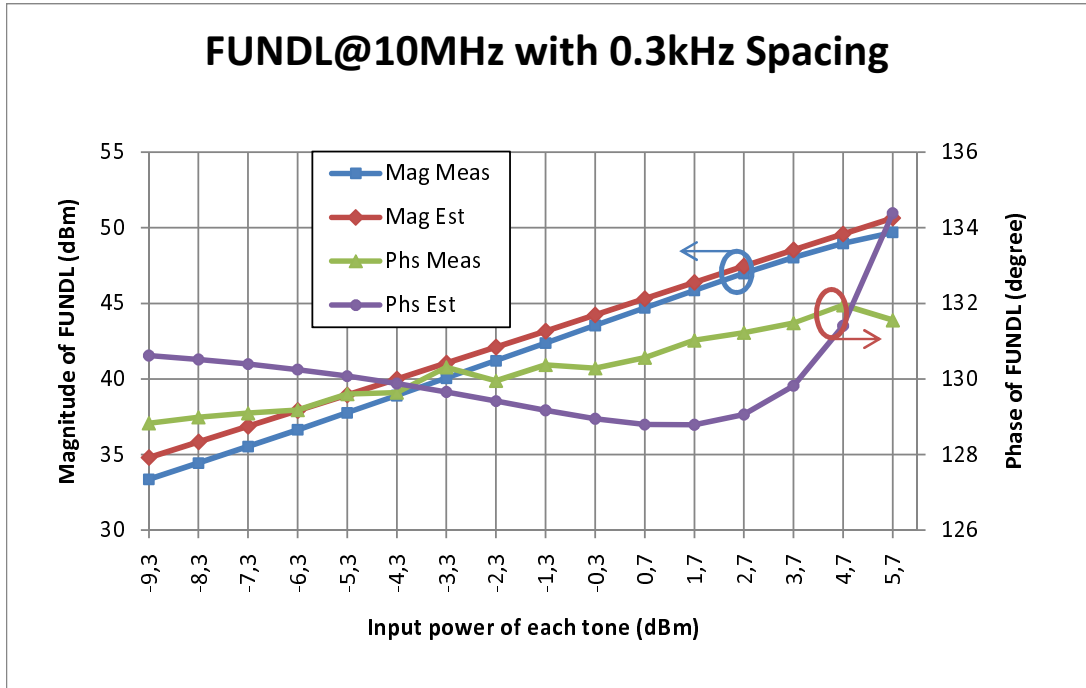
Figure 4.16: Comparison between magnitudes and phases of measurement and EOM model outputs for 12MHz/1kHz input excitation for a) ImdL b) ImdU c) FundL and d) FundU components



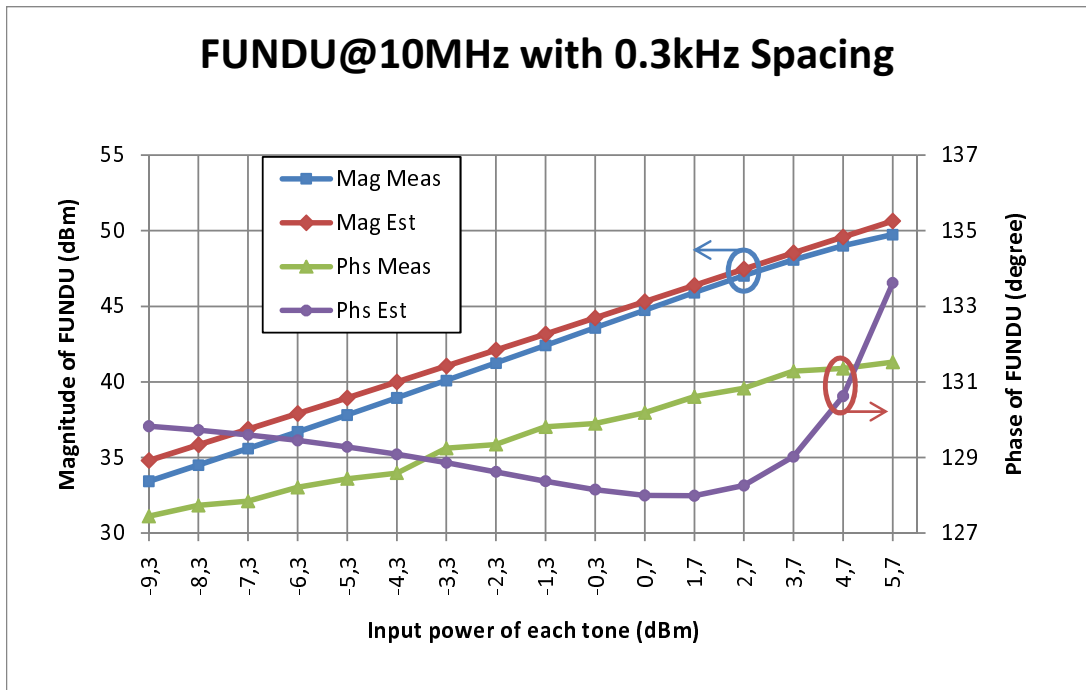
(a) Comparison of magnitude and phase of IMDL which is estimated by EOM model



(b) Comparison of magnitude and phase of IMDU which is estimated by EOM model

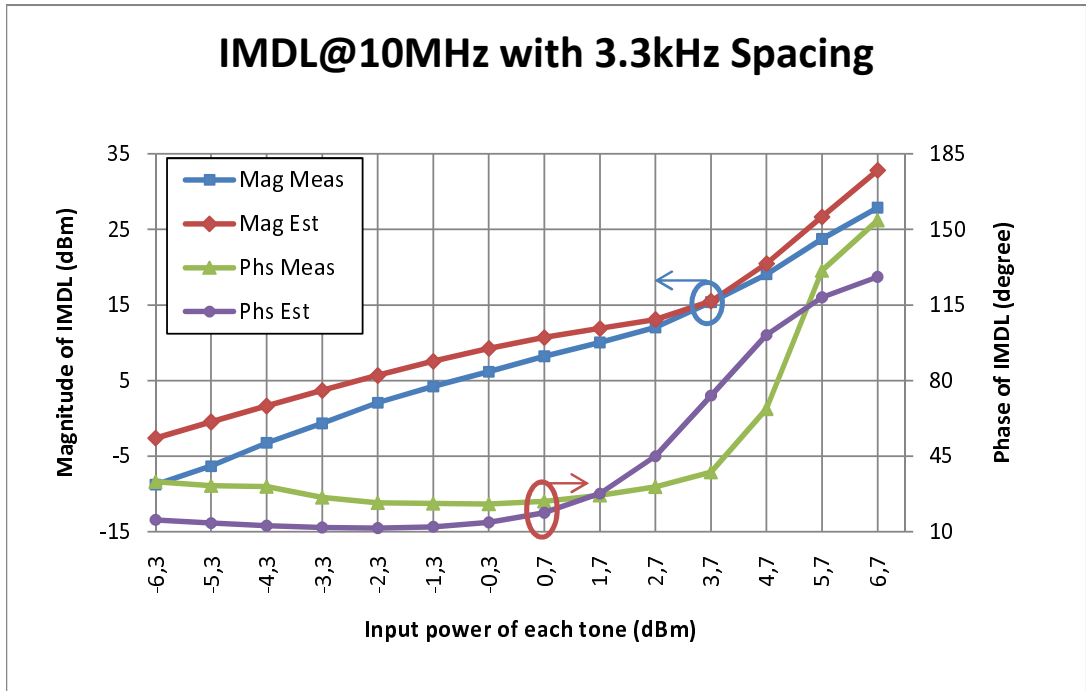


(c) Comparison of magnitude and phase of FUNDL which is estimated by EOM model

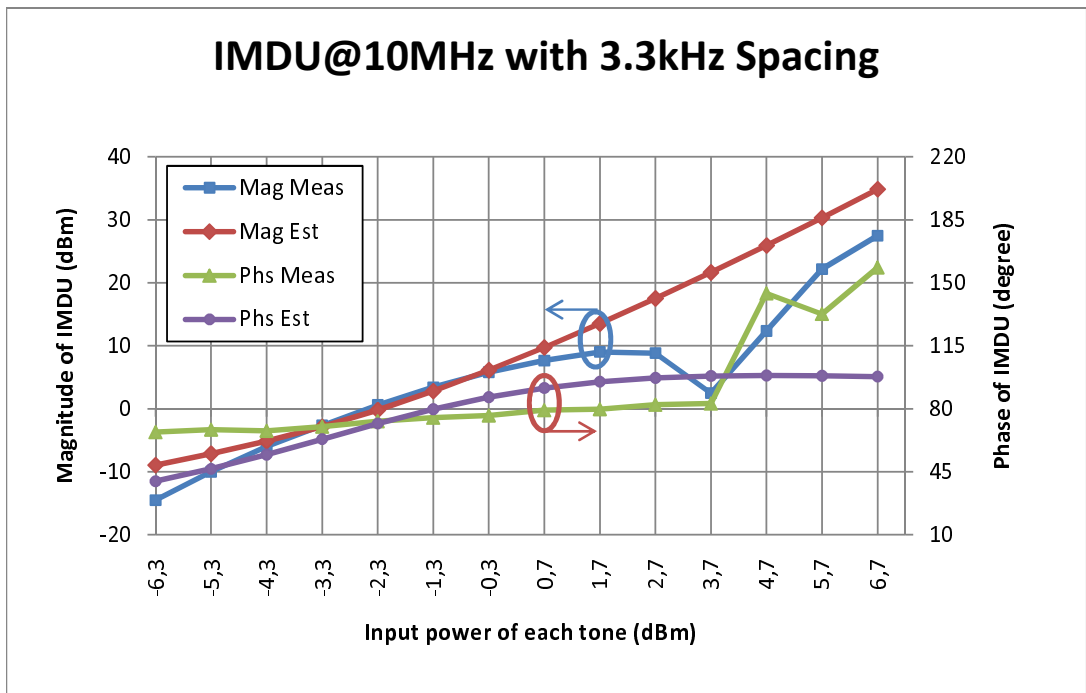


(d) Comparison of magnitude and phase of FUNDU which is estimated by EOM model

Figure 4.17: Comparison between magnitudes and phases of measurement and EOM model outputs for 10MHz/300Hz input excitation for a) ImdL b) ImdU c)FundL and d) FundU components



(a) Comparison of magnitude and phase of IMDL which is estimated by EOM model



(b) Comparison of magnitude and phase of IMDU which is estimated by EOM model

#### 4.6.2 EOM model Validity Range Investigation for Unequal Four-Tone excitation

The measurement setup given in Figure 3.1 is used to create unequal four-tone excitation and measure the amplifier response. Asymmetric two-tone signal is created in the Matlab program and loaded to the AWSG. AWSG output is connected to the "I" input of I/Q modulator. Four-tone signal which is created at the output of I/Q modulator is applied to the amplifier. There is  $10dBc$  power level difference between inner and outer tones.

Frequency spectra of created signal for the sample amplifier is measured and given in Figure 4.19. Although only a four-tone signal is created at the output of I/Q modulator, adjacent tones are seen in the measurement results. There are approximately  $-40dBc$  power at the adjacent channels w.r.t. inner tone for the worst case. These unwanted signals in the adjacent channel may result from imperfection of I/Q modulator which is used for DSBSC signal generation. Amplifier responses are measured for 18 different input power excitation levels ( $18dB$  dynamic range). Measurement results and model estimations are given in Figure 4.20 for five different input power levels (power level of outer tones are  $-8.78dBm$ ,  $-4.77dBm$ ,  $-1.76dBm$ ,  $0.25dBm$  and  $2.25dBm$ ) as an example. The measurement results and the model estimation for other excitation are given in Appendix C. Frequency spectral data of measured input and measured amplifier response to this input for 18 different excitation power levels are tabulated as given in Table 4.5 and Table 4.6, respectively. Then 12-tone signal is created in the matlab in time domain using the power levels given in Table 4.5 in order to add measurement setup imperfections to the model estimation. Amplifier response is calculated in time domain by using the EOM model equation which is given in (4.7) taking  $K = 5$ . Frequency spectra of model output is calculated using "fft" command of Matlab to be able to compare model estimation and measured output tone-by-tone. While calculating the frequency spectra using "fft" command, filtering is used in order to get rid of the limited time effect. Calculated frequency spectra of model estimation is listed in Table 4.7 and NMSE values are listed in Table 4.8.

Although model parameters are found according to the two-tone measurement results, model estimation errors are in acceptable region for in-band tones as seen in Table 4.8. Region of interest is shaded with light gray color in that table. Region of interest is determined according to the maximum power of output signal for that excitation level which shouldn't be exceed the  $55.32dBm$  power level. Since the maximum total power is  $55.32dBm$  for two-tone modeling. Thus, while comparing model estimation and measurement results for unequal-four-tone, this

region is focused first then the region having white background color is interested. There is always better than  $-17dB$  normalized square error in in-band signals. While power level of the first lower adjacent channel is smaller than the far-off tones in measurement results as shown in Table 4.8, power level of the first lower adjacent channel in estimated values is bigger than the magnitude of far-off tones. This is an unexpected behavior and this is neither a randomly occurred measurement error nor a system noise. Reason of this unexpected behavior is one of the future works. Thus, normalized square error for the lower band first adjacent channel ( $IMDL_1$ ) are not as good as expected value. In contrast to this, the errors for both lower and upper far-off tones are good. While the NMSE value of IMDL for  $10MHz/1kHz$  was better than the NMSE of IMDU, NMSE of IMDL for  $10MHz/300kHz$  is worse than NMSE for IMDU. Conversely, NMSE for IMDL for  $10MHz/3.3kHz$  is better than the NMSE of IMDU. In other words, when signal separation is decreased, NMSE of IMDU is getting better, conversely, when frequency separation increased NMSE of IMDL is getting better w.r.t. the NMSE of  $1kHz$  separation situation as given in Table 4.4.  $IMDL_1$  mostly effected from  $FUNDL_2$  and  $FUNDL_1$  interactions. Considering the fact that there is  $500Hz$  frequency separation between  $FUNDL_2$  and  $FUNDL_1$ , relatively better performance in the  $IMDU_1$  than  $IMDL_1$  is expected result.

Table 4.5: Measured frequency spectra of unequal four-tone signal created by I/Q modulator

Excitation Index	$P_{in}$ in dBm (measured)									
	9.998.250 Hz	9.998.750 Hz	9.999.250 Hz	9.999.750 Hz	10.000.250 Hz	10.000.750 Hz	10.001.250 Hz	10.001.750 Hz	10.002.250 Hz	10.002.750 Hz
	$IMDL_3$	$IMDL_2$	$IMDL_1$	$FUNDL_2$	$FUNDL_1$	$FUNDU_1$	$FUNDU_2$	$IMDU_1$	$IMDU_2$	$IMDU_3$
1	-87.74	-91.62	-80.38	-12.79	-22.79	-22.78	-12.79	-83.37	-87.97	-83.71
2	-85.04	-83.99	-85.18	-11.78	-21.78	-21.77	-11.78	-77.78	-80.86	-81.90
3	-88.97	-85.64	-78.76	-10.77	-20.77	-20.77	-10.77	-75.90	-88.14	-75.02
4	-84.93	-85.06	-84.59	-9.79	-19.77	-19.79	-9.78	-74.25	-83.62	-80.03
5	-83.59	-77.93	-77.34	-8.78	-18.78	-18.77	-8.77	-80.23	-77.39	-77.78
6	-70.80	-77.52	-76.03	-7.78	-17.77	-17.76	-7.77	-74.64	-74.90	-70.84
7	-74.38	-74.79	-68.88	-6.77	-16.76	-16.76	-6.77	-65.23	-74.32	-75.39
8	-69.93	-72.27	-77.57	-5.78	-15.78	-15.77	-5.78	-77.69	-74.31	-72.10
9	-67.64	-69.81	-66.91	-4.77	-14.77	-14.76	-4.77	-77.49	-69.40	-71.10
10	-66.75	-77.04	-65.82	-3.76	-13.76	-13.75	-3.76	-68.83	-70.83	-67.48
11	-71.18	-76.87	-66.45	-2.76	-12.75	-12.75	-2.75	-68.62	-69.04	-70.57
12	-69.63	-66.69	-65.83	-1.76	-11.76	-11.75	-1.76	-66.20	-68.55	-69.54
13	-67.87	-65.63	-61.81	-0.77	-10.77	-10.74	-0.76	-65.32	-64.53	-65.03
14	-60.32	-60.14	-61.07	0.25	-9.74	-9.74	0.25	-65.10	-60.16	-58.71
15	-57.91	-57.48	-60.09	1.25	-8.73	-8.74	1.26	-62.46	-56.58	-56.04
16	-55.57	-55.04	-58.61	2.25	-7.74	-7.74	2.25	-58.41	-54.31	-55.79
17	-51.39	-51.92	-55.28	3.25	-6.75	-6.73	3.26	-53.83	-51.78	-51.37
18	-48.02	-49.09	-52.51	4.26	-5.72	-5.73	4.27	-54.49	-49.02	-47.92

Table 4.6: Measured frequency spectra of the amplifier response to the unequal four-tone excitation

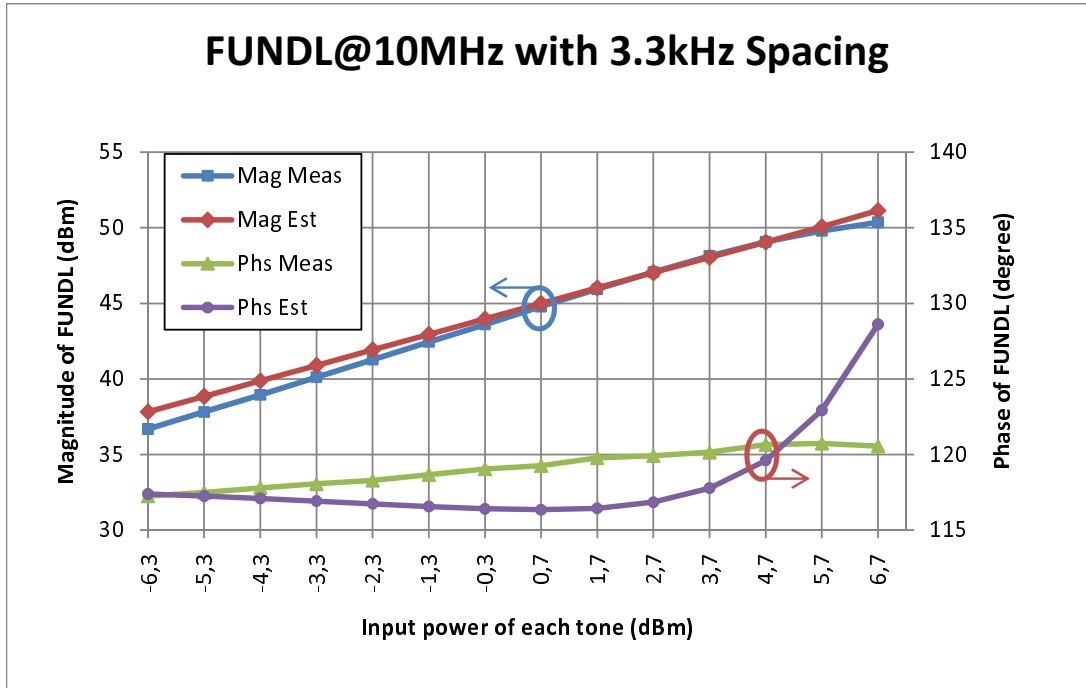
Excitation Index	$P_{out}$ in dBm (measured)									
	$IMDL_3$	$IMDL_2$	$IMDL_1$	$FUNDL_2$	$FUNDL_1$	$FUNDU_1$	$FUNDU_2$	$IMDU_1$	$IMDU_2$	$IMDU_3$
1	-18.80	-19.64	-29.21	30.22	20.22	20.22	30.22	-29.10	-26.93	-24.40
2	-14.89	-16.78	-22.79	31.28	21.28	21.27	31.27	-23.89	-23.20	-24.40
3	-11.99	-14.17	-19.83	32.35	22.36	22.35	32.34	-21.11	-20.18	-18.74
4	-9.63	-11.33	-17.51	33.44	23.46	23.45	33.44	-17.27	-16.47	-14.76
5	-7.08	-9.01	-14.89	34.55	24.57	24.57	34.54	-15.75	-13.80	-12.58
6	-4.82	-6.70	-12.55	35.68	25.71	25.69	35.67	-12.44	-12.22	-9.91
7	-2.14	-4.08	-9.95	36.80	26.84	26.83	36.80	-10.55	-8.73	-7.55
8	0.10	-1.75	-8.02	37.97	28.03	28.00	37.96	-8.54	-6.64	-5.41
9	2.32	0.30	-5.29	39.14	29.19	29.19	39.12	-5.95	-3.89	-2.82
10	4.14	2.48	-3.79	40.33	30.40	30.38	40.32	-4.21	-1.79	-0.56
11	5.89	4.11	-2.01	41.52	31.60	31.57	41.51	-2.36	-0.11	0.90
12	7.58	5.59	-0.39	42.70	32.77	32.75	42.69	-0.98	0.75	1.87
13	9.06	7.04	0.41	43.90	33.97	33.93	43.88	0.06	1.52	3.07
14	10.44	8.43	1.70	45.08	35.14	35.09	45.06	1.36	1.73	3.54
15	11.69	9.60	2.34	46.25	36.27	36.23	46.22	1.18	0.25	1.31
16	12.63	10.59	3.92	47.35	37.29	37.24	47.32	2.28	-1.01	-9.07
17	15.39	13.94	10.37	48.28	38.03	37.96	48.25	9.33	12.81	13.13
18	21.35	20.74	17.57	49.05	38.45	38.37	49.01	17.27	21.01	21.43

Table 4.7: Frequency spectra of model output calculated in Matlab by using FFT command for unequal four-tone excitation

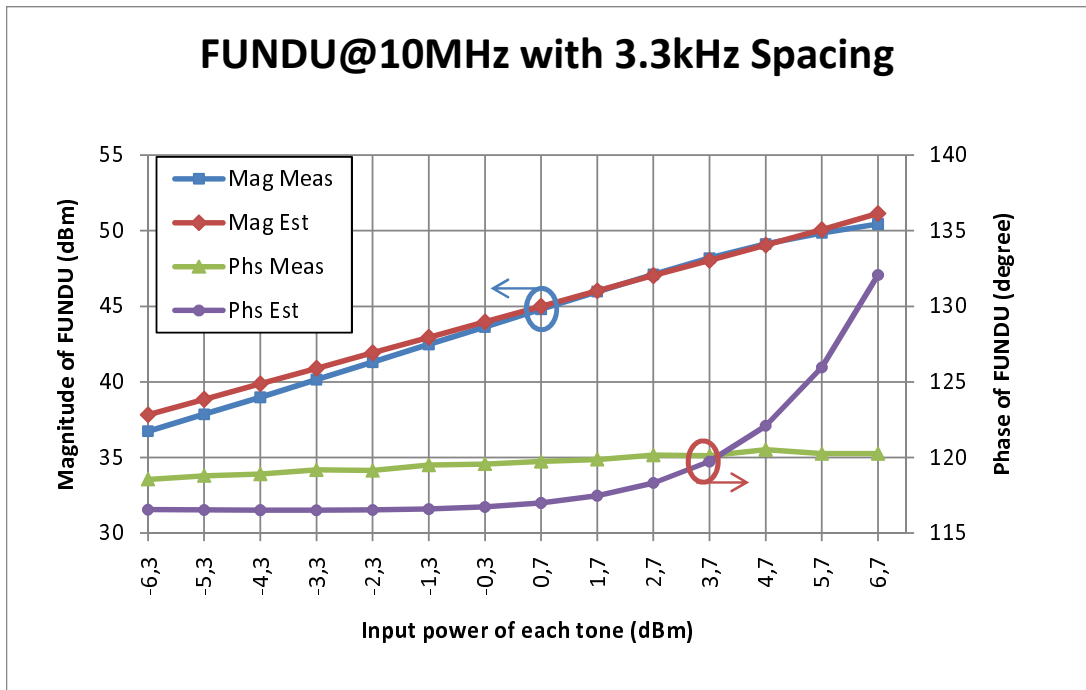
Excitation Index	$P_{estimated}$ in dBm (Model estimation; Calculated by matlab)									
	$IMDL_3$	$IMDL_2$	$IMDL_1$	$FUNDL_2$	$FUNDL_1$	$FUNDU_1$	$FUNDU_2$	$IMDU_1$	$IMDU_2$	$IMDU_3$
1	-17.13	-19.18	-16.24	31.26	21.35	21.35	31.25	-17.37	-20.31	-18.31
2	-14.99	-16.80	-14.59	32.29	22.39	22.39	32.28	-15.04	-17.91	-16.37
3	-13.08	-14.87	-12.25	33.32	23.43	23.42	33.32	-13.05	-16.53	-13.91
4	-10.96	-12.85	-10.55	34.33	24.46	24.44	34.33	-11.12	-14.47	-12.64
5	-8.84	-10.48	-8.23	35.37	25.49	25.49	35.36	-9.63	-12.21	-10.66
6	-6.18	-8.46	-6.17	36.40	26.55	26.54	36.39	-7.45	-10.20	-8.31
7	-4.43	-6.34	-3.77	37.44	27.60	27.59	37.42	-4.81	-8.38	-6.89
8	-2.26	-4.33	-2.29	38.47	28.63	28.63	38.44	-3.90	-6.67	-4.97
9	-0.20	-2.32	0.02	39.52	29.70	29.69	39.49	-2.10	-4.71	-3.20
10	1.71	-0.84	1.81	40.58	30.77	30.76	40.54	-0.23	-3.37	-1.40
11	3.27	0.72	3.29	41.63	31.84	31.81	41.59	1.06	-2.15	-0.17
12	4.90	2.31	4.58	42.68	32.90	32.87	42.62	2.01	-1.51	0.91
13	6.28	3.28	5.68	43.73	33.95	33.93	43.66	2.29	-1.25	1.66
14	7.73	4.66	6.50	44.80	35.03	34.98	44.72	2.51	-0.09	2.28
15	9.07	7.45	8.84	45.86	36.09	36.02	45.77	6.74	5.39	4.01
16	11.92	12.85	14.28	46.91	37.12	37.06	46.80	13.96	12.55	9.69
17	17.26	19.27	20.89	47.95	38.17	38.13	47.84	20.97	19.37	16.92
18	23.50	25.54	27.28	49.00	39.41	39.34	48.88	27.37	25.65	23.60

Table 4.8: Normalized square error of measured value and estimated model output

Excitation Index	NMSE (dB)									
	$IMDL_3$	$IMDL_2$	$IMDL_1$	$FUNDL_2$	$FUNDL_1$	$FUNDU_1$	$FUNDU_2$	$IMDU_1$	$IMDU_2$	$IMDU_3$
1	-13.50	-25.33	10.76	-17.90	-17.16	-17.13	-17.94	9.13	1.15	0.14
2	-38.06	-54.16	3.93	-18.12	-17.38	-17.21	-18.15	4.95	3.65	3.65
3	-18.58	-22.26	2.89	-18.54	-17.66	-17.65	-18.54	3.69	-2.56	-2.56
4	-16.96	-15.90	1.80	-19.37	-18.28	-18.42	-19.37	0.26	-11.18	-11.18
5	-14.71	-16.12	1.22	-20.10	-19.01	-19.00	-20.10	0.20	-12.14	-12.14
6	-16.75	-14.74	0.71	-21.23	-19.92	-19.68	-21.27	-2.18	-13.92	-13.92
7	-12.71	-12.81	0.31	-22.34	-20.77	-20.75	-22.55	-0.56	-22.15	-22.15
8	-12.47	-11.82	-0.59	-24.54	-22.78	-22.47	-24.76	-3.01	-25.65	-25.65
9	-11.98	-11.69	-1.48	-26.87	-24.42	-24.47	-27.34	-5.07	-27.49	-27.49
10	-12.25	-9.96	-0.87	-30.83	-27.29	-27.21	-31.87	-4.69	-20.67	-20.67
11	-11.70	-9.80	-1.50	-38.00	-30.96	-30.93	-40.47	-6.32	-18.68	-18.68
12	-11.52	-10.04	-2.25	-51.07	-36.96	-37.04	-42.48	-7.72	-19.53	-19.53
13	-11.24	-9.08	-1.57	-34.01	-50.45	-60.64	-32.15	-10.65	-16.51	-16.51
14	-11.42	-9.07	-2.66	-30.12	-38.54	-38.34	-28.31	-16.94	-17.37	-17.37
15	-11.71	-13.18	0.93	-27.15	-33.89	-32.54	-25.87	-0.95	-8.79	-8.79
16	-22.12	-10.54	7.22	-26.09	-33.96	-33.43	-24.62	9.07	17.70	17.70
17	-12.42	-1.44	7.45	-28.60	-35.83	-34.46	-26.64	9.00	-5.22	-5.22
18	-11.04	-2.65	6.28	-45.34	-18.67	-18.58	-36.07	6.85	-10.91	-10.91

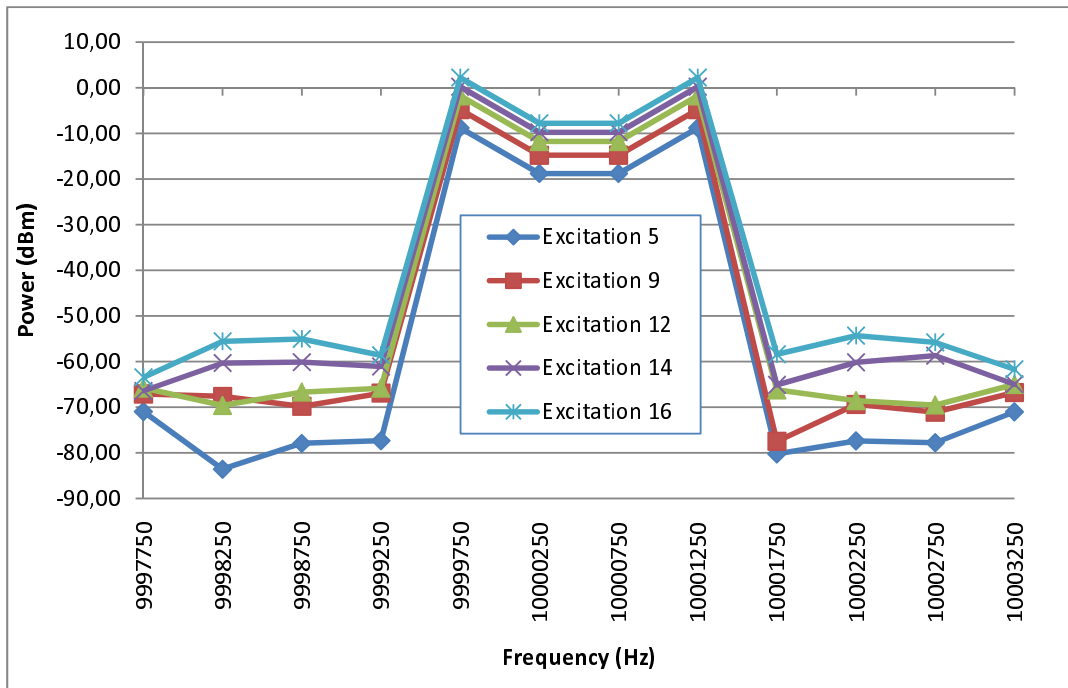


(c) Comparison of magnitude and phase of FUNDL which is estimated by EOM model

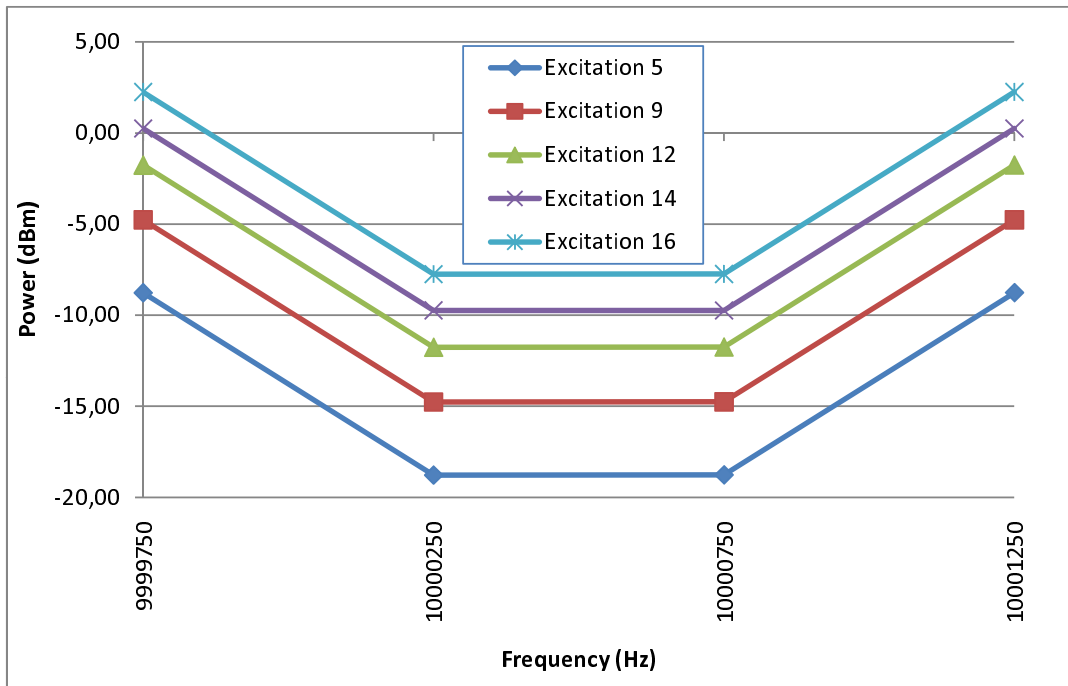


(d) Comparison of magnitude and phase of FUNDU which is estimated by EOM model

Figure 4.18: Comparison between magnitudes and phases of measurement and EOM model outputs for 10MHz/3.3kHz input excitation for a) ImdL b) ImdU c) FundL and d) FundU components

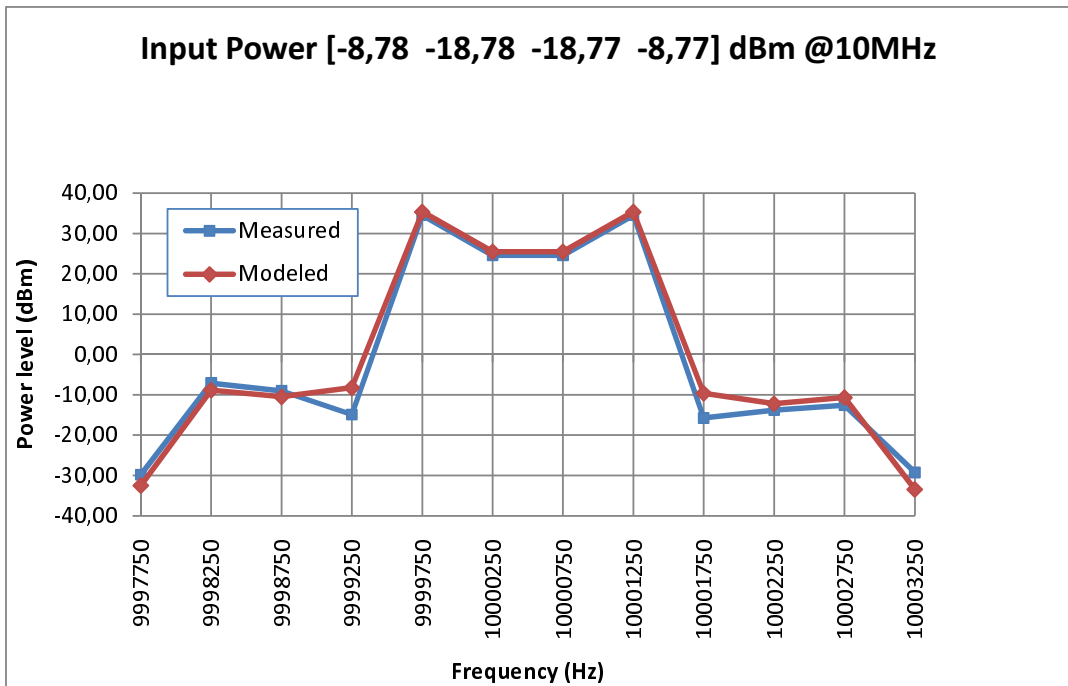


(a) Full range

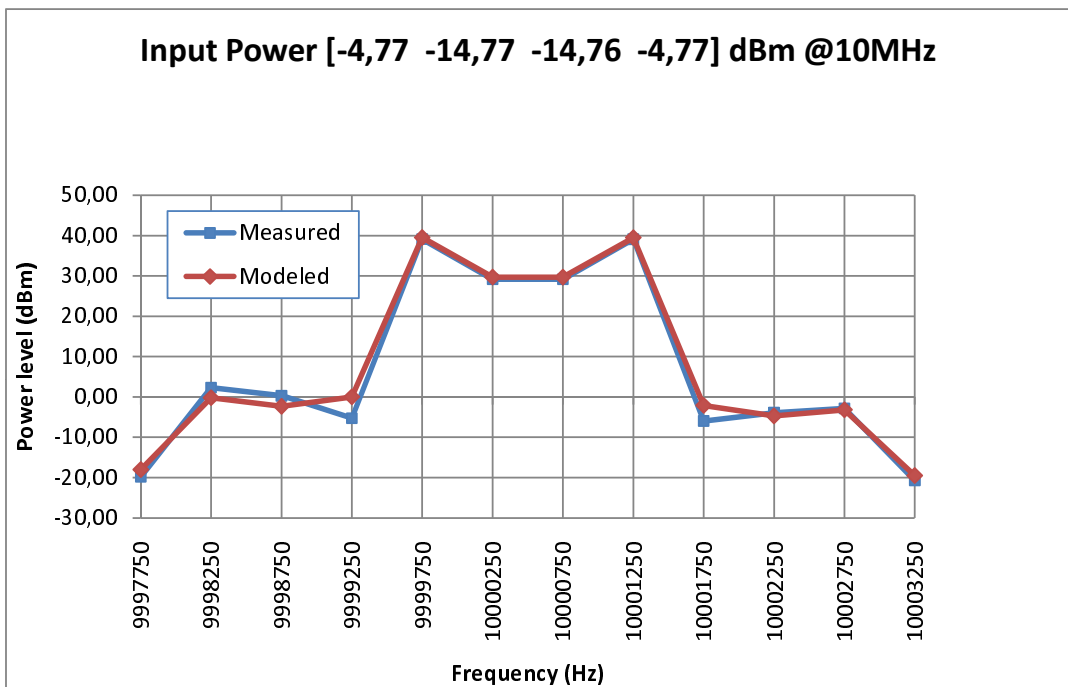


(b) Fundamental tones

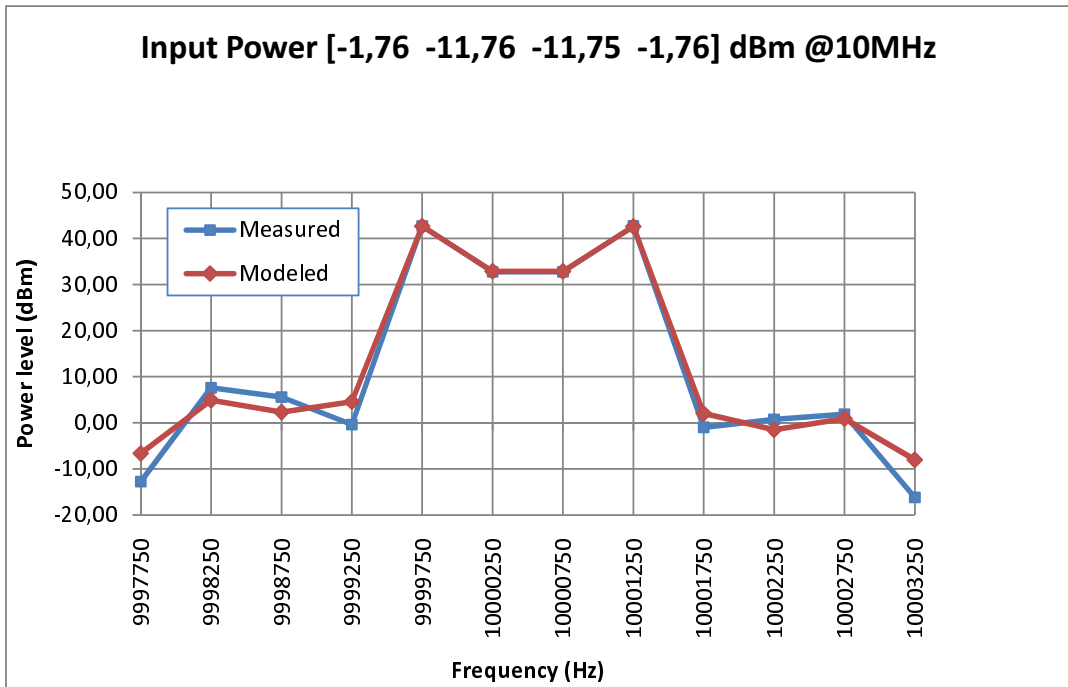
Figure 4.19: Measured frequency spectra of five sample excitation signal for unequal four-tone for a)full range and b)zoomed to fundamental tone



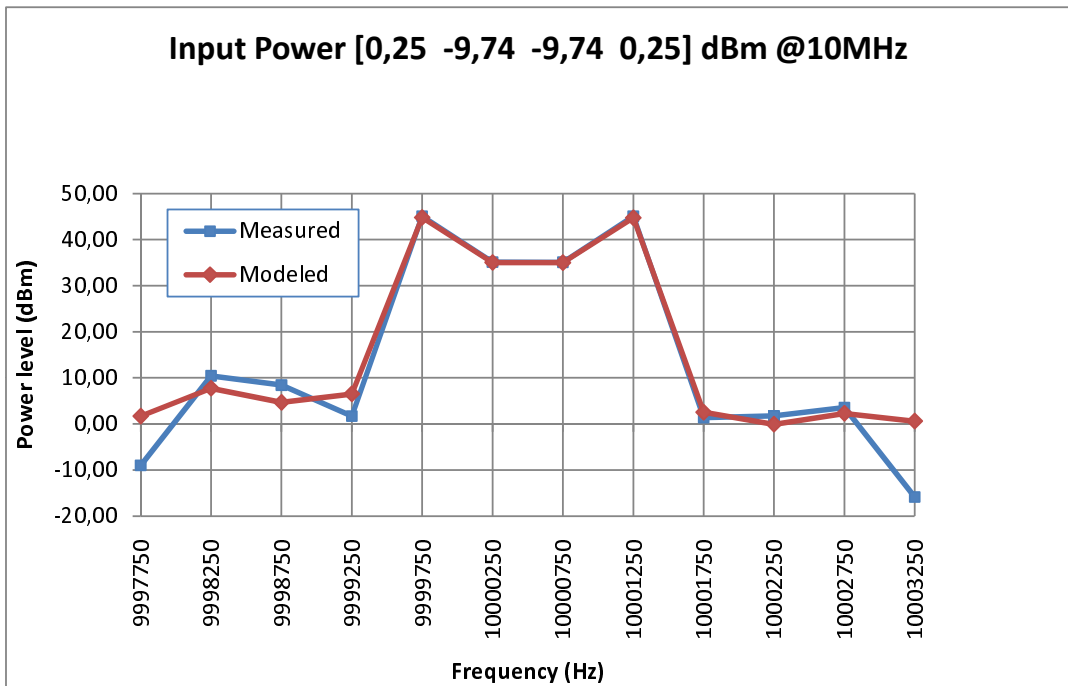
(a) Model estimation and measurement results for Excitation 5



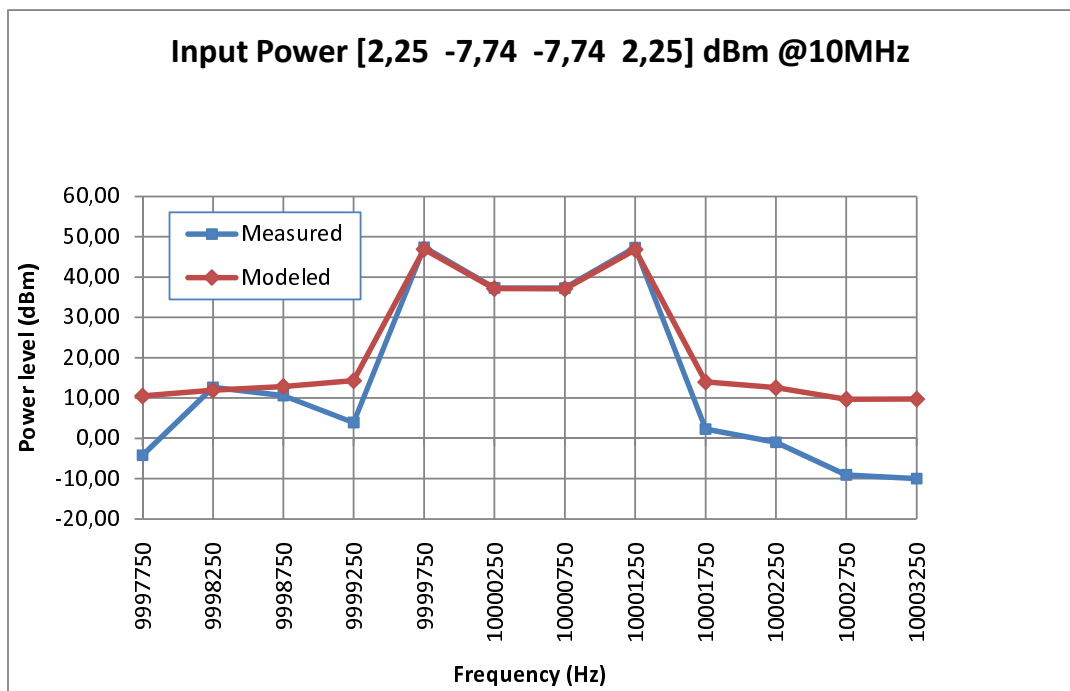
(b) Model estimation and measurement results for Excitation 9



(c) Model estimation and measurement results for Excitation 12



(d) Model estimation and measurement results for Excitation 14



(e) Model estimation and measurement results for Excitation 16

Figure 4.20: Comparison between measurement results and model outputs for four-tone input excitation for five different power levels ( $-8.18dBm$  to  $2.25dBm$ ).

## 4.7 Summary

Power series expression is used frequently in behavioral amplifier modeling techniques with additional component having dynamic behavior according to frequency because GPSE doesn't have ability to represent asymmetry in IMD and FUND components. Hence there is asymmetry in the measurement results of magnitude and phase of IMDL and IMDU, behavioral modeling has to have at least one dynamic component in order to create asymmetry. One possible solution is to use dynamic linear filter with power series and another way to create asymmetry is to add time delay term to the each order term of polynomial like Memory Polynomial Modeling with unit delay.

Asymmetry creation mechanism depends on vector addition. Equations of IMD components for EOM modeling are composed of vectors having same magnitude but different phase, it is expected that there will be asymmetry between IMDL and IMDU. Hence, time delay terms are added to the each order of power series in order to have asymmetry representation ability to the model which is developed under this thesis. Unlike the baseband Memory polynomial, unequal time delay terms are added to each term of polynomial. Effective channel length is changing according to average power which is carried by that channel. It is obvious that average power of each term ( $V_{in}(t)$ ,  $V_{in}^3(t)$ ) are not equal. So, time delay which is added to the each order should not be equal. A new modeling technique is developed which has unequal time delay terms and named as Odd Order Modeling(OOM) since it consists of only odd terms of polynomial series. This model definition is flexible and model order can be increased but model order is limited to 9 in this dissertation for simplicity.

An optimization program is prepared to find model coefficients because it is almost impossible to find them arithmetically. OOM model parameters are extracted according to two-tone  $10Mz/1kHz$  excitation measurement results by optimization program. Model performance of OOM and GPSE modeling techniques are compared by using NMSE metric. Although performance of OOM couldn't be define as *perfect*, OOM gives better result than GPSE.

As a next step, addition of even order terms to the model equation is considered not only to improve the model performance but also to simplify the model equation. The way that is needed to add even order terms to modeling equation has been published previously for *baseband modeling technique*. However, there is no modeling technique using even order

terms in modeling equation for passband modeling. Even order terms' contribution to IMD and FUND is proven mathematically for passband excitation signal. Hence this modeling technique contains even order terms as well as odd order terms, this new technique is named as Even Order modeling (EOM). EOM order is limited to 5 instead of 9 for a simpler model. Even though the number of terms are almost equal for OOM (having 9 order) and EOM (having 5<sup>th</sup>), EOM is simple model for multi-tone investigation (i.e. expansion of 5<sup>th</sup> order of two-tone input is simpler than expansion of 9<sup>th</sup> order of two-tone input).

EOM model parameters are extracted by using the same optimization program after making some modifications, and model performance is compared both with GPSE and OOM. EOM modeling technique's estimations are much more better than the others' estimations for 10Mz/1kHz excitation. Also, EOM validity range is investigated. To do this, model performance is investigated for the signals of which center frequency is swept while tone spacing is 1kHz and then tone spacing is swept while FUNDL tone frequency is 10MHz. Although the EOM performance is the best for the signal having different frequency( $f_0 \pm \%20$ ), GPSE performance became comparable with EOM for the signal having higher frequency separation.

Although model parameters are extracted according to two-tone measurement result, model performance is checked for unequal four-tone signal. EOM performance is as good as expected with one exception. Unexpectedly, error for the lower band first IMD is bigger than expected value.

## CHAPTER 5

### Baseband Applications of EOM Modeling

#### 5.1 Introduction

While EOM modeling is worked on, passband applications are focused on and developed. EOM modeling technique is verified with different passband signals as demonstrated in the previous chapter. In this chapter baseband application results of EOM modeling are given. EOM modeling technique required modification for baseband applications. Modified version of EOM is named as Memory Polynomial with Shaped Delay (MPSD). While extracting the model parameters and comparing model performance, digitally modulated signals are used.

In the first part, MPSD model is extracted for GSM-EDGE signal. When the bandwidth of input signal is narrow; the thermal memory effect dominates the electrical memory. When the bandwidth of the excitation signal is wider, the electrical memory effect dominates [7].

Thermal memory dominates the electrical memory since amplifier is excited with GSM-EDGE signal having  $200\text{kHz}$  bandwidth in the first part. Thermal memory effect is modeled with RC network which represent the thermal resistance and capacitance in [7], [51]. Afterward, MPSD modeling technique is used in DPD application.

In the second part, MPSD model is extracted for WCDMA signal. MPSD models are extracted for five different excitation scenarios. Memory Polynomial Modeling (MPM) estimation errors and the MPSD estimation errors are compared. Comparison is assessed based on three different metrics which are Normalized mean square error (NMSE), adjacent channel error power ratio (ACEPR) and Memory effect modeling ratio (MEMR). NMSE is dominated by in-band error, ACEPR is dominated by out-of-band error and MEMR represents both in-

band and out-of-band error.

## 5.2 Modification on EOM modeling

EOM model definition for passband is given in (4.7) as follows;

$$V_o(t) = \sum_{k=1}^K (a_{2k-1} + a_{2k} \cdot V_{env}(t - \tau_{2k-1})) V_i^{2k-1}(t - \tau_{2k-1}) \quad (5.1)$$

Modification is needed for baseband application of EOM modeling in order to improve model performance although it is not necessary. The mathematical representation of the modified version of EOM modeling, namely MPSD, is as follows:

$$y_{MPSD}[n] = \sum_{s=0}^{M-1} \sum_{k=1}^K a_{k,s} |x[n - \tau(k, s)]|^{k-1} \cdot x[n - \tau(k, s)] \quad (5.2)$$

where definition of  $\tau(k, s)$  is given in (5.3).

$$\tau(k, s) = \begin{cases} 0 & s = 0 \\ avg + \tau_0 e^{-\alpha k} & s \neq 0 \end{cases} \quad (5.3)$$

where "avg" is the average delay value, " $\tau_0$ " is the maximum delay and " $\alpha$ " is the decay ratio. The "avg" is related to Drain-Source average channel length that depends on average power applied to the transistor [52].

Mathematical representation of Memoryless modeling (GPSE), Memory polynomial Modeling (MPM) with unit delay and Memory Polynomial Modeling with Sparse Delay are given in (2.20), (2.35) and (2.38), respectively. These modeling techniques are used to compare with the MPSD model. Advantage of MPSD model is that, there is no need to add extra delay line in order to use high delay value. Conversely, if a higher delay value is needed for instance MPM with unit delay model, extra delay line should be added in that case model becomes more complex.

### 5.2.1 Evaluation Metrics

In order to demonstrate the proposed modeling approach performance, some evaluation metrics need to be reviewed. Normalized mean square error (NMSE) is the metric which indicates

the overall accuracy of a PA modeling. NMSE has already been reviewed in Section 4.4.

Another metric, memory effect modeling ratio (MEMR), is defined as the ratio of rms error that cannot be modeled with M delay tap to the rms error that cannot be modeled with memoryless modeling. Mathematical representation of MEMR is given as:

$$MEMR = 1 - \frac{\|E^{(M)}\|}{\|E^{(0)}\|} \quad (5.4)$$

where  $\|E^{(M)}\|$  represents rms error between measured value and estimated value by the model having M delay tap,  $\|E^{(0)}\|$  represents rms error between measured value and estimated value by the memoryless model. "MEMR value becomes 0 when the memory effects are not accounted and becomes 1 when the whole memory effects are modeled" [53].

Adjacent channel error power ratio (ACEPR) is another metric which is used to express the ratio of error at the adjacent channel power to the main channel power. Mathematical definition of ACEPR is given as:

$$ACEPR = 10 \log \left( \frac{\frac{1}{2} \left( \int_{\text{Low ad ch}} |E(f)|^2 + \int_{\text{Up ad ch}} |E(f)|^2 \right)}{\int_{\text{Main ch}} |Y_{meas}(f)|^2} \right) \quad (5.5)$$

where  $Y_{meas}$  and E represents Fourier transforms of measured value and error between measured and estimated signals.

## 5.2.2 Extraction Algorithm for MPSD

Model extraction consists of two stages: 1) delay coefficient extraction stage ("avg", " $\tau_0$ " and " $\alpha$ ") and 2) model coefficient extraction (" $a_{k,s}$ " coefficients). The detail of the proposed technique is described below. When the MPSD model with memory depth of 2 has been considered, the first set of memories are set to zero to represent the static nonlinear behavior of the PA. The second set of the memory terms has been considered as follows:

- Step 1: "m" values are set to zero for second delay line.
- Step 2: " $a_{k,s}$ " coefficients are calculated using Least Square (LS) algorithm.
- Step 3: Model estimation error is calculated by using NMSE and MEMR metrics.

- Step 4: If NMSE/MEMR value is better than predefined threshold, the delay values are stored as well as NMSE/MEMR.
- Step 5: "m" value is increased one step and then previous 4 steps are repeated. The delay value for upper order shouldn't be greater than the delay value for lower order.
- Step 6: Delay values are sorted in decreasing order according to corresponding NMSE/MEMR value.
- Step 7: The delay value placed on top is chosen in order to find "avg", " $\tau_0$ " and " $\alpha$ " value by using (5.3).
- Step 8: If Step 7 fails, these values are assumed as irrelevant and then the values placed at one lower rank in the ordered list are chosen.

The coefficient set which gives the least estimation error has been selected as the model coefficients. The above procedure have been developed in MATLAB and evaluated in the following section.

Figure 5.1 shows the shaped memory delay values of the MPSD model which are found by using (5.3) for the 101-WCDMA signal as an example. The delay values are rounded to the closest integer values to fit the memory of the discrete model. In Figure 5.1 the blue line with star marker shows the calculated delay values and the red circles show the rounded delay values considered in the MPSD model.

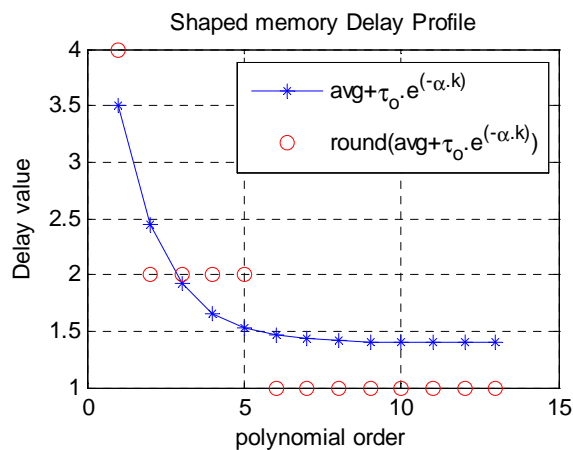


Figure 5.1: Shaped memory delay values for 101-WCDMA excitation scenario

### 5.3 Thermal Memory Effect Modeling and Linearization Application

As it is explain in Section 2.2 thermal memory effect dominates the electrical memory effect when amplifier is excited with the signal having narrow bandwidth. There is a limit which defines the boundary of region where thermal memory effect dominates. This boundary may be different for different amplifier because it depends on amplifier structure such as package, die size. But, there is a measurement technique to find this limit [8]. In order to separate the regions magnitudes of IMDL and IMDU are measured while the excitation frequency separation is sweeping. IMDL and IMDU response of a sample amplifier line up (Class B driver amplifier and LDMOS-45 W peak power amplifier is in cascade connected) is measured and plotted as given in Figure 5.2 while tone-spacing of two-tone signal is sweeping from  $200kHz$  to  $5.8MHz$ . Average power level of excitation signal is smaller than  $P_{1dB}$ . Thermal memory effect dominates electrical memory effect for this amplifier line-up when frequency separation is smaller than  $480kHz$  as seen from Figure 5.2. Similarly, electrical memory effect dominates the thermal memory effect when tone spacing is greater than  $2MHz$ . It is obvious that thermal memory dominates the electrical memory effect for this amplifier line-up when it is excited with GSM-EDGE signal. A modeling technique which has ability to represent thermal memory effect should be used in order to get accurate estimation, asymmetry in the IMD is resulted from thermal memory effect. At this point, MPSD model advantage is came in to the forefront.

Linearization with DPD technique is repeatedly explained [54, 41], and applied with different modeling technique, so it is straight forward. An amplifier response is shown in Figure 5.3 [54]. Before linearization, an amplifier output is represented as  $P_{out}$  when the amplifier is excited with the power level of  $P_{in}$ . If linearization could be done perfectly, the amplifier output would be  $P_{out-pd}$ .

In order to prevent confusion, EOM model explained up to now is defined as "Forward Model" and the new modeling which distort the input signal in order to get linear output is defined as "Inverse Model". Inverse model should increase input power level to  $P_{in-pd}$  so that amplifier output will be  $P_{out-pd}$ . Inverse model gain characteristic is given in Figure 5.4 [54]. That's why Inverse model is required for DPD application.

Difference between Forward model and Inverse model is just input and output signal defini-

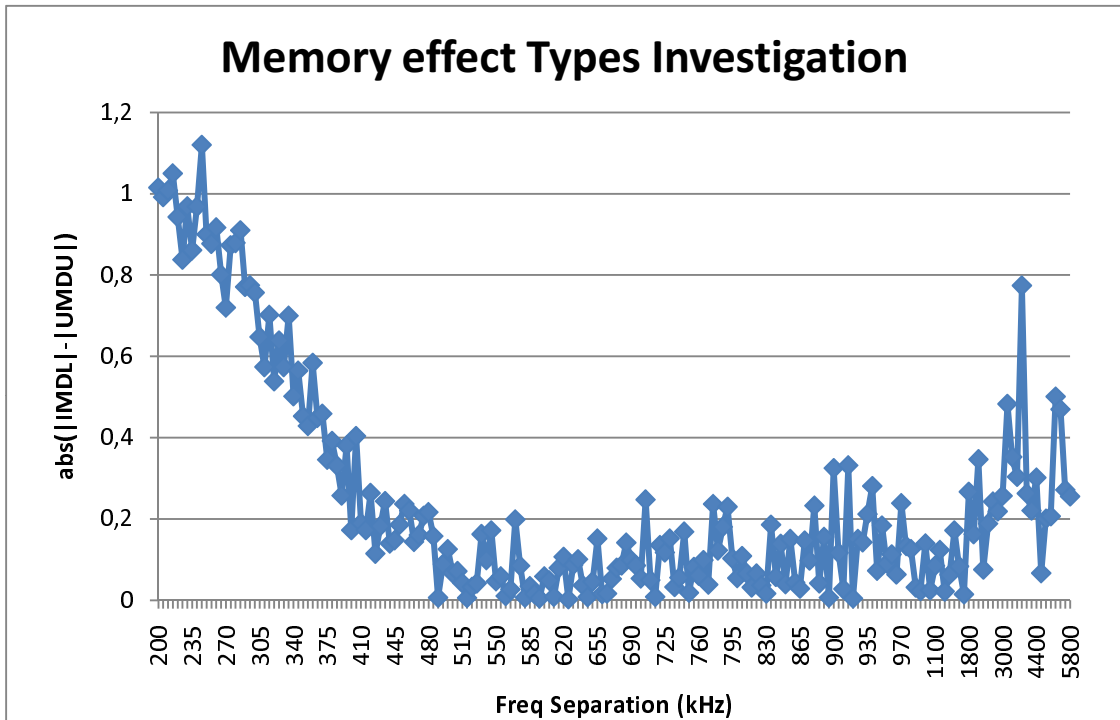


Figure 5.2: Difference between magnitude of IMDL and magnitude of IMDU to distinguish the region where thermal memory effect dominates

tion. While Forward model parameters are being extracted, input power of the real-amplifier is chosen as input and output power chosen as output. However, while Inverse model parameters are being extracted, a fictitious amplifier is assumed and output of real amplifier is chosen as input of fictitious amplifier. Similarly input of real amplifier is chosen as output of the fictitious amplifier. Then, model parameters of the fictitious amplifier is extracted and defined as Inverse model parameters.

The sample amplifier line-up is excited with GSM-EDGE signal and the output of line-up is measured at baseband. Then four different forward models are extracted for the different number of tap by using measurement results. Model performances are listed in Table 5.1. MPM with unit delay models are extracted for two tap to six tap. There is a very small improvement when the number of taps is increased from two to six since thermal memory effect is dominant in this measurement and much more previous samples are required to represent thermal memory effect. MEMR values of the MPM with sparse delay is bigger than the MEMR value of the MPM with unit delay which means that sparse delay performance is better than the unit delay performance since sparse delay can take greater delay value. MPSD performance is the best one as it is seen from Table 5.1. Even though the number of delay taps is chosen as two

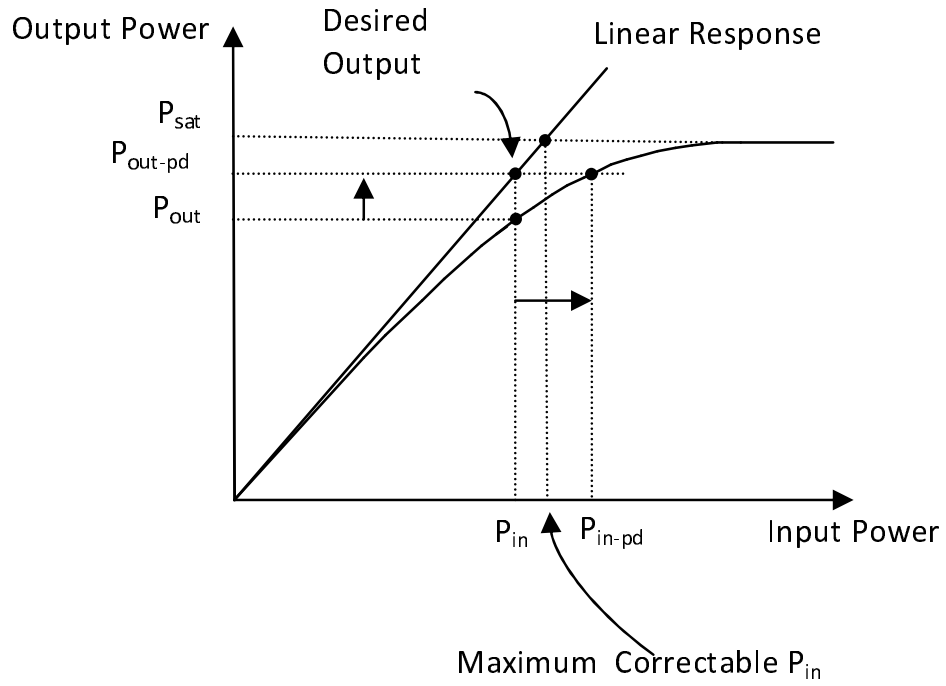


Figure 5.3: DPD and an amplifier output power versus input power [54]

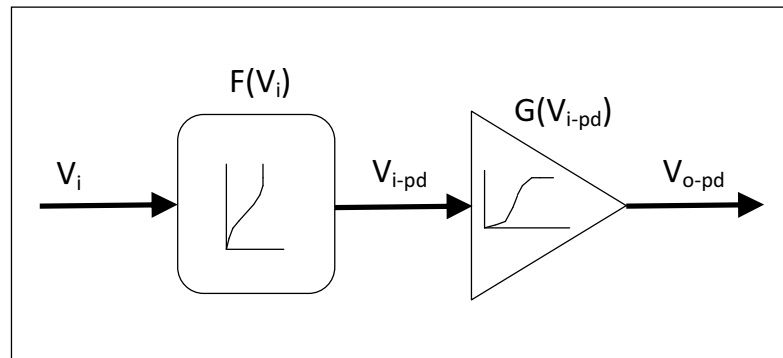


Figure 5.4: Linearization line-up [54]

for MPSD (line 10 in Table 5.1) and chosen as four tap for MPM with sparse delay (line 9), performance of the MPSD is better. Afterward, inverse models of four modeling techniques are extracted and MEMR and NMSE values are listed in Table 5.2. Again MPSD shows the best performance as seen in Table 5.2.

After inverse models of for four modeling techniques are extracted, the amplifier is excited with the distorted input. There is improvement in the IMD level of DPD output. Improvement of MPSD is better than the improvement of MPM with sparse delay model.

Table 5.1: Forward Models' performance comparison for GPSE, MPM with unit delay, MPM with sparse delay and MPSD

Index	Polynomial Order	Number of Tap	MEMR	NMSE	Modeling Type
1	6	1	0.000	-38.34	GPSE
2	6	2	0.296	-39.87	MPM unit delay
3	6	3	0.298	-39.88	MPM unit delay
4	6	4	0.299	-39.88	MPM unit delay
5	6	5	0.299	-39.89	MPM unit delay
6	6	6	0.299	-39.89	MPM unit delay
7	6	2	0.435	-40.82	MPM sparse delay
8	6	3	0.447	-40.91	MPM sparse delay
9	6	4	0.455	-40.97	MPM sparse delay
10	6	2	0.526	-41.58	MPSD
11	6	3	0.608	-42.41	MPSD

Table 5.2: Inverse Models' performance comparison of GPSE, MPM with unit delay, MPM with sparse delay and MPSD

Polynomial Order	Number of Tap	MEMR	NMSE	Modeling Type
10	1	0.000	-38.37	GPSE
10	2	0.263	-39.70	MPM unit delay
10	2	0.433	-40.84	MPM sparse delay
10	2	0.545	-41.79	MPSD

#### 5.4 Electrical Memory Effect Modeling Application

The proposed MPSD model is evaluated using the modulated WCDMA signals for a high power (300-W peak power) Doherty PA operating in the 2110MHz - 2170MHz frequency band. Six different WCDMA excitation signals with up to 4-carrier are used in the model validation. WCDMA signals along with their corresponding, "avg", " $\tau_0$ " and " $\alpha$ " parameters and the delay values for the different nonlinearity order are listed in Table 5.3.

The delay values corresponding to the higher order terms are always less than the delay values

Table 5.3: Delay Values

WCDMA	avg	$\tau$	$\alpha$	m											
				2	1	1	1	1	1	1	1	1	1	1	1
1	0	1.5	0.05	2	1	1	1	1	1	1	1	1	1	1	1
11	0.6	1.9	0.11	3	2	2	2	2	2	2	1	1	1	1	1
101	1.4	2.1	0.7	4	2	2	2	2	1	1	1	1	1	1	1
111	1.4	2.1	0.7	4	2	2	2	2	1	1	1	1	1	1	1
1001	1.48	3.02	1.2	5	2	2	2	2	1	1	1	1	1	1	1
1111	1.48	3.02	2.6	5	2	1	1	1	1	1	1	1	1	1	1

corresponding to the lower order terms. Since higher order generates very high frequency, corresponding delay time is decreased. If we assume there is capacitance which result in memory effect, time constant for the signal having high frequency is smaller than the signal having small frequency. As the bandwidth of the signal getting wider the " $\alpha$ " became in increasing order which yields decreasing in the delay value for higher order terms. In contrast, the delay value for the first term is increasing when the bandwidth of input increases.

Table 5.4: Comparison of the MPM and MPSD Models based on the MEMR, NMSE and ACEPR values

WCDMA	MEMR		NMSE		ACEPR	
	MPM	MPSD	MPM	MPSD	MPM	MPSD
1	0.039	0.059	-43.436	-43.617	-53.18	-53.29
11	0.162	0.168	-42.926	-42.994	-51.57	-51.73
101	0.426	0.452	-39.109	-39.512	-45.95	-46.63
111	0.414	0.432	-39.820	-40.088	-46.77	-46.99
1001	0.293	0.327	-35.323	-35.746	-40.22	-42.86
1111	0.416	0.437	-37.444	-37.763	-44.69	-45.14

The MPSD model with two sets of delay taps is compared with MPM model with the same number of delay taps. The comparison is based on the MEMR, NMSE, and ACEPR metrics between the estimated output of the model and the measured output signal from the PA.

Table 5.4 lists the comparison results between the MPM and the MPSD models for nonlinearity order of 13 ( $K=13$ ) and the memory depth of 2 ( $M=2$ ). In this case, the numbers of coefficients are similar for both models. It can be said that MPSD model estimate the output

better than MPM model for adjacent channel by considering Table 5.4.

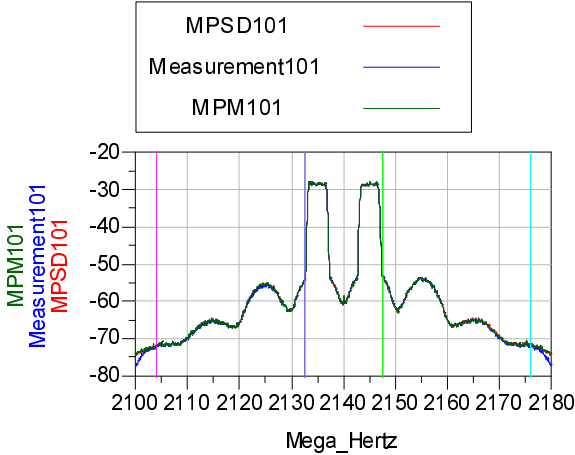


Figure 5.5: Frequency spectra of model estimation and measurement result for 101\_WCDMA excitation scenario

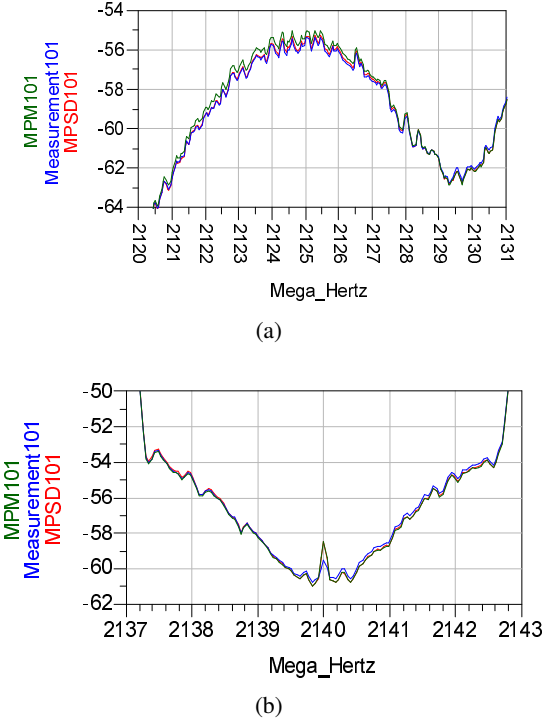


Figure 5.6: Zoomed version frequency spectra of model estimation and measurement results for 101\_WCDMA excitation scenario

Considering the MEMR and NMSE metrics listed in Table 5.4, the MPSD model has slightly

better performance over for the MPM model. Especially for the 1-carrier signal, the MEMR of the MPSD model is approximately two times better than the MEMR of the MPM model. MPSD model is developed to improve MPM model error. If the number of delay line is chosen equal both for MPM and for MPSD model, MPSD model gives better result than MPM model.

The power spectral density (PSD) of estimated output of the MPM and MPSD models are compared with the measured output of the PA for the 101\_WCDMA excitation scenario and plotted in Figure 5.5. In Figure 5.5 the vertical lines represent the boundary of channels. Zoomed version of measured and estimated by MPM and MPSD frequency spectra are given in Figure 5.6.

## 5.5 Summary

In this chapter, baseband applications of EOM are investigated. At first, modeling equation is modified. This modified version of EOM is named as Memory Polynomial with Shaped Delay (MPSD). MPSD model is used to model thermal memory effect and electrical memory effect.

In the first part of this chapter, Thermal memory effect modeling capability of MPSD is investigated. After proved that thermal memory effect dominates the electrical memory for the sample amplifier for the signal having bandwidth is narrower than  $480kHz$ , sample amplifier response is measured for GSM-EDGE signal. Four different models are extracted by using those measurement results and compared. MPSD model gives the best result. Then, inverse models are extracted for DPD application. Again MPSD gives the best estimation result for inverse modeling. Amplifier output is measured for both with DPD and without DPD cases and plotted on the same graph. MPSD model decreased the power level of IMD signal more than MPM.

In the second part, MPM coefficients and MPSD coefficients are extracted for six different excitation scenarios to model a 300W peak power amplifier. Comparison is assessed by using three different metrics, MEMR, NMSE and ACEPR. Although both modeling techniques have same number of delay line and model order, MPSD model estimation error is always lower than MPM model.

## CHAPTER 6

### Conclusion and Future work

#### 6.1 Conclusion

In this dissertation, two different behavioral modeling techniques, namely Odd Order Modeling (OOM) and Even Order Modeling (EOM) are proposed and introduced in order to get model of asymmetric intermodulation distortion and to represent memory effect. A measurement setup is developed in order to measure magnitude and phase of amplifier response. Then, one of these modeling techniques, EOM, is used in Digital Pre-Distorter (DPD) application at baseband.

Representation of a system as a black-box having mathematical relation between input and output is defined as "Behavioral Model". Behavioral modeling is important especially for the designers working in inter disciplinary areas.

Behavioral model should satisfy the requirements of the usage purposes:

Behavioral model should be compact and easy to use. If behavioral model includes so many operators, it will be difficult to use it in another system. It should make easier to design a new system having that amplifier instead of making it complicated. Behavioral model should estimate the output accurately according to the input signal as well. Model estimation error should be in the range of acceptable region. Acceptable region may be different for different applications. These two requirements are the main aim of this dissertation. In addition to those, there is another aim, the model estimation should be calculated easily. There are a number of behavioral models in the literature such as General Power Series Expression (GPSE), Volterra Series, Wiener-Hammerstein Models, Multi-Slice Behavioral Modeling. Each of

them has some disadvantages such as kernel parameter measurement requirement, complicated transfer function requirement, cannot model asymmetry.

Measurement results of input and output are required to find relation between them. Measurement step is the first and one of the important steps of behavioral modeling since model success directly affected by the measurement results accuracy. Thus, a new measurement setup is developed. One-tone AM/AM & AM/PM, two-tone AM/AM & AM/PM and four-tone AM/AM response can be measured by using this measurement setup. Hence OOM model and EOM model defined as passband model, measurement setup is designed to measure frequency spectra of signal instead of measuring the time domain baseband I/Q data. Two signal generators are used to create two-tone signal. In order to measure phase, one more signal generator as a phase reference, one digital attenuator for wider dynamic range are added to the measurement setup. The 10MHz reference signal generated by the one of signal generators is transferred to the others for phase lock. However, phase difference between IMDL and IMDU couldn't be measured since phase reference is lost when the frequency of signal generator is changed. To overcome this problem, arbitrary wave shape generator (AWSG) is added to the measurement setup to create four-tone signal having zero phase difference between each other. A computer on which "Agilent VEE" program works is added to the measurement setup and connected to the each instruments via GPIB cables to take data quickly for repetitive measurements. Phase of signal is calculated by measuring only magnitude instead of injecting the signal having 180° out-of-phase. While phase calculation technique takes 6second, 180° out-of-phase signal injection requires more than that. This is not acceptable for phase measurement for excitation signal having wide dynamic range because signal generator local oscillator's phase reference is changing over time, slowly. Therefore, the shorter time we spent for measurement the more correct phase measurement will be done. In order to get rid of temperature changing bad effect, phase measurement is started after signal generator running at least two hour. In addition to this, air condition is running during measurement time.

Another special phase measurement setup is prepared to check phase calculation technique. Phase of through line is measured while the phase of signal generator is sweeping with 1° steps for 360° range. 1° phase change is observed for successive step except the region which close to 0° phase difference. This small error resulted from nature of cosine function used in the phase calculation equation. During this measurement for 360 steps, the power level of and

the frequency of signal generators did not changed.

Phase of through line is measured again while power levels of signal generators are sweeping with  $1dB$  steps by using main measurement setup. Although constant phase difference is expected, there is change in the measured phase which is bigger than acceptable error. Source of this error may be the fine power level adjustment unit and the AM/PM behavior of the amplifier which is used at the output stage of signal generator. Since the change in the phase is constant according to power level, phase calibration step is added to the phase measurement process. Look-Up-Table (LUT) which contains the phase change related with power level is prepared. After finishing the phase calibration step, phase of through line is measured a number of times for  $16dB$  dynamic range and the phase of FUNDL component of sample amplifier is measured for a number of times for  $20dB$  dynamic range. Each of repetitive measurement is performed at different time and by using different LUT. There is a small difference among repetitive measurement results.

After the measurement setup is prepared, input and output response of sample amplifier are measured. A sample amplifier having maximum gain is  $45.7dB$  around working frequency, saturation peak power is more than  $390W$  ( $56dBm$ ) and output  $P_{1dB}$  is  $53.35dBm$ , is examined in this dissertation. This sample amplifier is composed of more than one stage (driver and two Class AB amplifier is connected in a push-pull structure as a main amplifier).

At the beginning, working frequency is decided as  $10MHz$  and the frequency separation is decided as  $1kHz$  for two-tone excitation. Since the amplifier has been designed for  $1MHz - 30MHz$  frequency band by manufacturer, amplifier responses are measured at  $2.5MHz$ ,  $10MHz$  and  $30MHz$ .  $10MHz$  measurement results are given in this dissertation as an example.  $1kHz$  has no special meaning. At that frequency separation amplifier response is dominated by thermal memory, and modeling thermal memory with memory polynomial is one of the original contributions of this thesis. Another measurements are needed for verification. So, amplifier responses are measured for different working frequency having same frequency separation and for different frequency separation having same working frequency ( $f_o \pm \%20$ ). Moreover, amplifier responses are measured for  $10MHz/300Hz$  and  $10MHz/3.3kHz$ . In addition to these measurements, amplifier response for unequal four-tone excitation is measured for  $18dB$  dynamic range.

While measuring amplifier response for any excitation, two propellers were running just be-

side amplifier in order to hold up environment temperature constant.

Asymmetry at the IMD components may reach  $10\text{dB}$  as in  $10\text{MHz}/1\text{kHz}$  excitation measurement result. This asymmetry is resulted from memory effect. Thus, in order to increase DPD linearization success, behavioral model should have ability to model memory effect. In other words, there should be asymmetry between output components of model estimation. GPSE modeling technique is easy to use in any system but it is unable to create asymmetry at the IMD components. So, introduced new modeling techniques are based on power series modeling technique. Asymmetry at the IMD components can be created by adding time delay to the each term of the power series expansion. Phase of IMD is determined by multiplication of frequency and delay term. Asymmetry creation mechanism is based on vector addition having same magnitude but different phase. As it can be seen from phasor representation of IMDL and IMDU, IMD components are composed of vectors having same magnitude but different phase. Asymmetry creation mechanism represented by using vectors as given in Section 4.2.1 in detail. Addition of the same time delay value to the all order terms also creates asymmetry as it is done in other modeling type, such as Memory Polynomial with Unit Delay or Memory Polynomial with Sparse Delay. However, Hu *et al.* [52] proposed that effective channel length of transistor is affected by the average power transferred by that channel. Average power of the first order and the third order of input signal are different (i.e. effective channel length for the signal created by the first order and for the signal created by the third order are different). Therefore, the time delay values for the each polynomial order are defined as unequal in the introduced modeling techniques (OOM and EOM). One of the other original contributions of this thesis is modeling amplifier behavior with power series having **unequal time delay terms**. This is the first modeling technique in the literature which uses unequal time delay terms.

Since even terms do not have any contribution to neither IMD nor FUND components, proposed model is composed of odd order polynomial series having unequal time delay terms.

Model parameters are found by equating the measurement results and IMD & FUND component phasor representation equations. Optimization tool of Matlab programme is used to find model coefficients since phasor representation equation of IMD & FUND are not linear. Cost function of optimization program is defined to minimize square error between estimated value and measurement result.

In order to compare model success, GPSE model is extracted as well. GPSE coefficients are chosen as complex number in order to have phase modeling ability. At that time a metric is needed to compare these models. Normalized mean square error (NMSE) metric is preferred since it is mostly used one by the researchers. Overall performance of OOM is better than GPSE.

In literature, it is mentioned that even order term improves model success, but there isn't any paper which shows even order terms contribution to the IMD and FUND components for **passband modeling**. If even order terms are added to the modeling polynomial series directly, it is impossible to improve model estimation. Since envelope of input signal changes the bias point of amplifier, it should have positive effect on modeling. So, envelope of input signal is added to even order terms in order to get contribution to the IMD and FUND components. This new modeling technique is named as EOM and contribution of envelope term to the IMD and FUND components is mathematically proved in Chapter B. Polynomial order is decreased to 5 for EOM modeling for the same amplifier. So, even order terms make simpler the model by reducing model order. Although EOM modeling technique is using 5<sup>th</sup> order, it has at least 10dB better NMSE value for IMD components than GPSE which uses 9<sup>th</sup> order for 10MHz/1kHz excitation situation. EOM modeling is more flexible to the working frequency change than GPSE. While frequency separation is decreased, EOM estimation is still better, but when frequency separation is increased, EOM estimation is worse than GPSE. This is an exceptional situation. EOM model can be improved to overcome this exceptional situation. This is one of the future works as well.

EOM model performance is checked for unequal four-tone, although model parameters are found by using two-tone measurement results only. EOM performance is good for inband tones and for far-off tones. First lower band adjacent tone ( $IMDL_1$ ) estimation error is greater than expected error. This may result from misaligned fundamental tones interactions. Model may be modified to satisfy this situation.

Finally, baseband application of EOM model is investigated for both thermal memory effect dominated and electrical memory effect dominated measurement results situations. At the beginning, EOM model is modified for baseband application and named as Memory Polynomial with Shaped delay (MPSD). MPSD performance is compared with three other modeling techniques (GPSE, MPM with unit delay and MPM with sparse delay). EOM gives always the

best result. Moreover, MPSD model is used in DPD circuit to diminish the intermodulation power level for the thermal memory effect dominated situation.

## 6.2 Future Research

In this dissertation, a new measurement setup is proposed to measure AM/AM and AM/PM response of amplifier. Phase is measured/calculated by measuring magnitudes of signals. Measurement error is always less than  $1^\circ$ . However, if the phase difference is close to  $0^\circ$  error may increase to  $6^\circ$  due to nature of cosine function used in calculation procedure. One of the future works would be to improve measurement setup to overcome this problem. There could be used another function to verify measurement results.

One of the other future research, may be the first one, would be try to understand the reason of unexpected change in the IMD behavior when frequency separation is changed. After find the reason, EOM model would be modified to get flexible gain according to frequency separation change.

Power level of lower band first adjacent tone ( $IMDL_1$ ) is less than the power level of the far-off tones for unequal four-tone excitation measurement results. Conversely, power level of  $IMDL_1$  is greater than the far-off tones at the model estimation. The reason of this diminishing in the power level of  $IMDL_1$  would be investigated for another amplifiers. If this is general amplifier behavior, EOM model will be modified to satisfy this behavior.

One of the main goal of developing behavioral model is to use it in linearization system. This modeling technique is used in DPD for linearization and good performance is observed at baseband. One of the future work would be to use this modeling technique in linearization at passband with appropriate method.

## REFERENCES

- [1] K. Remley, D. Williams, D. Schreurs, and J. Wood, "Simplifying and interpreting two-tone measurements," *IEEE Transactions on Microwave Theory and Techniques*, vol. 52, no. 11, pp. 2576–2584, 2004.
- [2] N. Borges de Carvalho and J. C. Pedro, "A comprehensive explanation of distortion sideband asymmetries," *Microwave Theory and Techniques, IEEE Transactions on*, vol. 50, no. 9, pp. 2090–2101, 2002.
- [3] J. E. Chen, "Modeling rf systems," <http://http://www.designers-guide.org/Modeling/modeling-rf-systems.pdf>, March 2005, accessed December 2010.
- [4] J. Wood and D. E. Root, *Fundamentals of Nonlinear behavioral modeling for RF and Microwave Design*. Artech House, 2005.
- [5] J. Vuolevi, T. Rahkonen, and J. Manninen, "Measurement technique for characterizing memory effects in rf power amplifiers," in *Radio and Wireless Conference, 2000. RAWCON 2000. 2000 IEEE*, 2000, pp. 195 –198.
- [6] W. John and R. David, "Fundamentals of nonlinear behavioral modeling for rf & microwave design," *Geodynamica Acta*, vol. 21, no. 5-6, 2008.
- [7] S. Boumaiza and F. Ghannouchi, "Thermal memory effects modeling and compensation in rf power amplifiers and predistortion linearizers," *Microwave Theory and Techniques, IEEE Transactions on*, vol. 51, no. 12, pp. 2427 – 2433, Dec. 2003.
- [8] O. Tornblad, B. Wu, W. Dai, C. Blair, G. Ma, and R. Dutton, "Modeling and measurements of electrical and thermal memory effects for rf power Idmos," in *Microwave Symposium, 2007. IEEE/MTT-S International*, Jun. 2007, pp. 2015 –2018.
- [9] J. Vuolevi, T. Rahkonen, and J. Manninen, "Measurement technique for characterizing memory effects in rf power amplifiers," *IEEE Transactions on Microwave Theory and Techniques*, vol. 49, no. 8, pp. 1383–1389, 2001.
- [10] A. L. Walker, "Behavioral modeling and characterization of nonlinear operation in rf and microwave systems," Ph.D. dissertation, North Carolina State University, 2005.
- [11] J. He, J. S. Yang, Y. Kim, and A. Kim, "System-level time-domain behavioral modeling for a mobile wimax transceiver," in *Behavioral Modeling and Simulation Workshop, Proceedings of the 2006 IEEE International*, Sep. 2006, pp. 138 –143.
- [12] W. Jang, "Modeling asymmetric distortion in multichannel radio frequency communication systems," Ph.D. dissertation, North Carolina State University, 2006.
- [13] M. Steer, P. Khan, and R. Tucker, "Relationship between volterra series and generalized power series," *Proceedings of the IEEE*, vol. 71, no. 12, pp. 1453 – 1454, dec 1983.

- [14] D. D. Weiner and J. F. Spina, *Sinusoidal analysis and modeling of weakly nonlinear circuits*. Van Nostrand Reinhold (New York), 1980.
- [15] K. Y. Huang, L. Yiming, and L. Chien-Ping, "A time-domain approach to simulation and characterization of rf hbt two-tone intermodulation distortion," *Microwave Theory and Techniques, IEEE Transactions on*, vol. 51, no. 10, pp. 2055–2062, 2003.
- [16] P. Arno, F. Launay, J. Fournier, and J. Grasset, "A simple rf power amplifier characterization using am-am, am-pm measurements based on cdma signal statistics," in *Microwave Conference, 2004. 34th European*, vol. 2, 2004, pp. 693–696.
- [17] K. Gharaibeh and M. Steer, "Modeling distortion in multichannel communication systems," *Microwave Theory and Techniques, IEEE Transactions on*, vol. 53, no. 5, pp. 1682 – 1692, May 2005.
- [18] G. Heiter, "Characterization of nonlinearities in microwave devices and systems," *Microwave Theory and Techniques, IEEE Transactions on*, vol. 21, no. 12, pp. 797 – 805, Dec. 1973.
- [19] V. Volterra, *Theory of Functionals and of Integro-differential Equations*. Dover, New York, 1959.
- [20] S. Maas, B. Nelson, and D. Tait, "Intermodulation in heterojunction bipolar transistors," *Microwave Theory and Techniques, IEEE Transactions on*, vol. 40, no. 3, pp. 442 –448, Mar. 1992.
- [21] S. Maas, "Third-order intermodulation distortion in cascaded stages," *Microwave and Guided Wave Letters, IEEE*, vol. 5, no. 6, pp. 189 –191, Jun. 1995.
- [22] N. B. Carvalho and J. C. Pedro, "Two-tone imd asymmetry in microwave power amplifiers," in *Microwave Symposium Digest., 2000 IEEE MTT-S International*, vol. 1, 2000, pp. 445–448 vol.1.
- [23] R. Roy and J. Sherman, "A learning technique for volterra series representation," *Automatic Control, IEEE Transactions on*, vol. 12, no. 6, pp. 761 – 764, dec 1967.
- [24] S. Boyd, Y. Tang, and L. Chua, "Measuring volterra kernels," *Circuits and Systems, IEEE Transactions on*, vol. 30, no. 8, pp. 571 – 577, Aug. 1983.
- [25] C. Evans, D. Rees, L. Jones, and M. Weiss, "Periodic signals for measuring nonlinear volterra kernels," *Instrumentation and Measurement, IEEE Transactions on*, vol. 45, no. 2, pp. 362 –371, Apr. 1996.
- [26] T. Wang and T. Brazil, "A volterra mapping-based s-parameter behavioral model for nonlinear rf and microwave circuits and systems," in *Microwave Symposium Digest, 1999 IEEE MTT-S International*, vol. 2, June 1999, pp. 783 –786.
- [27] F. Verbeyst and M. Vanden Bossche, "The volterra input-output map of a high-frequency amplifier as a practical alternative to load-pull measurements," *Instrumentation and Measurement, IEEE Transactions on*, vol. 44, no. 3, pp. 662 –665, Jun. 1995.
- [28] M. Maqusi, "Characterization of nonlinear distortion in hrc multiplexed cable television systems," *Circuits and Systems, IEEE Transactions on*, vol. 32, no. 6, pp. 605 – 609, Jun. 1985.

- [29] G. Orenco, P. Colantonio, A. Serino, F. Giannini, G. Ghione, M. Pirola, and G. Stegmayer, "Time-domain neural network characterization for dynamic behavioral models of power amplifiers," in *Gallium Arsenide and Other Semiconductor Application Symposium, 2005. EGAAS 2005. European*, 2005, pp. 189–192.
- [30] W. Greblicki and M. Pawlak, "Nonparametric identification of hammerstein systems," *Information Theory, IEEE Transactions on*, vol. 35, no. 2, pp. 409–418, Mar. 1989.
- [31] K. Narendra and P. Gallman, "An iterative method for the identification of nonlinear systems using a hammerstein model," *Automatic Control, IEEE Transactions on*, vol. 11, no. 3, pp. 546–550, Jul. 1966.
- [32] W. Greblicki, "Nonparametric identification of wiener systems by orthogonal series," *Automatic Control, IEEE Transactions on*, vol. 39, no. 10, pp. 2077–2086, Oct. 1994.
- [33] S. Billings and S. Fakhouri, "Identification of nonlinear systems using the wiener model," *Electronics Letters*, vol. 13, no. 17, pp. 502–504, 18 1977.
- [34] E.-W. Bai, "An optimal two stage identification algorithm for hammerstein-wiener nonlinear systems," in *American Control Conference, 1998. Proceedings of the 1998*, vol. 5, Jun. 1998, pp. 2756–2760 vol.5.
- [35] P. Crama and Y. Rolain, "Broadband measurement and identification of a wiener-hammerstein model for an rf amplifier," in *ARFTG Conference Digest, Fall 2002. 60th*, 2002, pp. 49–57.
- [36] M. Sano and L. Sun, "Identification of hammerstein-wiener system with application to compensation for nonlinear distortion," in *SICE 2002. Proceedings of the 41st SICE Annual Conference*, vol. 3, Aug 2002, pp. 1521–1526 vol.3.
- [37] F. Taringou, B. Srinivasan, R. Malhame, and F. Ghannouchi, "Hammerstein-wiener model for wideband rf transmitters using base-band data," in *Microwave Conference, 2007. APMC 2007. Asia-Pacific*, Dec 2007, pp. 1–4.
- [38] F. Ghannouchi, F. Taringou, and O. Hammi, "A dual branch hammerstein-wiener architecture for behavior modeling of wideband rf transmitters," in *Microwave Symposium Digest (MTT), 2010 IEEE MTT-S International*, May 2010, pp. 1692–1695.
- [39] H. Ku, M. McKinley, and J. Kenney, "Quantifying memory effects in rf power amplifiers," *Microwave Theory and Techniques, IEEE Transactions on*, vol. 50, no. 12, pp. 2843–2849, Dec 2002.
- [40] L. Ding, G. Zhou, D. Morgan, Z. Ma, J. Kenney, J. Kim, and C. Giardina, "Memory polynomial predistorter based on the indirect learning architecture," in *Global Telecommunications Conference, 2002. GLOBECOM '02. IEEE*, vol. 1, nov 2002, pp. 967–971 vol.1.
- [41] J. Kim and K. Konstantinou, "Digital predistortion of wideband signals based on power amplifier model with memory," *Electronics Letters*, vol. 37, no. 23, pp. 1417–1418, Nov 2001.
- [42] H. Zhou, G. Wan, and L. Chen, "A nonlinear memory power amplifier behavior modeling and identification based on memory polynomial model in soft-defined short-wave transmitter," in *Wireless Communications Networking and Mobile Computing (WiCOM), 2010 6th International Conference on*, sept. 2010, pp. 1–4.

- [43] K. Hyunchul, M. D. McKinley, and J. S. Kenney, "Extraction of accurate behavioral models for power amplifiers with memory effects using two-tone measurements," in *Microwave Symposium Digest, 2002 IEEE MTT-S International*, vol. 1, 2002, pp. 139–142.
- [44] J. Nan, J. Li, and Y. Liu, "Study and simulation of power amplifier behavioral model with sparse delay taps," in *Microwave, Antenna, Propagation and EMC Technologies for Wireless Communications, 2009 3rd IEEE International Symposium on*, oct. 2009, pp. 793–796.
- [45] C. Crespo-Cadenas, J. Reina-Tosina, and M. J. Madero-Ayora, "Phase characterization of two-tone intermodulation distortion," in *Microwave Symposium Digest, 2005 IEEE MTT-S International*, 2005, p. 4 pp.
- [46] S. Futatsumori, M. Furuno, T. Hikage, T. Nojima, A. Akasegawa, T. Nakanishi, and K. Yamanaka, "Precise measurement of imd behavior in 5-ghz hts resonators and evaluation of nonlinear microwave characteristics," *Applied Superconductivity, IEEE Transactions on*, vol. 19, no. 3, pp. 3595–3599, 2009.
- [47] J. P. Martins and N. B. Carvalho, "Multitone phase and amplitude measurement for nonlinear device characterization," *Microwave Theory and Techniques, IEEE Transactions on*, vol. 53, no. 6, pp. 1982–1989, 2005.
- [48] L. Seung-Yup, L. Yong-Sub, and J. Yoon-Ha, "A novel phase measurement technique for im3 components in rf power amplifiers," *Microwave Theory and Techniques, IEEE Transactions on*, vol. 54, no. 1, pp. 451–457, 2006.
- [49] A. Walker, M. Steer, and K. G. Gard, "A vector intermodulation analyzer applied to behavioral modeling of nonlinear amplifiers with memory," *Microwave Theory and Techniques, IEEE Transactions on*, vol. 54, no. 5, pp. 1991–1999, 2006.
- [50] O. Hammi, M. Younes, and F. Ghannouchi, "Metrics and methods for benchmarking of rf transmitter behavioral models with application to the development of a hybrid memory polynomial model," *Broadcasting, IEEE Transactions on*, vol. 56, no. 3, pp. 350–357, sept. 2010.
- [51] F. Yong-sheng, L. Yuan-an, and N. Jing-chang, "Research of electro-thermal memory effect of rf power amplifier based on ldmos fet," in *Environmental Electromagnetics, The 2006 4th Asia-Pacific Conference on*, Aug 2006, pp. 787–791.
- [52] G. Hu, C. Chang, and Y.-T. Chia, "Gate-voltage-dependent effective channel length and series resistance of ldd mosfet's," *Electron Devices, IEEE Transactions on*, vol. 34, no. 12, pp. 2469–2475, dec 1987.
- [53] H. Ku and J. S. Kenney, "Behavioral modeling of rf power amplifiers considering imd and spectral regrowth asymmetries," in *Microwave Symposium Digest, 2003 IEEE MTT-S International*, vol. 2, 2003, pp. 799–802 vol.2.
- [54] S. P. S. By Kelly Mekechuk, Wan-Jong Kim and J. H. Kim, "Linearizing power amplifiers using digital predistortion, eda tools and test hardware," [http://www.highfrequencyelectronics.com/Archives/Apr04/HFE0404\\_Stapleton.pdf](http://www.highfrequencyelectronics.com/Archives/Apr04/HFE0404_Stapleton.pdf), April 2004, accessed May 2011.

## Appendix A

### Intermediate Steps of Phase Difference Calculation Equation Derivation

$$m_{tot} \angle \phi_{tot} = m_{SG1} \angle \phi_1 + m_{SG2} \angle \phi_2$$

$$\begin{aligned} |m_{tot}| &= |m_{SG1} \angle \phi_1 + m_{SG2} \angle \phi_2| \\ &= \sqrt{[m_{SG1} \cdot \cos(\phi_1) + m_{SG2} \cdot \cos(\phi_2)]^2 + [m_{SG1} \cdot \sin(\phi_1) + m_{SG2} \cdot \sin(\phi_2)]^2} \end{aligned}$$

$$\begin{aligned} (m_{tot})^2 &= [m_{SG1} \cdot \cos(\phi_1) + m_{SG2} \cdot \cos(\phi_2)]^2 + [m_{SG1} \cdot \sin(\phi_1) + m_{SG2} \cdot \sin(\phi_2)]^2 \\ (m_{tot})^2 &= (m_{SG1})^2 \cdot (\cos(\phi_1))^2 + (m_{SG2})^2 \cdot (\cos(\phi_2))^2 \\ &\quad + 2 \cdot m_{SG1} \cdot m_{SG2} \cdot \cos(\phi_1) \cdot \cos(\phi_2) + 2 \cdot m_{SG1} \cdot m_{SG2} \cdot \sin(\phi_1) \cdot \sin(\phi_2) \\ &\quad + (m_{SG1})^2 \cdot (\sin(\phi_1))^2 + (m_{SG2})^2 \cdot (\sin(\phi_2))^2 \\ &= (m_{SG1})^2 \cdot [(\cos(\phi_1))^2 + (\sin(\phi_1))^2] + (m_{SG2})^2 \cdot [(\cos(\phi_2))^2 + (\sin(\phi_2))^2] \\ &\quad + 2 \cdot m_{SG1} \cdot m_{SG2} \cdot \cos(\phi_1) \cdot \cos(\phi_2) + 2 \cdot m_{SG1} \cdot m_{SG2} \cdot \sin(\phi_1) \cdot \sin(\phi_2) \\ &= (m_{SG1})^2 + (m_{SG2})^2 + 2 \cdot m_{SG1} \cdot m_{SG2} \cdot \cos(|\phi_1 - \phi_2|) \end{aligned}$$

$$\cos(|\phi_1 - \phi_2|) = \frac{(m_{tot})^2 - (m_{SG1})^2 - (m_{SG2})^2}{2 \cdot m_{SG1} \cdot m_{SG2}}$$

$$|\phi_1 - \phi_2| = \cos^{-1} \left( \frac{(m_{tot})^2 - (m_{SG1})^2 - (m_{SG2})^2}{2 \cdot m_{SG1} \cdot m_{SG2}} \right)$$

## Appendix B

### Expansion for the polynomial order terms

$$V_i = (V_1 \cdot \cos(\omega_1 \cdot t) + V_1 \cos(\omega_2 \cdot t))$$

$$V_{env} = \frac{8V_1}{\pi} + \frac{8V_1}{3\pi} \cdot \cos(\Delta\omega t) + \frac{8V_1}{15\pi} \cos(2\Delta\omega t) + \frac{8V_1}{35\pi} \cos(3\Delta\omega t)$$

$$V_o(t) = \sum_{k=1}^K (a_{2k-1} + a_{2k} \cdot V_{env}(t - \tau_{2k-1}) \cdot (V_i^{2k-1}(t - \tau_{2k-1})))$$

$$V_o|_{K=3}(t) = a_1 \cdot V_i(t - \tau_1) + a_2 \cdot V_{env} \cdot V_i(t - \tau_1) + a_3 \cdot V_i^3(t - \tau_1) \\ + a_4 \cdot V_{env} \cdot V_i^4(t - \tau_1) + a_5 \cdot V_i^5(t - \tau_1) \quad \text{if set } K=3, \text{ and omit } 6^{th} \text{ order}$$

$$a_1 V_i(t - \tau_1) = V_1 a_1 \cos \omega_1 t \cos \omega_1 \tau_1 + V_1 a_1 \cos \omega_2 t \cos \omega_2 \tau_1 + V_1 a_1 \sin \omega_1 t \sin \omega_1 \tau_1 \\ + V_1 a_1 \sin \omega_2 t \sin \omega_2 \tau_1$$

$$a_2 \cdot V_{env} \cdot V_i(t - \tau_1) = a_2 \left( \frac{4V_1}{\pi} + \frac{8V_1}{3\pi} \cos(\Delta\omega(t - \tau_1)) - \frac{8V_1}{15\pi} \cos(2\Delta\omega(t - \tau_1)) \right. \\ \left. + \frac{8V_1}{35\pi} \cos(3\Delta\omega(t - \tau_1)) + \frac{8V_1}{63\pi} \cos(4\Delta\omega(t - \tau_1)) \right) \cdot (V_1 \cos(\omega_1(t - \tau_1)) + V_1 \cos(\omega_2(t - \tau_1)))$$

$$= \frac{4}{3\pi} V_1^2 a_2 \cos(t\omega_1 - \tau_1\omega_1 + t\omega\Delta - \omega\Delta\tau_1) - \frac{2}{3\pi} V_1^2 a_2 \cos(t\omega_1 + \tau_1\omega_1 - t\omega\Delta - \omega\Delta\tau_1) \\ - \frac{1}{3\pi} V_1^2 a_2 \cos(t\omega_1 + \tau_1\omega_1 - t\omega\Delta + \omega\Delta\tau_1) + \frac{1}{\pi} V_1^2 a_2 \cos(t\omega_1 - \tau_1\omega_1 - t\omega\Delta + \omega\Delta\tau_1) \\ + \frac{1}{3\pi} V_1^2 a_2 \cos(\tau_1\omega_1 - t\omega_1 + t\omega\Delta - \omega\Delta\tau_1) + \frac{2}{3\pi} V_1^2 a_2 \cos(t\omega\Delta - \tau_1\omega_1 - t\omega_1 + \omega\Delta\tau_1) \\ - \frac{3}{140\pi} V_1^2 a_2 \cos(t\omega_1 + \tau_1\omega_1 - 3t\omega\Delta + \omega\Delta\tau_1) - \frac{1}{3\pi} V_1^2 a_2 \cos(t\omega_2 + \tau_1\omega_2 - t\omega\Delta + \omega\Delta\tau_1) \\ + \frac{1}{3\pi} V_1^2 a_2 \cos(t\omega\Delta - \tau_1\omega_1 - t\omega_1 - \omega\Delta\tau_1) + \frac{2}{15\pi} V_1^2 a_2 \cos(t\omega_1 + \tau_1\omega_1 - 2t\omega\Delta - 2\omega\Delta\tau_1) \\ + \frac{1}{30\pi} V_1^2 a_2 \cos(t\omega_1 + \tau_1\omega_1 - 2t\omega\Delta + 2\omega\Delta\tau_1) - \frac{2}{35\pi} V_1^2 a_2 \cos(t\omega_1 + \tau_1\omega_1 - 3t\omega\Delta - \omega\Delta\tau_1) \\ + \frac{3}{140\pi} V_1^2 a_2 \cos(t\omega_1 - \tau_1\omega_1 - 3t\omega\Delta + \omega\Delta\tau_1) - \frac{2}{3\pi} V_1^2 a_2 \cos(t\omega_2 + \tau_1\omega_2 - t\omega\Delta - \omega\Delta\tau_1) \\ + \frac{4}{3\pi} V_1^2 a_2 \cos(t\omega_2 - \tau_1\omega_2 + t\omega\Delta - \omega\Delta\tau_1) + \frac{1}{\pi} V_1^2 a_2 \cos(t\omega_2 - \tau_1\omega_2 - t\omega\Delta + \omega\Delta\tau_1) \\ - \frac{1}{70\pi} V_1^2 a_2 \cos(\tau_1\omega_1 - t\omega_1 + 3t\omega\Delta + \omega\Delta\tau_1) + \frac{1}{3\pi} V_1^2 a_2 \cos(\tau_1\omega_2 - t\omega_2 + t\omega\Delta - \omega\Delta\tau_1) \\ + \frac{2}{3\pi} V_1^2 a_2 \cos(t\omega\Delta - \tau_1\omega_2 - t\omega_2 + \omega\Delta\tau_1) - \frac{7}{30\pi} V_1^2 a_2 \cos(t\omega_1 - \tau_1\omega_1 - 2t\omega\Delta + 2\omega\Delta\tau_1) \\ - \frac{4}{15\pi} V_1^2 a_2 \cos(t\omega_1 - \tau_1\omega_1 + 2t\omega\Delta - 2\omega\Delta\tau_1) + \frac{1}{70\pi} V_1^2 a_2 \cos(t\omega_1 - \tau_1\omega_1 - 3t\omega\Delta - \omega\Delta\tau_1) \\ - \frac{3}{140\pi} V_1^2 a_2 \cos(t\omega_2 + \tau_1\omega_2 - 3t\omega\Delta + \omega\Delta\tau_1) - \frac{1}{30\pi} V_1^2 a_2 \cos(\tau_1\omega_1 - t\omega_1 + 2t\omega\Delta - 2\omega\Delta\tau_1) \\ - \frac{3}{140\pi} V_1^2 a_2 \cos(\tau_1\omega_1 - t\omega_1 + 3t\omega\Delta - \omega\Delta\tau_1) + \frac{2}{35\pi} V_1^2 a_2 \cos(3t\omega\Delta - \tau_1\omega_1 - t\omega_1 + \omega\Delta\tau_1) \\ + \frac{1}{3\pi} V_1^2 a_2 \cos(t\omega\Delta - \tau_1\omega_2 - t\omega_2 - \omega\Delta\tau_1) - \frac{2}{35\pi} V_1^2 a_2 \cos(t\omega_1 + \tau_1\omega_1 - 3t\omega\Delta - 3\omega\Delta\tau_1) \\ - \frac{1}{140\pi} V_1^2 a_2 \cos(t\omega_1 + \tau_1\omega_1 - 3t\omega\Delta + 3\omega\Delta\tau_1) - \frac{5}{126\pi} V_1^2 a_2 \cos(t\omega_1 + \tau_1\omega_1 - 4t\omega\Delta - 2\omega\Delta\tau_1)$$



$$\begin{aligned}
&= \frac{9}{4} V_1^3 a_3 \cos(t\omega_1 - \tau_1\omega_1) + \frac{9}{4} V_1^3 a_3 \cos(t\omega_2 - \tau_1\omega_2) + \frac{1}{4} V_1^3 a_3 \cos(3t\omega_1 - 3\tau_1\omega_1) \\
&+ \frac{1}{4} V_1^3 a_3 \cos(3t\omega_2 - 3\tau_1\omega_2) + \frac{3}{4} V_1^3 a_3 \cos(t\omega_1 - 2t\omega_2 - \tau_1\omega_1 + 2\tau_1\omega_2) \\
&+ \frac{3}{4} V_1^3 a_3 \cos(t\omega_1 + 2t\omega_2 - \tau_1\omega_1 - 2\tau_1\omega_2) + \frac{3}{4} V_1^3 a_3 \cos(2t\omega_1 + t\omega_2 - 2\tau_1\omega_1 - \tau_1\omega_2) \\
&+ \frac{3}{4} V_1^3 a_3 \cos(2t\omega_1 - t\omega_2 - 2\tau_1\omega_1 + \tau_1\omega_2)
\end{aligned}$$

$$a_4 \left( \frac{8V_1}{\pi} + \frac{8V_1}{3\pi} \cos(\Delta\omega t) + \frac{8V_1}{15\pi} \cos(2\Delta\omega t) + \frac{8V_1}{35\pi} \cos(3\Delta\omega t) \right) (V_1 \cos(\omega_1(t - \tau_3)) + V_1 \cos(\omega_2(t - \tau_3)))^3$$

$$\begin{aligned}
&= \frac{1}{4\pi} V_1^4 a_4 \cos(\omega_1\tau_3 - 2\omega_2t - \omega_1t + \Delta\omega t) - \frac{1}{4\pi} V_1^4 a_4 \cos(\omega_1t + 2\omega_2t + \omega_1\tau_3 - \Delta\omega t) \\
&- \frac{1}{8\pi} V_1^4 a_4 \cos(\omega_1t - 2\omega_2t + \omega_1\tau_3 - \Delta\omega t) + \frac{3}{8\pi} V_1^4 a_4 \cos(2\omega_2t - \omega_1t + \omega_1\tau_3 + \Delta\omega t) \\
&+ \frac{1}{4\pi} V_1^4 a_4 \cos(\omega_2t - 2\omega_1t + \omega_2\tau_3 + \Delta\omega t) - \frac{1}{40\pi} V_1^4 a_4 \cos(\omega_1t - 2\omega_2t + \omega_1\tau_3 - 2\Delta\omega t) \\
&- \frac{3}{8\pi} V_1^4 a_4 \cos(\omega_1t - 2\omega_2t - \omega_1\tau_3 - \Delta\omega t) - \frac{1}{20\pi} V_1^4 a_4 \cos(\omega_1t + 2\omega_2t + \omega_1\tau_3 - 2\Delta\omega t) \\
&- \frac{1}{4\pi} V_1^4 a_4 \cos(\omega_1t + 2\omega_2t - \omega_1\tau_3 - \Delta\omega t) + \frac{1}{4\pi} V_1^4 a_4 \cos(\Delta\omega t - 2\omega_2t - \omega_1\tau_3 - \omega_1t) \\
&+ \frac{1}{8\pi} V_1^4 a_4 \cos(2\omega_2t - \omega_1t - \omega_1\tau_3 + \Delta\omega t) + \frac{1}{4\pi} V_1^4 a_4 \cos(\omega_2t - 2\omega_1t - \omega_2\tau_3 + \Delta\omega t) \\
&+ \frac{1}{4\pi} V_1^4 a_4 \cos(\omega_2\tau_3 - \omega_2t - 2\omega_1t + \Delta\omega t) - \frac{1}{4\pi} V_1^4 a_4 \cos(2\omega_1t + \omega_2t + \omega_2\tau_3 - \Delta\omega t) \\
&- \frac{3}{280\pi} V_1^4 a_4 \cos(\omega_1t - 2\omega_2t + \omega_1\tau_3 - 3\Delta\omega t) - \frac{3}{40\pi} V_1^4 a_4 \cos(\omega_1t - 2\omega_2t - \omega_1\tau_3 - 2\Delta\omega t) \\
&- \frac{3}{140\pi} V_1^4 a_4 \cos(\omega_1t + 2\omega_2t + \omega_1\tau_3 - 3\Delta\omega t) - \frac{1}{20\pi} V_1^4 a_4 \cos(\omega_1t + 2\omega_2t - \omega_1\tau_3 - 2\Delta\omega t) \\
&+ \frac{1}{20\pi} V_1^4 a_4 \cos(\omega_1\tau_3 - 2\omega_2t - \omega_1t + 2\Delta\omega t) + \frac{3}{40\pi} V_1^4 a_4 \cos(2\omega_2t - \omega_1t + \omega_1\tau_3 + 2\Delta\omega t) \\
&+ \frac{1}{20\pi} V_1^4 a_4 \cos(\omega_2t - 2\omega_1t + \omega_2\tau_3 + 2\Delta\omega t) + \frac{1}{4\pi} V_1^4 a_4 \cos(\Delta\omega t - \omega_2t - \omega_2\tau_3 - 2\omega_1t) \\
&- \frac{1}{20\pi} V_1^4 a_4 \cos(2\omega_1t + \omega_2t + \omega_2\tau_3 - 2\Delta\omega t) - \frac{1}{4\pi} V_1^4 a_4 \cos(2\omega_1t + \omega_2t - \omega_2\tau_3 - \Delta\omega t) \\
&- \frac{1}{4\pi} V_1^4 a_4 \cos(2\omega_1t - \omega_2t + \omega_2\tau_3 - \Delta\omega t) - \frac{9}{280\pi} V_1^4 a_4 \cos(\omega_1t - 2\omega_2t - \omega_1\tau_3 - 3\Delta\omega t) \\
&- \frac{3}{140\pi} V_1^4 a_4 \cos(\omega_1t + 2\omega_2t - \omega_1\tau_3 - 3\Delta\omega t) + \frac{3}{140\pi} V_1^4 a_4 \cos(\omega_1\tau_3 - 2\omega_2t - \omega_1t + 3\Delta\omega t) \\
&+ \frac{1}{20\pi} V_1^4 a_4 \cos(2\Delta\omega t - 2\omega_2t - \omega_1\tau_3 - \omega_1t) + \frac{9}{280\pi} V_1^4 a_4 \cos(2\omega_2t - \omega_1t + \omega_1\tau_3 + 3\Delta\omega t) \\
&+ \frac{1}{40\pi} V_1^4 a_4 \cos(2\omega_2t - \omega_1t - \omega_1\tau_3 + 2\Delta\omega t) + \frac{3}{140\pi} V_1^4 a_4 \cos(\omega_2t - 2\omega_1t + \omega_2\tau_3 + 3\Delta\omega t) \\
&+ \frac{1}{20\pi} V_1^4 a_4 \cos(\omega_2t - 2\omega_1t - \omega_2\tau_3 + 2\Delta\omega t) + \frac{1}{20\pi} V_1^4 a_4 \cos(\omega_2\tau_3 - \omega_2t - 2\omega_1t + 2\Delta\omega t) \\
&- \frac{3}{140\pi} V_1^4 a_4 \cos(2\omega_1t + \omega_2t + \omega_2\tau_3 - 3\Delta\omega t) - \frac{1}{20\pi} V_1^4 a_4 \cos(2\omega_1t + \omega_2t - \omega_2\tau_3 - 2\Delta\omega t) \\
&- \frac{1}{20\pi} V_1^4 a_4 \cos(2\omega_1t - \omega_2t + \omega_2\tau_3 - 2\Delta\omega t) - \frac{1}{4\pi} V_1^4 a_4 \cos(2\omega_1t - \omega_2t - \omega_2\tau_3 - \Delta\omega t) \\
&+ \frac{3}{140\pi} V_1^4 a_4 \cos(3\Delta\omega t - 2\omega_2t - \omega_1\tau_3 - \omega_1t) + \frac{3}{280\pi} V_1^4 a_4 \cos(2\omega_2t - \omega_1t - \omega_1\tau_3 + 3\Delta\omega t) \\
&+ \frac{3}{140\pi} V_1^4 a_4 \cos(\omega_2t - 2\omega_1t - \omega_2\tau_3 + 3\Delta\omega t) + \frac{3}{140\pi} V_1^4 a_4 \cos(\omega_2\tau_3 - \omega_2t - 2\omega_1t + 3\Delta\omega t) \\
&+ \frac{1}{20\pi} V_1^4 a_4 \cos(2\Delta\omega t - \omega_2t - \omega_2\tau_3 - 2\omega_1t) - \frac{3}{140\pi} V_1^4 a_4 \cos(2\omega_1t + \omega_2t - \omega_2\tau_3 - 3\Delta\omega t) \\
&- \frac{3}{140\pi} V_1^4 a_4 \cos(2\omega_1t - \omega_2t + \omega_2\tau_3 - 3\Delta\omega t) - \frac{1}{20\pi} V_1^4 a_4 \cos(2\omega_1t - \omega_2t - \omega_2\tau_3 - 2\Delta\omega t) \\
&+ \frac{3}{140\pi} V_1^4 a_4 \cos(3\Delta\omega t - \omega_2t - \omega_2\tau_3 - 2\omega_1t) - \frac{3}{140\pi} V_1^4 a_4 \cos(2\omega_1t - \omega_2t - \omega_2\tau_3 - 3\Delta\omega t) \\
&- \frac{1}{8\pi} V_1^4 a_4 \cos(\omega_1t + \omega_1\tau_3 - 2\omega_2\tau_3 - \Delta\omega t) - \frac{1}{4\pi} V_1^4 a_4 \cos(\omega_1t + \omega_1\tau_3 + 2\omega_2\tau_3 - \Delta\omega t) \\
&+ \frac{1}{8\pi} V_1^4 a_4 \cos(\omega_2t - 2\omega_1\tau_3 + \omega_2\tau_3 + \Delta\omega t) + \frac{1}{4\pi} V_1^4 a_4 \cos(\omega_1\tau_3 - \omega_1t - 2\omega_2\tau_3 + \Delta\omega t) \\
&- \frac{1}{8\pi} V_1^4 a_4 \cos(\omega_1\tau_3 - \omega_1t + 2\omega_2\tau_3 + \Delta\omega t) - \frac{1}{40\pi} V_1^4 a_4 \cos(\omega_1t + \omega_1\tau_3 - 2\omega_2\tau_3 - 2\Delta\omega t) \\
&- \frac{1}{20\pi} V_1^4 a_4 \cos(\omega_1t + \omega_1\tau_3 + 2\omega_2\tau_3 - 2\Delta\omega t) + \frac{1}{8\pi} V_1^4 a_4 \cos(\omega_1t - \omega_1\tau_3 - 2\omega_2\tau_3 - \Delta\omega t) \\
&- \frac{1}{4\pi} V_1^4 a_4 \cos(\omega_1t - \omega_1\tau_3 + 2\omega_2\tau_3 - \Delta\omega t) - \frac{1}{8\pi} V_1^4 a_4 \cos(\omega_2t - 2\omega_1\tau_3 + \omega_2\tau_3 - \Delta\omega t) \\
&+ \frac{1}{8\pi} V_1^4 a_4 \cos(\omega_2t - 2\omega_1\tau_3 - \omega_2\tau_3 + \Delta\omega t) - \frac{1}{4\pi} V_1^4 a_4 \cos(\omega_2t + 2\omega_1\tau_3 + \omega_2\tau_3 - \Delta\omega t) \\
&+ \frac{1}{4\pi} V_1^4 a_4 \cos(\Delta\omega t - \omega_1\tau_3 - 2\omega_2\tau_3 - \omega_1t) + \frac{1}{8\pi} V_1^4 a_4 \cos(2\omega_2\tau_3 - \omega_1\tau_3 - \omega_1t + \Delta\omega t) \\
&+ \frac{1}{4\pi} V_1^4 a_4 \cos(\omega_2\tau_3 - 2\omega_1\tau_3 - \omega_2t + \Delta\omega t) - \frac{1}{8\pi} V_1^4 a_4 \cos(2\omega_1\tau_3 - \omega_2t + \omega_2\tau_3 + \Delta\omega t)
\end{aligned}$$



$$\begin{aligned}
& + \frac{1}{8\pi} V_1^4 a_4 \cos(-\omega_2 t - \omega_2 \tau_3 - \Delta\omega t) + \frac{1}{40\pi} V_1^4 a_4 \cos(\omega_1 \tau_3 - 3\omega_1 t + 2\Delta\omega t) \\
& - \frac{1}{40\pi} V_1^4 a_4 \cos(3\omega_1 t + \omega_1 \tau_3 - 2\Delta\omega t) - \frac{1}{8\pi} V_1^4 a_4 \cos(3\omega_1 t - \omega_1 \tau_3 - \Delta\omega t) \\
& + \frac{1}{8\pi} V_1^4 a_4 \cos(\omega_2 \tau_3 - 3\omega_2 t + \Delta\omega t) - \frac{3}{280\pi} V_1^4 a_4 \cos(\omega_1 t + 3\omega_1 \tau_3 - 3\Delta\omega t) \\
& + \frac{39}{280\pi} V_1^4 a_4 \cos(\omega_2 t - \omega_2 \tau_3 - 3\Delta\omega t) + \frac{69}{280\pi} V_1^4 a_4 \cos(\omega_2 t - \omega_2 \tau_3 + 3\Delta\omega t) \\
& - \frac{1}{8\pi} V_1^4 a_4 \cos(\omega_2 t + 3\omega_2 \tau_3 - \Delta\omega t) + \frac{1}{40\pi} V_1^4 a_4 \cos(2\Delta\omega t - 3\omega_1 \tau_3 - \omega_1 t) \\
& + \frac{3}{280\pi} V_1^4 a_4 \cos(\omega_2 \tau_3 - \omega_2 t - 3\Delta\omega t) + \frac{33}{280\pi} V_1^4 a_4 \cos(\omega_2 \tau_3 - \omega_2 t + 3\Delta\omega t) \\
& + \frac{1}{40\pi} V_1^4 a_4 \cos(-\omega_2 t - \omega_2 \tau_3 - 2\Delta\omega t) + \frac{1}{5\pi} V_1^4 a_4 \cos(2\Delta\omega t - \omega_2 \tau_3 - \omega_2 t) \\
& + \frac{1}{8\pi} V_1^4 a_4 \cos(\Delta\omega t - 3\omega_2 \tau_3 - \omega_2 t) + \frac{3}{280\pi} V_1^4 a_4 \cos(\omega_1 \tau_3 - 3\omega_1 t + 3\Delta\omega t) \\
& + \frac{1}{40\pi} V_1^4 a_4 \cos(2\Delta\omega t - \omega_1 \tau_3 - 3\omega_1 t) + \frac{1}{24\pi} V_1^4 a_4 \cos(\Delta\omega t - 3\omega_1 \tau_3 - 3\omega_1 t) \\
& + \frac{1}{24\pi} V_1^4 a_4 \cos(3\omega_1 \tau_3 - 3\omega_1 t + \Delta\omega t) - \frac{3}{280\pi} V_1^4 a_4 \cos(3\omega_1 t + \omega_1 \tau_3 - 3\Delta\omega t) \\
& - \frac{1}{40\pi} V_1^4 a_4 \cos(3\omega_1 t - \omega_1 \tau_3 - 2\Delta\omega t) + \frac{1}{3\pi} V_1^4 a_4 \cos(3\omega_1 t - 3\omega_1 \tau_3 + \Delta\omega t) \\
& + \frac{1}{8\pi} V_1^4 a_4 \cos(\Delta\omega t - \omega_2 \tau_3 - 3\omega_2 t) - \frac{1}{8\pi} V_1^4 a_4 \cos(3\omega_2 t + \omega_2 \tau_3 - \Delta\omega t) \\
& - \frac{1}{40\pi} V_1^4 a_4 \cos(\omega_2 t + 3\omega_2 \tau_3 - 2\Delta\omega t) + \frac{3}{280\pi} V_1^4 a_4 \cos(3\Delta\omega t - 3\omega_1 \tau_3 - \omega_1 t) \\
& + \frac{3}{280\pi} V_1^4 a_4 \cos(-\omega_2 t - \omega_2 \tau_3 - 3\Delta\omega t) + \frac{3}{35\pi} V_1^4 a_4 \cos(3\Delta\omega t - \omega_2 \tau_3 - \omega_2 t) \\
& + \frac{3}{280\pi} V_1^4 a_4 \cos(3\Delta\omega t - \omega_1 \tau_3 - 3\omega_1 t) - \frac{3}{280\pi} V_1^4 a_4 \cos(3\omega_1 t - \omega_1 \tau_3 - 3\Delta\omega t) \\
& + \frac{7}{24\pi} V_1^4 a_4 \cos(3\omega_1 t - 3\omega_1 \tau_3 - \Delta\omega t) - \frac{1}{24\pi} V_1^4 a_4 \cos(3\omega_1 t + 3\omega_1 \tau_3 - \Delta\omega t) \\
& + \frac{1}{40\pi} V_1^4 a_4 \cos(\omega_2 \tau_3 - 3\omega_2 t + 2\Delta\omega t) - \frac{1}{40\pi} V_1^4 a_4 \cos(3\omega_2 t + \omega_2 \tau_3 - 2\Delta\omega t) \\
& - \frac{1}{8\pi} V_1^4 a_4 \cos(3\omega_2 t - \omega_2 \tau_3 - \Delta\omega t) - \frac{3}{280\pi} V_1^4 a_4 \cos(\omega_2 t + 3\omega_2 \tau_3 - 3\Delta\omega t) \\
& + \frac{1}{40\pi} V_1^4 a_4 \cos(2\Delta\omega t - 3\omega_2 \tau_3 - \omega_2 t) + \frac{1}{120\pi} V_1^4 a_4 \cos(2\Delta\omega t - 3\omega_1 \tau_3 - 3\omega_1 t) \\
& + \frac{1}{120\pi} V_1^4 a_4 \cos(3\omega_1 \tau_3 - 3\omega_1 t + 2\Delta\omega t) + \frac{7}{120\pi} V_1^4 a_4 \cos(3\omega_1 t - 3\omega_1 \tau_3 - 2\Delta\omega t) \\
& + \frac{1}{15\pi} V_1^4 a_4 \cos(3\omega_1 t - 3\omega_1 \tau_3 + 2\Delta\omega t) - \frac{1}{120\pi} V_1^4 a_4 \cos(3\omega_1 t + 3\omega_1 \tau_3 - 2\Delta\omega t) \\
& + \frac{3}{280\pi} V_1^4 a_4 \cos(\omega_2 \tau_3 - 3\omega_2 t + 3\Delta\omega t) + \frac{1}{40\pi} V_1^4 a_4 \cos(2\Delta\omega t - \omega_2 \tau_3 - 3\omega_2 t) \\
& + \frac{1}{24\pi} V_1^4 a_4 \cos(\Delta\omega t - 3\omega_2 \tau_3 - 3\omega_2 t) + \frac{1}{24\pi} V_1^4 a_4 \cos(3\omega_2 \tau_3 - 3\omega_2 t + \Delta\omega t) \\
& - \frac{3}{280\pi} V_1^4 a_4 \cos(3\omega_2 t + \omega_2 \tau_3 - 3\Delta\omega t) - \frac{1}{40\pi} V_1^4 a_4 \cos(3\omega_2 t - \omega_2 \tau_3 - 2\Delta\omega t) \\
& + \frac{1}{3\pi} V_1^4 a_4 \cos(3\omega_2 t - 3\omega_2 \tau_3 + \Delta\omega t) + \frac{3}{280\pi} V_1^4 a_4 \cos(3\Delta\omega t - 3\omega_2 \tau_3 - \omega_2 t) \\
& + \frac{1}{280\pi} V_1^4 a_4 \cos(3\Delta\omega t - 3\omega_1 \tau_3 - 3\omega_1 t) + \frac{1}{280\pi} V_1^4 a_4 \cos(3\omega_1 \tau_3 - 3\omega_1 t + 3\Delta\omega t) \\
& + \frac{1}{40\pi} V_1^4 a_4 \cos(3\omega_1 t - 3\omega_1 \tau_3 - 3\Delta\omega t) + \frac{1}{35\pi} V_1^4 a_4 \cos(3\omega_1 t - 3\omega_1 \tau_3 + 3\Delta\omega t) \\
& - \frac{1}{280\pi} V_1^4 a_4 \cos(3\omega_1 t + 3\omega_1 \tau_3 - 3\Delta\omega t) + \frac{3}{280\pi} V_1^4 a_4 \cos(3\Delta\omega t - \omega_2 \tau_3 - 3\omega_2 t) \\
& - \frac{3}{280\pi} V_1^4 a_4 \cos(3\omega_2 t - \omega_2 \tau_3 - 3\Delta\omega t) + \frac{7}{24\pi} V_1^4 a_4 \cos(3\omega_2 t - 3\omega_2 \tau_3 - \Delta\omega t) \\
& - \frac{1}{24\pi} V_1^4 a_4 \cos(3\omega_2 t + 3\omega_2 \tau_3 - \Delta\omega t) + \frac{1}{120\pi} V_1^4 a_4 \cos(2\Delta\omega t - 3\omega_2 \tau_3 - 3\omega_2 t) \\
& + \frac{1}{120\pi} V_1^4 a_4 \cos(3\omega_2 \tau_3 - 3\omega_2 t + 2\Delta\omega t) + \frac{7}{120\pi} V_1^4 a_4 \cos(3\omega_2 t - 3\omega_2 \tau_3 - 2\Delta\omega t) \\
& + \frac{1}{15\pi} V_1^4 a_4 \cos(3\omega_2 t - 3\omega_2 \tau_3 + 2\Delta\omega t) - \frac{1}{120\pi} V_1^4 a_4 \cos(3\omega_2 t + 3\omega_2 \tau_3 - 2\Delta\omega t) \\
& + \frac{1}{280\pi} V_1^4 a_4 \cos(3\Delta\omega t - 3\omega_2 \tau_3 - 3\omega_2 t) + \frac{1}{280\pi} V_1^4 a_4 \cos(3\omega_2 \tau_3 - 3\omega_2 t + 3\Delta\omega t) \\
& + \frac{1}{40\pi} V_1^4 a_4 \cos(3\omega_2 t - 3\omega_2 \tau_3 - 3\Delta\omega t) + \frac{1}{35\pi} V_1^4 a_4 \cos(3\omega_2 t - 3\omega_2 \tau_3 + 3\Delta\omega t) \\
& - \frac{1}{280\pi} V_1^4 a_4 \cos(3\omega_2 t + 3\omega_2 \tau_3 - 3\Delta\omega t) + \frac{6}{\pi} V_1^4 a_4 \cos(\omega_1 t - 2\omega_2 t - \omega_1 \tau_3 + 2\omega_2 \tau_3) \\
& + \frac{6}{\pi} V_1^4 a_4 \cos(\omega_1 t + 2\omega_2 t - \omega_1 \tau_3 - 2\omega_2 \tau_3) + \frac{6}{\pi} V_1^4 a_4 \cos(2\omega_1 t + \omega_2 t - 2\omega_1 \tau_3 - \omega_2 \tau_3) \\
& + \frac{6}{\pi} V_1^4 a_4 \cos(2\omega_1 t - \omega_2 t - 2\omega_1 \tau_3 + \omega_2 \tau_3) + \frac{18}{\pi} V_1^4 a_4 \cos(\omega_1 t - \omega_1 \tau_3) \\
& + \frac{18}{\pi} V_1^4 a_4 \cos(\omega_2 t - \omega_2 \tau_3) + \frac{2}{\pi} V_1^4 a_4 \cos(3\omega_1 t - 3\omega_1 \tau_3) \\
& + \frac{2}{\pi} V_1^4 a_4 \cos(3\omega_2 t - 3\omega_2 \tau_3) + \frac{1}{8\pi} V_1^4 a_4 \cos(\omega_2 t - 2\omega_1 t - 2\omega_1 \tau_3 + \omega_2 \tau_3 + \Delta\omega t) \\
& - \frac{1}{4\pi} V_1^4 a_4 \cos(\omega_1 t - 2\omega_2 t + \omega_1 \tau_3 - 2\omega_2 \tau_3 - \Delta\omega t) - \frac{1}{8\pi} V_1^4 a_4 \cos(\omega_1 t - 2\omega_2 t + \omega_1 \tau_3 + 2\omega_2 \tau_3 - \Delta\omega t)
\end{aligned}$$



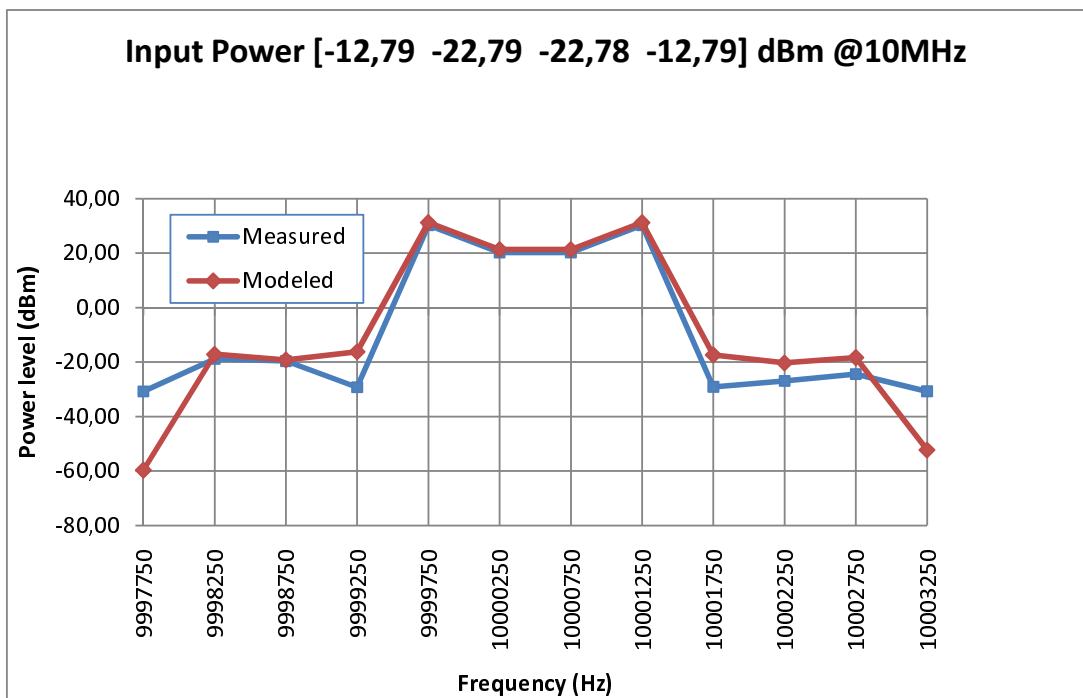
$$\begin{aligned}
& + \frac{3}{35\pi} V_1^4 a_4 \cos(2\omega_1 t + \omega_2 t - 2\omega_1 \tau_3 - \omega_2 \tau_3 + 3\Delta\omega t) - \frac{3}{280\pi} V_1^4 a_4 \cos(2\omega_1 t + \omega_2 t + 2\omega_1 \tau_3 - \omega_2 \tau_3 - 3\Delta\omega t) \\
& + \frac{9}{140\pi} V_1^4 a_4 \cos(2\omega_1 t - \omega_2 t - 2\omega_1 \tau_3 + \omega_2 \tau_3 - 3\Delta\omega t) + \frac{3}{35\pi} V_1^4 a_4 \cos(2\omega_1 t - \omega_2 t - 2\omega_1 \tau_3 + \omega_2 \tau_3 + 3\Delta\omega t) \\
& - \frac{3}{280\pi} V_1^4 a_4 \cos(2\omega_1 t - \omega_2 t + 2\omega_1 \tau_3 + \omega_2 \tau_3 - 3\Delta\omega t) - \frac{1}{40\pi} V_1^4 a_4 \cos(2\omega_1 t - \omega_2 t + 2\omega_1 \tau_3 - \omega_2 \tau_3 - 2\Delta\omega t) \\
& + \frac{3}{280\pi} V_1^4 a_4 \cos(3\Delta\omega t - 2\omega_2 t - \omega_1 \tau_3 - 2\omega_2 \tau_3 - \omega_1 t) + \frac{3}{280\pi} V_1^4 a_4 \cos(2\omega_2 \tau_3 - 2\omega_2 t - \omega_1 \tau_3 - \omega_1 t + 3\Delta\omega t) \\
& + \frac{3}{280\pi} V_1^4 a_4 \cos(2\omega_2 t - \omega_1 t - \omega_1 \tau_3 - 2\omega_2 \tau_3 + 3\Delta\omega t) + \frac{3}{140\pi} V_1^4 a_4 \cos(2\omega_2 t - \omega_1 t - \omega_1 \tau_3 + 2\omega_2 \tau_3 + 3\Delta\omega t) \\
& + \frac{3}{280\pi} V_1^4 a_4 \cos(3\Delta\omega t - \omega_2 t - 2\omega_1 \tau_3 - \omega_2 \tau_3 - 2\omega_1 t) + \frac{3}{280\pi} V_1^4 a_4 \cos(2\omega_1 \tau_3 - \omega_2 t - 2\omega_1 t - \omega_2 \tau_3 + 3\Delta\omega t) \\
& - \frac{3}{280\pi} V_1^4 a_4 \cos(2\omega_1 t - \omega_2 t + 2\omega_1 \tau_3 - \omega_2 \tau_3 - 3\Delta\omega t)
\end{aligned}$$

$$a_5 V^3(t - \tau_5) = a_5((V_1 \cos(\omega_1(t - \tau_5)) + V_1 \cos(\omega_2(t - \tau_5))))^5$$

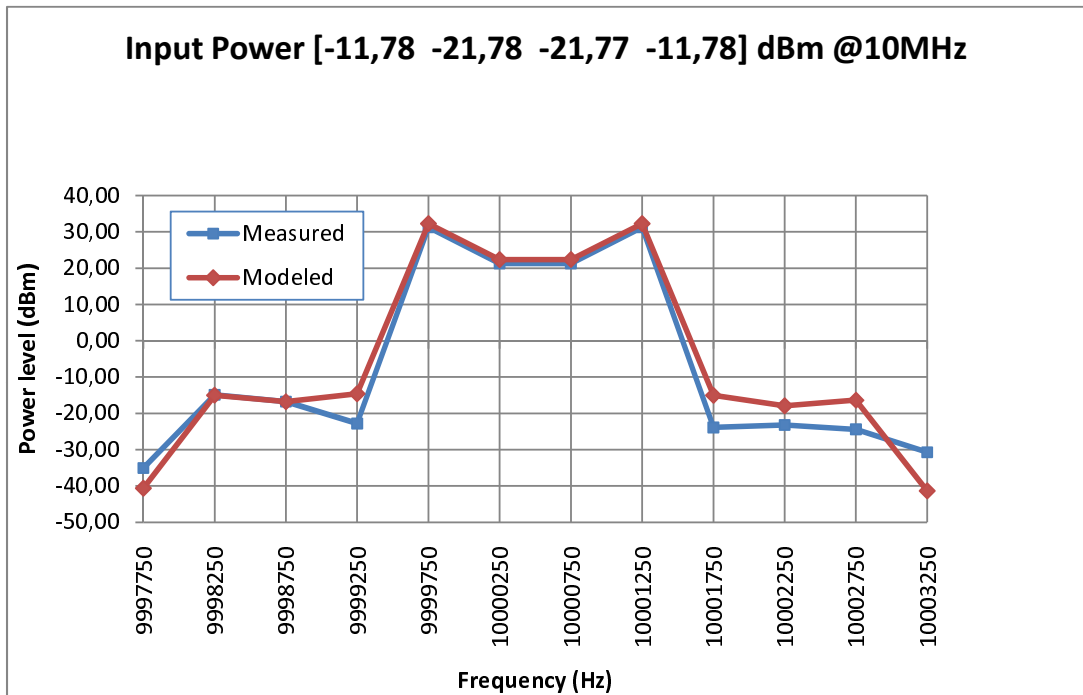
$$\begin{aligned}
& = \frac{25}{4} V_1^5 a_5 \cos(\omega_1 t - \omega_1 \tau_5) + \frac{25}{4} V_1^5 a_5 \cos(\omega_2 t - \omega_2 \tau_5) + \frac{25}{16} V_1^5 a_5 \cos(3\omega_1 t - 3\omega_1 \tau_5) \\
& + \frac{25}{16} V_1^5 a_5 \cos(3\omega_2 t - 3\omega_2 \tau_5) + \frac{1}{16} V_1^5 a_5 \cos(5\omega_1 t - 5\omega_1 \tau_5) + \frac{1}{16} V_1^5 a_5 \cos(5\omega_2 t - 5\omega_2 \tau_5) \\
& + \frac{25}{8} V_1^5 a_5 \cos(\omega_1 t - 2\omega_2 t - \omega_1 \tau_5 + 2\omega_2 \tau_5) + \frac{25}{8} V_1^5 a_5 \cos(\omega_1 t + 2\omega_2 t - \omega_1 \tau_5 - 2\omega_2 \tau_5) \\
& + \frac{25}{8} V_1^5 a_5 \cos(2\omega_1 t + \omega_2 t - 2\omega_1 \tau_5 - \omega_2 \tau_5) + \frac{25}{8} V_1^5 a_5 \cos(2\omega_1 t - \omega_2 t - 2\omega_1 \tau_5 + \omega_2 \tau_5) \\
& - \frac{25}{128} V_1^5 a_5 \cos(\omega_2 t - 4\omega_1 t - 2\omega_1 \tau_5 + \omega_2 \tau_5) - \frac{5}{256} V_1^5 a_5 \cos(\omega_2 t - 4\omega_1 t + 2\omega_1 \tau_5 + \omega_2 \tau_5) \\
& + \frac{15}{256} V_1^5 a_5 \cos(2\omega_2 t - 3\omega_1 t + \omega_1 \tau_5 + 2\omega_2 \tau_5) - \frac{5}{64} V_1^5 a_5 \cos(\omega_2 t - 4\omega_1 t - 2\omega_1 \tau_5 - \omega_2 \tau_5) \\
& + \frac{15}{256} V_1^5 a_5 \cos(\omega_2 t - 4\omega_1 t + 2\omega_1 \tau_5 - \omega_2 \tau_5) - \frac{15}{256} V_1^5 a_5 \cos(4\omega_1 t - \omega_2 t - 2\omega_1 \tau_5 + \omega_2 \tau_5) \\
& + \frac{5}{64} V_1^5 a_5 \cos(4\omega_1 t - \omega_2 t + 2\omega_1 \tau_5 + \omega_2 \tau_5) - \frac{15}{256} V_1^5 a_5 \cos(3\omega_1 t - 2\omega_2 t - \omega_1 \tau_5 - 2\omega_2 \tau_5) \\
& - \frac{5}{32} V_1^5 a_5 \cos(\omega_2 t - 4\omega_1 t - 4\omega_1 \tau_5 + \omega_2 \tau_5) - \frac{5}{512} V_1^5 a_5 \cos(\omega_2 t - 4\omega_1 t + 4\omega_1 \tau_5 + \omega_2 \tau_5) \\
& + \frac{5}{256} V_1^5 a_5 \cos(4\omega_1 t - \omega_2 t - 2\omega_1 \tau_5 - \omega_2 \tau_5) + \frac{25}{128} V_1^5 a_5 \cos(4\omega_1 t - \omega_2 t + 2\omega_1 \tau_5 - \omega_2 \tau_5) \\
& + \frac{5}{16} V_1^5 a_5 \cos(\omega_1 t - 4\omega_2 t - \omega_1 \tau_5 + 4\omega_2 \tau_5) + \frac{5}{16} V_1^5 a_5 \cos(\omega_1 t + 4\omega_2 t - \omega_1 \tau_5 - 4\omega_2 \tau_5) \\
& + \frac{5}{64} V_1^5 a_5 \cos(\omega_2 t - 4\omega_1 t - 4\omega_1 \tau_5 - \omega_2 \tau_5) + \frac{155}{512} V_1^5 a_5 \cos(\omega_2 t - 4\omega_1 t + 4\omega_1 \tau_5 - \omega_2 \tau_5) \\
& + \frac{5}{16} V_1^5 a_5 \cos(4\omega_1 t + \omega_2 t - 4\omega_1 \tau_5 - \omega_2 \tau_5) + \frac{5}{512} V_1^5 a_5 \cos(4\omega_1 t - \omega_2 t - 4\omega_1 \tau_5 + \omega_2 \tau_5) \\
& - \frac{5}{64} V_1^5 a_5 \cos(4\omega_1 t - \omega_2 t + 4\omega_1 \tau_5 + \omega_2 \tau_5) + \frac{5}{8} V_1^5 a_5 \cos(2\omega_1 t - 3\omega_2 t - 2\omega_1 \tau_5 + 3\omega_2 \tau_5) \\
& + \frac{5}{8} V_1^5 a_5 \cos(2\omega_1 t + 3\omega_2 t - 2\omega_1 \tau_5 - 3\omega_2 \tau_5) + \frac{5}{256} V_1^5 a_5 \cos(2\omega_2 t - 3\omega_1 t - 3\omega_1 \tau_5 + 2\omega_2 \tau_5) \\
& + \frac{5}{64} V_1^5 a_5 \cos(2\omega_2 t - 3\omega_1 t + 3\omega_1 \tau_5 + 2\omega_2 \tau_5) - \frac{5}{64} V_1^5 a_5 \cos(3\omega_1 t - 2\omega_2 t - 3\omega_1 \tau_5 - 2\omega_2 \tau_5) \\
& + \frac{5}{8} V_1^5 a_5 \cos(3\omega_1 t - 2\omega_2 t - 3\omega_1 \tau_5 + 2\omega_2 \tau_5) - \frac{5}{256} V_1^5 a_5 \cos(3\omega_1 t - 2\omega_2 t + 3\omega_1 \tau_5 - 2\omega_2 \tau_5) \\
& + \frac{5}{8} V_1^5 a_5 \cos(3\omega_1 t + 2\omega_2 t - 3\omega_1 \tau_5 - 2\omega_2 \tau_5) + \frac{5}{512} V_1^5 a_5 \cos(4\omega_1 t - \omega_2 t - 4\omega_1 \tau_5 - \omega_2 \tau_5) \\
& + \frac{5}{32} V_1^5 a_5 \cos(4\omega_1 t - \omega_2 t + 4\omega_1 \tau_5 - \omega_2 \tau_5) - \frac{15}{256} V_1^5 a_5 \cos(2\omega_2 t - 3\omega_1 t + \omega_1 \tau_5) \\
& - \frac{45}{512} V_1^5 a_5 \cos(\omega_2 t - 4\omega_1 t + \omega_2 \tau_5) + \frac{15}{256} V_1^5 a_5 \cos(3\omega_1 t - 2\omega_2 t - \omega_1 \tau_5) \\
& + \frac{55}{512} V_1^5 a_5 \cos(\omega_2 t - 4\omega_1 t - \omega_2 \tau_5) - \frac{55}{512} V_1^5 a_5 \cos(4\omega_1 t - \omega_2 t + \omega_2 \tau_5) \\
& + \frac{45}{512} V_1^5 a_5 \cos(4\omega_1 t - \omega_2 t - \omega_2 \tau_5) - \frac{5}{256} V_1^5 a_5 \cos(2\omega_2 t - 3\omega_1 t - 3\omega_1 \tau_5) \\
& - \frac{5}{64} V_1^5 a_5 \cos(2\omega_2 t - 3\omega_1 t + 3\omega_1 \tau_5) + \frac{5}{64} V_1^5 a_5 \cos(3\omega_1 t - 2\omega_2 t - 3\omega_1 \tau_5) \\
& + \frac{5}{256} V_1^5 a_5 \cos(3\omega_1 t - 2\omega_2 t + 3\omega_1 \tau_5)
\end{aligned}$$

## Appendix C

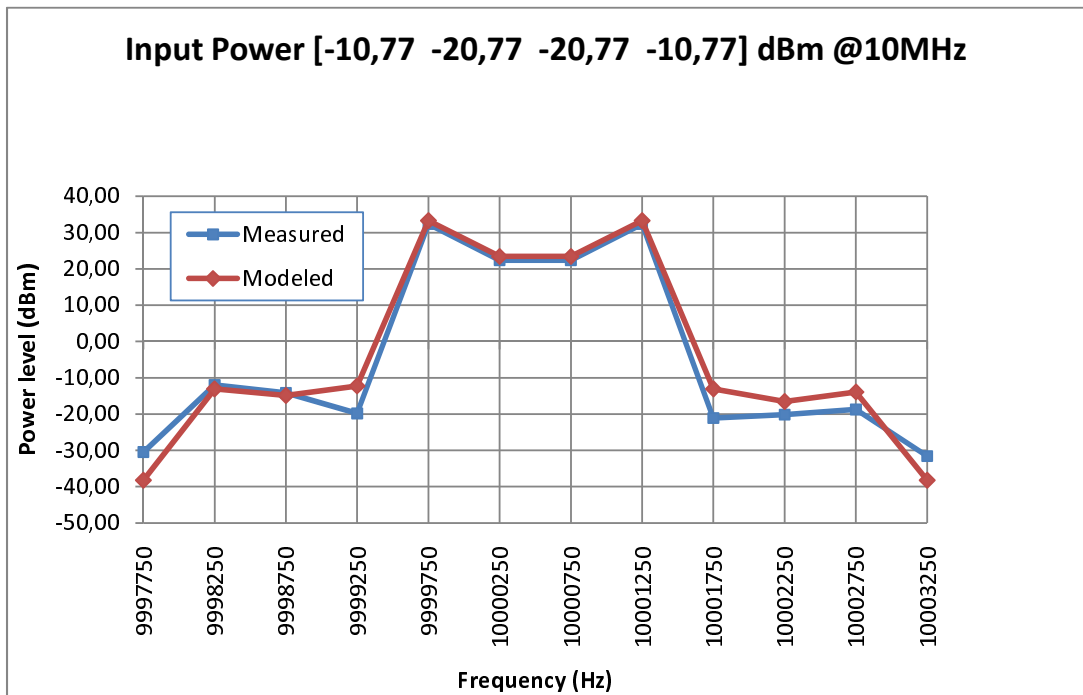
### Unequal Four-Tone Comparison Graphs



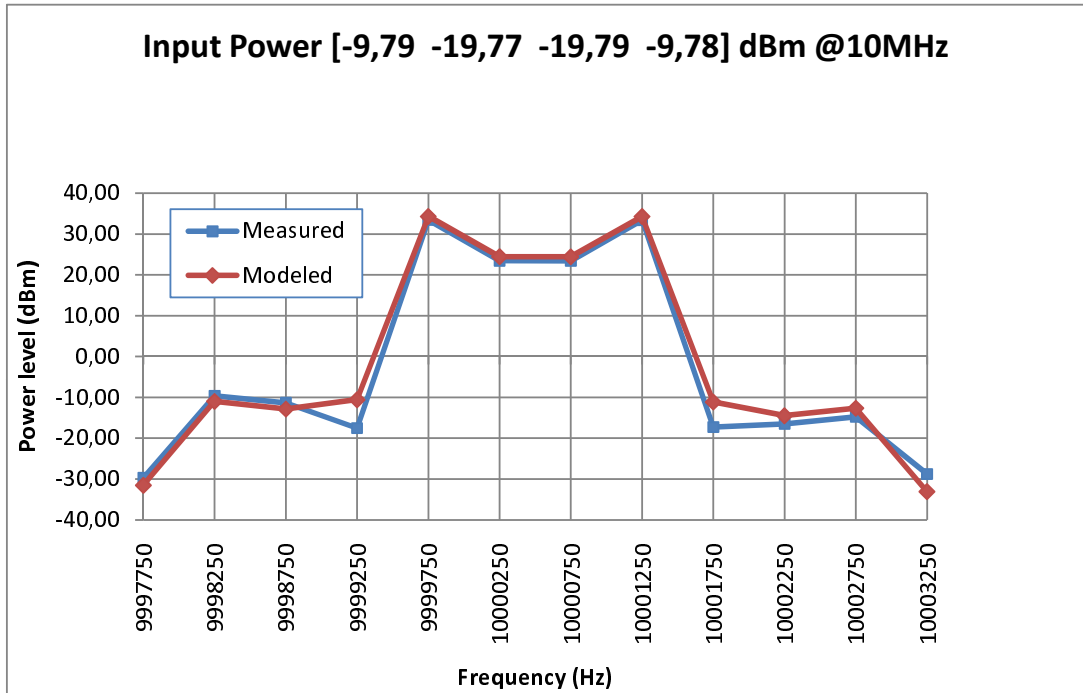
(a) Model estimation and measurement result for Excitation 1



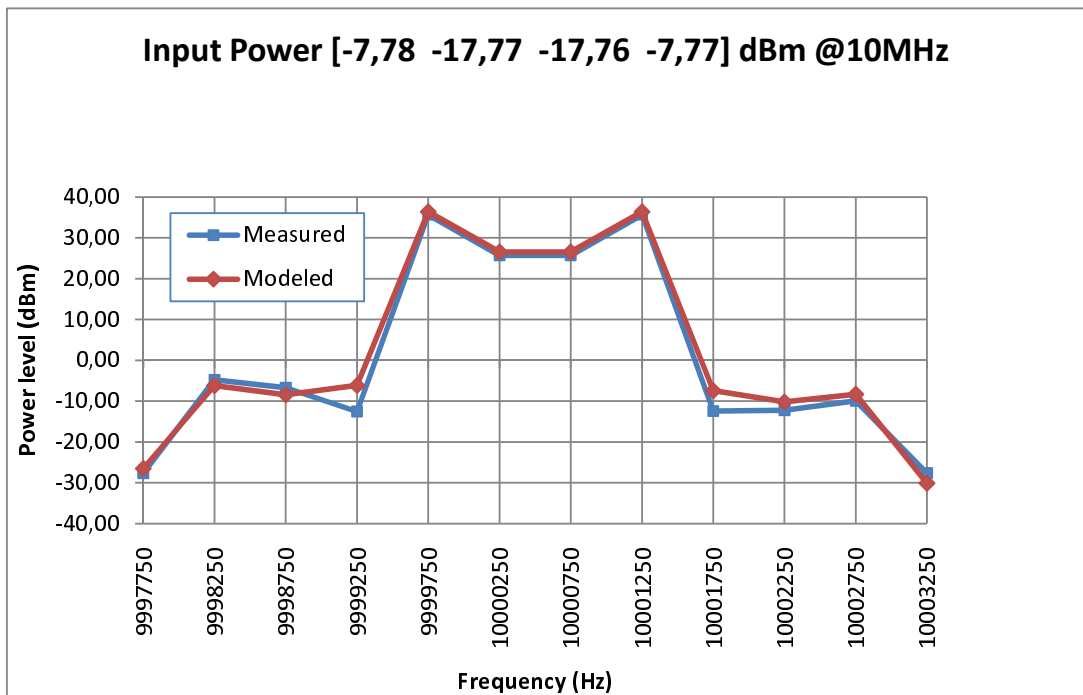
(b) Model estimation and measurement result for Excitation 2



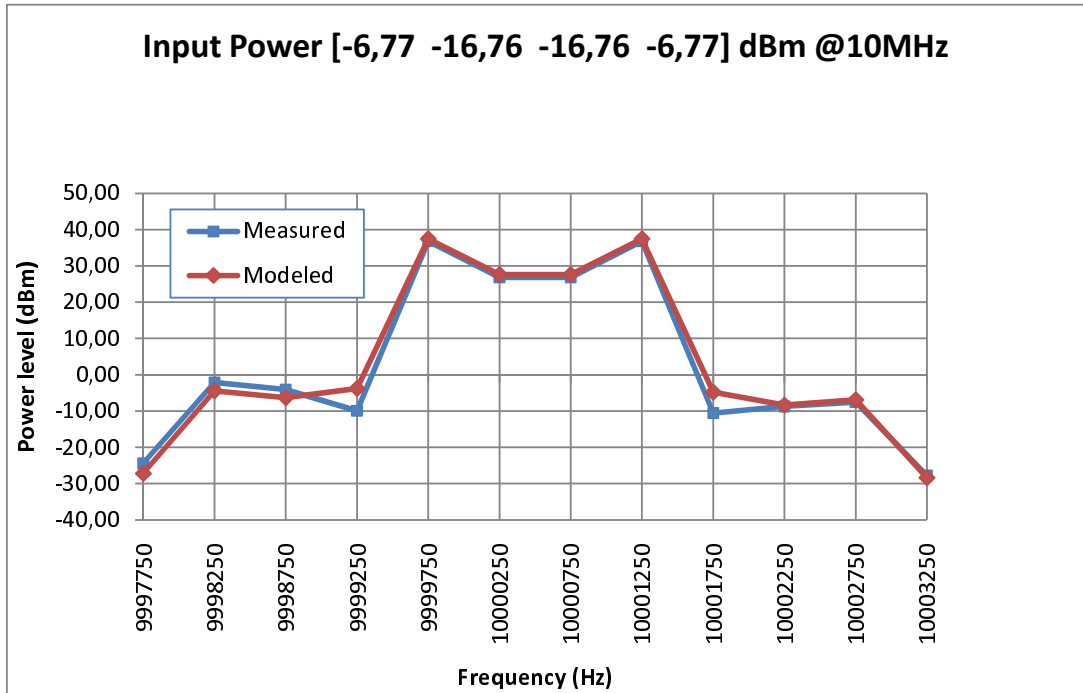
(c) Model estimation and measurement result for Excitation 3



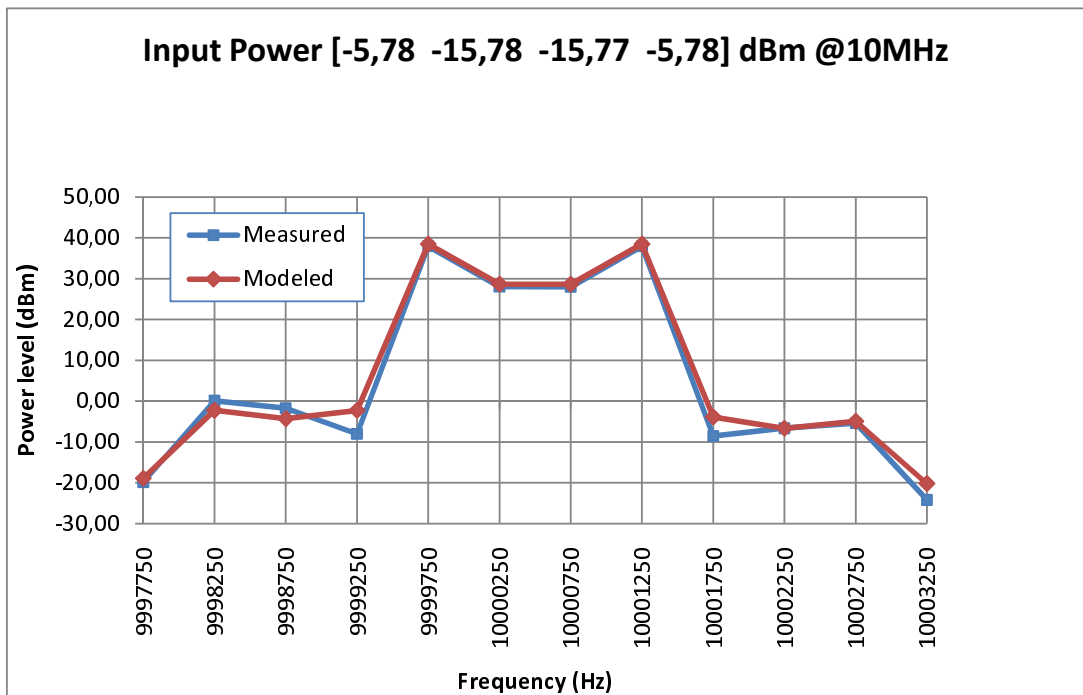
(d) Model estimation and measurement result for Excitation 4



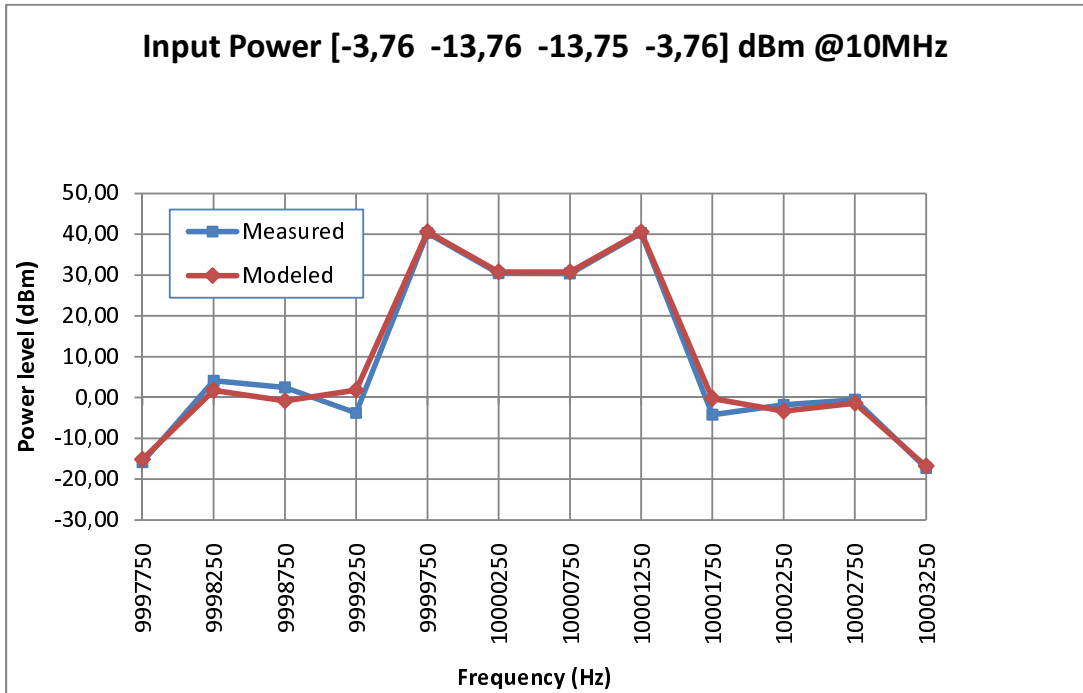
(e) Model estimation and measurement result for Excitation 6



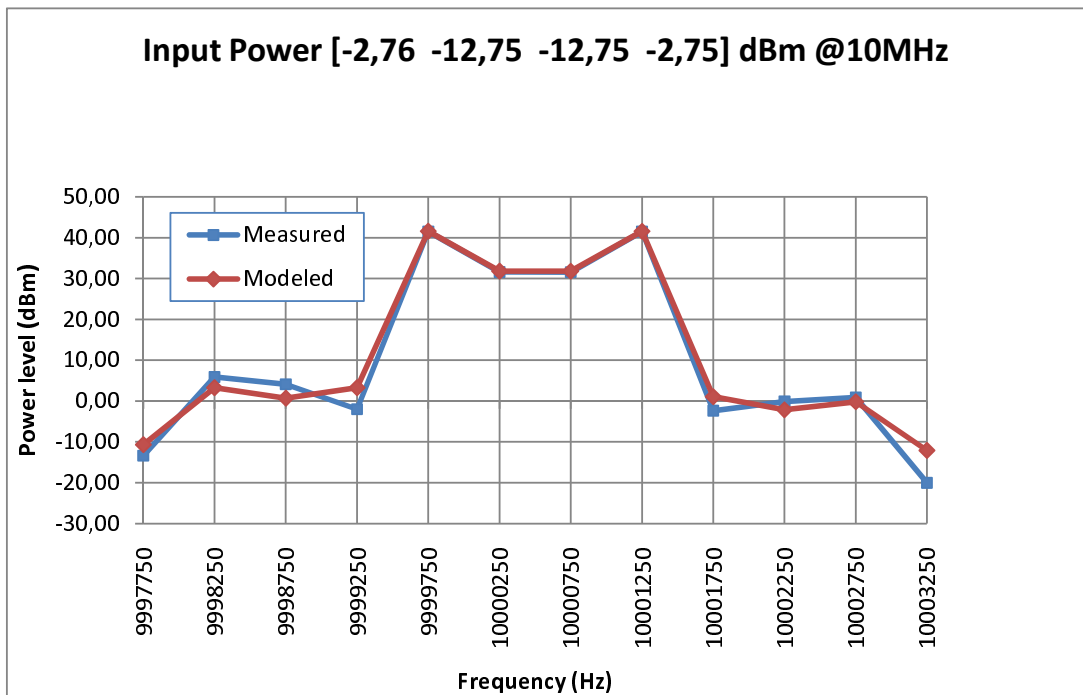
(f) Model estimation and measurement result for Excitation 7



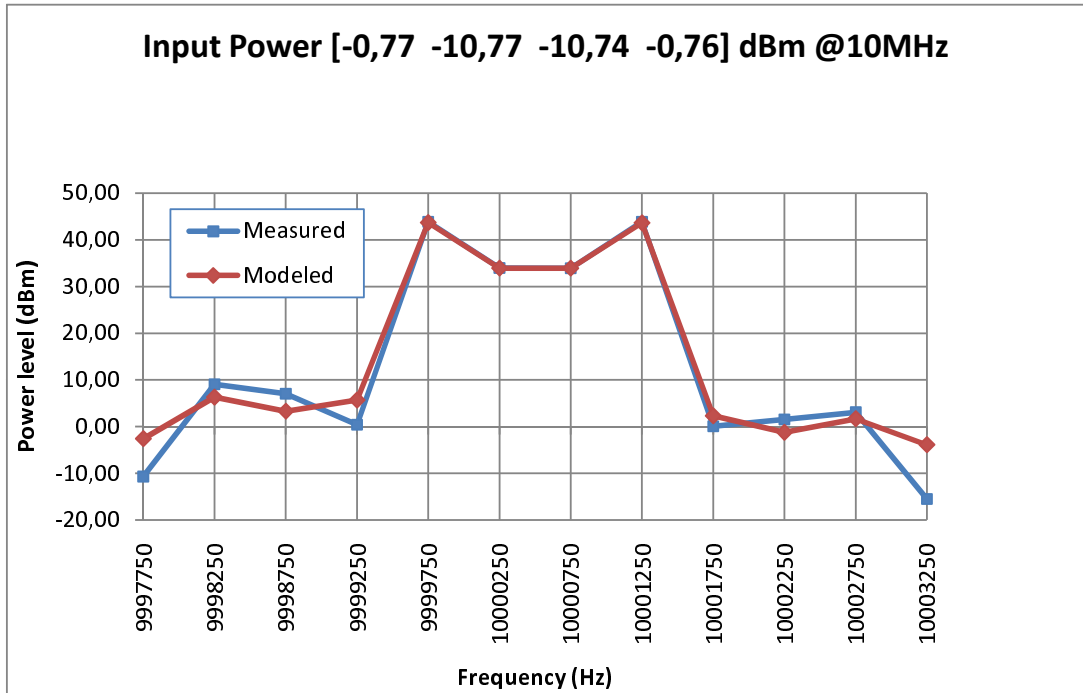
(g) Model estimation and measurement result for Excitation 8



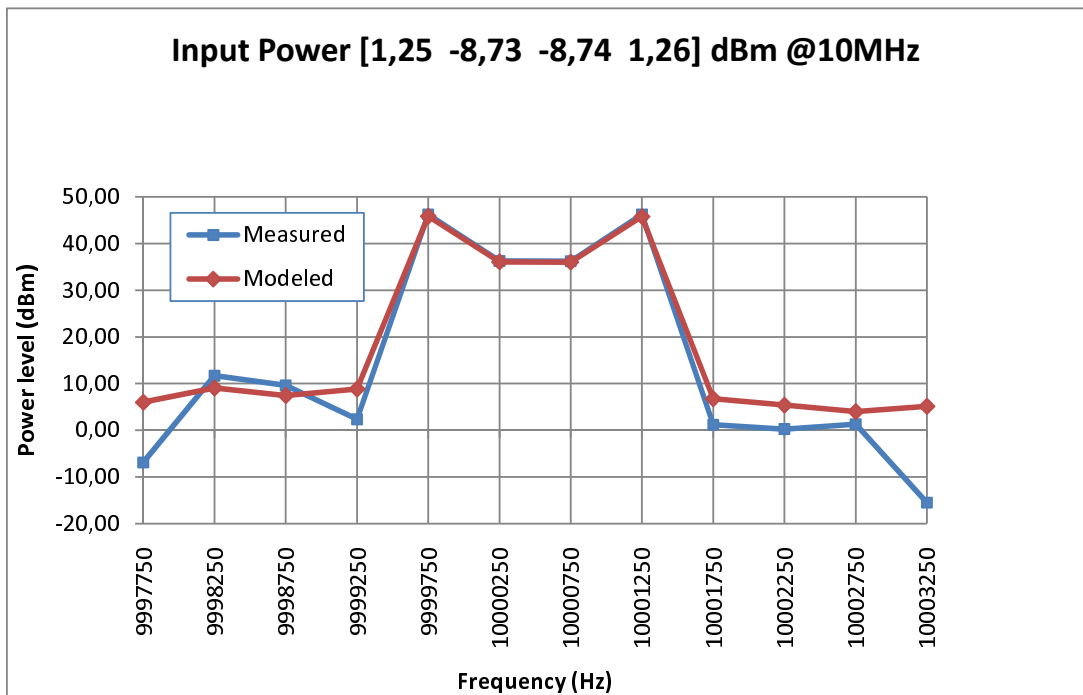
(h) Model estimation and measurement result for Excitation 10



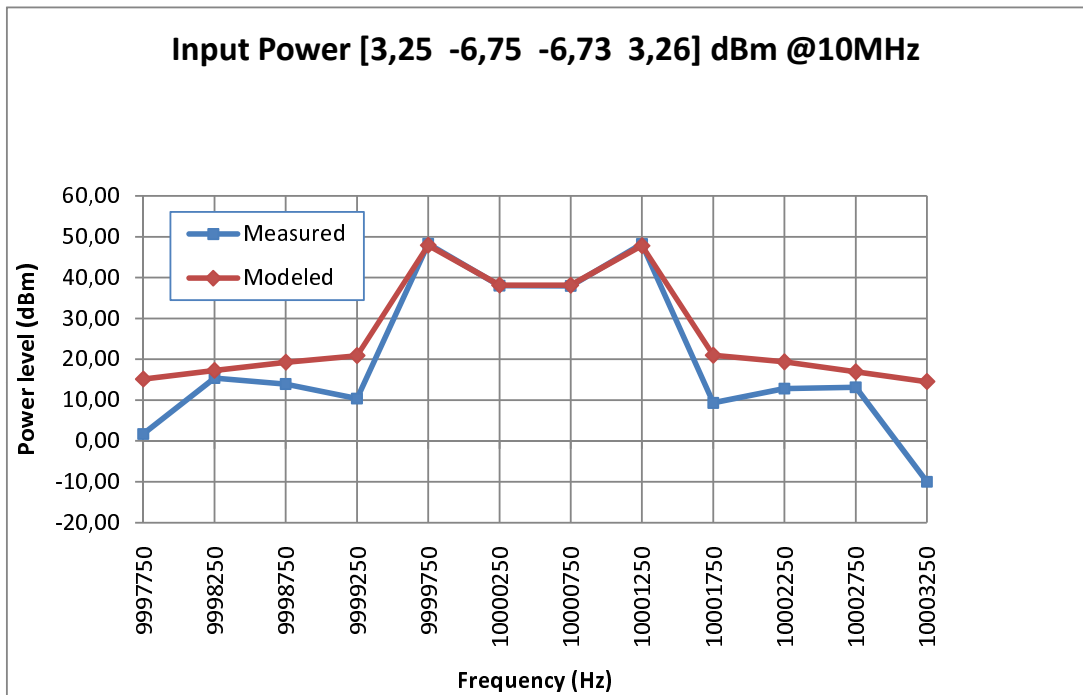
(i) Model estimation and measurement result for Excitation 11



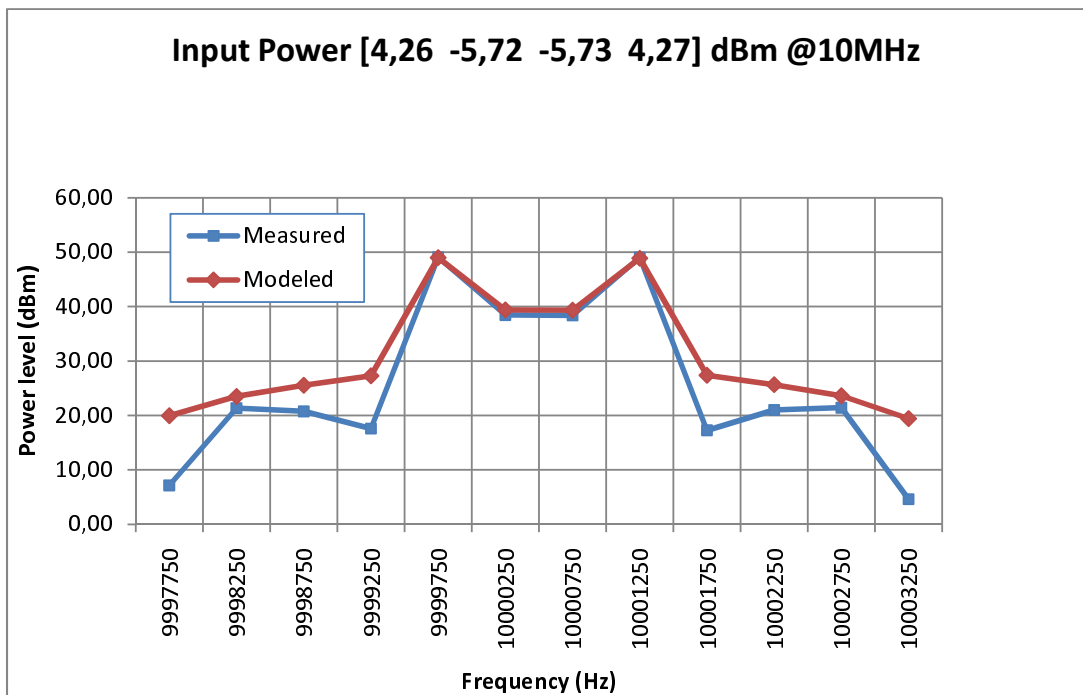
(j) Model estimation and measurement result for Excitation 13



(k) Model estimation and measurement result for Excitation 15



(l) Model estimation and measurement result for Excitation 17



(m) Model estimation and measurement result for Excitation 18

Figure C.1: Comparison between measurement and model outputs for four-tone (10MHz/1kHz) input excitation for five different power levels (-12.8dBm to 4.26dBm).

# CURRICULUM VITAE

## PERSONAL INFORMATION

Surname, Name : Yüzer, Ahmet Hayrettin  
Nationality : Turkish (TC)  
Date and Place of Birth : 1977 , İskenderun  
email : yuzer@metu.edu.tr, hayrettin\_yuzer@yahoo.com,  
hayrettinyuzer@gmail.com

## EDUCATION

Degree	Institution	Year of Graduation
PhD	: METU, Electrical and Electronics Engineering, Ankara	2011
MSc	: İnönü Univ. ,Electrical and Electronics Engineering, Malatya	2002
BS	: İnönü Univ., Electrical and Electronics Engineering, Malatya	1999
High School	:Ahmet Akıncı, Malatya	1994

## WORK EXPERIENCE

Year	Place	Enrollment
2002–	: METU, Electrical and Electronic Eng. Dep.	Research and Teaching Assistant
1999 – 2002	: İnönü Univ., Electrical and Electronic Eng. Dep.	Research and Teaching Assistant
1998–1999	: İnönü Univ.,Faculty of Engineering	Computer Lab. Assistant

## FOREIGN LANGUAGES

English

## PUBLICATIONS

1. Ahmet Hayrettin Yuzer, S. Aidin Bassam, Fadhel M. Ghannouchi, Simsek Demir, *Memory Polynomial with Shaped Memory Delay Profile*, being prepared
2. Ahmet Hayrettin Yuzer, S. Aidin Bassam, Fadhel M. Ghannouchi, Simsek Demir, *Thermal Memory Effect Modeling with Memory Polynomial*, being prepared
3. A. H. Yuzer and S. Demir, *Behavioral Modeling*, submitted to AEÜ – International Journal of Electronics and Communications.
4. A. H. Yuzer and S. Demir, *A nonlinear model for amplifiers with memory* in Microwave Symposium (MMS), 2010 Mediterranean, Aug 2010, pp. 277–280.
5. A. H. Yuzer and S. Demir, *A new phase measurement technique for rf power amplifier only measuring magnitudes* in Progress In Electromagnetics Research Symposium Cambridge, USA, July 2010, pp. 170–173.
6. A. H. Yuzer and S. Demir, *Behavioral modeling of asymmetric intermodulation distortion of nonlinear amplifier* in Progress In Electromagnetics Research Symposium Cambridge, USA, July 2010, pp. 1115–1119.
7. A. H. Yuzer and S. Demir, *Improved behavioral modeling of nonlinear amplifiers with phase asymmetry* in 5th International Advanced Technologies Symposium (IATS 09), May 2009, pp. 580–584.
8. A. H. Yuzer and S. Demir, *Güç, yükselticilerde davranışsal modelleme ile arakipleme bozulmasının modellenmesi* in URSI Ulusal Konferansı 2008, Akdeniz Ü niversitesi, Oct 2008, pp. 133–136.
9. A. H. Yuzer and S. Demir, *Vektör modülatör mmic uygulama devreleri* in URSI Ulusal Konferansı 2006, Hacettepe Üniversitesi, Sep 2006, pp. 432–434.